UNIVERSITY OF LIVERPOOL

Department of Mathematics

A Combined Experimental and Mathematical Study of Evolution of Microbial Community Composed of Interacting *Staphylococcus* Strains

Thesis Submitted in Accordance With The Requirements of

The University of Liverpool for The Degree of Doctor in Philosophy

By

Nouf Saleh Alghamdi

Contents

Abstract

The emergence of the phenomenon known as AMR (anti-microbial resistance), or to be more specific, ABR (anti-bacterial resistance), is the result of the gradual decrease in the efficacy of antibiotics and the increase in the cost of producing new antibiotics [29, 97, 101, 169]. Hence, alternative solutions to prevent the spread of the pathogenic species are required [7, 127]. Observing and studying microbial ecosystems is considered one way to provide an opportunity for a deeper understanding of the essential mechanisms of life [65, 190]. The human body shelters a diverse collection of microbial species [37, 199]. The basic instinct of survival drives these populations to engage in constant competition with each other for space and resources [188]. Some species compete by manufacturing lethal compounds, toxins that do not affect their population and are directed against the other interacting populations [151]. Consequently, the affected populations evolve defences, mutating against these attacks to ensure their existence [132, 182, 188].

A significant number of theoretical and experimental population studies indicate that the interactions within and between bacterial species can impede and even prevent the colonisation of other populations [122, 182, 188, 199]. An ecosystem is a complex system of dynamic interactions among organisms as well as between organisms and the environment.

Mathematical modelling is a crucial tool to analyse and investigate the underlying phenomena and understand the diverse scales at which these systems act. Continuous models represented by differential equations are a suitable approach that can effectively offer and deliver descriptions and explanations of the outcome from microscopic behaviours [11, 134, 147].

In this thesis, a combined experimental and mathematical study of the evolution of microbial communities is presented. The aim was to investigate the role of skin bacteria invasion and competition in limiting pathogenic species growth and colonisation, and to determine and reveal factors and conditions that alter and influence the dynamics of interactions between species. The focus in this study was *Staphylococcus aureus* as it is considered a major human pathogen that shows colonisation traits distinct from the more abundant skin antimicrobial-secreting residents, *S. epidermidis* and *S. hominis* [132, 134]. The method adopted when conducting this study was based on two approaches: experimental and mathematical.

A series of laboratory experiments were carried out to determine, analyse and describe the characteristics of the evolved species, as well as the interactions between species, where toxin-producing and non-producing isolates of *S. epidermidis* interacted with populations of *S. aureus*. The evolution of resistance by *S. aureus* was also investigated experimentally by performing the deferred inhibition assays before and after the interactions.

Several mathematical models were developed and introduced to understand, explain, and predict the behaviour of the involved species. The use of the Tilman model [203], when a single population consumes limited resources, enables the stimulation of the growth curves of the involved species and the estimation of the consumption rate for each strain. Also, a mathematical term was defined to link the inhibitory parameters by solving the inhibitory variable when modelling the inhibition assays.

The interaction phenomenon is modelled in both types of environments by extending a classic two-species *Lotka-Volterra* competition in one spatial dimension to incorporate adaptation by one species, *S. aureus*, and toxin production by another, *S. epidermidis* [12, 54, 148]. The modelling hypothesis in this study predicts that most *S. aureus* SH1000 will adapt to the produced toxins given enough time. This hypothesis was tested in the laboratory (by performing the post-interactions inhibition assays) and in silico (by changing the initial conditions, assuming that most of the *S. aureus* SH1000 were adapted). Also, when the interactions were performed under structured conditions, the evolved populations formed a circular spot which was maintained during the daily transfer process. The impact of the initial location of resistance in the evolved bacterial lawn on the interference dynamics was examined by extending the model to the 2D n-species competition-diffusive model.

The novelty and significance of the study presented in this thesis lies in the fact that, unlike that found in a previous study, [122], the manipulation of spatial structures, the level of toxicity, and initial frequencies did not prevent the emergence of resistance in the evolved *S. aureus* populations. The evolved *S. aureus* populations were able to dominate their opponents regardless of the environmental conditions. However, it was found that the level of toxicity and environmental regulations made it harder for evolved *S. aureus* populations to recover.

In addition, the findings of this study concur with the findings of the previous study in that when interacting under mixed conditions, all *S. epidermidis* isolates were unable to successfully invade or restrict the invasions by *S. aureus*. However, *S. epidermidis* was more likely to persist at low frequencies and avoid extinction in both environments.

Furthermore, both studies found that structured environments favour the production of inhibitory toxins. The structured environments and the higher level of toxicity assisted the evolved *S. epidermidis* populations in improving their survival chances. However, unlike the findings of the previous study [122], no extinction or total decolonisation was

observed in any performed interactions.

Another point of conflict was that, according to the experimental findings of this thesis, a negative association was observed between the initial density of the *S. aureus* population and its ability to recover, i.e., when performing mutual invasions, the evolved *S. aureus* were able to recover faster when they were the invaders rather than the residents. However, according to the results obtained in [122], invasion of *S. aureus* into a toxin-producing *S. epidermidis* resident was positively frequency-dependent, with the highest initial frequencies invading the fastest and with lower initial frequencies becoming extinct. The oscillations of the evolved population density were more evident when the interactions were conducted under mixed conditions and started from different initial concentrations.

Most of the evolved inhibitory *S. epidermidis* strains produced larger inhibition zones against the ancestral *S. aureus* indicating the occurrence of mutations in *S. epidermidis* populations as well.

Another aspect of the novelty presented in this thesis is that the findings suggest that the farther the mutations are created from the centre of the spot, the longer it takes to recover and finally dominate. Biologically this can be justified as the concentration of toxins is relatively low compared to the centre of the spot. Also, it is known that the emergence of mutations is positively proportional to the hostility of the surrounding conditions [24, 113, 154]. However, the emergence of resistance away from the centre of the spot contributed positively to the producer since the *S. aureus* populations are non-motile [28, 84], and this feature gives a better opportunity for the evolved *S. epidermidis* populations to have access to nutrients and consequently maintain their existence for a longer period.

Mathematically, the findings of this study show that the two-variable model was not sufficiently complex to capture the dynamics of interactions observed in the experimental data. However, the three-variable model succeeded in simulating the interaction dynamics that were experimentally observed when performing what were considered non-inhibitory interactions. The inhibitory interactions were modelled by adding the fourth variable to represent the inhibitory production by *S. epidermidis* populations. Finally, the four-variable model was able to simulate the evolution of inhibitory interactions when imposing different conditions according to the type of environment incubating these interactions.

Chapter 1

General Introduction

The emergence of antimicrobial resistance (AMR) is considered one of the most serious public health issues of the twenty-first century [7, 169]. The rapid growth of this phenomenon threatens the efficacy of the old methods of prevention and treatment of an ever-increasing range of infections [29, 97, 169]. AMR refers to resistance observed in all microbial communities, including bacteria, parasites, viruses, and fungi. As a result, common medications are no longer effective in preventing and treating diseases caused by such microorganisms [97, 169].

This study focuses on antibacterial resistance (ABR), which is currently a significant issue due to the high rates of resistance identified in bacteria that cause common diseases that range in their severity from mild to life-threatening and the complexity of their consequences [101, 169].

The description of antibiotic activity by Alexander Fleming at the beginning of 1943 contributed to changing the destiny of mankind [46, 193]. Fleming's discovery helped to eliminate many epidemics and infections and saved millions of lives [7, 136]. Antibiotics have transformed the practice of medicine by facilitating advances across the entire range of clinical care, including safer childbirth, surgery, organ transplants, and myeloablative chemotherapy treatments [7, 190]. However, while people died in the pre-antibiotic era, we stand today at the threshold of the post-antibiotic era [65]. Over the last several decades, bacteria causing common or serious infections have evolved resistance to each new antibiotic introduced onto the market [7, 127]. Faced with this fact, it is imperative to act to avoid a global disaster in healthcare.

Antibiotic Resistance Leading Factors

Antibiotic resistance is a natural phenomenon resulting from the exposure of microorganisms to antibiotic medicines [7, 169]. Under the pressure of antibiotics, vulnerable bacteria are eliminated or suppressed, whereas bacteria that are inherently resistant or have acquired antibiotic-resistant characteristics have a better chance of surviving and proliferating. Antibiotic resistance is a result of both overuse and incorrect use of antibiotics (wrong selection, inadequate dose, and poor adherence to treatment guidelines).

Antibiotic resistance can be traced back to four basic sources: community and hospital-based human medicine, livestock production, and the environment [65, 169].

Implications of Antibiotic Resistance

Estimating the impact of antibiotic resistance on mortality and public health budgets is challenging, and there is little research addressing this area [29, 169]. However, bacteria developed resistance in such a rapid way that pharmaceutical companies have decided that creating new antibiotics is not in their best interest, Fig (1.1), and the need to find an alternative to these solutions has become pressing [65, 190]. In addition, the treatment of common infections in newborns in intensive care is becoming increasingly complicated and sometimes impossible [191]. *Staphylococcal* species, primarily *S. aureus* and *S. epidermidis*, cause 60-70% of infections in these units, and multiple cases of methicillin-resistant *S. aureus* (MRSA) have been observed [157].
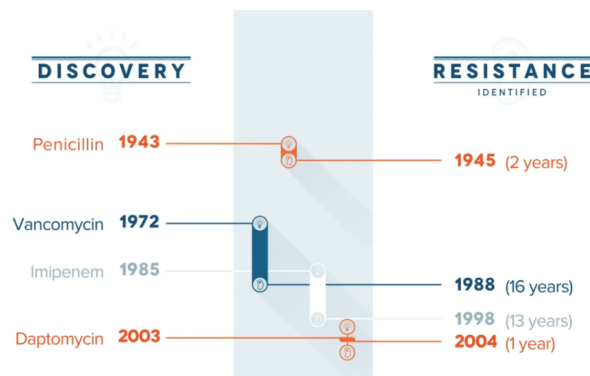
Figure 1.1: **A timeline of the discovery and resistance of antibiotics.** Taken from [128].

Furthermore, inadequate economic incentives for the pharmaceutical development of novel antimicrobial medicines have compounded the problem [49]. When infections evolve resistant to first-line antimicrobials, treatment must be transferred to second- or third-line medications, which are considerably more expensive, as well as necessitating specialist equipment, lengthier hospital stays, and patient isolation protocols [49, 128].

Innovative Methods to Limit Antimicrobial Resistance

Antimicrobial resistance poses significant challenges for global health care, and because resistance is inevitable, researchers must react and introduce alternative strategies to address antimicrobial resistance [185], for instance by developing new drug applicants, immunisations, and generating novel methods of treatment that are less likely than conventional antibiotics to cause resistance.

Several novel approaches have been investigated to address antimicrobial resistance, as seen in (Table 1.1), which demonstrates the main approaches with some examples of each approach.

Type of Approach	Examples
Antibiotic Development	• Identifying novel sources of naturally occurring antibiotics, (iChip platform) [125] • Producing antibiotics from untapped sources, (Marine microbes) • Antimicrobial peptides, (Bacteriocins) [10]
Boosting the Immune system	• Vaccines [40, 160] • Monoclonal antibodies [158] • Investigating the signalling pathways and receptors of the natural immune system [78]
Microbial community manipulations	• Microbiota transplant and live bio-therapeutics (the microbiota includes bacteria, fungi, and viruses) [132, 199]. • Bacteriophages (viruses that infect and kill bacteria). • Innovative phage-derived techniques [182]
Anti-virulence Approaches	• Antitoxin antibodies for the treatment of *C difficile* • Inhibitors of the secretion system that prevent the release of bacterial virulence factors (eg, for *P seudomonas* infection) • Preventing the creation of biofilms by using coatings for devices that include substances that stop bacterial communication (quorum sensing) [221]
Diagnostics	• Tests to differentiate between bacterial and viral causes of respiratory disease • Magnetic resonance imaging (MRI) • Procalcitonin levels in the blood indicate bacterial infection [183, 222]

Table 1.1: **Summary of novel approaches to address antimicrobial resistance.**

Indeed, many of these approaches have shown promising outcomes. For instance, through the first approach, scientists have been able to identify teixobactin, an antibiotic compound with a novel mechanism of action [10, 125].

Boosting the immune system provides additional options for treatment and prevention and shows the capability of preventing bacterial infection. Furthermore, it is considered as an attractive approach due to the low toxicity, extended serum half-life of certain monoclonal antibodies, and the absence of standard, drug-mediated selective pressure [40, 78, 158, 160]. It is also a promising approach for patients with inadequate immunisation responses and can reduce the antibiotic dosage, duration of treatment, or both [13, 60].

Microbial community manipulations limit the colonisation of multidrug resistant or-

ganisms in patients [132, 199]. Phage therapy shows significant clinical benefit when treating antibiotic-resistant suppurative infections [188], chronic, antibiotic resistant P $aeruginosa$ infections [213], and bacterial infections caused by wounds and burns [37]. Phage therapy is also utilised to generate engineered products that can modify bacterial cells, including their antibiotic-resistance mechanisms and virulence factors [182]. However, many of these approaches are still in the early stages of development [125], or could be improved with methods that better model physiologic conditions [53]. Thus, further investigations are required to cover all the challenges arising from each approach [13, 37, 41, 53, 60, 183, 222].

1.1   Motivation

The motivation for this study was the desire to perform further investigations into one of these novel approaches that is associated with the manipulation of the bacterial community. The study of manipulations of microbial communities is vital in the fight against antibiotic resistance since, as previously indicated, bacterial populations rapidly evolve resistance [190]. Consequently, resistance to new antibiotics is now a matter of time [128]. In addition, the rising cost of developing new antibiotics has necessitated the development of alternative treatments for microbial infections [49]. Also, as shown in (Table 1.1), this sort of approach demonstrated promising results [188, 199], for instance, when utilised to treat C $difficile$ infections [37]. However, the application of this method to decolonise patients with multi-drug-resistant pathogens is still under consideration [199].

Little research has been conducted to investigate the role of de-colonising bacteria in $S.$ $aureus$ carriage. Three studies characterised nasal species distributions by using 16S rRNA gene sequencing, and scientists have hypothesised species-level interactions based on these patterns[61, 212, 219]. $S.$ $aureus$ was found to have a positive correlation with $Corynebacterium$ $pseudodipthericum$ and a negative correlation with $Finegoldia$ $magna$ and $Corynebacterium$ $accolens$ in one of these studies [212], while the other study demonstrated that $S.$ $aureus$ interacts at the species level with $C.$ $accolens$ and $C.$ $pseudodiphthericum$ and thus concluded that these are the most significant interactions between bacteria in terms of $S.$ $aureus$ carriage [219]. Additionally, that research revealed differences in the ecological relations between nasal niches, emphasising the dynamic complexity of bacterial relationships on host epithelial surfaces [219].

The inspiration for this thesis is a study performed in Dr Malcolm Horsburgh's laboratory to investigate the decolonisation theory [122]. The focus of the laboratory study was on the opportunistic pathogen $Staphylococcus$ $aureus$, which colonises the lower nasal

airway of humans.

The research presented in [122] concluded that manipulating the nasal microbial population could be utilised to reduce colonisation of *S. aureus*, potentially limiting transmission and infection rates. The hypothesis of the study presented in this thesis is that this suppression is due to competition and inhibition between bacterial species.

Thus, in this thesis the aim is to:

- Analyse the experimental results obtained in Dr. Malcolm Horsburgh's laboratory during the investigation into the dynamics of the population formed by interacting *S. epidermidis* and *S. aureus* species.

- Develop mathematical models to explain and simulate the dynamics of interacting populations observed in laboratory experiments.

- Perform laboratory experiments to:

  1. Analyse and define the distinguishing characteristics of the evolved species.
  2. Examine and explain species interactions.
  3. Analyse and describe the influence of the inhibitory productions on the outcomes of the interactions.
  4. Analyse and describe the influence of the environmental structure on the outcomes of the interactions.
  5. Identify and reveal factors and conditions that alter the dynamics of species interactions.
  6. Provide additional justification for the introduced models.

- Examine inhibitory production and resistance evolution in the invasion and competition of skin bacteria.

- Fit model parameters to experimental data.

1.2 Biological Background

Although there is evidence suggesting that many environments possess a carrying capacity at a level that allows coexistence of species, as well as evidence supporting the idea of cooperative interaction between them, the consequences of species interaction remain relatively unknown [4]. With regard to bacterial cells, modelling allows for the deepening of our understanding of their growth and the way in which they interact. Modelling the interaction of bacterial species has a diverse range of real-world applications, including safe food production and medicinal use. Since bacterial interaction within and

between species can restrain and prevent the colonisation of other populations, mathematical modelling of their interactions allows scientists to generate an understanding of the conditions and circumstances required for preventing and eliminating the colonisation of opportunistic pathogens [148].

1.2.1 Bacterial Properties

In this section, many important concepts regarding the growth of microbial populations, such as binary fission, exponential growth, generation time, and growth curve, will be explored.

(a)

(b)
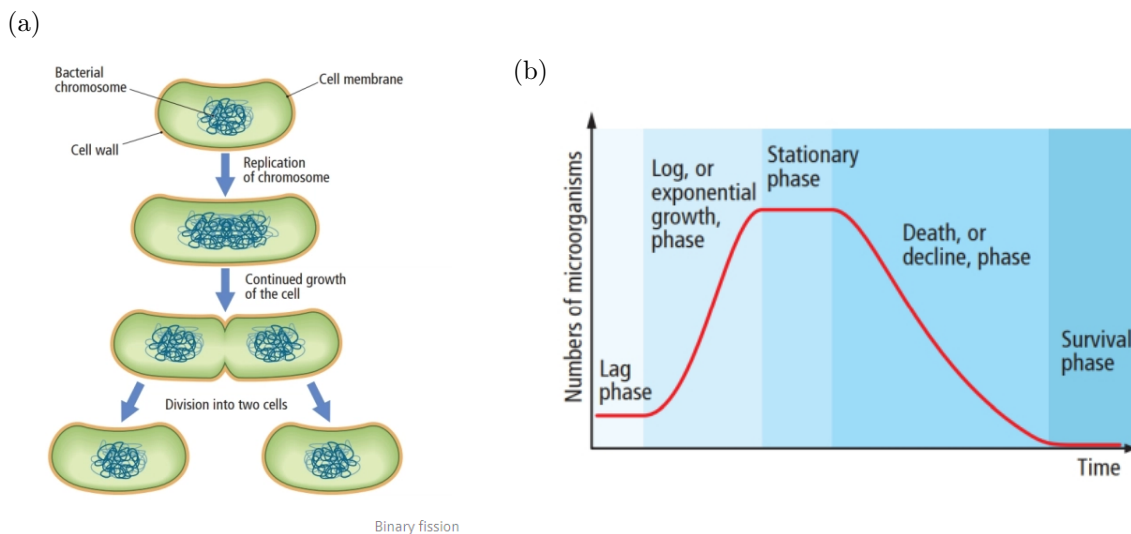
Figure 1.2: **Bacterial properties.** Panel (a): steps of binary fission process in bacteria, through chromosome replication and cell development, a parent cell divides into two identical daughter cells. Panel (b): an illustration of the bacterial growth curve. Taken from [179].

Binary Fission

All bacteria are prokaryotes, meaning that bacteria are single-celled organisms [197]. Bacteria reproduce asexually through a process identified as binary fission [179]. A bacterial cell will metabolise and grow to be double its regular size, then two daughter cells that are genetically identical to the mother cell will be produced through this process (see Fig 1.2a).

Population Growth

Bacterial growth is defined by an increase in cell number rather than cell size [103]. In each round of binary fission reproduction, the number of bacterial cells is doubled. The cumulative number of cells arising from a single cell via binary fission is calculated as:

$$\text{Number of cells at } n = \text{initial number of cells} \times 2^n,$$

where n is the number of generations. This type of reproduction is known as logarithmic or exponential growth [5].

Generation Time

Generation time is the amount of time required for a population to grow twice its initial density. The abundance of resources and space determines the growth of populations. Under appropriate environmental conditions, bacterial cells can continue to double at a constant rate. Doubling time varies among bacterial species. In some species generation time can be as short as ten minutes, whereas it might require days in other species. Most bacteria have relatively short generation times (1-3 hours) [45, 184].

Growth Curve

The bacterial population cycle passes through four distinct primary phases [179].

• The **lag phase** is when bacteria adjust to the growing environment [197]. At this point the individual bacteria are still developing and unable to divide. RNA, enzymes, and other compounds are synthesised by bacteria during their lag period of growth [45]. As they do not immediately replicate in a new medium, cells change relatively slowly during the lag phase. The lag phase, which can last anywhere between an hour and many days, is characterised by minimal to zero cell division [6]. The cells are not inactive during this stage [24].

• Cell doubling occurs during the **log phase** (also known as the logarithmic phase or the exponential phase) [172]. The rate at which new bacteria form is proportional to the population's current density. If growth remains unrestricted, the number of cells and the rate of population expansion both double with each consecutive period of time [178]. Plotting the natural logarithm of cell number against time yields a straight line for this form of exponential growth [179]. In this case, the slope of the line represents the specific growth rate of the organism, which is the measure of the number of divisions per cell per unit time [172]. The actual growth (the slope of the line in Fig 1.2b) is determined by the culture conditions [23], which influence the frequency of cell division cycles and the chance of both daughter cells surviving. However, exponential growth cannot be sustained permanently since the medium eventually is depleted of nutrients and becomes loaded with waste [5].

• Depletion of vital nutrients and/or production of inhibitory products such as organic acids are common causes of the **stationary phase**. When the growth and death rates are equal, the process reaches a stationary phase [197]. The growth factors (i.e., temperature, acidity, water activity, oxygen, micronutrients, toxins) limit the number of new cells that may be generated, so the rate of cell growth coincides with the rate of cell death. As shown in Fig (1.2b), the flat horizontal linear section of the curve during the stationary period is the consequence of this phase. During the stationary phase, mutations can occur [24, 113, 154].

• Bacteria die during the **death phase** (decline phase). This may be due to nutrient

limitations, environmental temperatures that are above or below the species' tolerance band, or other harmful factors [197].

There is increasing evidence that DNA damage is responsible for many of the mutations that occur in the genomes of the stationary phase bacteria or starved and compromised bacteria [24, 113, 154]. Such damage is believed to be significantly induced by reactive oxygen species created within organisms themselves (endogenously generated) [24].

The basic bacterial growth model highlights clonality, asexual binary division, short development time relative to replication, low death rate, need to transition from dormant to reproductive state, or condition of media, and lab-adapted strains' ability to exhaust resources. However, even in batch culture, the four phases are not well-defined [154]. For cells to replicate in synchrony, there must be constant and clear inducements. Moreover, their exponential phase growth is often not at a constant rate but rather at a slowly decaying rate. There is a continual stochastic response to reproduction and dormancy forces in the face of diminishing nutrient concentrations and rising waste concentrations [154].

1.2.2 The Ecology of *Staphylococcus*

There are approximately thirty species of *Staphylococcus*, ten of which are easily recognised as human commensals [63]. *Staphylococci* are naturally occurring bacteria, and their interactions with humans are generally asymptomatic [134]. However, two species, *S. aureus* and *S. epidermidis*, are known as opportunistic pathogens and cause most diseases, ranging from mild skin infections to life-threatening disorders such as endocarditis and septicemia [126, 134].

A comparison will be presented to determine the fundamental similarities and differences between these two species (Table 1.2). Before proceeding, it is necessary to explain the difference between opportunistic and pathogenic bacteria. Any disease-causing microorganism is considered a pathogen [93]. Primary or opportunistic pathogens are the two main types of pathogens. Regardless of a host's microbiome or immune system, a primary pathogen can infect and cause disease. However, an opportunistic pathogen can take advantage of a situation such as a compromised immune system, sickness, or abnormal microbiome [93].

Criterion	Similarities and differences
Characteristics / Taxonomy	*Staphylococcus* species are Gram-positive, non-motile, non-sporing *cocci* that range in diameter from 0.5 to 1.5 μm and can be found single, in pairs, or in irregular clusters. In certain cases, colonies are white, cream, or even yellow or orange [28].

Environmental conditions	Both species are mesophiles, with optimal growth temperatures ranging from $30°C$ to $37°C$. They are facultative anaerobes with a fermentative metabolism [156].
Virulence	*S. aureus* infections are more virulent and can induce acute and chronic illness, whereas *S. epidermidis* infections were uncommon before the emergence of modern medicine [134]. A comparative genomic investigation has found that *S. aureus* and *S. epidermidis* share a core set of genes, with each organism expressing species-specific genes. The extra *S. aureus* genes are horizontally acquired genomic islands that encode virulence components not found in *S. epidermidis* [69, 134]. Additional research has been conducted to determine the factors that contributed to *S. aureus* being more virulent. Several hypotheses were studied to explain this phenomenon, with a focus on adaptability, transmission, and habitat [134].
Adaptability	*S. aureus* strains preserve a certain peptide, whereas *S. epidermidis* does not. This peptide's pheromone activity may have contributed to the evolution of vancomycin- resistant strains of *S. aureus*. As *S. epidermidis* does not secrete this peptide, it can be argued that this microorganism is less adaptable than *S. aureus* [57, 134, 150]. Furthermore, there is evidence that both *S. aureus* and *S. epidermidis* have recently acquired the methicillin-resistant islands, suggesting they acquire DNA at a similar rate. However, *S. aureus* maintains more virulence genes on islands than *S. epidermidis* [134].
Transmission	*S. epidermidis* is more efficient at transferring between hosts than *S. aureus*. This was suggested by an analysis of the transmission properties of these species, which reveals three factors contributing to this phenomenon [134]. • The absence of host barriers preventing colonisation by *S. epidermidis*. Whereas, only a sub-population of humans is colonised by *S. aureus* [106, 134]. • The transmission process between healthy hosts is less complicated in *S. epidermidis* than in *S. aureus* [17, 134]. • The phenomenon of Agr interference: when a host is colonised by *S. aureus* of one Agr type, the competitive nature of Agr interference will inhibit the colonisation of any newly transmitted strains of a different Agr type. Similler inhibition was not observed between different Agr sequence types in *S. epidermidis* species [48, 58, 99, 100, 124, 134].

Habitat	*S. aureus* primarily colonises the moist squamous epithelium of the human anterior nares. *S. epidermidis* is the most common *staphylococcal* species found on human skin, where host defences are weak in comparison to immune components acting in the anterior nares. As a result, the persistence of a bacteria in the skin environment vs. the nasal environment would necessitate different microbial adaptations [134].

Table 1.2: **A summary of the similarities and differences between *S. aureus* and *S. epidermidis*.**

1.2.3 Ecological Communities: Types of Interacting Species

A group of microorganisms form a population. Several populations construct a community. There are different types of interactions within and between these communities. In this section some of these interactions will be described and the consequences or evolution of each type of them [114, 139, 176].

Competition

While competition is most often characterised as the interaction of individuals seeking a limited resource, it may also be defined more broadly as the direct or indirect contact of organisms that results in a change in fitness when the organisms share the same resource. Typically, the consequence is unfavourable to the weaker competitors. However, several factors moderate the severity of competition, and thus competitors might coexist.

Symbiosis

A symbiotic relationship between populations can be defined as long and close interactions that tend to maintain the coexistence of the engaged populations. This type of interaction takes multiple forms, for instance: mutualism occurs when all the involved populations benefit from the interactions; commensalism when one of the engaged population benefits from this relationship while the other population neither gained nor harmed; parasitism, is considered beneficial to one of the populations whereas the other population is harmed, and amensalism refers to one population being harmed or inhibited and the other remaining unaffected.

Predation

This type of interaction can be simply defined as a form of relationship between two populations in which one of them is the predator that captures and depends on the other population that serves as the prey.

The Effect of Interactions on The Involved Populations

As shown in (Table 1.3), these interactions may contribute positively or negatively to the ecosystem. Constant feedback and recovery mechanisms keep those populations

in check and under control to maintain the stability of the ecosystems. The effect and consequences of the previous interference can be summarised in the following table:

Type of Interaction	The effect of A to B	The effect of B to A
Competition	−	−
Mutualism	+	+
Commensalism	+	0
Amensalism	0	−
Predation and parasitism	+	−

Table 1.3: **Types of interactions between populations A and B.** (−) indicates a negative feedback, (+) a positive feedback and (0) no feedback.

1.3   Mathematical Background

Bacteria in nature generate different communities whose structure and function change dynamically in response to environmental variables [139]. As an adaptive system, bacterial species exhibit higher-order features that are not inherent to individual species but are the result of their interactions [24].

Mathematical models can aid in the comprehension of the fundamental principles underlying the dynamics and emergent characteristics of natural and synthetic bacterial communities. In addition, mathematical models provide crucial information for the evolution of these communities [91].

1.3.1   An Overview of Mathematical Models in Bacterial Growth and Competition

In this section, an overview of the mathematical tools that were used to simulate bacterial growth and competition is provided. In food safety research, mathematical models of microbial growth are the most widely used approach. Since these models have been thoroughly overviewed in [120, 159], and in [161], a brief overview of the most notable will suffice for this background. Mathematical models can be evaluated based on the following criteria:

- The number of parameters should be as few as possible to maximise consistency and, consequently, explanatory power.

- The more logical and comprehensible the parameters, the more mechanistic and explanatory power the model possesses.

- The more phases of microbial growth that are represented in a model, the more accurate it is.

Additionally, primary, secondary, and tertiary models have been frequently used to categorise mathematical models [159]. Primary models may be empirical or phenomenological in nature, or they can describe inactivation or survival, or they can be rate growth models. They are sometimes a combination of one or more of the models listed in the (Table 1.4), where a is the bacterial lower asymptote, μ_{max} is the maximum specific growth rate, λ is the lag time, Y_{max} is the bacterial upper asymptote, $e =$ exponent (2.718281828), t is the sampling time, S is the concentration of the limiting substrate S for growth, and K_s is the "half-velocity constant". As previously noted, the bacterial population cycle consists of distinct primary phases. Typically, changes in growth rate result in a sigmoidal curve with a lag phase immediately after $t = 0$, followed by an exponential phase, and then a stationary phase [177].

Model	Equation
Gompertz [68]	$y = a.\exp\left[-\exp(b - cx)\right]$
Modified Gompertz [138]	$y = A\exp\left\{-\exp\left[\dfrac{\mu_{max}e}{A}(\lambda - t) + 1\right]\right\}$
Logistic [227]	$y = \dfrac{a}{[1 + \exp(b - cx)]}$
Modified Logistic [228]	$y = \dfrac{A}{\left\{1 + \exp\left[\dfrac{4\mu_{max}}{A}(\lambda - t) + 2\right]\right\}}$
Three-phase linearised growth or Buchanan model [25, 92]	$Y = \begin{cases} A, & \text{if } X < \text{Lag}, \\ A + K(X - \lambda), & \text{if } \lambda \leq X \leq X_{max}, \\ Y_{max}, & \text{if } X \geq X_{max} \end{cases}$
Monod equation [111, 217]	$\mu = \mu_{max}\left(\dfrac{S}{S + K_s}\right)$

Table 1.4: **Models for microbial growth.**

Various mathematical functions, such as the Logistic [227], Gompertz [68], Buchanan three-phase [25], and more models, can be used to fit the sigmoidal curve. Most sigmoidal growth curve equations incorporate mathematical parameters $(a, b, c, ...)$ rather than biological parameters $(A, \mu_{max}, \text{and } \lambda)$. Parameters without biological meaning are hard to estimate. Thus, all growth models were modified to use $(A, \mu_{max}, \text{and } \lambda)$. This was done by constructing a formula for the biological parameters as a function of the

fundamental function parameters [227]. In contrast to the "classical growth models" [25, 68, 92, 138, 227, 228], the Monod model [111, 217] establishes the concept of a growth-controlling ("limiting") substrate.

In the next part of the overview, different approaches will be demonstrated to modelling microbial growth and competition (Table 1.5). The objective of this method is to make the presentation as accessible as possible. Thus, the level of mathematical complexity required to describe how the model's ecology arises from the mathematics is limited. There are consumers, microorganisms, plants, or animals that are part of a certain ecosystem, and resources in Tilman's model [203].

"The Tilman model" examines the general form of the equations for multiple species, $N_i(t)$ seeking multiple resources, $R_i(t)$, as well as the model's assumptions [203]. The general form of the model is given by the system of equations [195]:

$$\begin{cases} \dot{N_i}(t) = f_i(R_1, R_2, \ldots)N_i(t) - m_i N_i(t), \\ \dot{R_j}(t) = g_j(R_j) - \sum_i q_{ji}(R_1, R_2, \ldots)f_i(R_1, R_2, \ldots)N_i(t). \end{cases}$$

Here f_i is the relative growth rate of consumer N_i, m_i is the inherent net mortality rate of the consumer N_i, g_j is the growth rate of any given resource and q_{ji} is the rate for resource R_j consumed by N_i. Here $g_j(R_j) = a_j(s_j - R_j)$, it illustrates the constrained exponential growth of the resource density towards s_j in the absence of consumers.

Assumptions	System of Equations
A single species consuming a single resource	$\begin{cases} \dot{N_1}(t) = f_{N_1}(R_1(t))N_1(t) - m_{N_1}N_1(t), \\ \dot{R_1}(t) = a_{R_1}(s_{R_1} - R_1(t)) - q_{R_1 N_1}f_{N_1}(R_1(t))N_1(t) \end{cases}$
Two species seeking the same resource	$\begin{cases} \dot{N_1}(t) = f_{N_1}(R_1)N_1(t) - m_{N_1}N_1(t), \\ \dot{N_2}(t) = f_{N_2}(R_1)N_2(t) - m_{N_2}N_2(t), \\ \dot{R_1}(t) = a_{R_1}(s_{R_1} - R_1(t)) - q_{R_1 N_1}f_{N_1}(R_1(t))N_1(t) - \\ q_{R_1 N_2}f_{N_2}(R_1(t))N_2(t) \end{cases}$
A single species consuming two resources	$\begin{cases} \dot{N_1}(t) = f_{N_1}(R_1(t), R_2(t))N_1(t) - m_{N_1}N_1(t), \\ \dot{R_1}(t) = a_{R_1}(s_{R_1} - R_1(t)) - q_{R_1 N_1}f_{N_1}(R_1(t), R_2(t))N_1(t), \\ \dot{R_2}(t) = a_{R_2}(s_{R_2} - R_2(t)) - q_{R_2 N_1}f_{N_1}(R_2(t), R_1(t))N_1(t) \end{cases}$

Two species competing for two resources	$\begin{cases} \dot{N_1}(t) = f_{N_1}(R_2(t), R_1(t))N_1(t) - m_{N_1}N_1(t), \\ \dot{N_2}(t) = f_{N_2}(R_2(t), R_1(t))N_2(t) - m_{N_2}N_2(t), \\ \dot{R_1}(t) = a_{R_1}(s_{R_1} - R_1(t)) - q_{R_1 N_1}f_{N_1}(R_1(t), R_2(t))N_1(t) - \\ q_{R_1 N_2}f_{N_2}(R_1(t), R_2(t))N_2(t), \\ \dot{R_2}(t) = a_{R_2}(s_{R_2} - R_2(t)) - q_{R_2 N_1}f_{N_1}(R_1(t), R_2(t))N_1(t) - \\ q_{R_2 N_2}f_{N_2}(R_1(t), R_2(t))N_2(t) \end{cases}$

Table 1.5: **Different modifications of the Tilman model.**

All the mathematical models of bacterial growth in this literature were built on the simple premise that nutrient intake and cellular growth are directly linked. Growth is frequently considered to be proportional to nutrient availability, and the conversion process is assumed to be immediate [192]. More advanced approaches when modelling the competition between bacterial populations can be demonstrated when the growth-limiting resource is not in a form that microorganisms can directly consume and must first be converted into an intermediate product by cell-bound extracellular enzymes [192].

Mathematical modelling of toxin-mediated bacterial competition has exclusively focused on growth in chemostats, as established by Lenski and Hattingh in [118], who modelled the dynamics of two species competing for a single limiting resource in the presence of a substance that inhibits the growth of one species. Conditions that enable steady coexistence were described in their work, given that (i) the susceptible species is more successful in utilising the limited resources and (ii) the resistant species eliminates the inhibitor from the environment. However, if the resistant species does not clear the inhibitor from the environment or manufactures the inhibitor, coexistence is dynamically unstable.

In addition, the review presented in [91] provides a detailed introduction to inhibitory interactions, in terms of the internal and external sources of toxins and the effects of these substances (indirectly by polluting the incubating environment or directly by affecting the competitor). The survey shows that different mathematical methods are needed to solve biologically similar problems that at a later stage present similar qualitative aspects. Small modifications in the mathematical model involve significantly different methods. For example, in external inhibitor models, direct or indirect impacts offer the same phase descriptions, but the mathematical procedures required are completely different. The difference in behaviour between internal and external inhibitors, on the other hand, is significant. Moreover, according to this review, these issues can be considered as part of a larger category of interactions that might be classed as hostile. Another study defines this

as the use of energy, time, or other resources to diminish the fitness of other individuals [95]. The internal inhibitor models presented in [91] would fit within this category. They present an alternative model with lattice dynamics (similar to colonies in agar) that yields *Lotka-Volterra* type equations in the completely mixed situation. The study presented in [30], shows an alternative model based on cellular automata.

Even though the earliest work modelled toxin production using inhibitory paired reactions [118] (which is, in fact, traditional *Lotka-Volterra* competition), later studies [90] incorporated a new dependent variable reflecting toxin concentration. The study presented in [90] investigated a model of competition in a chemostat between two species for a single nutrient, one of which can generate a toxin against its opponent at the expense of its reproductive capacity.

Although limit cycles have been observed in the chemostat [226], and in a three-strain model involving interactions between a toxin producer and both resistant and susceptible competitors [152], the majority of the reviewed literature focuses on the existence and stability of constant solutions to ordinary differential equation models. It is worth noting that this particular work [152] established the first continuous, spatially homogenous model of the competitive interaction between inhibitory- producing, resistant, and sensitive bacteria.

Additional research has included the analysis of rare mutations [1] and the introduction of a detailed model that incorporates bacteria in different growth phases and the recycling of organic material from dead bacteria by Levin [119], although in this instance, the toxins were applied externally rather than being produced by the competitors.

1.3.2   Modelling The Dynamics of Single Population

The use of mathematical modelling in several biological fields developed significantly throughout the last century. Regarding the bacterial species, modelling has become an important tool to understand the details of their growth, transmission and many other aspects. In addition, studying the mechanisms of interaction between species, as well as predicting their strength and any other outcomes become possible by using mathematical models. This type of data has many applications, for example when studying the impacts of infectious diseases on populations [148].

Logistic Growth Model

Assume there is a population $N(t)$ at time t, the change of population over time takes the form:

$$\frac{dN}{dt} = [a - b] N, \implies N(t) = N(0) e^{(a-b)t},$$

where a and b are positive constants, and when $a > b$, the population proliferates ex-

ponentially. If the opposite case occurs, it decays. Eventually, an adjustment must be made to accommodate such exponential expansion. As proposed by Verhulst, [12], when a population becomes too large, a self-limiting process should exist. Thus:

$$\frac{dN}{dt} = r\,N\left(\frac{K-N}{K}\right),$$

where r is a positive parameter representing the growth rate, which means it has a similar shape of exponential when N is very small, at the beginning of a population trajectory, and levels off as N becomes large. By introducing the carrying capacity K the biological concept that simply represents the ceiling of the potential population density, so the intrinsic rate would be multiplied by $(K-N)/K$, [206, 204]. Non-dimensional form of the logistic equation is given as:

$$\dot{u} = u\,(1-u)\,. \tag{1.1}$$

This is obtained after the rescaling of the variables, namely, $u = N/K$ and $\tau = rt$. This equation has two steady states $u = 0$ and $u = 1$, which are unstable and stable respectively.

Solution of the equation (1.1) is given as:

$$u(t) = \frac{u_0 e^{rt}}{(1 - u_0 + u_0 e^{rt})}, \tag{1.2}$$

where $u_0 = u(t = 0)$ is the initial size of the population. As shown in figure (1.3, A), there is a negative association between the initial abundance: capacity ratio of a population's size and the time consumed to ultimately converge to the equilibrium point.
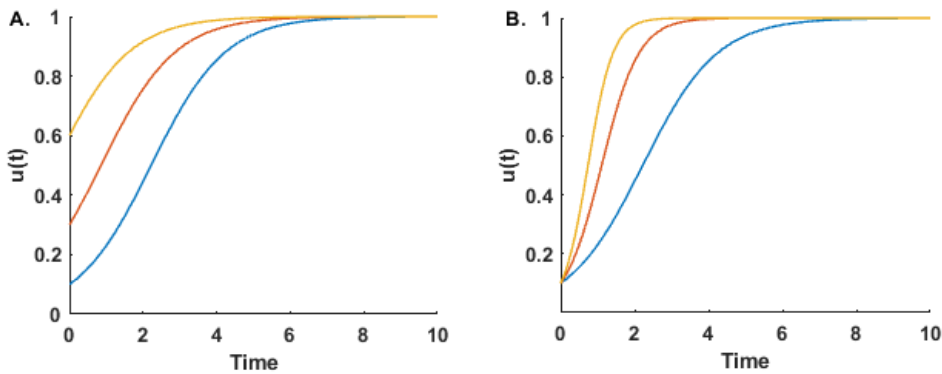
Figure 1.3: **Plots of solution (1.2).** Panel A: $r = 1$ and $u_0 = 0.1$ (blue), 0.3 (orange) and 0.6 (yellow). Panel B: $u_0 = 0.1$ and $r = 1$ (blue), $r = 2$ (orange) and $r = 3$ (yellow).

Meaning if we choose 0.1, as the initial size of population before iteration using the logistic equation; we can surmise that it would take more time to ultimately reach the equilibrium point than a starting size of 0.6 would, if we fixed the growth rate at $r = 1$.

By simplifying the equation (1.2), we get:

$$u(t) = \frac{1}{e^{-rt}\left(\dfrac{1}{u_0} - 1\right) + 1}.$$

Now, $e^{-rt} \to 0$ as $t \to \infty$, therefore $u \to 1$ as $t \to \infty$ for any u_0, showing how a population will always tend to its carrying capacity over time. Furthermore, as shown in figure (1.3, B), for a starting size of 10% capacity, and a growth rate of $r = 1$. As a result, its behaviour shows a very slight hesitation to enter its log phase after its initial lag phase, with its now diminished ability to increase in size, in contrast when using higher growth rates, $r = 2$ or $r = 3$. However, with higher growth rate it should take less time for the initial population size to enter its exponential growth phase and converge to the second equilibria.

Logistic Growth Model in Spatially Distributed System

Fisher equation is frequently used in heat and mass transfer, chemistry, biology and ecology [55]. In mathematics Fisher equation is also known as Kolmogorov Petrovsky-Piscounov equation or Fisher KPP equation. Fisher equation describes the process of interaction between diffusion and reaction [55, 108]. The classic simplest case of a non-linear reaction diffusion equation is:

$$u_t = D\,u_{xx} + r\,u\,(1 - u), \tag{1.3}$$

where r and D are positive parameters representing the growth rate and the diffusion coefficient respectively.

The diffusion term captures the macroscopic behaviour of numerous micro-particles in Brownian motion as a result of their random movements and interactions [194, 38]. Whereas the inhomogeneous term, the reaction term, is directly associated with the growth [148]. It was suggested by Fisher [107] as a deterministic version of a stochastic model for the spatial spread of a favoured gene in the context of population dynamics to describe the spatial spread of an advantageous allele and explore its travelling wave solutions [56].

Furthermore, Fisher equation considered as the natural extension of the logistic growth population model discussed in previously. When the population disperses through linear diffusion [54, 73]. By considering (1.3). It is convenient at the start, to rescale (1.3) by writing:

$$x^* = x\,\sqrt{\frac{r}{D}}\ ,\ \ t^* = r\,t.$$

By canceling the asterisks for notational simplicity, (1.3) becomes:

$$u_t = u_{xx} + u\,(1 - u). \tag{1.4}$$

In the spatially homogeneous situation the steady states are $u = 0$ and $u = 1$, which are unstable and stable respectively. This proposes to look for travelling wavefront solutions to (1.4) for which $0 \leq u \leq 1$; negative u has no physical meaning with what we have in mind for such models. If the travelling wave solution exists it can be written in this form:

$$u(x,t) = U(x - ct) = U(y), \text{where } y = x - ct,$$

where c is the wave speed. We assume $c \geq 0$ since (1.4) is invariant if $x \to -x$, c may be negative or positive.

$$\frac{\partial U}{\partial t} = -c\,U', \quad \frac{\partial U}{\partial x} = U', \quad \frac{\partial^2 U}{\partial x^2} = U''.$$

Substituting this travelling wave form into (1.4), $U(y)$ satisfies:

$$U'' + c\,U' + U\,(1 - U) = 0. \tag{1.5}$$

By studying (1.5) for U in the (U, V) phase plane where:

$$U' = V, \text{ so that, } V' = -c\,V - U\,(1 - U).$$

This system has two steady states for (U, V), that is, $(0, 0)$ and $(1, 0)$. To determine the stability of the steady states we need a linear stability analysis as following:

$$A = \begin{bmatrix} \dfrac{\partial U'}{\partial U} & \dfrac{\partial U'}{\partial V} \\ \dfrac{\partial V'}{\partial U} & \dfrac{\partial V'}{\partial V} \end{bmatrix},$$

$$A = \begin{bmatrix} 0 & 1 \\ -1 + 2\,U & -c \end{bmatrix}. \tag{1.6}$$

By implementing this point into the matrix (1.6), we obtain:

$$A_{(0,0)} = \begin{bmatrix} 0 & 1 \\ -1 & -c \end{bmatrix}.$$

Similarly for (1,0), we obtain;

$$A_{(1,0)} = \begin{bmatrix} 0 & 1 \\ 1 & -c \end{bmatrix}.$$

The eigenvalues λ for the singular points are;

$$(0,0): \lambda = \frac{-c \pm \sqrt{c^2 - 4}}{2}, \implies \begin{cases} \text{stable node,} & \text{if } c^2 \geq 4, \\ \text{stable spiral,} & \text{if } c^2 < 4, \end{cases}$$

24

$$(1,0): \lambda = \frac{-c \pm \sqrt{c^2 + 4}}{2}, \implies \text{saddle point.}$$

From this analysis as shown in Fig (1.4), we conclude that if $c \geq c_{min} = 2$, the origin is a stable node, Fig (1.4a). If $c^2 < 4$ then the origin is a stable spiral, this means U oscillates around this point. Although travelling wave solutions exist where $c < 2$, they are not considered as real solutions since $U < 0$ indicates a negative population, which is physically unrealistic. This is shown with the spiralling of the trajectories around the origin as illustrated in Fig (1.4b), meaning they enter the negative quadrants at certain points. From continuity point of view, there is a trajectory from $(1,0)$ to $(0,0)$ located entirely in the quadrant $U \geqslant 0, U' \leqslant 0$ with $0 \leqslant U \leqslant 1$ for all wavespeeds $c \geqslant c_{min} = 2$. Hence, for a real travelling wave solution to exist, all wave speeds must satisfy $c \geq c_{min} = 2$. For our initial dimensional equation (1.3), all wave speeds must satisfy:

$$c \geq c_{min} = 2\sqrt{rD}.$$

In both cases the steady state $(1,0)$ is a saddle point. On the other hand, the resultant wave speed is also defined by the shape of the wave profiles [148].

(a)   (b)
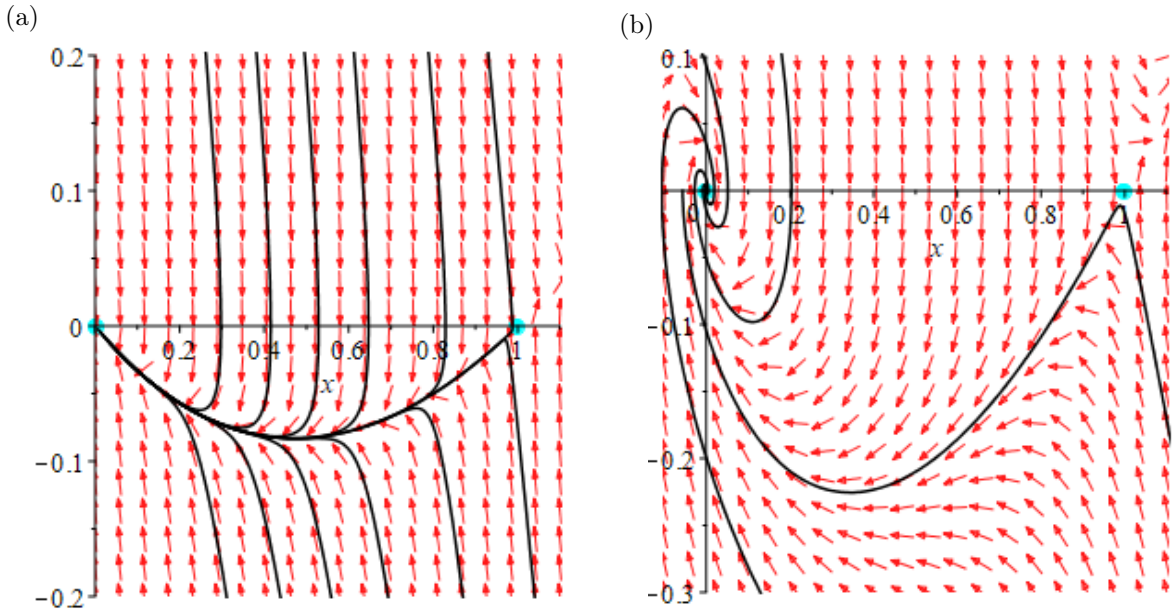
Figure 1.4: **Phase portrait for the system (1.5).** Direction field is shown by red arrows and sample phase trajectories in black curves. Panel (a): when $c \geqslant c_{min} = 2$, the steady state $(0,0)$ is a stable node. Panel (b): when $c^2 < 4$, the steady state $(0,0)$ is a stable spiral. Model parameters: panel (a), c=3, panel (b), c=1. Produced using Maple codes.

For example, if the wave profile has the form $e^{-\alpha y}$, the change in α leads to change the shape of the profile and consequently affects the wave speed. In this situation, the wave speed will decay instead of being given by a step function. The wave speed can be any

value, as long as it is higher than the minimum condition. The shape of the wave profile can also be affected by changing the initial conditions of the system.

1.3.3 Modelling The Dynamics of Interacting Populations in Spatially Homogeneous Systems

The general model for two interacting populations can be described as:

$$\begin{cases} \dot{N}_1 = f(N_1, N_2), \\ \dot{N}_2 = g(N_1, N_2). \end{cases}$$

The two functions, N_1 and N_2, describe the evolution of each population over time. The partial derivatives of this system quantify the effects of each species [9, 21, 180, 200]; $\frac{\partial f}{\partial N_1}$ and $\frac{\partial g}{\partial N_2}$ represent the self-replicating effect of species N_1 and N_2, respectively. $\frac{\partial f}{\partial N_2}$ and $\frac{\partial g}{\partial N_1}$ represent the effect of species N_2 on species N_1, and N_1 on N_2 respectively. The partial derivatives $\frac{\partial f}{\partial N_2}$ and $\frac{\partial g}{\partial N_1}$ determine the type of interaction, as following:

(i) $\frac{\partial f}{\partial N_2} > 0$, $\frac{\partial g}{\partial N_1} < 0$, represents N_1 population preying on N_2 population.

(ii) $\frac{\partial f}{\partial N_2} < 0$, $\frac{\partial g}{\partial N_1} > 0$, represents N_2 population preying on N_1 population.

(iii) $\frac{\partial f}{\partial N_2} < 0$, $\frac{\partial g}{\partial N_1} < 0$, indicates competition between the species N_1 and N_2.

(iv) $\frac{\partial f}{\partial N_2} > 0$, $\frac{\partial g}{\partial N_1} > 0$, demonstrates a mutually beneficial relationship between the interacting species, i.e., (a symbiotic system).

To further investigate the two species system, the stationary points that exist can be calculated as solutions to:

$$\begin{cases} \dot{N}_1 = f(N_1, N_2) = 0, \\ \dot{N}_2 = g(N_1, N_2) = 0. \end{cases}$$

To calculate the exact values of N_1 and N_2 at which the system is at equilibrium, simultaneous equations are used. Having solved to find all stationary points within the system, the stability of each point can be evaluated using the system's Jacobian matrix, which is the matrix of all first order partial derivatives of a function [9, 21]:

$$J = \begin{bmatrix} \dfrac{\partial f}{\partial N_1} & \dfrac{\partial f}{\partial N_2} \\ \dfrac{\partial g}{\partial N_1} & \dfrac{\partial g}{\partial N_2} \end{bmatrix}.$$

26

To determine the stability of the obtained equilibrium points, the values of N_1 and N_2 at each point should be implanted into the Jacobian. The eigenvalues of this matrix can be calculated by using its characteristic equation, defined as:

$$det(J - \lambda I) = 0.$$

The real parts of the obtained values of λ_1, λ_2 determine the stability of each point. The specific stability behaviour influenced by the existence of real and imaginary components of the eigenvalues, together with the signs of the real components and the distinctness of their values [9, 21, 180, 200].

Lotka-Volterra Predator-Prey Model

Since Volterra [207] introduced and proposed his model for the predation of one species by another to explain and show how the populations of species could permanently oscillate, Fig (1.5B), such approach and methodology made the scientists eager to know and investigate the dynamic models of interacting populations. Given the fact that the dynamics of the involved population were affected by the interaction of species, this curiosity has stimulated the development of modelling approaches to analyse such effects. As mentioned previously, in a simple community within two-species systems there exists mainly three types of interaction: Predator-Prey condition, shown in Fig (1.5), which causes the decline of one population's growth rate, at the same time as increasing the rate of the other population [11]; competition, the interaction which affects both population's respective growth rates and symbiosis. The consequence of the symbiotic type of interaction is the improvement of both population's growth rates [208, 104]. Volterra proposed his simple Predator-Prey model which defines the predation of one species by another [11].

Assuming $N(t)$ represents the populations of prey and $P(t)$ predators at time t, then Volterra's model is:

$$\begin{cases} \dot{N} = N(a - bP), \\ \dot{P} = P(cN - d), \end{cases} \tag{1.7}$$

where a, b, c and d are positive constants. The term aN represents the growth rate of the prey, which means with the absence of the predator the prey species would grow exponentially. However, the growth rate of the predator species cNP is associated with the presence of the prey, which means the absence of the prey species will cause a decline in the predator populations, denoted by the $-dP$ term. Finally, the term $-bP$ represents the effect of the predator species on the prey population. To find the stationary point of

this system (1.7), these equations must be solved in the following form:

$$\begin{cases} N(a - bP) = 0, & \text{if } N = 0, \text{ or } P = \dfrac{a}{b}, \\[2mm] P(cN - d) = 0, & \text{if } P = 0, \text{ or } N = \dfrac{d}{c}. \end{cases}$$

Hence, two steady states $(N, P) = (0, 0)$; and $(N, P) = (d/c, a/b)$ are obtained. To determine the stability of the steady states the Jacobian of communities are necessary:

$$J = \begin{bmatrix} a - bP & -bN \\ cP & cN - d \end{bmatrix}.$$

The steady state $(N, P) = (0, 0)$ has eigenvalues of $\lambda_1 = a$ and $\lambda_2 = -d$, indicating that it is unstable. The Jacobian in the second steady state, $(N, P) = (d/c, a/b)$, has the imaginary eigenvalues $\lambda_{1,2} = \pm i \sqrt{ad}$. Since both values are complex, and the real parts equal to zero, $(d/c, a/b)$ can be determined as seen in Fig (1.5A), as centre point. The phase trajectory equation for this point is calculated through solutions to $\frac{dP}{dN}$. This is:

$$\frac{dP}{dN} = \frac{P(cN - d)}{N(a - bP)}.$$

Integration of this equation (through the use of separation of variables) gives:

$$\ln |P^a N^d| - bP - cN = \text{constant}.$$

Lotka-Volterra Competition Model

Here the aim is to model the interactions between two species. Therefore, the first step is to define this interaction.

> **Inter-Specific Competition**, in ecology, is a type of interaction in which individuals of different species compete for the same limited resources in an ecosystem (e.g. food or living space) [4].

By considering the competition for the same limited resources, i.e., territory or food, between two or more species, which might lead to inhibit each other's growth, a general principle is observed to hold in nature: specifically, when two species compete for the same limited resources the results or the outcomes of such process cause one of the competing species to become extinct. This principle is demonstrated by *Lotka-Volterra* competition model. Here a simple competition model is presented by taking into account the basic 2-species *Lotka-Volterra* competition model, N_1 and N_2, with each population having logistic growth in the absence of the other [147, 225]. Realistic approaches were
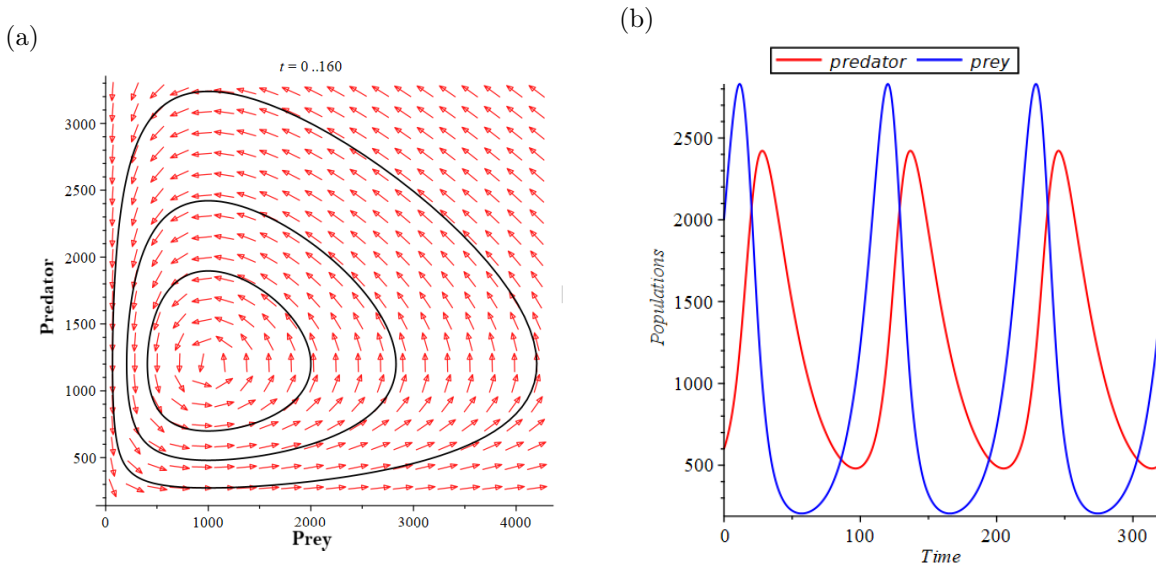
Figure 1.5: **Dynamics in *Lotka-Volterra* Predator–Prey model** (1.7). Panel (a): vector field (red arrows) and phase plane trajectories (black loops) for the system (1.7). Trajectories are shown for $N_0 = 2000$ and $P_0 = 600, 1200, 3000$ (smallest to largest). Panel (b): shows the change in each population of species N (prey, blue) and P (predator, red) over time for $N_0 = 2000, P_0 = 600$. Model parameters: $a = 0.1, b = 8 \times 10^{-5}, c = 4 \times 10^{-5}, d = 0.04$.

the reasons behind adding and including the logistic growth into the *Lotka-Volterra* systems. To highlight the principle, the straightforward model which yet reflects many of the properties of more complicated models is considered, particularly regarding stability [148, 153]. Thus, the following is considered:

$$\begin{cases} \dfrac{dN_1}{dt} = r_1 N_1 \left(1 - \dfrac{N_1}{K_1} - a_1 \dfrac{N_2}{K_1} \right), \\ \dfrac{dN_2}{dt} = r_2 N_2 \left(1 - \dfrac{N_2}{K_2} - a_2 \dfrac{N_1}{K_2} \right), \end{cases} \tag{1.8}$$

where r_1, r_2, K_1, K_2, a_1, and a_2 are all positive constants, the r stands for the linear birth rate and the K represent the carrying capacity for each species. The a_1 and a_2 are defined as the competition coefficients which measure the competitive effect of N_2 on N_1 and N_1 on N_2 respectively. The competitive effect of each species is defined as the number of individuals of one population that are equivalent to one individual of the other species, in terms of their use of resource. They are generally not equal [179, 5, 45, 148]. If $a_1 = a_2 = 0$, the species are said to be independent of one another, since this indicates that there is no interspecific competition.

To analytically study this model (1.8), this system needs to be non-dimensionalised. Non-dimensionalisation refers to removing the physical dimensions of an equation and replacing them with appropriate variables, to parameterize the problem by making the system without unit [148]. One of the advantages of non-dimensionalisation is scaling the quantities to compare outcomes with greater simplicity, relative to an appropriate unit.

For example, since the values N and K are physical quantities concerning the population size, using a substitution which divides N by K restricts the potential and possible values of our new variables to between 0 and 1, with 1 representing the carrying capacity of the population. Also reducing the number of parameters involved is an advantage of the non-dimensionalisation method [148]. Again, this creates a simpler basis for comparison of the results. The system is non-dimensionalised using the following substitutions:

$$u = \frac{N_1}{K_1}, \quad v = \frac{N_2}{K_2}, \quad \tau = r_1 t, \ \rightarrow \ \frac{d}{dt} = \frac{d\tau}{dt}\frac{d}{d\tau} = r_1 \frac{d}{d\tau}. \tag{1.9}$$

The u and v terms eliminate the population dimension from the system, which means that the value of u and v are restricted between 0 and 1. Hence, comparing the relative populations in proportion to their maximum capacity is made easier. Since the system is also dependent on time, τ is used to non-dimensionalise the time parameter by equating the right hand side to the same time dependency.

The equations (1.8) after the substitutions (1.9) transform into:

$$\begin{cases} \dot{u} = u\,(1 - u - b_1\,v) = f_1(u,v), \\ \dot{v} = r\,v\,(1 - v - b_2\,u) = f_2(u,v), \end{cases} \tag{1.10}$$

where $b_1 = a_1 * K_2/K_1$, $b_2 = a_2 * K_1/K_2$ and $r = r_2/r_1$. By setting $f_1(u,v) = f_2(u,v) = 0$, the steady states and the phase plane singularities, u^*, v^* are obtained, which from (1.10) are:

$$(u^*, v^*) = (0,0),\ (1,0),\ (0,1),\ \left(\frac{1 - b_1}{1 - b_1\,b_2}, \frac{1 - b_2}{1 - b_1\,b_2}\right), \tag{1.11}$$

where u^* and v^* represent the solutions to equations (1.10). The solution involving b_1, b_2 represents an equilibrium in which coexistence of species is possible, but is only stable for values of $b_1, b_2 < 1$, any other case is irrelevant. However, the last equilibrium point is only considered if $u^* \geq 0$ and $v^* \geq 0$ are finite, in which case $b_1 . b_2 \neq 1$. To determine the stability of the steady states the Jacobian of communities is needed:

$$A_{(u^*,v^*)} = \begin{bmatrix} 1 - 2\,u - b_1 v & -b_1 u \\ -r\,b_2 v & r\,(1 - 2\,v - b_2 u) \end{bmatrix}. \tag{1.12}$$

The first steady state in (1.11), which is $(0,0)$, is unstable. By implementing this point into the matrix (1.12), the following is obtained:

$$A_{(0,0)} = \begin{bmatrix} 1 & 0 \\ 0 & r \end{bmatrix}.$$

The eigenvalues $\lambda_1 = 1$, $\lambda_2 = r$, are positive. For the second equilibrium point from (1.11), $(1,0)$, the matrix (1.12) gives:

$$A_{(1,0)} = \begin{bmatrix} -1 & -b_1 \\ 0 & r\,(1 - b_2) \end{bmatrix}.$$

The eigenvalues: $\lambda_1 = -1$, $\lambda_2 = r\,(1 - b_2)$, hence:

$$(u^*, v^*) = (1,0), \quad \text{is} \quad \begin{cases} \text{stable,} & \text{if} \quad b_2 > 1, \\ \text{unstable,} & \text{if} \quad b_2 < 1. \end{cases} \tag{1.13}$$

Similarly for the third equilibrium point, $(0,1)$, the eigenvalues are $\lambda_1 = -r$, $\lambda_2 = 1 - b_1$ and so:

$$(u^*, v^*) = (0,1), \quad \text{is} \quad \begin{cases} \text{stable,} & \text{if} \quad b_1 > 1, \\ \text{unstable,} & \text{if} \quad b_1 < 1. \end{cases} \tag{1.14}$$

Finally for the last equilibrium point from (1.11), if it exists in the positive quadrant, the matrix (1.12) takes this form:

$$A = \frac{1}{1 - b_1 b_2} \begin{bmatrix} b_1 - 1 & b_1\,(b_1 - 1) \\ r\,b_2\,(b_2 - 1) & r\,(b_2 - 1) \end{bmatrix},$$

which has the eigenvalues:

$$\lambda_{1,2} = \frac{(b_1 - 1) + r(b_2 - 1) \pm \sqrt{[(b_1 - 1) + r(b_2 - 1)]^2 - 4r(1 - b_1 b_2)(b_1 - 1)(b_2 - 1)}}{2(1 - b_1 b_2)}. \tag{1.15}$$

This equilibrium point is stable for all $b_1 < 1$ and $b_2 < 1$, as such values would produce two negative eigenvalues. To verify this, each part of the equation will be looked at individually. $(1 - b_1 b_2)$ is always positive for $b_1, b_2 < 1$, since b_1 multiplied by b_2 is smaller than one. Hence, the denominator $2(1 - b_1 b_2)$ is always positive, meaning the numerator must be always negative to generate two negative eigenvalues. Since $(b_1 - 1)$ and $(b_2 - 1)$ will be negative, it follows that their sum will also be negative. For reference, we will use:

$$(b_1 - 1) + r(b_2 - 1) = \alpha.$$

By considering the terms under the square root, the first term $[(b_1 - 1) + r(b_2 - 1)]^2 = \alpha^2$ and is always positive since it involves squaring a negative value. For the added term we will use:

$$4r(1 - b_1 b_2)(b_1 - 1)(b_2 - 1) = \beta,$$

which will be always positive as a result of the product of multiplying the two negative terms $(b_1 - 1), (b_2 - 1)$, meaning the positive value β is subtracted from another positive value α^2. Now there are two cases:

$$\alpha^2 > \beta,$$

$$\alpha^2 < \beta.$$

The first case, the value of $\alpha^2 - \beta$, where $\alpha^2 > \beta$, means the resultant value will be less than $|\alpha|$, hence, any case in which it is added or subtracted from our first negative term α, the result will be negative. This means there is always a positive denominator, with an always negative numerator, resulting in two always negative eigenvalues. For the other case where $\alpha^2 < \beta$, $\alpha^2 - \beta < 0$, the resultant square root will be imaginary. Thus, we have the negative real value $\alpha \pm$ the imaginary result in the numerator. Joining this with the positive denominator means the real part of both resultant eigenvalues is negative, with the stability being defined by the real parts of the values. As the resultant eigenvalues are always negative. Hence, for any values $b_1, b_2 < 1$ the equilibrium is stable, either node or spiral.

As mentioned previously, the stability of this point depends on the values of b_1 and b_2. There are several cases to take into consideration, all of which have ecological implications.

The different cases are:

(i) $b_1 < 1$, $b_2 < 1$. There is a stable steady state where both competing populations can exist as in Fig (1.6a). In terms of the original parameters in (1.8) this corresponds to $a_1 \frac{K_2}{K_1} < 1$ and $a_2 \frac{K_1}{K_2} < 1$. So, assume $K_1 \approx K_2$ than the interspecific competition which is determined by the values of a_1 and a_2 is not too strong. On the other hand, if their capacities are different and their competition coefficients are approximately the same, it is not easy to determine the implications of this case until the dimensionless groupings b_1 and b_2 are formed and compared.

(ii) $b_1 > 1$, $b_2 > 1$. n this case, assume that both populations have an approximate carrying capacity, hence, a_1, a_2 are not small. According to the analysis of the model all three non-trivial equilibriums can exist. However, from equations $(1.13) \rightarrow (1.15)$ only $(1, 0)$ and $(0, 1)$ are stable points as shown in Fig (1.6b). Mainly it depends on the starting of each species. If the initial conditions lie in domain (1), then $u \to 1, v \to 0$, and it is the other way around if the initial conditions lie in the domain (2). Furthermore, the extinction of one species is predicted even if the initial conditions lie on the separatrix because the present of random fluctuations will drive one of the competing populations to tend to zero.

(iii) $b_1 < 1$, $b_2 > 1$. As shown in Fig (1.6c), also from (1.13), the stronger competition of u dominates and the other species v dies out or eventually becomes extinct.
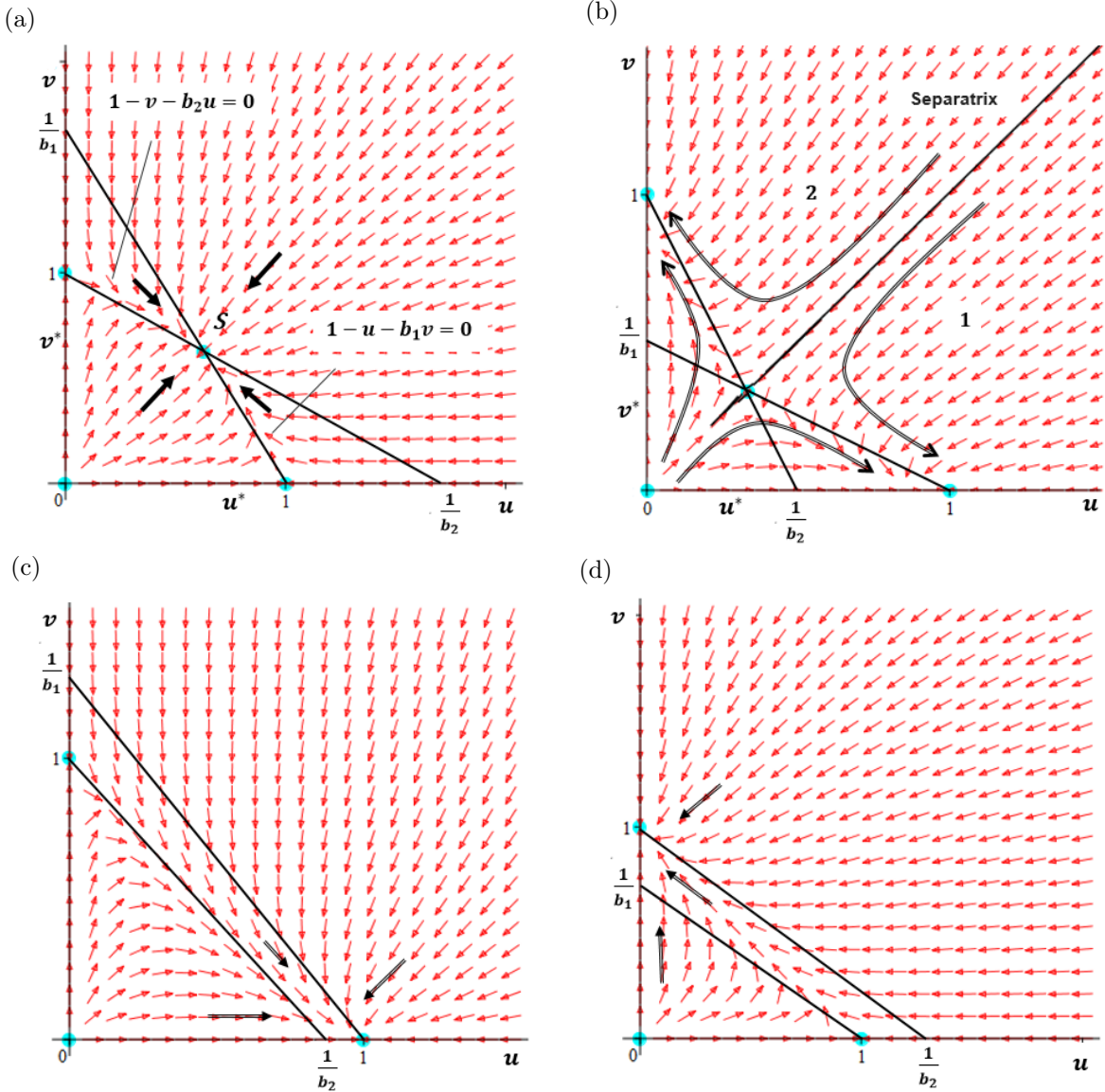
Figure 1.6: **Phase portraits for four dynamical regimes in the system** (1.10)**.** Direction fields are shown by red arrows, null-clines - by (straight) black lines and phase trajectories - by arrowed black lines. Panel (a): $b_1 = b_2 = 0.5$. Panel (b): $b_1 = b_2 = 1.1$. Panel (c): $b_1 = 0.9$, $b_2 = 1.1$. Panel (d): $b_1 = 1.1$, $b_2 = 0.9$. $r = 1$ in all panels. Produced using Maple codes.

(iv) $b_1 > 1$, $b_2 < 1$. Here it is the other way round from (1.14), the stronger competition of v dominates and drives the other species u to extinction, as illustrated in Fig (1.6d).

Note that the cases (iii) and (iv) always result in species elimination and in case (ii) it is certainly due to natural fluctuations of populations. Hence, conditions for competitive exclusions can be determined as shown in Fig (1.6).

The case in which $b_1 = b_2 = 1$ is a special case. With the usual stochastic, naturally-randomly determined variability, it is unlikely in the real world to hold exactly. Therefore, even in this case a competitive exclusion of one or the other competing populations also occurs [148].

1.3.4 Modelling The Dynamics of Interacting Populations in Spatially Distributed Systems

As indicated previously, the evolution of spatially homogeneous populations may be modelled by ordinary differential equations, for instance, by the logistic-growth model. The interaction of competing populations can be described by a system of coupled equations, one of which is the famous *Lotka-Volterra* model [104, 225], introduced in the previous section. In a spatially heterogeneous setting, the population number varies in space and may diffuse in the environment. This gives the class of reaction-diffusion equations and their systems.

Turing found that the stationary solution to a diffusion system may become unstable even if the steady state of the corresponding system without diffusion is stable [148]. Thus, the stability analysis is much more involved than in the spatially homogeneous case. Roughly speaking, in the long-time limit, one may have extinction or coexistence of the species. After introducing the analytic study of the *Lotka-Volterra* competition system in homogenous situation, the aim in this section is to expand the analytic study to include the *Lotka-Volterra* competition system in inhomogeneous situation by introducing the diffusive terms of the respective species, N_1 and N_2. This creates the system:

$$\begin{cases} \dfrac{\partial N_1}{\partial t} = D_1 \dfrac{\partial^2 N_1}{\partial x^2} + r_1 N_1 \left(1 - \dfrac{N_1}{K_1} - a_1 \dfrac{N_2}{K_1} \right), \\ \dfrac{\partial N_2}{\partial t} = D_2 \dfrac{\partial^2 N_2}{\partial x^2} + r_2 N_2 \left(1 - \dfrac{N_2}{K_2} - a_2 \dfrac{N_1}{K_2} \right), \end{cases} \tag{1.16}$$

where D_1, D_2, r_1, r_2, K_1, K_2, a_1 and a_2 are all positive constants. In the population N_1, the term D_1 represents the diffusion coefficient, r_1 the linear birth rate, K_1 term represents the maximum carrying capacity of the population. The a_1 term measures the competitive effect of N_2 on N_1, the same description of the parameters applies to the other population. The system (1.16) will be non-dimensionalised, by defining the dimensionless dependent variables:

$$u = \frac{N_1}{K_1}, \quad v = \frac{N_2}{K_2}, \tag{1.17}$$

dimensionless space and time

$$x^* = x \sqrt{\frac{r_1}{D_1}} \ , \ t^* = r_1 t. \tag{1.18}$$

This system is now dimensionless. However, the number of parameters is further reduced

if:

$$D = \frac{D_2}{D_1}, \quad r = \frac{r_2}{r_1}, \quad b_1 = a_1 \frac{K_2}{K_1}, \quad b_2 = a_2 \frac{K_1}{K_2}. \tag{1.19}$$

By inserting the values from (1.17),(1.18) and (1.19) into the equations in (1.16), this means the following dimensionless system has been created:

$$\begin{cases} u_t = u_{xx} + u\left(1 - u - b_1\,v\right), \\ v_t = D\,v_{xx} + r\,v\left(1 - v - b_2\,u\right). \end{cases} \tag{1.20}$$

The values of b_1 and b_2 indicate the nature of the competition. For $b_1, b_2 < 1$, the competition is described as weak. For either $b_1 < 1, b_2 > 1$, or other way around, there is weak strong competition between the species. Finally, for $b_1, b_2 > 1$, strong competition occurs. The system (1.20) will have an infinite number of solutions. To obtain a unique solution, initial conditions and boundary conditions must be defined. The initial conditions will be given and be subject to change during the numerical calculations. However, the boundary conditions remain constant. Neumann boundary conditions are imposed, meaning the normal derivatives of each dependent variable are specified at the boundary. To achieve this type of boundary condition, the points U_1 and U_n are introduced next to the boundary. In the MATLAB code, $U_1 = U_2$, and $U_n = U_{n-1}$ is defined so that the boundaries U_1, and U_n, are never affected. Hence, the boundary conditions can also be described as zero flux, since the gradients between the points U_1 and U_2, as well as between U_n and U_{n-1}, are zero.

Propagating Wave Solutions for A Competitive Reaction-Diffusion Model

If the travelling wave solution exists it can be written in this form:

$$u(x,t) = U(x + ct),$$

where c is the wave speed. Substituting this travelling waveform into (1.20), yields:

$$\begin{cases} cU' = U'' + U\left(1 - U - b_1\,V\right), \\ cV' = D\,V'' + r\,V\left(1 - V - b_2\,U\right). \end{cases} \tag{1.21}$$

To determine the wavefront solution, this system (1.21) must be transformed into the system of four first order ODEs:

$$\begin{cases} U' = W, \\ W' = cW - U\left(1 - U - b_1\,V\right), \\ V' = Z, \\ Z' = \frac{1}{D}\left(cZ - r\,V\left(1 - V - b_2\,U\right)\right). \end{cases} \tag{1.22}$$

By setting $U' = W' = V' = Z' = 0$, the steady states are obtained which from (1.22) are:

$$(U^*, W^*, V^*, Z^*) = (0,0,0,0), \ (1,0,0,0), \ (0,0,1,0), \ \left(\frac{1-b_1}{1-b_1b_2}, 0, \frac{1-b_2}{1-b_1b_2}, 0 \right).$$

To determine the stability of the equilibrium points the Jacobian of the communities is needed:

$$J_{[U^*,W^*,V^*,Z^*]} = \begin{bmatrix} 0 & 1 & 0 & 0 \\ -1 + 2U + b_1V & c & b_1U & 0 \\ 0 & 0 & 0 & 1 \\ \dfrac{rb_2V}{D} & 0 & \dfrac{-r + 2rV + rb_2U}{D} & \dfrac{c}{D} \end{bmatrix}.$$

These steady states are in fact extensions of the four steady states in the spatially homogeneous case, with zeroes for the variables W and Z. Here, as there is only interest in the points $(0,0)$, $(1,0)$ and $(0,1)$, it was decided to neglect the coexistence equilibrium point because it is not constrained by obvious parameters, along with the eigenvalues for this state being simply too long to be included.

For travelling wavefront solutions to exist, for each point imaginary eigenvalues should be prevented [148]. In other words, all eigenvalues for each point must be real. Therefore, it is necessary to find the minimum value of c that satisfies this condition, in turn providing minimum wave speed requirements for each equilibrium point.

For the equilibrium point $(0, 0)$, we have four eigenvalues, $\lambda_{1,2} = \dfrac{c \pm \sqrt{c^2 - 4}}{2}$, and $\lambda_{3,4} = \dfrac{c \pm \sqrt{c^2 - 4Dr}}{2D}$. For $\dfrac{c \pm \sqrt{c^2 - 4}}{2}$, we require $c > c_{min} = 2$, with $c < 2$ indicating a spiral node. Similarly, for $\dfrac{c \pm \sqrt{c^2 - 4Dr}}{2D}$, we require $c > c_{min} = 2\sqrt{Dr}$.

As these wave speed requirements rely on the eigenvalues for the state $(0,0)$, any travelling wavefront solutions that can be found will involve transitions from this state. On the other hand, it can be noted that there is an inconsistency between the two wave speed requirements since they are only equal if $Dr = 1$. This discrepancy will be explored by finding the eigenvector corresponding to each eigenvalue. It is know that:

$$(J - \lambda I)\, e = 0.$$

Thus, for $\lambda_{1,2,3,4}$ the corresponding eigenvectors are:

$$e_1 = \begin{bmatrix} \frac{2}{c+\sqrt{c^2-4}} \\ 1 \\ 0 \\ 0 \end{bmatrix}, e_2 = \begin{bmatrix} \frac{2}{c-\sqrt{c^2-4}} \\ 1 \\ 0 \\ 0 \end{bmatrix}, e_3 = \begin{bmatrix} 0 \\ 0 \\ \frac{2D}{c+\sqrt{c^2-4Dr}} \\ 1 \end{bmatrix}, e_4 = \begin{bmatrix} 0 \\ 0 \\ \frac{2D}{c-\sqrt{c^2-4Dr}} \\ 1 \end{bmatrix}.$$

Through the observation of the obtained eigenvectors it can be concluded that, the wave speed requirement $c_{min} > 2$ applies only to the wavefronts for species U, while $c_{min} > 2\sqrt{Dr}$ applies to wavefronts for species V.

Similar analysis shows that for the equilibrium point $(1,0)$, $c > c_{min} = 2\sqrt{Dr(1-b_2)}$ is required. This wave speed requirement results from the eigenvalues relating to the state $(1,0)$, meaning any numerical simulations involving transitions from this point will stick to this wave speed minimum. Unlike the state $(0,0)$, this wave speed requirement can correspond to wave profiles of both species.

Finally, for the equilibrium point $(0,1)$, $c > c_{min} = 2\sqrt{1-b_1}$ is required. Any numerical results involving transitions from the state $(0,1)$ must follow this wave speed requirement. Again, this wave speed requirement can apply to wavefronts for both species.

1.4 Numerical Integration of Differential Equations

Most of the PDEs cannot be solved analytically. The separation of variables method works only for some simple cases, to be specific, usually not for inhomogeneous and non-linear PDEs. Numerical methods require that the PDE become discretised on a grid. Finite difference methods are often used in science, replacing differential equations with difference equations.

1.4.1 Finite Difference Approximations of Derivatives

The finite difference is basically a numerical method for approximating a derivative [94, 135, 140]. In a numerical study, finite-difference methods (FDM) are a class of numerical methods for solving differential equations by approximating derivatives with finite differences [140]. Both the spatial domain and time interval are discretised, or divided into a finite number of steps, and the value of the solution at these discrete points is approximated by solving algebraic equations containing finite differences and values from nearby points. Here the aim is to use finite difference method by the Taylor series expansion. In the classification of partial differential equations, particularly in

heat transfer and fluid mechanics problems, there appears first and second derivatives of dependent variables. Such differential of the dependent variables must be expressed as an approximate expression so that computer programs such MATLAB and others can be employed to obtain a solution [94, 135, 140]. By considering the continuous function $u(x)$ the aim is to find the first and the second derivatives using this method. To apply such a method, discrete points or grids are needed, i.e., it is necessary to divide the domain into uniform discrete points. Generally, in one-dimensional these points are represented by index i in the $x-$direction, and the index j in $y-$direction will be used in a two-dimensional domain.

By using Taylor series expansion:

$$u(x + \Delta x) = u(x) + \sum_{n=1}^{\infty} \frac{(\Delta x)^n}{n!} \frac{\partial^n u}{\partial x^n},$$

$$u(x + \Delta x) = u(x) + \Delta x \, u'(x) + \frac{\Delta x^2}{2!} u''(x) + \frac{\Delta x^3}{3!} u'''(x) + ... + R, \qquad (1.23)$$

$$u'(x) = \frac{u(x + \Delta x) - u(x)}{\Delta x} - \boxed{\frac{\Delta x}{2!} u''(x) - \frac{\Delta x^2}{3!} u'''(x) - ... - R,}$$

where the boxed terms are known as, TE, the the truncation error. TE means the difference between the partial derivatives and the finite difference approximation. Note that the error of this approximation is termed as $O(\Delta x)$, and knowing that $\Delta x \gg \Delta x^2 \gg \Delta x^3$. Hence, the first term of the truncation error known as the leading term will contribute maximum error.

Rewriting the approximation in terms of i index:

$$u'(x) = \frac{u_{i+1} - u_i}{\Delta x} + O(\Delta x) \implies \text{Forward difference approximation}$$

Similarly for $u(x - \Delta x)$:

$$u(x - \Delta x) = u(x) - \Delta x \, u'(x) + \frac{\Delta x^2}{2!} u''(x) - \frac{\Delta x^3}{3!} u'''(x) + ... + R. \qquad (1.24)$$

Alternative schemes, central and backward:

$$\text{Central:} \quad u'(x) \simeq \frac{u(x + \Delta x) - u(x - \Delta x)}{2 \, \Delta x}.$$

$$\text{Backward:} \quad u'(x) \simeq \frac{u(x) - u(x - \Delta x)}{\Delta x}.$$

Now the use of Taylor expansion will be extended to find the second derivatives approximation. Adding the equations (1.23) and (1.24), gives:

$$u''(x) = \frac{u(x + \Delta x) - 2\,u(x) + u(x - \Delta x)}{\Delta x^2} + O(\Delta x)^2. \qquad (1.25)$$

The expression in (1.25) represents the central difference approximation of the second derivatives.

1.4.2 Numerical Integration of Parabolic PDEs

Numerical solution schemes are frequently referred to as being explicit or implicit. The computation is known to be explicit when a direct computation of the dependent variables can be made in terms of known quantities [94, 137, 140].

In contrast, when the dependent variables are defined by coupled sets of equations, and either a matrix or iterative technique is required to obtain the solution, the numerical method in this case is implicit. Under certain conditions, implicitly formulated equations are almost always solved using iterative techniques, for instance, if the governing equations of the dynamics are non-linear and the number of unknown variables is very large. Iterations are used to introduce a solution through a sequence of steps from a starting state to a final, converged state. This is true whether the required solution is either one step or a final steady-state result. In either case, the iteration steps are similar to a time-like process. Obviously, the iteration steps usually do not correspond to a realistic time- dependent behaviour. In fact, it is this aspect of an implicit method that makes it attractive for steady-state computations, as the number of iterations required for a solution is often much smaller than the number of time steps required for an accurate transient that asymptotically approaches steady conditions.

The consequences of using an implicit versus an explicit solution method for a time-dependent problem have two aspects. One aspect has to do with numerical stability and the other with numerical accuracy [94, 135, 140]. The main reason for using implicit solution approaches, which are more complex to program and involve more computational work in each solution step, is to allow for large time-step sizes. A simple qualitative model will help to clarify how this works. Considering the heat conduction equation:

$$\frac{\partial u}{\partial t} = \frac{\partial^2 u}{\partial x^2},$$

and by using the backward difference approximation for the first derivative in time and central difference approximation for the second derivative in space, the following is obtained:

$$\frac{u_x^t - u_x^{t-\Delta t}}{\Delta t} = \frac{u_{x+\Delta x}^t - 2\,u_x^t + u_{x-\Delta x}^t}{\Delta x^2}.$$

Rearranging the equation gives:

$$u_x^{t-\Delta t} = u_x^t - \frac{\Delta t}{\Delta x^2}\left[u_{x+\Delta x}^t - 2\,u_x^t + u_{x-\Delta x}^t\right].$$

Rewriting the above approximation at the time level $(t + \Delta t)$, yields:

$$u_x^t = u_x^{t+\Delta t} - \frac{\Delta t}{\Delta x^2}\left[u_{x+\Delta x}^{t+\Delta t} - 2\,u_x^{t+\Delta t} + u_{x-\Delta x}^{t+\Delta t}\right] \implies \text{Implicit method} \qquad (1.26)$$

To show and explain the explicit method, the same example for the heat conduction equation is used, but by using the forward difference approximation for the first derivative in time and central difference approximation for the second derivative in space:

$$\frac{u_x^{t+\Delta t} - u_x^t}{\Delta t} = \frac{u_{x+\Delta x}^t - 2\,u_x^t + u_{x-\Delta x}^t}{\Delta x^2}.$$

Rearranging the equation gives:

$$u_x^{t+\Delta t} = u_x^t + \frac{\Delta t}{\Delta x^2}\left[u_{x+\Delta x}^t - 2\,u_x^t + u_{x-\Delta x}^t\right] \implies \text{Explicit method} \qquad (1.27)$$

As can be seen, both methods, (1.26) and (1.27), involve two levels in time. However, in the implicit method more terms of the next level above are included, see Fig (1.7a), which means in an explicit numerical method the rate of change in u would be evaluated in terms of known quantities at the previous time step t. An implicit method, in contrast, would evaluate some or all of the terms in the rate of change in terms of unknown quantities at the new time step $t + \Delta t$, see Fig (1.7b). Thus, new quantities then appear on both the left and right side of the u-equation, it is said to be an implicit definition of the new $t + \Delta t$ values. Typically, a matrix or iterative solution must be used to compute the new quantities.
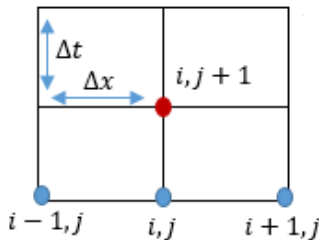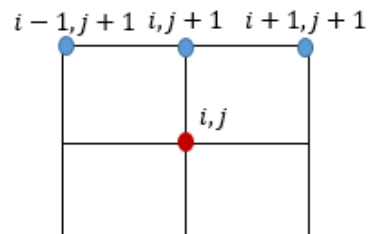
Figure 1.7: **The stencils for the *Euler's* method for the heat equation.** Panel (a): explicit method. Panel (b): implicit method.

Numerical stability is determined by the behaviour of the solution as the time-step Δt is increased. If the solution remains well-behaved for arbitrarily large values of the

time step, the method is determined to be unconditionally stable. Such a situation never occurs with explicit methods, as they are always conditionally stable. This is clearly observed by dividing the u-equation by Δt and then letting $\Delta t \to \infty$. In this limit there are no $t + \Delta t$ terms remaining in the equation so no solution exists for $u_x^{t+\Delta t}$, indicating that there must be some limit on the size of the time step for there to be a solution, whereas in implicit methods a solution for the unknowns at level $t + \Delta t$ may be obtained for any size time step. Obviously, the solution for very large times may not be accurate unless the implicit construction has been carefully constructed [137].

Both explicit (1.27) and implicit (1.26) give the first order approximation to the exact solution of the problem. For it to be useful, the numerical scheme should not only approximate the exact solution but also be stable. Stability of numerical schemes are studied by various methods of which the Von Neumann stability analysis [27, 200] is most commonly used. According to this analysis, the explicit scheme (1.27) is stable under the following condition:

$$\beta = \frac{D\Delta t}{\Delta x^2} \leq \frac{1}{2}. \tag{1.28}$$

Therefore, for the (FTCS) scheme to be stable this condition must be satisfied, which means if the diffusion coefficient and the space step is fixed, then accordingly we need to define or choose the value of the time step Δt that satisfy the stability condition to obtain a stable solution.

By using the von Neumann stability analysis, it can also be shown that the implicit scheme (1.26) is stable under the following condition:

$$\frac{1}{1 + 4\,\beta} \leq 1 \text{ where } \beta = \frac{D\Delta t}{\Delta x^2}.$$

Therefore, the implicit scheme, (BTCS), is unconditionally stable as the stability condition will be always satisfied. Regarding the accuracy issue, for larger time steps, the implicit scheme is preferable since it is less computationally demanding. The explicit scheme is the least accurate and can be unstable, but it is also the easiest to implement and the least numerically intensive. However, a general rule is that the time-step sizes for explicit stability and accuracy are usually equivalent. Thus, when $\frac{\Delta t}{\Delta x^2} > 0.5$, an explicit method would be unstable, but implicit methods simply under-relax more to maintain the stability of the iterative solution. In conclusion, when Δt is sufficiently small, the accuracy of both explicit and implicit methods can be comparable [27, 200].

1.4.3 Adaptation of Numerical Algorithm to Competitive Reaction–Diffusion System

Inserting the previous approximations into this system of equations, yields:

$$\begin{cases} u_t = u_{xx} + u\,(1 - u - b_1\,v)\,, \\ v_t = D\,v_{xx} + r\,v\,(1 - v - b_2\,u)\,. \end{cases} \tag{1.29}$$

$$u_t = \frac{u(t + \Delta t) - u(t)}{\Delta t} \quad \longrightarrow \quad \text{forward time} \tag{1.30}$$

$$u_{xx} = \frac{u(x + \Delta x) - 2\,u(x) + u(x - \Delta x)}{\Delta x^2} \quad \longrightarrow \quad \text{central space} \tag{1.31}$$

Thus, the first equation will take this form:

$$\frac{u_x^{t+\Delta t} - u_x^t}{\Delta t} = \left(\frac{u_{x+\Delta x}^t - 2u_x^t + u_{x-\Delta x}^t}{\Delta x^2}\right) + u_x^t\,(1 - u_x^t - b_1 v_x^t),$$

rearranging gives:

$$u_x^{t+\Delta t} = u_x^t + \Delta t\left[\left(\frac{u_{x+\Delta x}^t - 2u_x^t + u_{x-\Delta x}^t}{\Delta x^2}\right) + u_x^t\,(1 - u_x^t - b_1 v_x^t)\right].$$

Similarly,

$$v_x^{t+\Delta t} = v_x^t + \Delta t\left[D\left(\frac{v_{x+\Delta x}^t - 2v_x^t + v_{x-\Delta x}^t}{\Delta x^2}\right) + r\,v_x^t\,(1 - v_x^t - b_2 u_x^t)\right].$$

As mentioned previously, the system (1.29) will have an infinite number of solutions. To obtain a unique solution, initial conditions and boundary conditions must be defined. Therefore, the initial conditions:

$$\begin{cases} u(x, 0) = u_0(x), \\ v(x, 0) = v_0(x), \end{cases}$$

are set with certain chosen functions $u_0(x)$ and $v_0(x)$. Also, the Neumann boundary condition is applied:

$$u_x(0, t) = u_x(L, t) = v_x(0, t) = v_x(L, t) = 0 \ \forall\ t > 0.$$

This method will be used for all upcoming simulations in Chapters 2-3 after discretising the space and time units to satisfy the stability and accuracy of conditions.

1.4.4   2-D Spatially Extended *Lotka-Volterra* Models

Although a 1-dimensional spatial domain is a useful modelling tool in certain circumstances (e.g., modelling long, thin regions), spatial domains are also expected to be in 2- or 3-dimensions. Therefore, the following 2-D spatially extended *Lotka-Volterra* system is considered:

$$\begin{cases} u_t = D_u \left(u_{xx} + u_{yy} \right) + u \left(1 - u - b_1 \, v \right), \\ v_t = D_v \left(v_{xx} + v_{yy} \right) + r \, v \left(1 - v - b_2 \, u \right), \end{cases} \tag{1.32}$$

where $(x, y) \in \Omega \subseteq \mathbb{R}^2$ for some set Ω.

Axially Symmetric Case of The Laplace Equation

As a starting point, radially symmetric solutions are considered. The relationship between plane polar coordinates and cartesian coordinates are given as:

$$x = r \cos \theta, \ y = r \sin \theta,$$

where,

$$r = \sqrt{x^2 + y^2}, \ \text{and} \ \theta = \tan^{-1} \left(\frac{y}{x} \right).$$

Hence, the Laplacian in polar coordinates can be written as:

$$\frac{\partial^2}{\partial x^2} + \frac{\partial^2}{\partial y^2} = \frac{\partial^2}{\partial r^2} + \frac{1}{r} \frac{\partial}{\partial r} + \frac{1}{r^2} \frac{\partial^2}{\partial \theta^2}, \tag{1.33}$$

where r is the radial distance and θ is the angle.
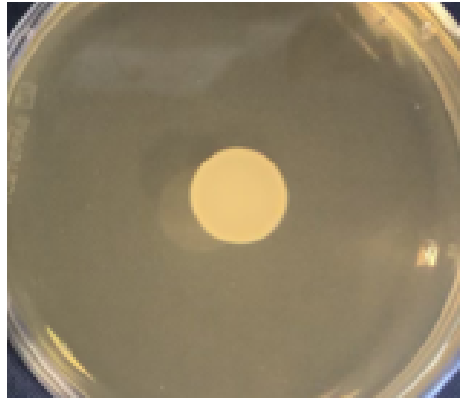
Figure 1.8: **Image of the bacterial colony growing in a Petri dish:** The image indicates the radially symmetric shape of the colony.

As shown in Fig (1.8), the interacted populations form a circular spot in the middle of the plate and expand symmetrically. As a result, according to [146], the functions only depend on r (radially symmetric), and the expression in (1.33) reduces to:

$$\frac{\partial^2}{\partial x^2} + \frac{\partial^2}{\partial y^2} = \frac{\partial^2}{\partial r^2} + \frac{1}{r} \frac{\partial}{\partial r}.$$

Therefore, the system (1.32), takes the following form:

$$
\begin{cases}
u_t = D_u \left[u_{rr} + \dfrac{1}{r} u_r \right] + r_u\, u\,(1 - u - b_1\, v), \\[2mm]
v_t = D_v \left[v_{rr} + \dfrac{1}{r} v_r \right] + r_v\, v\,(1 - v - b_2\, u).
\end{cases}
\tag{1.34}
$$

When $r = 0$, u_r needs to be equal to zero to ensure symmetry, and a similar condition would be expected to hold when $r = \infty$. As in acceptable solutions, the anticipation is u_r to be limited and bounded. As a result, the system (1.34) can be approximated by the following system for sufficiently large r:

$$
\begin{cases}
u_t = D_u\, u_{rr} + r_u\, u\,(1 - u - b_1\, v), \\[2mm]
v_t = D_v\, v_{rr} + r_v\, v\,(1 - v - b_2\, u).
\end{cases}
\tag{1.35}
$$

Calculating Laplasian in General (Axially Asymmetric) Two-Dimensional Case

A commonly used central difference approximation for the Laplacian in the case of even spacial discretisation, $\Delta x = \Delta y$, is given as:

$$
\Delta_1 u_{i,j} = \frac{u_{i+1,j} + u_{i-1,j} + u_{i,j+1} + u_{i,j-1} - 4\, u_{i,j}}{\Delta x^2}.
\tag{1.36}
$$

This scheme involves four neighbours as shown in Fig (1.9a). It is known that this scheme gradually results in an asymmetry in the simulations as illustrated in Fig (1.9b): concentric waves are more rhombic than circular. An alternative scheme for calculating Laplasian would better involve four diagonal members as shown in Fig (1.9c):

$$
\Delta_2 u_{i,j} = \frac{u_{i+1,j+1} + u_{i-1,j+1} + u_{i-1,j+1} + u_{i-1,j-1} - 4\, u_{i,j}}{2\, \Delta x^2}.
\tag{1.37}
$$
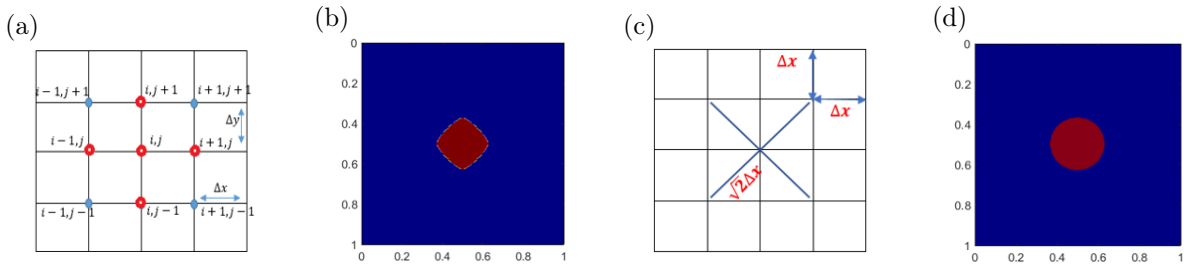
Figure 1.9: **Numerical Schemes.** Panel (a): demonstration of the typical scheme using four adjacent points (red dots) in two-dimensional space using the FTCS (forward time- centred space) approach incorporated into (1.36). Panel (b): an illustration of the simulated spot produced by the use of the standard form of the Laplacian operator presented in (1.36). Panel (c): demonstration of the neighbouring points incorporated into (1.37). Panel (d): an illustration of the simulated spot produced by the use the Laplacian operator presented in (1.38).

However, this scheme also involves formation of the artificial asymmetry. A better result is obtained by combining the schemes presented in (1.36) and (1.37). According to

44

[16, 205], it is known that the best proportion to avoid artificial asymmetry is given as the following:

$$\Delta u = \frac{2}{3}\Delta_1 u + \frac{1}{3}\Delta_2 u.$$

Thus:

$$\Delta u = \frac{4 * (u_{i+1,j} + u_{i-1,j} + u_{i,j+1} + u_{i,j-1}) + u_{i+1,j+1} + u_{i-1,j+1} + u_{i-1,j+1} + u_{i-1,j-1} - 20\,u_{i,j}}{6\,\Delta x^2}$$

(1.38)

As shown in Fig (1.9d), the simulations produced using this approach (1.38) were much more isotropic than those generated using the standard scheme [16, 205]. This numerical scheme was used for two-dimensional simulations performed in Chapter 4.

1.5 Implication of The Presented Information to Our Research

When modelling the interactions between bacterial species to simulate the data presented in Chapter 2, which reflects the behaviour of evolved populations under mixed conditions, was first begun the *Lotka-Volterra* equations were used, a simple model of the population dynamics of species competing for a common resource. In Chapter 2, after estimating the diffusion coefficients of the involved species, the spatial variations were simply disregarded and it was concluded that the use of competitive *Lotka-Volterra* equations in spatially- homogeneous systems presented earlier in (1.10), the two-variable model and the three-variable model, were sufficient to produce and generate simulations comparable to the reported experimental data. Furthermore, the steady solutions to the system were analytically derived in the case when the bacteria were completely immobile, i.e., when bacterial diffusivity vanished, and the stability conditions were fulfilled for all the equilibriums, (1.13), (1.14), and (1.15).

As explained in Chapters 3 and 4, after obtaining the precise data and laboratory information regarding the diffusion coefficients of the evolved populations, it was decided to extend the competitive *Lotka-Volterra* equations to incorporate the diffusion term to account for the space variation and reflect the reality of the experimental methods regardless of their weak impact. Thus, two competing bacterial populations in a one-dimensional domain (1.20) were considered as a starting point.

Later, the spatially- extended *Lotka-Volterra* model of two-species competition in one dimension was modified to explicitly account for the presence of a susceptible fraction in one species, which was inhibited by the other. In addition, when modelling the inhibitory

interactions, the three-variable model was later extended to include the production of the toxin by one species to inhibit the other evolved species. With the knowledge that even non-motile bacteria exhibit some movement due to mechanical forces within the cell and the local environment [28], the system was then numerically solved for small bacterial diffusivities. This made it possible to characterise an invasion as a travelling wave connecting two single-species colonies.

As the developed systems cannot be solved analytically, the PDE must be discretised on a grid using numerical methods. Thus, using the explicit numerical schemes presented in (1.30) and (1.31), it was possible to obtain an approximated solution for the system (1.29). This system has an infinite number of potential solutions. To obtain a unique solution, initial conditions and boundary conditions must be specified.

In the final part of this study presented in Chapter 4, it was decided to investigate the position of resistance emergence and its influence on the interaction dynamics. Such effects are only manifested and realised in two dimensions. Therefore, by using the 2-D spatially extended *Lotka-Volterra* models presented in (1.32), and after the choice was made to broaden the diffusion term to include additional neighbouring points as presented in (1.38), it was possible to show the effect of the initial position of mutations.

1.6   Thesis Outline

This thesis consists of five chapters.

Chapter 1: General Introduction

In this chapter, a comprehensive introduction is provided that includes a general explanation of the issue which motivated this study, its causes, and the consequences of its emergence, as well as a discussion of some of the approaches and measures used to limit the spread of this problematic phenomenon.

After exploring these aspects, the motivation and aims of this study are introduced along with some biological background about the bacterial species that were the focus of this study as well as bacterial properties, such as population growth, generation time, and growth curve. Furthermore, some ecological community concepts are reviewed, for example, types of interactions between species and the effects of different interactions on the involved populations.

In this chapter, a mathematical background is also presented, which includes an overview of mathematical models in bacterial growth and competition. In addition to the analysis of models for single species in spatially homogeneous and inhomogeneous situations, models for the dynamics of interacting populations in both situations are also analysed, such as predator-prey models, *Lotka-Volterra* systems, and competition models, along with the analytic solutions for such models wherever possible. Finally, an alternative

approach is reviewed and discussed, which is the use of discrete variable methods to obtain an accurate approximation to the solution of an initial value problem, i.e., numerical methods.

Chapter 2: Mathematical Analysis of The Experimental Data in The Context of The Dynamics of Non-inhibitory Microbial Interactions and Resistance Evolution

In this chapter, the aim is to analyse the experimental results obtained in Dr Malcolm Horsburgh's laboratory during an investigation into the dynamics of the population formed by interacting *S. epidermidis* and *S. aureus* bacteria, and to develop mathematical models to explain and reproduce the dynamics of interacting populations observed in laboratory experiments. Also, the aim is to fit model parameters to experimental data.

Moreover, an overview of the experiments performed in Dr. Malcolm Horsburgh's lab and reported in (Libberton et al., Evolutionary Applications, 2015) [122] was presented. This can be explained and concluded briefly as the competition experiments in which toxin-producing (B180, B155) and non-producing (B115, B035) nasal isolates of *S. epidermidis* invaded from three starting frequencies (0.1, 0.01 and 0.001) resident populations of toxin-sensitive *S. aureus* (SH1000). Conversely, to test whether *S. aureus* invasion could be restricted by *S. epidermidis* populations, the reciprocal invasions were performed. All competitions were propagated for 7 days with the daily transfer of communities to a fresh medium; in half of the replicates, population structure was maintained at each transfer, whereas in the other half of the replicates, the population structure was homogenised at each transfer.

Based on these reported data, this phenomenon was modelled by extending the classic two-species *Lotka-Volterra* competition model where the first model depended on two variables representing the concentrations of *S. aureus* and *S. epidermidis*. Although this model concurred with the experimental data regarding the final states of the competing populations (at day 7), the two-variable model was, in some cases, unable to simulate the dynamics and the behaviour of the evolved populations during the first days of the competition. Hence, this model was improved by introducing an extra variable. By adding this variable, the meta-population assumptions were made, assuming that the evolved *S. epidermidis* populations consist of two fractions. The susceptible fraction, which represents the majority of the population and their existence, caused the reported declining behaviour of *S. epidermidis* populations at the beginning of the invasions, and the adopted fraction, which represents one percent of the total population density, resulted in the recovery process observed in the reported experimental data.

As a result of the addition of the adopted section, the simulations obtained by the three-variable model were conformable with the experimental data in terms of the dynamics of the competing populations as well as the final states of the evolved populations.

However, as attempts were made to model the mutual invasions between the inhibitory populations of *S. epidermidis* and toxin-sensitive *S. aureus* populations, many aspects were not clear, which resulted in conflicting statements. Thus, it was decided that further experiments were required to understand different biological aspects.

Chapter 3: A Combined Experimental and Theoretical Study of The Dynamics of Interacting Populations in A Mixed Environment

Many obstacles were encountered when attempting to model the inhibitory interactions. Such difficulties, reviewed in detail at the end of chapter 2, prevented the introduction of a mathematical model that could simulate the obtained behaviour observed in the presented data. In addition to these challenges, it was essential to re-perform these experiments before developing mathematical models to represent the inhibitory interactions in order to:

• Obtain a comprehensive understanding of the nature of these interferences.

• Extend the duration of these interactions until the difference in evolved population density was no longer substantial.

• Clarify several concepts that were neither presented nor addressed in the paper reviewed in Chapter 2.

Neglecting such information was not a deficiency; it may not have been considered biologically significant. Thus, this chapter introduces a combined theoretical-experimental study that covers different aspects of the evolution of single and multi-species populations to understand the mechanisms governing the evolution of microbial populations and the roles of different factors involved in bacterial interactions. The dynamics of interactions in mixed environments between the susceptible strain of *S. aureus* (SH1000) and different inhibitor-producing strains of *S. epidermidis* (B180, B155, and TU3298), differing in their level of toxicity, were experimentally studied.

The aim of this chapter was to investigate several microbial evolution studies suggesting that manipulating some of the environmental factors surrounding these interactions may contribute to inhibiting the pathogenic species.

A set of experiments were performed to determine the growth rate and doubling time for the involved strains by incubating replicates for each strain at $37^\circ C$ for $24\,h$ and taking OD_{600} readings at 30-min intervals. Another set of experiments were performed to analyse the toxicity level and evolution of each strain separately. Also, a series of experiments were conducted involving mutual invasions of toxin-producing populations of *S. epidermidis* and susceptible populations of *S. aureus* with varied initial frequencies. Furthermore, pre and after-invasion toxin-mediated inhibition assays were performed to analyse the effect of the toxins secreted by the ancestral *S. epidermidis* strains and the evolved *S. epidermidis* strains on the ancestral and evolved *S. aureus* strains.

The findings regarding the growth rate and doubling time experiments indicate that

the *S. epidermidis* strains had comparable growth rates to the *S. aureus* strain (SH1000). Regarding the inhibition assays, three isolates were toxin producers, as revealed in a deferred inhibition assay in which the bacteria killed the *S. aureus* [zone of clearing when a lawn of *S. aureus* strain SH1000 was sprayed over them [151]]. Of the three toxin-producing *S. epidermidis* strains, B180 produced an inhibition area that was around five times smaller than that of B155, and B155 produced an inhibition area that was around two times smaller than that of TU3298.

Regarding the competition experiments, all interaction experiments resulted in *S. aureus* dominance with coexistence between the evolved populations, regardless of initial frequency and toxicity levels. Also, a positive association was observed between the level of toxicity expressed by *S. epidermidis* and the time consumed by *S. aureus* populations to adapt to this toxicity. In addition, a positive relationship was found between the level of *S. epidermidis* toxicity and its ability to survive and avoid extinction while interacting with *S. aureus*. Invasions by toxin-producing *S. epidermidis* stains were eventually impeded by the evolution of resistance by *S. aureus* populations. On the other hand, evolved resistance promotes *S. aureus* invasion.

In order to explain the experimental findings of this study, several mathematical models were developed which were used for simulation of the bacterial dynamics in the above experiments. Regarding the growth rate experiments, the simplest case of the Tilman model [203] was used. The case of a single consumer and a single resource was investigated. Regarding the toxin-mediated inhibition, only the effect of the inhibitions without the competitions were considered by introducing two bacterial populations into a one-dimensional domain. The producer, *S. epidermidis* stains, produces an antimicrobial toxin which inhibits the other, susceptible, *S. aureus* populations. The third variable represents the toxins produced by the producer, *S. epidermidis* populations, at a certain rate and which degraded at another rate. Rates are defined by fitting the mathematical model to the obtained data using the least squares approximation to find the best coefficients.

In terms of the competition experiment, several mathematical models were developed. They were distinguished by level of toxicity. The first type of interactions concerned competition for resources between (B180: SH1000), since the toxins produced by B180 did not play a significant role in the outcomes, whereas the other type considered the inhibition and competition for resources between (B155: SH1000) and between (TU3298: SH1000).

The simulations of this study confirmed that the toxicity level can drastically affect the evolutionary outcomes. Additionally, the models reproduce and explain the way in which competitive interactions between toxin-producing bacteria and their susceptible/adapted counterparts influence the two-lineage community response to toxin exposure.

Mathematical experiments were performed to validate the predictions of the developed models. From these experiments, it was concluded that there is a positive correlation between the toxicity level of the interaction and the required resistance ratio to enable the evolved *S. aureus* to dominate. Also, under mixed conditions, an inverse relationship was noticed between the time required for the adaptive fracture of *S. aureus* to overcome the susceptible ratio and the growth rate of their opponent strain of *S. epidermidis*, i.e., the faster the evolved *S. epidermidis* strain grows, the more it forces its opponent to transform. Nevertheless, these forcing mechanisms imposed on the evolved *S. aureus* did not result in immediate dominance, indicating that the toxin producer co-evolved and adapted. However, in the absence of knowledge of the mechanism of inhibition, this remains unclear.

Chapter 4: A Combined Experimental and Theoretical Study of The Dynamics of Interacting Populations in A Spatially Structured Environment

This chapter provides a detailed and combined biological and mathematical study of interactions in natural bacterial communities and their implications and outcomes. All previous experiments that were conducted in Chapter 3, when populations of *S. aureus* were engaged in competition against different species of *S. epidermidis* under different settings, in terms of the initial concentrations of the interacted populations as well as the level of toxicity of *S. aureus* opponents, were repeated, including the preservation factor. This ensured that during these competitions the environmental structure of the evolved populations was maintained.

The aim of this chapter is to investigate how far the preservation of the environmental structure contributes to limiting the spread of the pathogenic strain (SH1000) and eliminating its colonisation; the extent to which this step will change the dynamics of the interactions and, consequently, the results of these interferences when comparing them with the outcomes of interactions conducted under mixed conditions.

Once again, the findings of this study regarding the interactions showed the coexistence of the evolved populations, which means no extinction was observed among the competitors. However, the findings also emphasised the critical role of spatial structure in altering and changing the course of interactions, especially if these interactions involve a high degree of toxicity. As demonstrated by the findings, maintaining spatial structure enables inhibitor-producing *S. epidermidis* to better prevent and promote invasions from and into the evolved *S. aureus* populations, since structured environments typically favour the manufacture of inhibitory toxins. Nevertheless, the evolved populations of *S. aureus* (SH1000) were able to overcome these complex and severe conditions.

Mathematically, the models based on logistic equations that were shown in the previous chapter were used. When simulating these interactions, the conditions of the environment were considered. The mathematical translation of this biological concept involves

reducing the concentrations at the end of each day without compromising the dimensions of the formed spots. When modelling the interactions under structured conditions, all the previous assumptions and model parameters that were used in mixed conditions simulations succeeded in producing comparable simulations with the experimental data only in low-toxin interactions. However, imposing these assumptions when the interaction involved a high level of toxicity failed to produce simulations that concurred with those obtained from the experimental data.

In this chapter, the attempts to obtain model simulations that coincide with the reported experimental data are also shown. They were all unable, to varying degrees, to generate simulations consistent with both invasion directions. However, the final attempt, which aimed to keep all parameters the same as the simulations under mixed conditions with only change to the parameter p_2, succeeded in producing realistic simulations. In the final section of this chapter, the impact of the initial location of resistance in the evolved spot on the interference dynamics was examined by extending the model to the 2D n- species competition-diffusive model.

The findings show that the farther the mutations are formed from the centre of the spot, the longer it takes to be able to recover and eventually dominate because the diffusion coefficient is weak. Biologically, this phenomenon is justified, as the appearance of the mutation on the edges of the spot signifies that it will be in contact with a relatively smaller number of cells, which contributes to slowing down the process of spreading these mutations and vice versa. Furthermore, given the fact that all evolved populations have weak motile coefficients, the emergence of mutations at the edge of the spot would give the other competitors a better chance to survive and maintain their existence for a longer period.

Chapter 5: Discussion

In this chapter, the conclusions are provided and a discussion offered of the findings presented throughout this study, including experimental and mathematical results, as well as highlighting the benefits of the findings for future research.

An overview of the research presented in this thesis is given by briefly exploring the problem, the hypothesis, and the focus of the study. The main goals of this study are also revisited, along with a summary of the methods used to achieve these goals.

A presentation of the experimental and mathematical findings is provided in this chapter. Each aim addressed throughout this study together with its results is presented. The points where the findings concur with those of previously undertaken study as well as points of disagreement are highlighted.

Finally, this research is concluded by suggesting several ideas for future work which would improve the outcomes of this research in providing a path to progression at the laboratory and mathematical levels.

Chapter 2

Mathematical Analysis of The Experimental Data in The Context of The Dynamics of Non-inhibitory Microbial Interactions and Resistance Evolution

2.1 Introduction

As stated previously, human airways are known as being the shelter for many bacterial species. Many of these species are harmless to the human body, while others are harmful [134].

Staphylococcus aureus colonisation of nasal cavities plays a crucial role in the lifecycle, epidemiology, and pathogenesis of *staphylococcal* contagion [4]. Maintaining the survival of other microbial communities sharing the same environment with *Staphylococcus aureus* requires them to be engaged in a constant competition with *Staphylococcus aureus* for resources and space. Toxin-producing competitor strains compete by manufacturing a lethal compound (toxins) that does not affect their population and are directed against *Staphylococcus aureus* [122]. Other populations, to protect their existence, evolve a defence against that attack [132].

Several studies determined that eliminating *S. aureus* from the nose is positively associated with reducing the incidence of *Staphylococcal* infections in certain patients [170, 171]. Taking into consideration the absence of long-term elimination strategies against *S. aureus* nasal carriage and the emergence of antibiotic resistance, new methods are necessary for the prevention of *Staphylococcal* disease.

Recent evidence suggests that interactions and competitions between bacterial species control the distribution of the opportunistic pathogen *Staphylococcus aureus* in the nasal airway of humans, either by preventing colonisation or by driving displacement [122]. Several experiments report a negative association between *S. epidermidis* and *S. aureus* across nasal communities, suggesting that these species are involved in one-way or mutual exclusion [148].

The purpose of this study is to construct simple in vitro populations of *S. epidermidis*

and *S. aureus* to test the hypothesis that toxin-mediated killing of competitor species (interference competition) could explain the observed negatively associated distributions of these species in nasal communities [81].

Thus, the presented study in this chapter aims to:

- Overview various biological aspects and experimental techniques described in (Libberton, Horsburgh, and Brockhurst, 2015) [122].

- Analyse the experimental results obtained in Dr. Malcolm Horsburgh's laboratory during the investigation into the dynamics of the population formed by interacting *S. epidermidis* and *S. aureus* species.

- Develop mathematical models to explain and simulate the dynamics of inhibitory and non-inhibitory interactions observed in laboratory experiments.

- Fit model parameters to experimental data.

2.2 Materials and Methods Used in (Libberton, Horsburgh, and Brockhurst, 2015) [122]

Several experiments were performed to observe and evaluate the influence and impact of the environmental structures, the presence of toxic substances, and the initial density of the interacted populations on the outcomes of competitions.
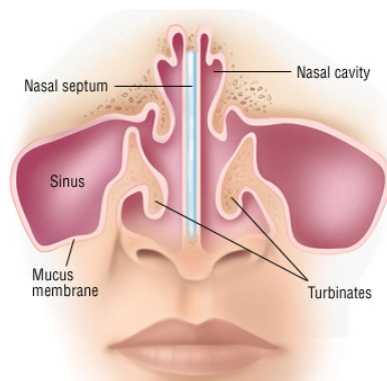
Figure 2.1: **Illustrations of the nasal cavity and nasal epithelium.** Taken from [81].

Four sequenced collections of *S. epidermidis* were used in the study. They are usually located in the human nasal airway where both *S. aureus* and *S. epidermidis* colonise and compete, see Fig (2.1). Furthermore, they are distinguished by their level of toxicity. Two isolates were toxin producers, as revealed in a deferred inhibition assay in which

S.aureus was killed, forming a clear zone when a lawn of *S. aureus* strain, SH1000, was sprayed over them. Two isolates were non-producers based on their inability to reduce the viability of strain SH1000. According to Table (2.1), the *S. epidermidis* strains had comparable growth rates to SH1000, which means that there is no significant difference between any of the *S. epidermidis* strains tested and the *S. aureus* strain SH1000 used in the study in terms of the population doubling time.

Species	Strain identification	Doubling time (Min)
S. aureus	SH1000	116.45
S. epidermidis	B035	123.34
S. epidermidis	B115	120.49
S. epidermidis	B155	110.11
S. epidermidis	B180	116.06

Table 2.1: **Identification and doubling times of strains used in this study.** The doubling times in minutes were compared to SH1000 (*S. aureus*) as a control using a *post hoc Dunnett's test.*

To test these hypotheses, the decolonisation studies presented earlier [132, 182, 188, 199], a competition study was conducted in which toxin-producing and non-producing nasal isolates of *S. epidermidis* were introduced at three different initial frequencies (0.1, 0.01, and 0.001) into toxin-sensitive *S. aureus* populations. To investigate if *S. aureus* invasion may be inhibited by *S. epidermidis* toxin production, reciprocal invasions were performed. All these invasions were performed in two types of environments (mixed and structured), see Fig (2.2).
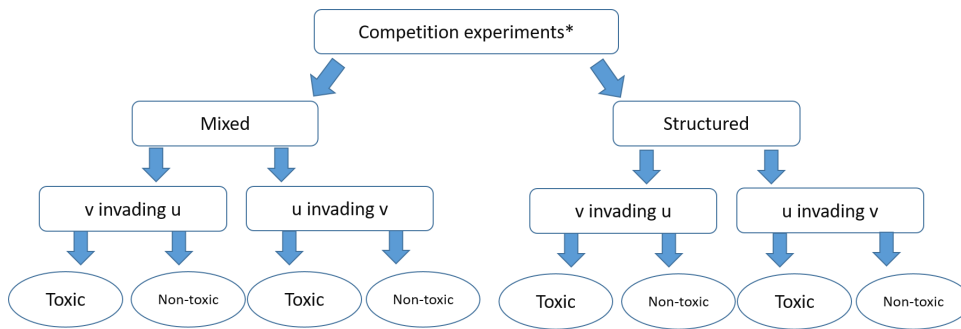
Figure 2.2: **Summary of the experiments reported in [122].** Here u is *S. aureus*, and v is *S. epidermidis.*

The cultured communities were transferred to a new agar plate every day for 7 days. Half of the replicates underwent a regime whereby the transfers were made by replica plating with velvet, Fig (2.3), to maintain spatial structure. While the other half of replicates underwent a mixed regime, the spatial structure was destroyed every 24 h, as the evolved populations were transferred by scraping the entire bacterial lawn off the

plate and diluting it in $10\,ml$ of sterile PBS, before thoroughly vortexing and pipetting $50\,\mu l$ onto a new plate to carry on the interaction experiments [179].
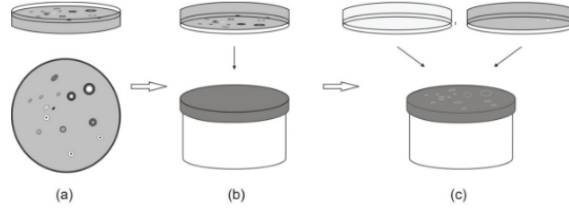
Figure 2.3: **Application of the replica-technique.** A microbiological technique in which the pattern of colonies growing on a culture plate is copied. Taken from [179].

The success of the invasions was determined and quantified through a calculation of the selection rate constant for each invader, which required the use of relative bacterial frequencies throughout the period. The following equation makes it possible to define the results of each invasion:

$$C_{ir} = \frac{\ln\left[N_i(7)/N_i(0)\right] - \ln\left[N_r(7)/N_r(0)\right]}{7days}. \tag{2.1}$$

Here, $N_i(0)$ and $N_r(0)$ represent the initial densities of both invader and resident populations, while $N_i(7)$ and $N_r(7)$ represent their densities after 7 days. Negative values in Fig(2.4) indicated that invasion was not possible, whereas positive values indicated invasion was possible. By assuming that both competing species have an exponential growth rate, the equations representing their growth can be written as follows:

$$N_i(t) = N_i(0)\,e^{r_i t} \implies e^{r_i t} = \frac{N_i(t)}{N_i(0)} \implies r_i = \frac{\ln\left(\frac{N_i(t)}{N_i(0)}\right)}{t}.$$

Similarly, the growth rate equation of the competing resident population can be written as follows:

$$r_R = \frac{\ln\left(\frac{N_R(t)}{N_R(0)}\right)}{t}.$$

Therefore, by using the equation (2.1), the success of invasions is quantified by subtracting the growth rates of the competing populations, $r_i - r_R$, so if the values are negative, the resident population has a higher growth rate while the positive values indicate that the invader population is in the dominant position [122].

2.3 Summary of Results Reported in [122]

Reported findings suggest that manipulation of the nasal microbial community could be used to limit colonisation by *S. aureus*, which might limit transmission and infection rates.

2.3.1 A Structured Environment Encourages The Invasion of Toxin-producing *S. epidermidis*

In a structured environment, all *S. epidermidi* strains were able to invade successfully, Fig (2.4a). However, the production of toxic substances by *S. epidermidis* enhanced the invasions, and the rate of invasions was higher than non-producing stains.
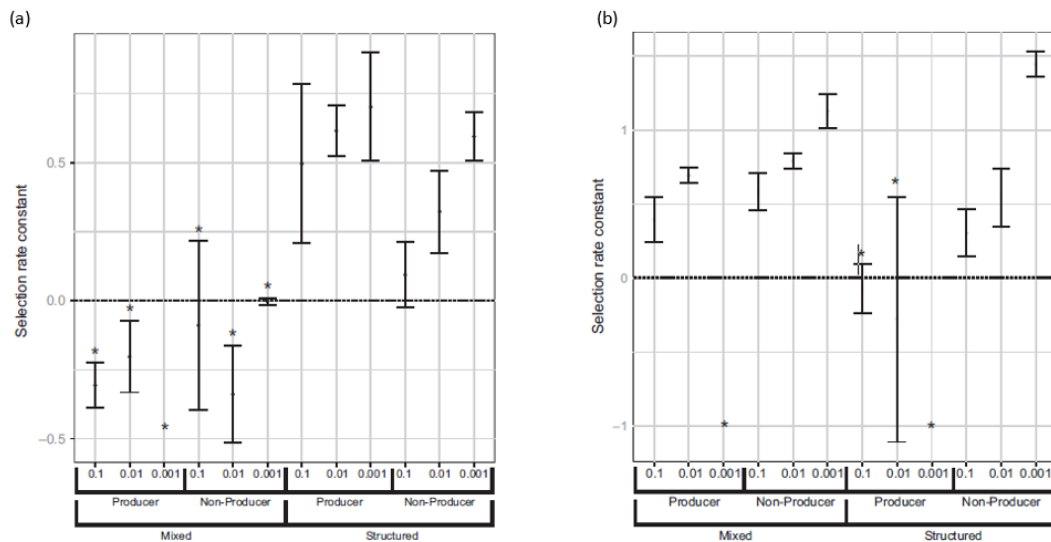
Figure 2.4: **Selection rate coefficients.** Panel (a): for toxin and non-toxin producing populations of *S. epidermidis* invading populations of *S. aureus*. Panel (b): for *S. aureus* (SH1000) invading populations of *S. epidermidis*. Both directions of invasions started at three different initial frequencies (1:10), (1:100) and (1:1000), pointed out as 0.1, 0.01, and 0.001 respectively in the *x*-axis. Each of the invasions was performed in mixed and structured environments. Negative values of the rate of invasions mean that the invasion did not occur, and they were marked by asterisks. Error bars represent the standard error of the mean. Taken from [122].

In a mixed environment, both toxin-producing and non-toxin-producing strains of *S. epidermidis* were unable to invade, and the invasions were restricted by the resident population of *S. aureus*. Furthermore, lower concentrations of the invaders vanished, whereas invaders that were initiated at relatively higher concentrations were most likely to exist and continue at low frequencies and avoid extinction.

2.3.2 The Emergence of Resistance in The Evolved *S. aureus* Populations Inhibits The Invasion by *S. epidermidis*

Inhibitor producing strains of *S. epidermidis* (B155, black) and (B180, blue) show different behaviours over time in a structured environment.
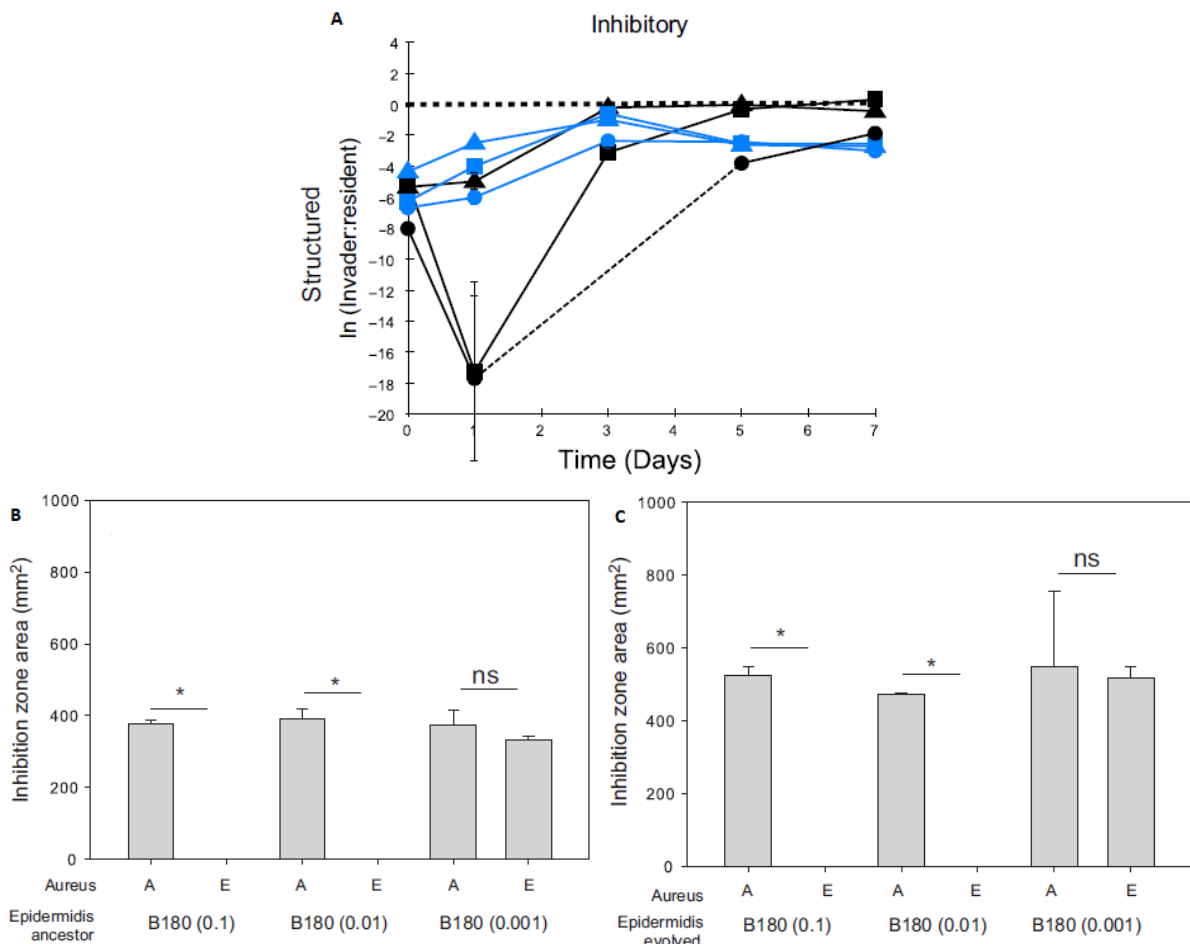
Figure 2.5: **The emergence of the resistence inhibits the invasion by *S. epidermidis.*** Panel A: toxin-producing (B155, black) and (B180, blue) isolates of *S. epidermidis* invading populations of *S. aureus* (SH1000) at frequencies of 0.1 (triangle), 0.01 (square) and 0.001 (circle) under a spatially structured regime. The *x*-axis is the time in days, and the *y*-axis is the natural log of the invader to resident ratio. The case when the population dipped below the experiment detection threshold was denoted by a dotted line in the time course, whereas the heavy dotted line at 0 on the *y*-axis indicates an equal invader to resident ratio. Panel B: the inhibition zone area (mm^2) produced by the toxin-producing *S. epidermidis* strains (the ancestral B180) against the ancestral SH1000 (A) and the evolved SH1000 (E). Panel C: the inhibition zone area (mm^2) produced by the toxin-producing *S. epidermidis* strains (the evolved B180) against the ancestral SH1000 (A) and the evolved SH1000 (E). Asterisks represent a significant difference between the inhibition zone areas of ancestral (A) and evolved (E) *S. aureus* strains. Taken from [122].

As illustrated in Fig (2.5A), all different concentrations of (B155) stain began to increase after the first day and moved toward the ratio of 1:1 invader to resident, whereas the starting frequencies of 0.1 and 0.01 of the other toxic strain (B180) increased gradually

until the third day, after which they decreased.

The decline in frequency of *S. epidermidis* strain (B180), (starting frequencies of 0.1 and 0.01), was justified by the evolution of resistance in the resident *S. aureus* populations

To prove this argument, spray assays were performed, Fig(2.5B, 2.5C), .5C), where ancestral (pure) and evolved resident clones of *S. aureus* were sprayed over pure and evolved *S. epidermidis* strain (B180).

These assays indicate that after 7 days, the resident population of *S. aureus* acquires and develops resistance against the invasions of the (B180) strain at the starting frequencies of 0.1 and 0.01, whereas when the invasion of the (B180) strain started at 0.001 frequency, the resistance of the resident population was not observed.
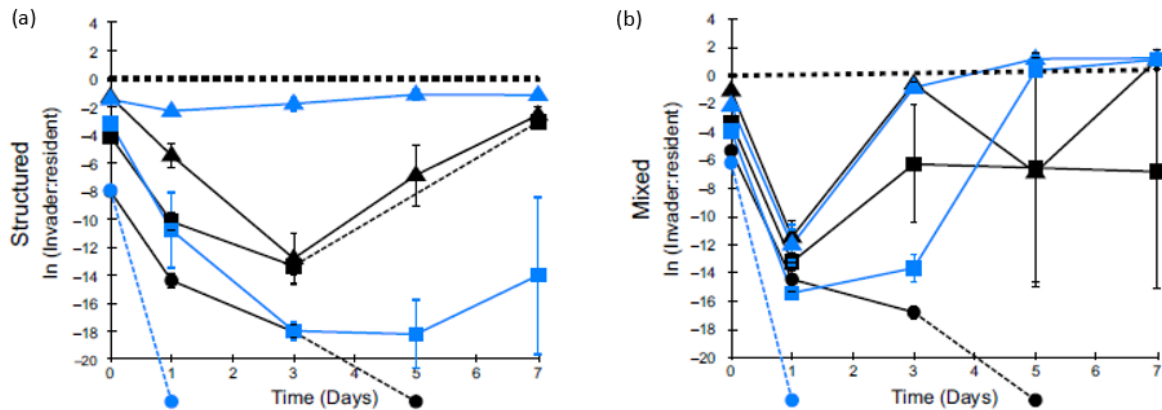
Figure 2.6: **Results of invasions by susceptible populations of *S. aureus* into inhibitory-producing populations of *S. epidermidis*.** Panel (a): *S. aureus* invading populations of toxin-producing (B155, black) and (B180, blue) *S. epidermidis* at frequencies of 0.1 (triangle), 0.01 (square) and 0.001 (circle) in a spatially structured regime. Panel (b): in a mixed regime. The x-axis is the time in days, and the y-axis is the natural log of the invader to resident ratio. A dotted line in the time course shows when the population dipped below the experiment detection threshold (for clarity, these lines also cross the x-axis if the population went to extinction). There is a heavy dotted line at 0 on the y-axis to indicate an equal invader to resident ratio. Error bars represent the standard error of the mean (n = 3). Taken from [122].

Moreover, when susceptible strains of *S. aureus* were sprayed over pure and evolved (B180), larger inhibition zones were produced by the evolved strain of *S. epidermidis* against *S. aureus* than the ancestral *S. epidermidis* strains, as shown in Fig (2.5C), which suggests that the emergence of the survival challenges, due to the progressive and increasing resistance of the resident population, led to modifying the invasive strain to become more virulent and aggressive. Thus, the evolved *S. epidermidis* may have upregulated production of the inhibitory toxins or developed alternative toxins.

2.3.3 Structured Environments Prevent *S. aureus* Invasions Into Inhibitory Populations of *S. epidermidis*

Here in this section, the results of the mutual invasions will be presented, [see Fig (2.4b)], when susceptible populations of *S. aureus* strain invaded toxic and non-toxic populations of *S. epidermidis* under spatially-structured and mixed conditions. In general, inhibitory-producing residents of *S. epidermidis* were more resistant to invasions than non-producing populations. Under spatially-structured conditions, toxic populations of *S. epidermidis* restricted and inhibited the invasions by *S. aureus*.

According to Fig (2.6a) and Fig (2.6b), there is a positive association between the initial frequencies of the invader and the speed of invasion. The highest initial concentration of the invader invaded fastest, while the lower concentrations vanished. If spatial structure is maintained, then inhibitor-producing bacteria can better prevent the invasion from low concentrations of *S. aureus*, whereas unstructured environments generally do not favour the production of inhibitory toxins.

2.3.4 The Appearance of Mutations Enhanced Invasions of *S. aureus*

The *Staphylococcus aureus* population was only able to invade the toxin-producing resident population of *S. epidermidis* under mixed conditions, as illustrated in Fig (2.4b), and Fig (2.6b).
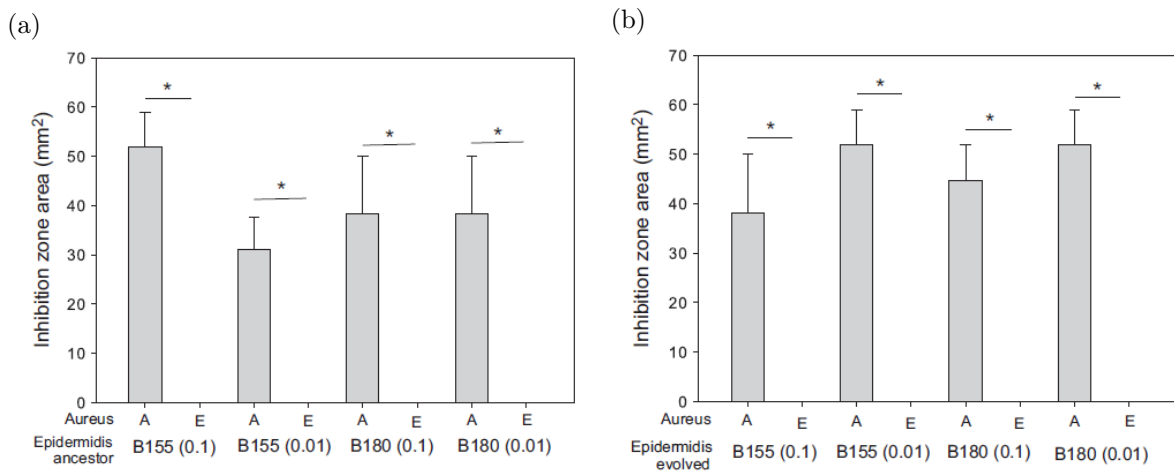
Figure 2.7: **The appearance of mutations enhanced invasions of *S. aureus*.** Panel (a): the inhibition zone area (mm^2) produced by the toxin-producing *S. epidermidis* strains (the ancestral B155, B180) against the ancestral SH1000 (A) and the evolved SH1000 (E). Panel (b): the inhibition zone area (mm^2) produced by the toxin-producing *S. epidermidis* strains (the evolved B155, B180) against the ancestral SH1000 (A) and the evolved SH1000 (E). Asterisks represent a significant difference between the inhibition zone areas of ancestral (A) and evolved (E) *S. aureus* strains. Taken from [122].

To determine whether the initiated resistance by *S. aureus* against the toxins produce

by *S. epidermidis* strains was the factor that supports the invasions in mixed environments, spray assays were performed where pure and evolved populations of *S. aureus* were sprayed over pure and evolved populations of *S. epidermidis* obtained from the toxin-producing resident populations.

In all cases pure and evolved toxin-producing populations of *S. epidermidis* showed no inhibition zones against the evolved populations of *S. aureus*; no inhibition zones were observed when spraying the evolved populations of *S. aureus* over both ancestral, Fig (2.7a), and evolved, Fig (2.7b), toxin-producing populations of *S. epidermidis*, which means that when the *S. aureus* strain was introduced into two different toxin-producing populations of *S. epidermidis*, (B155, B180), at relatively high frequencies (1 : 0.1) and (1 : 0.01), the evolved *S. aureus* populations were resistant to the toxins produced by both *S. epidermidis* strains.

The direction of invasions

	S. epidermidis → S. aureus				S. aureus → S. epidermidis			
Environmental structure	Structured		Mixed		Structured		Mixed	
Type of interactions	Inhibitory	Non-inhibitory	Inhibitory	Non-inhibitory	Inhibitory	Non-inhibitory	Inhibitory	Non-inhibitory
Species	B180 + SH1000	B115 + SH1000	B180 + SH1000	B115 + SH1000	SH1000 + B180	SH1000 + B115	SH1000 + B180	SH1000 + B115
	B155 + SH1000	B035 + SH1000	B155 + SH1000	B035 + SH1000	SH1000 + B155	SH1000 + B035	SH1000 + B155	SH1000 + B035
The invasion outcomes	Very successful	Successful	Not successful		Not successful		Successful	
Reasons	Toxins + environmental structures promote *S. epidermidis* invasions.	Environmental structures promote *S. epidermidis* invasions. Yet, resistance was observed.	The evolution of resistance by the *S. aureus* population.		Toxins + environmental structures inhibited *S. aureus* invasions.	*S. aureus* populations were able to successfully invade non-inhibitory resident populations of *S. epidermidis* regardless of the environmental structure. - The evolution of resistance enabled *S. aureus* populations to successfully invade inhibitory resident populations of *S. epidermidis*.		
The influence of initial population frequencies on the dynamics of interacted populations	(0.1 : 1) – Showed very osculated behaviour. (0.01 : 1) – Showed osculated behaviour. (0.001 : 1) – Invader went to extinction in most of interactions.				Invasions of *S. aureus* into resident populations of *S. epidermidis* were negatively frequency-dependent, with the lower frequency invaded better than the higher initial frequency. However, when the resident populations were inhibitory, the lowest density of *S. aureus* invaders went to extinction.			
Observations	- Similar colour codes indicate that the evolving populations exhibit similar behaviours. This means that in the first direction of invasions, when inhibitory and non-inhibitory isolates of epidermidis invaded resident populations of S. aureus, the environmental structure played a crucial role in determining the dynamics of interactions, whereas in the reverse direction, the dynamics of interactions differ based on the level of toxicity. - Several models suggest that the possibility of adapting to a hostile environment improves with higher population inflow [69, 88]. Increased immigration rates increase the likelihood that immigrants have advantageous mutations that have been pre-adapted to withstand extreme environments [87, 163]. - Spatial structure may hinder the spread of mutations because in spatially structured ecosystems, populations are composed of a number of semi-isolated subpopulations. As a colony expands, a decreasing proportion of the mutant population will compete with the ancestral genotype [75].							

Table 2.2: **A summary of the results presented in [122].**

61

2.4 Mathematical Translation of The Biological Concepts

In order to simulate the reported experimental outcomes, it must be taken into consideration that these outcomes reflect two types of interactions. The first type of interactions involved toxins, invasions, and interactions between *Staphylococcus aureus* (SH1000) and *Staphylococcus epidermidis* (B155, B180). The second type of interactions did not involve any toxin substances, where both evolved populations were competing for resources in the absence of other factors that might influence the outcomes, invasions, and interactions between *Staphylococcus aureus* (SH1000) and *Staphylococcus epidermidis* (B115, B035).

After observing and analysing the presented outcomes in the study, several conclusions were reached. In the first set of performed experiments, where toxin-producing and non-producing isolates of *Staphylococcus epidermidis* invaded resident populations of *S. aureus* (SH1000), the level of toxicity did not reflect a significant role in changing the outcomes. However, the environmental structure contributed to changing the behaviour of the interacting populations during the invasion process by preventing the reduction of the invasive strains at the beginning of the invasions in the structured environments. Hence, the dynamics of the interactions between these populations differ according to the environmental structure. From a holistic and general point of view, when isolates of *Staphylococcus epidermidis* invade populations of *S. aureus*, these invasions converge towards the same equilibrium point.

In the second part of the study, the second set of performed experiments, when toxin-producing and non-producing isolates of *Staphylococcus epidermidis* were invaded by populations of *S. aureus* (SH1000), the environmental structure did not influence the outcomes. However, the toxin production contributed to altering the outcomes of the invasions.

Before proceeding into mathematical programming and modelling of the obtained data, it is necessary to clarify some biological concepts that have been dealt with and programmed mathematically, for example the growth rate of competing populations as well as discrimination and application of the environmental structure mathematically.

2.4.1 Calculating The Growth Rate of The Involved Bacterial Species

According to the data presented in (Table 2.1), the *S. epidermidis* strains had comparable growth rates to SH1000. The table provides the doubling time for each strain in minutes. It is also known that these experiments were conducted in 7 days. Hence, to simulate and implement the time in the calculations, the time unit is defined by calculating the growth rate for each strain per day. Obtaining the doubling time of a bacterial population can only be done from the exponential growth phase. As a result, the equation that represents this phase is as follows:

$$y = y_0 \, e^{rt}, \tag{2.2}$$

where y is the concentration of the population, t is the time, y_0 is the value of y at time 0 and r is the the growth rate. Simply by re-arranging the equation (2.2), to be in this form:

$$t = \frac{\ln(y/y_0)}{r},$$

when $y = 1$, the time is denoted as t_1, thus:

$$t_1 = \frac{\ln(1/y_0)}{r},$$

when $y = 2$ (i.e., when y is doubled), the time is denoted as t_2, thus:

$$t_2 = \frac{\ln(2/y_0)}{r}.$$

Hence, the doubling time, which is denoted as T_d, can be calculated as follows:

$$T_d = t_2 - t_1 = \frac{\ln(2/y_0) - \ln(1/y_0)}{r},$$

$$T_d = t_2 - t_1 = \frac{\ln(2) - \cancel{\ln(y_0)} - \cancel{\ln(1)} + \cancel{\ln(y_0)}}{r},$$

as $\ln(1) = 0$, the equation simplifies to:

$$T_d = t_2 - t_1 = \frac{\ln(2)}{r} \implies r = \frac{\ln(2)}{T_d}.$$

The doubling time for each strain is given in minutes. From this information, it is possible to calculate the growth rate for each strain per minute, hour, and day as illustrated in (Table 2.3).

Strain	Growth rate per minute	per hour	per day
r_{SH1000}	0.00595	0.357	8.571
r_{B180}	0.00597	0.358	8.600
r_{B155}	0.0063	0.378	9.065
r_{B115}	0.00575	0.345	8.284
r_{B035}	0.00562	0.337	8.093

Table 2.3: **Estimation of the growth rate for strains used in this study.** Growth rates were estimated per minute, per hour, and per day.

2.4.2 Types of Environmental Structures

Initially, the environments were treated by considering the Petri dishes as zero-column vectors. The cultural spots were considered mathematical values representing the initial concentrations of the competing populations in the middle of those zero vectors. The length of these vectors represents the size of the dish, and the constructed matrix represents the evolution over time, Fig (2.8a). If L is the length of the vector, i.e., the size of the Petri dish, and n is the number of grid points, then Δx is the size of the space step.

$$\Delta x = L/n.$$

Similarly, the matrix represents the evolution of the competing populations over time, where t denotes the time, Δt the size of the time step, and h is the number of iterations. Thus the 1 space unit in the simulations in this study corresponds to $10\,cm$ in actual space measurements, and the 1-time unit corresponds to 1 day.
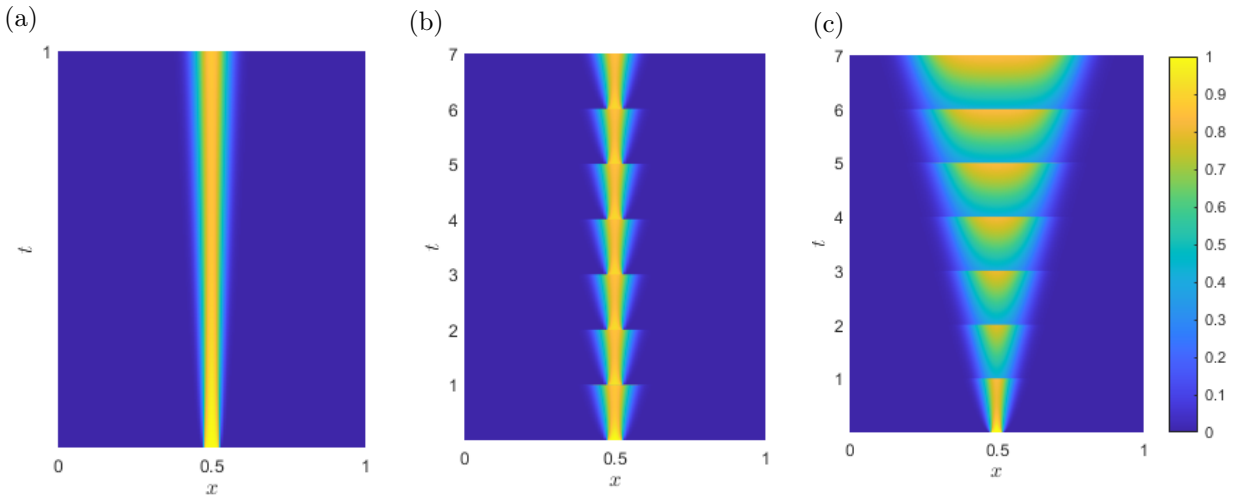
Figure 2.8: **Types of the environmental structure in simulations using the *Fisher* equation (1.3).** Panel (a): the mathematical simulation of the evolved population in a Petri dish for one day. Panel (b): a mathematical simulation of the evolution of a single population under mixed conditions for seven days. Panel (c): simulation of the evolution of a single population under structured conditions for seven days. The x-axis represents space (1 space unit corresponds to 10 cm). The y-axis represents time in days. In simulations: $\Delta x = 0.01, \Delta t = 0.004, D = 0.00045$ corresponds to $0.045\,cm^2/day$, and $r = 2$.

Biologically, the two types of environmental structures were distinguished when the competing populations were transferred into a new fresh medium every day. The communities were transferred to a new agar plate every day for seven days. Half of the replicates underwent a regime whereby the transfers were made by replica plating with velvet to maintain spatial structure. The other half of the replicates were subjected to a mixed regime in which the spatial structure was destroyed every 24 hours by scraping the entire bacterial lawn from the plate and transferring it to $10\,mL$ of sterile PBS before thoroughly vortexing and then pipetting $50\,\mu L$ onto a new plate to complete the transfer.

As a result, each day must be mathematically defined by specifying the number of iterations z.

$$z = h/t,$$

where z represents the number of iterations in one day. Therefore, during the simulations, whenever the vector where $mod(h, z) = 0$ is obtained, this mathematically means this is a new day. Therefore, as shown in Fig (2.8b), in a mixed environment, the obtained values in this vector were added and divided by the number of space grid points, and thus placed in the next column in the form of the spot, as illustrated initially. In the structured competitions, Fig (2.8c), all the obtained values were divided by the number of space grid points without the need to collect or add the values and placed as a spot in the upcoming vector to preserve the location of the values.

2.4.3 Types of Bacterial Motility and Distinguishing Features

It is fundamental to the study of any motility mechanism to determine whether it is active or passive [87]. Active motility involves an energy-dependent mechanism whereby the bacteria can control their direction. Passive motility is dependent on modulating the surroundings to generate movement. Active motility is generally distinguished from passive motility in two ways: (1) by demonstrating previously defined characteristics that are only associated with a known form of motility (e.g., observation of flagella on a bacterial cell suggests it may be capable of swimming motility) and/or (2) by identifying situations where the movement displayed can only be explained by active motility (e.g., the observation of the particular running movement of swimming bacteria cannot be explained by passive forces) [84].

Henrichsen conducted a significant study on defining motility as demonstrated in his paper, "Bacterial Surface Translocation: a survey and a classification". He performed a study of motile bacteria and analysed how they moved across surfaces and the features that defined the various types of observed movement [84]. Six types of motility were recognised and formally defined. Four were active, inherently requiring a molecular mechanism of propulsion: swimming, swarming, gliding, and twitching. Two forms of

movement were described as passive, where the motive force is generated by the bacterial community modifying the environment, resulting in sliding and darting movement. The definitions of the types of motility and the basis for each of them are summarised in (Table 2.4).

In conclusion, growing cultures of bacteria on solid medium differs from growing cultures of bacteria on liquid media, for instance the cultured bacterial population may be known to have active motility mechanism or if the surface, (BHI agar), is modified in a way to observe the passive, weak motility mechanism. Since none of these conditions applied to the conducted competitions, as *Staphylococcus* was historically regarded and considered as a non-motile organism, the Petri dishes were not modified to challenge the competing populations.

Hence, it can be determined that the outcomes of the conducted competitions will not differ greatly regardless of the type of the medium, which was confirmed when comparing the outcomes of competing populations in a tube and in a Petri dish. Mathematically, the diffusion coefficient in this case can be neglected or set $D \approx 0$, which is defined as the quantity of a substance which in diffusing from one region to another passes through each unit of cross section per unit of time when the volume-concentration gradient is unity, also called diffusivity [123, 211].

2.4.4 Estimating Diffusion Coefficients for Bacterial Species Assuming Brownian Motion

The impacts of motility and aggregation on the diffusion coefficient for bacteria were investigated in an aqueous system [79, 141]. The effects of cell concentrations, tube sizes, and dilution rates on the diffusion coefficient were examined. Generally, motile cells can diffuse about a thousand times faster than non-motile cells [79, 141]. The Stokes-Einstein equation provides a good estimate for the diffusion coefficient of large spherical molecules or particles in liquids. Movement of non-motile bacteria can be treated as diffusion of colloidal particles because colloidal particles extend from approximately $10\,nm$ to $1\,\mu m$ in diameter. Therefore, the Stokes-Einstein equation was used to estimate the diffusion coefficient for non-motile cells. The Stokes-Einstein equation is as follows:

$$D = \frac{K_B\,T}{6\pi\eta\,a},\tag{2.3}$$

where K_B is the Boltzman constant [105], T the temperature, η the viscosity of suspended medium, and a, the radius of the cell. By using the equation (2.3), a simple estimate can be made.

According to [80], the average cell radius of *S. aureus* is $440\,nm$, whereas as stated in

Type of motility	Example species	Original description in Henrichsen [84]
Swimming	*E. coli, P. aeruginosa*	"The micromorphological pattern is unorganised. The cells move individually and at random in the same manner as flagellated bacteria in wet mounts"
Swarming	*P. mirabilis, P. aeruginosa, B. subtilis*	"Swarming is a kind of surface translocation produced through the action of flagella but (it) is different from swimming. The movement is continuous and regularly follows the long axis of the cells, which are predominantly aggregated in bundles during the movement"
Twitching	*Neisseria, P. aeruginosa*	"Cells move predominantly singly although smaller moving aggregates occur. The movement appears as intermittent and jerky and do not regularly follow the long axis of the cell"
Gliding	*M. xanthus, Beggiatoa, Cyanobacteria*	"The movement is continuous and regularly follows the long axis of cells which are predominantly aggregated in bundles"
Sliding	*Streptococcus spp, S. aureus spreading*	"Sliding is a kind of surface translocation produced by the expansive forces in a growing culture in combination with special surface properties. The micromorphological pattern is that of a uniform sheet of closely packed cells In a single layer. The sheet moves slowly as a unit"
Darting	*Staphylococcus epidermidis*	"Darting is a kind of surface translocation produced by the expansive forces developed in an aggregate of cells inside a common capsule and resulting in the ejection of cells from the aggregate."

Table 2.4: **Different types of bacterial motility and distinguishing features.** A table outlining the feature as associated with motility both historically and the molecular basis/hypothetical explanations for it.

[112, 133], *S. epidermidis* is a gram-positive bacterium that appears spherical with a radius ranging between $250 - 750\,nm$ on light microscopy. In this study [122], a stage-top incubator was used to regulate the temperature to $37°C \approx 310K$, and the viscosity of the medium was estimated as the water viscosity. Plugging this temperature-dependent viscosity, $\eta = 0.69 \times 10^{-3} Kg\,m^{-1}s^{-1}$ [8, 189], into the Stokes-Einstein equation, yields:

$$D_{SH1000} = \frac{K_B T}{6\pi\eta\,a} \approx \frac{1.38 \times 10^{-23}\,m^2 Kg\,s^{-2}\,K^{-1} \times 310\,K}{6 \times 3.14 \times 0.69 \times 10^{-3} Kg\,m^{-1}s^{-1} \times 0.44 \times 10^{-6}\,m} = 7.48 \times 10^{-13}\,\frac{m^2}{s},$$
(2.4)

$$D_{B180} = \frac{K_B T}{6\pi\eta\,a} \approx \frac{1.38 \times 10^{-23}\,m^2 Kg\,s^{-2}\,K^{-1} \times 310\,K}{6 \times 3.14 \times 0.69 \times 10^{-3} Kg\,m^{-1}s^{-1} \times 0.5 \times 10^{-6}\,m} = 6.58 \times 10^{-13}\,\frac{m^2}{s}.$$
(2.5)

By converting the above units into the simulation units, i.e., $\frac{m^2}{s}$ into $\frac{cm^2}{day}$, equations (2.4) and (2.5) take this form:

$$D_{SH1000} = \frac{7.48 \times 10^{-13} \times 10^4}{1.16 \times 10^{-5}} = 6.45 \times 10^{-4}\,\frac{cm^2}{day}, \tag{2.6}$$

$$D_{B180} = \frac{6.58 \times 10^{-13} \times 10^4}{1.16 \times 10^{-5}} = 5.67 \times 10^{-4}\,\frac{cm^2}{day}. \tag{2.7}$$

As mentioned previously, *S. aureus* and *S. epidermidis* are considered non-motile species [28], and the expansion of the colony is caused by population growth [84], as explained in (Table 2.4) under the type of motility known as sliding. However, as noted earlier, both types of interactions in terms of the environmental structure, mixed and structured, were conducted in Petri dishes. Hence, for accuracy, it was necessary to estimate the diffusion coefficients of the evolved populations to determine if the evolved population motility, estimated in equations (2.6), and (2.7), affect and change the interaction dynamics or whether it can be ignored and neglected.

2.5   Modelling The Competitive Interactions in Mixed Environments

As previously stated, one type of interaction involved both populations competing for resources in the absence of other factors that could influence the outcomes of invasions and interactions between *Staphylococcus aureus* (SH1000) and *Staphylococcus epidermidis* (B115, B035). Hence, to mathematically simulate and model these types of interactions, competitive *Lotka-Volterra* equations [11, 148] were used. The system is similar to the

Lotka-Volterra equations for predation in that the equation for each species has one term for self-interaction and another term for interaction with other species. In the equations for predation, the base population model is exponential. For the competition equations, the logistic equation is the basis. The logistic population model, when used by ecologists, often takes the following form:

$$\frac{du}{dt} = r\, u \left(1 - \frac{u}{K}\right),$$

where u is the size of the population at a given time, r is the inherent per-capita growth rate, and K is the carrying capacity.

2.5.1 Two-variable Model

Given two populations, u and v, with logistic dynamics, the *Lotka-Volterra* formulation adds an additional term to account for the interactions of the species [148]. Furthermore, as explained earlier, by non-dimensionalising the system of equations and adding the diffusion term, the system of equations will take this form:

$$\begin{cases} \dfrac{\partial u}{\partial t} = D_u \dfrac{\partial^2 u}{\partial x^2} + r_u\, u\,(1 - u - b_1\, v), \\[2mm] \dfrac{\partial v}{\partial t} = D_v \dfrac{\partial^2 v}{\partial x^2} + r_v\, v\,(1 - v - b_2\, u), \end{cases} \tag{2.8}$$

where $u = u(x,t)$ and $v = v(x,t)$ are concentrations of S. aureus and S. epidermidis strains. Here:

- x is the space variable, so $x \in [0, L]$, where L is the length of the medium. (Size of Petri dish)

- t is the time variable, so $t \geq 0$.

- r the growth rate of the strains.

- D diffusion coefficient.

- b effect that each strain has on the other.

As illustrated in the previous section, growing bacteria cultures on solid mediums, such as Petri dishes, differs from growing bacteria cultures on liquid media such as tubes; for example, the cultured bacterial populations may be known to have an active motility mechanism or the surface (BHI agar) is modified to observe the passive, weak motility mechanism [23].

Since none of these conditions applied to these conducted competitions, *Staphylococcus* was historically regarded and considered as a non-motile organism [28, 84], and the

Petri dishes were not modified to challenge the competing populations. Hence, it can be determined that the outcomes of the conducted competitions do not differ greatly regardless of the type of the medium. This was confirmed when comparing the results of competing populations (SH1000+B155) in a tube and in a Petri dish.

Mathematically, simulations can also be compared that represent the outcomes of tube and Petri dish competitions by implementing the obtained diffusion coefficients of the evolved populations SH1000 and B180 in equations (2.6) and (2.7). If the results do not reflect a significant difference between these types of environments, then, in this case, the diffusion coefficient D can be neglected or set to the diffusion coefficient $D \approx 0$.

The principal reason behind such a procedure is that if it is proven that there is no significant difference in the outcomes of the two environments, it will be easier to find appropriate parameters to fit the model in this study to the obtained data by neglecting the space variation. The number of parameters that need to be determined will be reduced. Given the fact that if the space variation part (diffusion term) is maintained, the fitting process according to the (2.8) system of equations will go through four loops: the values of b_1 and b_2, also the time and space steps, since the growth rates were determined. Hence the fitting process will be time-consuming, especially when fitting the three-variable model as it contains extra parameters.

(a)　　　　　　　　　　　　　　　　　　　　　(b)
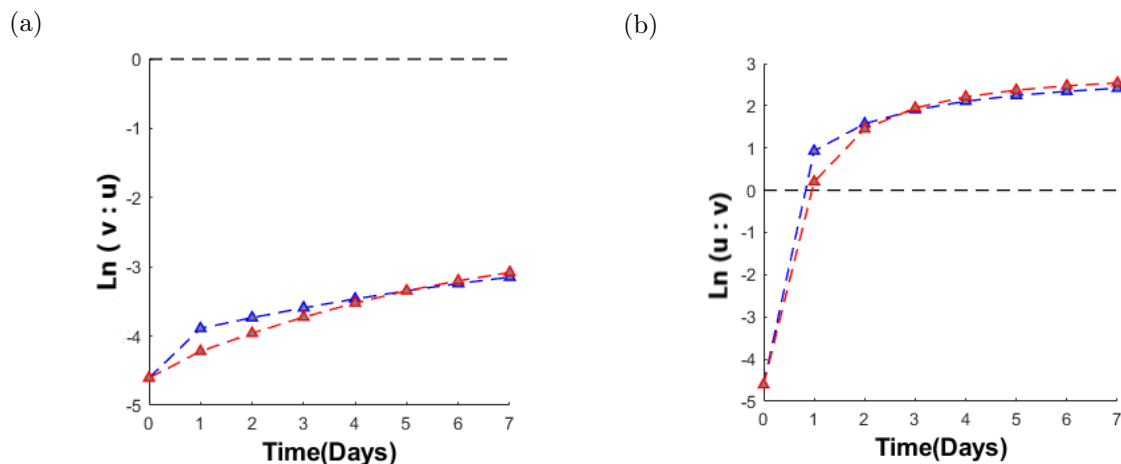
Figure 2.9: **Numerical simulations of competitive dynamics in models** (2.9) **and** (2.8)**.** Panel (a): the natural log of the invader to resident ratio when isolates of *S. epidermidis* (B180) invading populations of *S. aureus* (SH1000) at frequencies of 0.01. Panel (b): the natural log of the invader to resident ratio when isolates of *S. aureus* invading populations of *S. epidermidis* at frequencies 0.01. Blue line simulations are produced from (2.9), (tube). Red line simulations are produced from (2.8), (plate). Model parameters: $r_u = 8.571, r_v = 8.284, b_1 = 0.1, b_2 = 0.9, D_u = 0.0000065$ corresponds to $0.00065\, cm^2/day$ and $D_v = 0.0000057$ corresponds to $0.00057\, cm^2/day$. The x-axis is the time in days, and the y-axis is the natural log of the invader to resident ratio.

The difference between the tube and the dish mathematical simulations depends on the initial concentration of the competing populations. The initial concentrations of the competing populations in the tube can be represented by single values, e.g., $u_0 = 1, v_0 =$

0.01. In contrast, in the dish, vectors were constructed that represented the dish and the initial concentrations inserted for the competing populations as values in the middle of these vectors to represent the cultured mixed spot in the middle of the Petri dish. Since the growth rates for the competing populations were determined per day, the time unit was set to be $t = 7$, meaning seven days, which was the time consumed to conduct and perform the reported experiments.

Regarding the daily transfer of the competing population and introducing a fraction of the competing populations into a new medium, a dilution factor was fixed in both types of environments, where both competing populations were multiplied by this factor at the end of each day to dilute the concentrations and simulate the process of introducing the fraction of populations to a fresh new medium every day. Finally, as shown in Fig (2.9a), when isolates of *S. epidermidis* (B180) invade populations of *S. aureus* (SH1000), and Fig (2.9b), when isolates of *S. aureus* invade populations of *S. epidermidis* at frequencies 0.01, by obtaining the Matlab simulations and comparing the outcomes of different environments, it can be determined whether the motility of the bacterial population is considered to be passive or weak; the outcomes of the competing populations will not differ regardless of the incubator environment.

Hence, the diffusion term can be neglected to ease the mathematical simulations and fittings process. Thus, the system takes the following form:

$$
\begin{cases}
\dfrac{du}{dt} = r_u\, u\, (1 - u - b_1\, v), \\[2mm]
\dfrac{dv}{dt} = r_v\, v\, (1 - v - b_2\, u).
\end{cases}
\tag{2.9}
$$

2.5.2 Variation of Model Parameters

Many bacteria are of low motility, for example those typically colonising human skin or otherwise adhering to host cells [26, 72, 166]. Thus, after focusing on the case where bacterial motility rates are low and setting $0 \leq D \ll 1$, the variables b_1 and b_2 are varied to see all possible outcomes from the model.

It was decided to test different values of b_1 and b_2 when the population of *S. epidermidis* invaded the resident population of *S. aureus* at a frequency of (0.01: 1). Initially, the aim was to change both values of b_1 and b_2 while maintaining the ratio between these variables. For example, as illustrated in Fig (2.10a), which represents the profile of the interacted populations over time, and Fig (2.10b), which is the ratio between the evolved populations, $b_1 = 0.1, 0.5$ and 1, $b_2 = b_1/2$ was set.
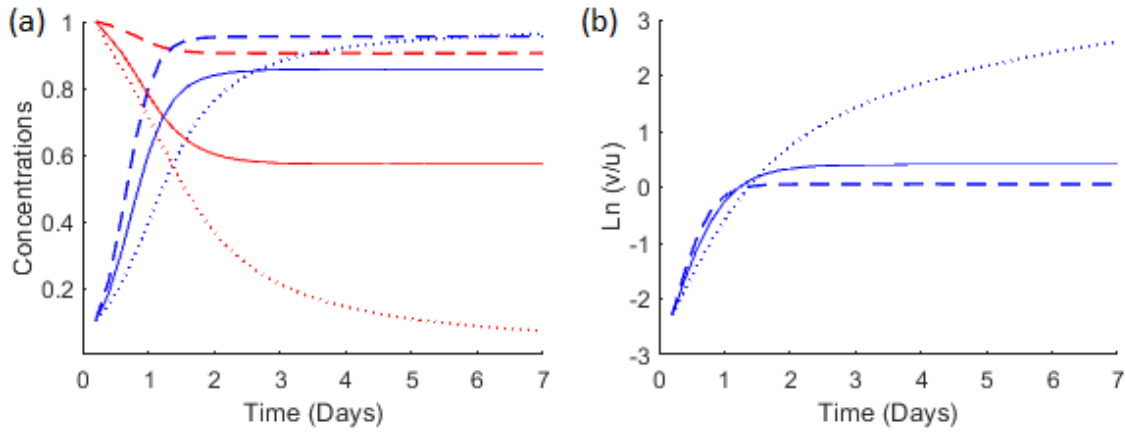
Figure 2.10: **The outcomes of the model** (2.9) **simulations when the ratio between** b_1 **and** b_2 **is fixed.** Panel (a): *S. epidermidis* (blue) invades populations of *S. aureus* (red) at an initial ratio of $(0.1 : 1)$. Dashed lines indicate weak interactions, where $b_1 = 0.1$ and $b_2 = 0.05$. Solid lines $b_1 = 0.5$ and $b_2 = 0.25$. Dotted lines represent strong interactions, where $b_1 = 1$ and $b_2 = 0.5$. Panel (b): the ratio between the evolved populations. Model parameters: $r_u = 8.571$ and $r_v = 8.284$. The x-axis in both panels is the time in days, the y-axis in panel (a) is the relative concentrations of invader and resident populations, and panel (b) is the natural log of the invader to resident ratio.

The findings in this study indicate that, in terms of time scale, the strength of the interactions is positively associated with the time consumed by both populations to reach the stationary phase. It was also found that different values of b_1 and b_2 lead to different equilibriums, Fig(2.10a). The dashed line represents the weakest interactions where both populations coexist and almost $u \approx v \approx 1$, hence, $\ln(v/u) \approx 0$.
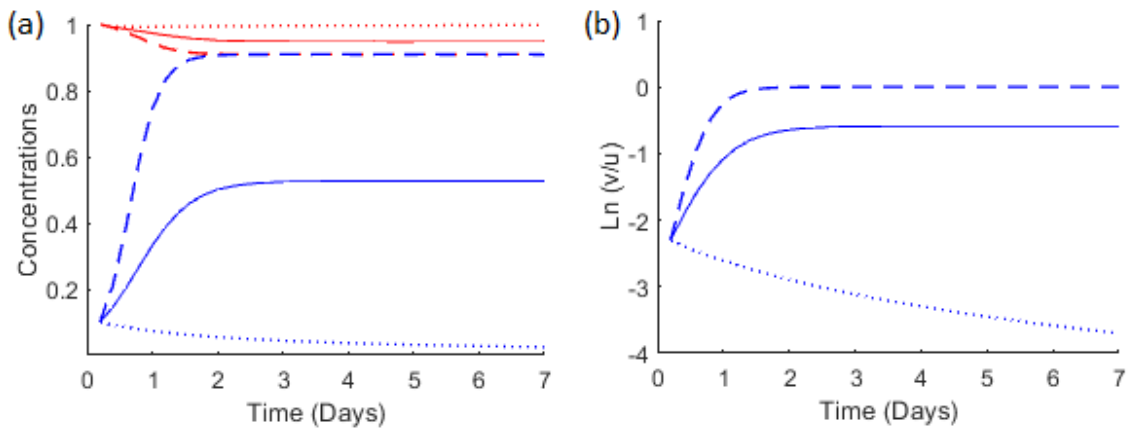
Figure 2.11: **The outcomes of the model** (2.9) **simulations when the value of** b_1 **is fixed, and the value of** b_2 **is varied.** Panel (a): *S. epidermidis* (blue) invades populations of *S. aureus* (red) at initial frequency of $0.1 : 1$. The value of b_1 is fixed to be equal to 0.1. Dashed lines indicate weak interactions, where $b_2 = 0.1$. Solid lines $b_2 = 0.5$. Dotted lines represent strong interactions, where $b_2 = 1$. Panel (b): the ratio between the evolved populations. Model parameters: $r_u = 8.571$ and $r_v = 8.284$. The x-axis in both panels is the time in days, the y-axis in panel (a) is the relative concentrations of invader and resident populations, and panel (b) is the natural log of the invader to resident ratio.

In addition, it was decided to vary one of the variables and fix the other to explore all possible outcomes, as shown in Fig (2.11a, b), when $(b_1 = 0.1, b_2 = 0.1)$ the invader (blue) successfully invaded the resident population, as illustrated by the dashed line.

However, the dotted line indicates that the invader population was inhibited and restricted by the resident population (red) at $(b_1 = 0.1, b_2 = 1)$.
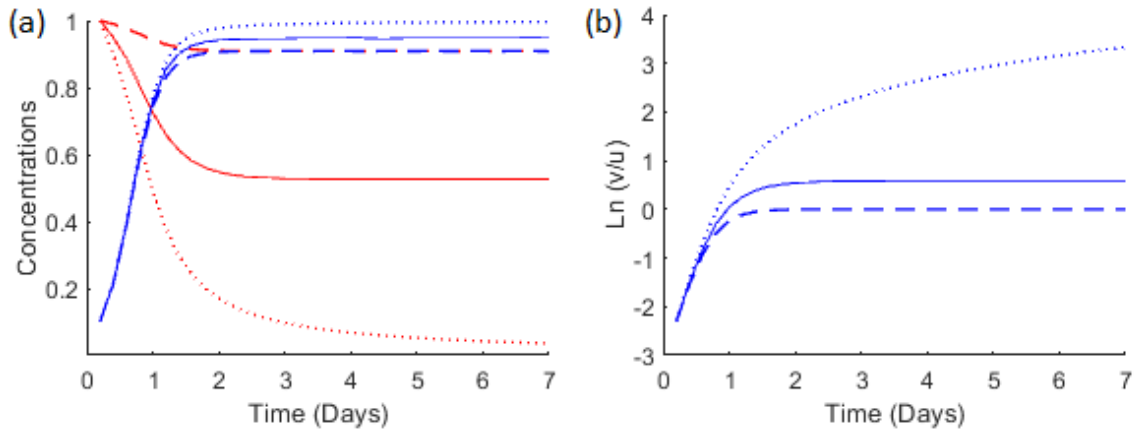
Figure 2.12: **The outcomes of the model** (2.9) **simulations when the value of b_2 is fixed, and the value of b_1 is varied.** Panel (a): *S. epidermidis* (blue) invades populations of *S. aureus* (red) at initial frequency of $0.1 : 1$. The value of b_2 is fixed to be equal to 0.1. Dashed lines indicate weak interactions, where $b_1 = 0.1$. Solid lines $b_1 = 0.5$. Dotted lines represent strong interactions, where $b_1 = 1$. Panel (b): the ratio between the evolved populations. Model parameters: $r_u = 8.571$ and $r_v = 8.284$. The x-axis in both panels is the time in days, the y-axis in panel (a) is the relative concentrations of invader and resident populations, and panel (b) is the natural log of the invader to resident ratio.

This can be presented contrariwise, as shown in Fig (2.12a), which represents the profile of the interacted populations over time, and Fig (2.12b), which is the ratio between the evolved populations, when the value of $(b_1 = 0.1, 0.5, 1)$, and the other variable b_2 is fixed at 0.1. It was noted that the invader population restricted the growth of the resident population and took over when $(b_1 = 1)$, as illustrated by the dotted line.
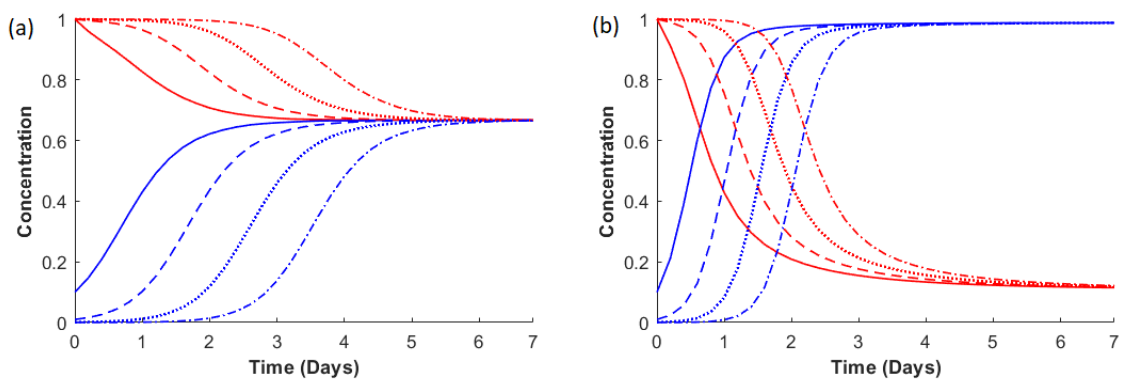
Figure 2.13: **The outcomes of the model** (2.9) **simulations assuming different initial concentrations.** *S. epidermidis* (blue) invading populations of *S. aureus* (red) at an initial frequency of $(0.1 : 1)$ solid lines, $(0.01 : 1)$ dashed lines, $(0.001 : 1)$ dotted lines, and $(0.0001 : 1)$ dashed dotted lines. Panel (a): $b_1 = b_2 = 0.5$. Panel (b): $b_1 = 0.9, b_2 = 0.1$. The x-axis is the time in days, and the y-axis is the relative concentrations of the evolved populations.

Finally, both variables were fixed to certain values and the initial concentration of the competing populations changed to be (invader: resident) $= (0.1 : 1), (0.01 : 1), (0.001 : 1)$

73

and $(0.0001 : 1)$. As shown in Fig (2.13a), when $b_1 = b_2 = 0.5$, and Fig (2.13b), when $b_1 = 0.9, b_2 = 0.1$, a negative association between the initial concentrations of the competing populations and the time consumed to reach the equilibrium can be concluded.

2.5.3 Fitting The Model to The Experimental Data

The time unit in system simulations (2.9) is defined as $t = 1$, corresponding to one day in actual experimental data by determining the growth rate for each strain per day, $r_u = 8.571$ and $r_v = 8.284$. Initial conditions:

$$u_0 = 1, v_0 = a \cdot u_0 \text{ where } a = 0.1, 0.01 \text{ or } 0.001.$$

This can be presented contrariwise when performing the mutual invasions.

(a)

(b)
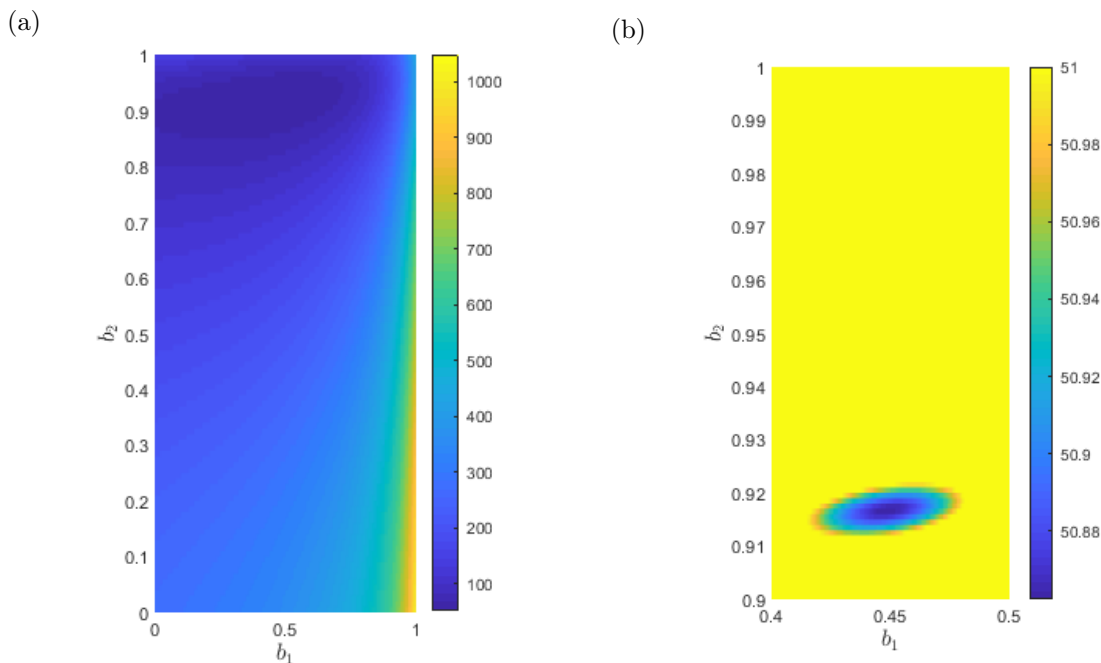
Figure 2.14: **The mean squared error of regression when estimating b_1 and b_2.** Fitting the model (2.9) parameters to the experimental data by varying the values of both variables, b_1 and b_2 and plotting the mean square error against them. Panel (a): surface plot of the errors for all initial concentrations, second method. Panel (b): surface plot of the same error spot after narrowing down both b's axes. The x-axis represents b_1 values, while the y-axis represents b_2 values.

To obtain the best fit with the lower error value, the least squares fitting technique was performed, which is a mathematical procedure for finding the best-fitting curve to a given set of points by minimising the sum of the squares of the offsets ("the residuals") of the points from the curve. The sum of the squares of the offsets is used instead of the absolute offset values as this allows the residuals to be treated as a continuously differentiable quantity. Also, by varying both values of b_1 and b_2, as shown in Fig (2.14), it was possible to find the best values for both variables to fit the experimental data.

Two methods were used to fit the experimental data to the model simulations. In the first method, it was decided to separate the experimental data based on the initial concentrations and find the best values for b_1 and b_2 with the lowest error value for each concentration. Thus, three different values with the minimum error recorded were obtained as following: when the initial ratio of concentration for the competing populations (invader: resident) is equal to (0.1:1), $b_1 = 0.687$ and $b_2 = 0.952$; when the initial ratio is equal to (0.01:1), $b_1 = 0.601$ and $b_2 = 0.95$; when the initial ratio is equal to (0.001:1), $b_1 = 0.332$ and $b_2 = 0.9$.

After obtaining three values for b_1 and b_2, the value for each parameter was averaged, as following:

$$b_1 = 0.687 + 0.601 + 0.332 = 1.62/3 = 0.54,$$

$$b_2 = 0.952 + 0.95 + 0.9 = 2.802/3 = 0.934.$$

According to the model (2.9), b_1 represents the effect of *S. epidermidis* on *S. aureus* while b_2 is the effect of *S. aureus* on *S. epidermidis*. As *S. aureus* had the advantage in the invasions, it is known that $b_2 > b_1$. However, from fitting the experimental data to the model simulation process, it was noted that there is a positive association between the initial concentrations and the strength of the effect on the other strain. When the initial ratio of concentrations between the competing strains were (0.1 : 1) the value of $b_1 = 0.687$ and $b_2 = 0.952$, while $b_1 = 0.332$ and $b_2 = 0.9$ when the initial ratio of concentrations between the competing strains were (0.001:1).

In the second method, shown in Fig (2.14), the aim was to find the best values for b_1 and b_2 corresponding to the minimum error for all the experimental data without separation by constructing a vector and inserting all the reported data into the same vector, where the first set of inputs represents the invasion by *S. epidermidis* into the population of *S. aureus* at the frequencies of (0.1: 1), (0.01: 1), and (0.001:1), respectively. The second set of inputs represents the opposite direction of invasions at the same order of frequencies.

After obtaining two sets of parameters from different fitting methods, the set of parameters that satisfied the minimum error was applied. As illustrated in Fig (2.15a), when using the set of parameters obtained from the first method, and Fig (2.15b) where parameters obtained from the second method, both methods yield almost similar error values. The technique with the minimum error was applied, fitting the whole data without separations.

The simulations of the two-variable model concurred with the actual results in terms of the last state of the competing populations, see Fig (2.15). However, the dynamics were different. If the black dots are closely examined, which represent the actual ratio between the interacted populations obtained from the experimental data, it will be apparent that when invasions by *S. epidermidis* populations were undertaken in mixed environments,

the resident populations of *S. aureus* were able to inhibit and restrict these invasions at the beginning of the invasion period. Afterwards, the invader populations were able to recover and reach the same invader-to-resident ratio as in the structured environment.
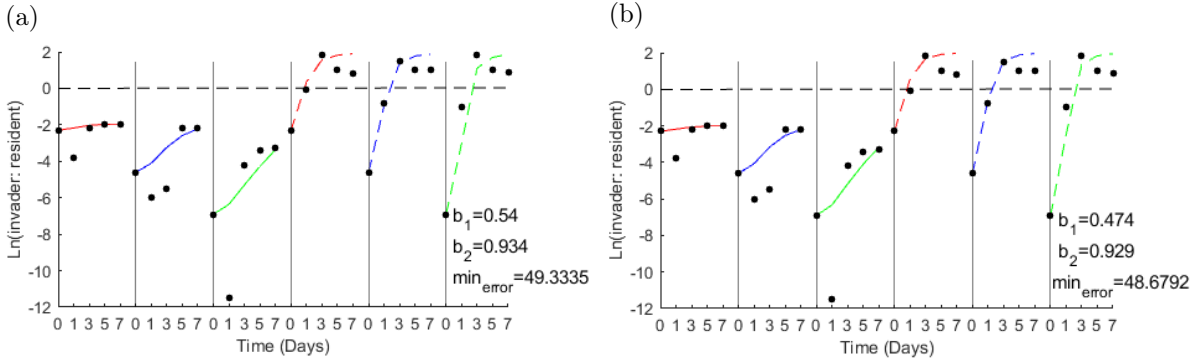
Figure 2.15: **Fitting the model** (2.9) **parameters to the experimental data presented in [122].** Panel (a): using the first method; averaged values of the parameters, $b_1 = 0.545$ and $b_2 = 0.934$, the minimum error is $= 49.334$. Panel (b): using the second method to define the parameters, $b_1 = 0.474$ and $b_2 = 0.929$, the minimum error is $= 48.679$. Black dots represent the experimental data, solid lines represent the (2.9) simulations when *S. epidermidis* is the invader, dashed lines when *S. aureus* is the invader. The x-axis is the time in days, and the y-axis is the natural log of the invader to resident ratio. Different colours indicate different initial ratios between the invader and resident, (0.1:1, red), (0.01:1, blue), and (0.001:1, green).

When susceptible populations of *S. aureus* invaded populations of *S. epidermidis* in different environmental structures, the model simulations were closer to the experimental data, except for the fact that in experimental observations in a structured environment, both populations tend to be equal, while in the model simulations there were no such observations.

2.5.4 Qualitative Difference Between Model Simulations and Experimental Results

The dynamics of actual experimental data indicate a non-monotonic behaviour, i.e., one population recovers and mutates against the invasion. The two-variable model cannot produce such behaviour. As demonstrated by the obtained figures representing the two variable model simulations, the rate of change in population concentrations over time $\frac{d}{dt}\left(\frac{u}{v}\right)$ does not change the sign (i.e., if one of the competing populations is increasing, it is always increasing, and if it is decreasing, it is always decreasing). To prove that theoretically, we start by defining the expression $\frac{d}{dt}\left(\frac{u}{v}\right)$ as following:

$$\frac{d}{dt}\left(\frac{u}{v}\right) = \frac{v\,u^{'} - u\,v^{'}}{v^2}.$$

From 2.9, u' and v' can be defined as:

$$\frac{d}{dt}\left(\frac{u}{v}\right) = \frac{\not{v}u(1 - u - b_1 v) - u\,r\not{v}(1 - v - b_2 u)}{\not{v}^2},$$

$$\frac{d}{dt}\left(\frac{u}{v}\right) = \frac{u}{v}\left((1 - u - b_1 v) - r(1 - v - b_2 u)\right),$$

$$\frac{d}{dt}\left(\frac{u}{v}\right) = \frac{u}{v}\left((1 - \not{r}) + (rb_2 - 1)u + (r - b_1)v\right).$$

Assume $\frac{u}{v} = x$, hence,

$$x' = xv((rb_2 - 1)x + (r - b_1)).$$

Therefore, for the function $\frac{u}{v}$ to change behaviour over time it must change its sign from positive to negative or vice versa. To change the sign, it must cross the zero. When the function approaches zero it stabilises i.e., $\frac{d}{dt}\left(\frac{u}{v}\right) = 0$, as shown in Fig(2.16).

Thus, it can be concluded that to simulate the observed non-monotonic behaviour, it is necessary to introduce a third variable to the previous model. From a biological point of view, the introduction of a third variable is to represent the adapted fraction of the populations.
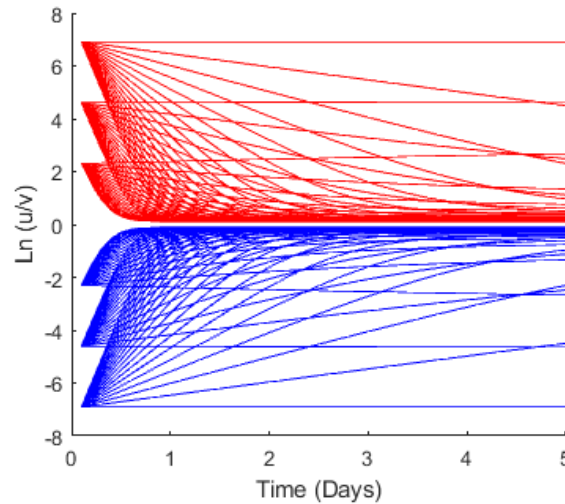
Figure 2.16: **Illustrations of monotonic behaviour of two variable model.** Blue lines when $u_0 = 0.1, 0.01$ and 0.001 and $v_0 = 1$. Red lines when $u_0 = 1$ and $v_0 = 0.1, 0.01$ and 0.001. b_1 varied between 0 to 0.9 by the step size 0.05, $b_2 = b_1 + 0.1$.

According to the findings presented in paper [122], another set of experiments were performed to test whether the evolution of inhibitory resistance by *S. aureus* was responsible for inhibiting invasions in a mixed environment, as shown in Figs (2.6,A,C). Ancestral and evolved *S. aureus* strains were sprayed over ancestral and evolved *S. epidermidis* toxin-producing residents.

In all cases, evolved *S. aureus* were resistant to the *S. epidermidis* toxin Fig (2.7). This was justified as follows: the more likely explanation for resistance evolution is that the higher inoculation frequencies increased the chance of these invading populations containing beneficial resistance mutations. Thus, in the following section of this chapter, the metapopulation concept will be presented, the term "metapopulation" referring to a group of spatially- separated populations of the same species that have some form of mutual interaction [70, 76, 88, 89, 163].

2.5.5 Three-variable Model

As previously highlighted, the simulations of the two-variable model concurred with the actual experimental findings in terms of the last state of the competing populations. However, the dynamics were different.

The dynamics observed in actual experimental data, when isolates of *S. epidermidis* invaded resident populations of *S. aureus*, indicated that many of the invasive strain individuals died before the later emergence of the adaptation behaviour. Generating and simulating such behaviour requires a third variable to be added to the previous system to represent the susceptible fraction of the invader populations.

Thus, the system of equations takes this form:

$$
\begin{cases}
\dfrac{du}{dt} = r_u\, u\, (1 - u - b_1\, v_s - b_2\, v_a), \\[2mm]
\dfrac{dv_s}{dt} = r_v\, v_s\, (1 - v_s - b_3\, u - v_a), \\[2mm]
\dfrac{dv_a}{dt} = r_v\, v_a\, (1 - v_a - b_4\, u - v_s),
\end{cases}
\tag{2.10}
$$

where u, v_s and v_a are concentrations of *S. aureus* and susceptible and adapted *S. epidermidis* strains, respectively. Initial conditions:

$$
u(0) = 1,\ v_s(0) + v_a(0) = a \,.\, u(0) \text{ where } a = 0.1, 0.01 \text{ or } 0.001 \text{ and } v_a/v_s = 0.01.
$$

This can be presented the other way around when performing the mutual invasions.

2.5.6 Fitting The Model to The Experimental Data

As illustrated previously, to obtain the best fit with the lowest error value the least squares fitting technique was performed and by varying values of b_1, b_2, b_3 and b_4 by constructing loops, it was possible to find the best values for the variables to fit the experimental data.
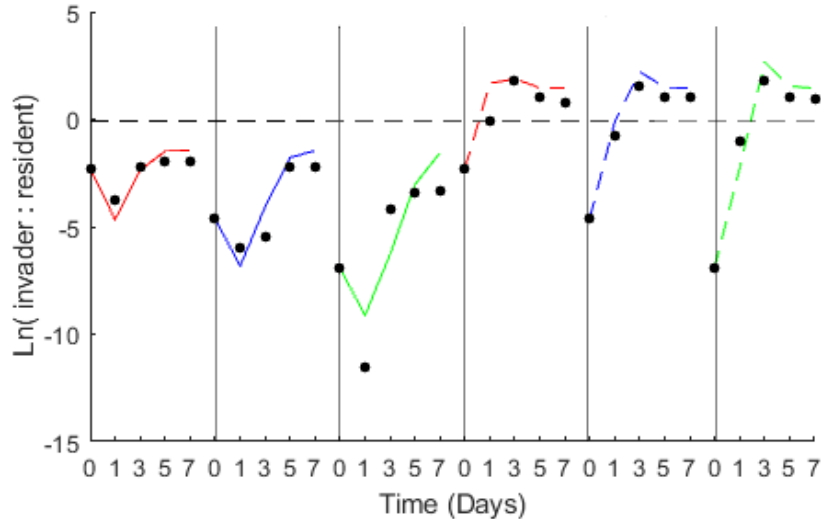
Figure 2.17: **Fitting the model** (2.10) **parameters to the experimental data presented in [122].** The best values for b_1, b_2, b_3 and b_4 with minimum error value for all concentrations. Black dots represent the experimental data, solid lines represent the (2.10) simulations when *S. epidermidis* is the invader, dashed lines when *S. aureus* is the invader. The x-axis is the time in days, and the y-axis is the natural log of the invader to resident ratio. Different colours indicate different initial ratios between the invader and resident, (0.1:1, red), (0.01:1, blue), and (0.001:1, green). Model parameters: $r_u = 8.571$, $r_v = 8.284$, $b_1 = 0.11$, $b_2 = 0.46$, $b_3 = 1.36$, and $b_4 = 0.79$.

The figure (2.17) depicts the model simulations (solid lines) plotted against the actual data (black dots) after obtaining the best values for b_1, b_2, b_3, and b_4 with the lowest error value across all concentrations.

The addition of the third variable to the system of PDEs improved the simulation outcomes to become closer to the dynamics and behaviour of the interacting populations that were observed in the experimental data. Furthermore, the addition of the third variable made it possible to observe the tendencies of both competing populations to equalise. Such behaviour was not obtained from two-variable model simulations.

2.6   Conclusions

The study presented in this chapter has several aims, as explained in the introduction. In this section, the overall outcomes achieved throughout the work in this chapter will be presented. Also, the difficulties and obstacles that prevented the achievement of the desired goals will be explored.

The first goal, which was to provide an overview of the aim and different biological aspects and experimental methods described in (Libberton, Horsburgh, and Brockhurst, 2015) [122], was set out in the first and second sections of this chapter. The presented study aimed to investigate the effects of spatial structure, frequency dependence, and resistance evolution on the dynamics of toxin and non-toxin mediated microbial invasions. Also, the aim was to test whether manipulating the factors that govern these interactions prevents the spread of the pathogenic species *S. aureus*.

The methods used in the investigation can be summarised briefly as mutual invasions being performed between toxin-producing and non-producing nasal isolates of *S. epidermidis* on the one hand and populations of toxin-sensitive *S. aureus* on the other. Invasions were launched at three different frequencies (0.1, 0.01, and, 0.001). All evolved communities were grown on solid agar for 7 days, with communities being moved to fresh medium every day. In half of the replicates, the population structure maintained the same with each transfer, while in the other half, the population structure changed with each transfer.

In addition, the aim was to provide an analysis of the experimental results obtained in Paper [122]. Such aim was addressed in depth in the third section of this chapter. Mainly the findings of Paper [122] suggested that alteration of the nasal microbial ecology may be utilised to restrict *S. aureus* colonisation, hence reducing transmission and infection rates.

Based on the reported data, it was possible to partially achieve the third and fourth aims, which concerned developing mathematical models to explain and simulate the inhibitory and non-inhibitory interactions observed in laboratory experiments, and to fit the introduced model parameters to experimental data.

As indicated previously, the study presented two types of interactions: inhibitory and non-inhibitory. It was possible to model non-inhibitory competitions mathematically by using two different models.

In general, when modelling the competitions, the aim is to begin by using the simplest model that could generate simulations satisfying the reported data and provide insight into the observed dynamics. This method seeks to make the presentation as accessible as possible by limiting the level of mathematical complexity required to describe how the model's ecology arises from mathematics and to address the criteria for evaluating the mathematical models presented earlier in Section (1.3.1), which indicates that the number of parameters should be as few as possible to maximise consistency and, consequently, explanatory power. Therefore, the first model was based on two variables representing the concentrations of the bacterial species involved.

Although this model concurred with the experimental data regarding the final states of the competing populations, (at day 7), the two-variable model was, in some cases, unable to simulate the dynamics and behaviour of the evolved populations during the first days of the competitions.

Hence, the model was improved by introducing an extra variable that represents the susceptible fraction of *S. epidermidis* populations to observe the declining behaviour of *S. epidermidis* populations at the beginning of their invasions into susceptible populations of *S. aureus*. As a result of this addition, the simulations obtained by the three-variable model conformed with the experimental data regarding the dynamics of the competing populations and the final states of the evolved populations.

For various reasons, the inhibitory interactions were not modelled in this chapter, perhaps the most salient being the inability to understand and justify some of the outcomes. For example:

1. The effect of inhibitory production was evident in one direction of invasion but not in the other:

   (a) **When toxin and non-toxin populations of S. epidermidis invaded populations of S. aureus**;
   The environmental structure had an effective role in changing the dynamics of interactions, regardless of the level of toxicity of these interactions.

   (b) **However, when toxin and non-toxin populations of S. epidermidis were invaded by populations of S. aureus**;
   The level of toxicity had an effective role in changing the dynamics of interactions regardless of the environmental structure.

   Thus, it was believed that it is difficult to introduce a model with fixed conditions that satisfy both directions of invasions.

2. Furthermore, from a mathematical point of view, the author of this thesis maintains that, unlike the non- inhibitory interactions, the inhibitory interactions stopped before the evolved populations stabilised or even converged to a certain point. Hence, it cannot be stated with certainty that the final ratio between the interacted population reported in this study, which was after 7 days, will remain stable.

Aside from these challenges, it was important to re-perform these experiments before developing mathematical models to represent the inhibitory interactions:

1. To obtain a comprehensive understanding of the nature of these interferences.

2. To extend the duration of these interactions until the difference in evolved population density was no longer substantial.

3. To clarify several concepts that are neither presented nor addressed in Paper [122].

Based on the above presented challenges, the opportunity was provided by Dr. Malcolm J. Horsburgh to perform further investigations and experiments to obtain a broader view and a better understanding of some biological aspects. Thus, the following chapter will introduce a combined experimental and theoretical study of the dynamics of interacting populations in a mixed environment.

Chapter 3

Study of The Dynamics of Interacting Populations in A Mixed Environment

3.1 Introduction

Over the years, the capacity to develop medicines to treat bacterial infections has resulted in significant progress in terms of reducing mortality rates [49]. The ability of bacteria to evolve, mutate, and reclaim control of the resident microbiome, on the other hand, demands the creation of alternative methods and approaches [65].

The importance of the microbiota in avoiding the colonisation and proliferation of the pathogens is increasingly recognised [74, 102]. Most of the mechanisms for this beneficial effect of probiotic bacteria are indirect and include modification of the immune system, improvement of the intestinal epithelial barrier, or competition with pathogens for nutrients [20, 71, 102, 130]. Bacteriocin proteins, which can kill pathogenic bacteria, are produced by several probiotic strains, and it has been demonstrated that an inhibitory generating *Escherichia coli* strain reduces colonisation by related pathogenic bacteria in the inflamed stomach of mice [181]. There is currently no proof that these systems are significant or common in humans. However, it is widely asserted that a probiotic diet improves human health [165, 181].

Several studies indicate that *S. epidermidis* and *S. aureus*, which are the two dominant species in the nasal microbial community [212, 219], have negatively correlated distributions across nasal communities, suggesting that these species participate in one-way or mutual exclusion [61, 121, 124, 212].

This method was demonstrated in the successful treatment of antibiotic-resistant bacteria that had been inhibited and restrained in growth when the host patient experienced a transplant from a healthy individual, helping to restore the beneficial resident bacteria by reproducing their abundance in the infected microbiome. When using the described population interactions, both bacterial strains will attempt to remain in a symbiotic environment, where they can transfer through all stages of their planned development until

eventually collapsing with minimum disturbance. When a resident species of bacteria acts in its own habitat in isolation, referred to in biological terminology as intra-specific competition, it aims to maintain the same level of growth regardless of any interaction from other species. If preyed upon, it must also have the essential characteristics, whether it be the ability to generate or suppress toxins or the potential to mutate against them, to restore and sustain its size. Interactions and continuous competitions among different bacterial species involve many complex aspects.

In the previous chapter, two models were developed which successfully simulate the interactions between non-inhibitory populations competing under mixed conditions. Regarding the inhibitory interactions, it was not possible to develop a model capable of simulating the reported data for various reasons. For instance, the effect of the toxins produced by the inhibitory populations was inconsistent in both directions of invasions. In addition, the interactions lasted only seven days, and the evolved populations had not yet settled.

Therefore, it was determined that to model the inhibitory interactions, it was necessary to introduce a new set of experiments to better investigate the hypothesis, which assumes that the interactions between bacterial communities limit the colonisation of pathogenic bacteria [122], and to conduct these interactions over a more extended period until these evolved populations converge toward a particular point or the change in their density is no longer significant. Thus, the study presented in this chapter aims to:

- Re-perform the experiments presented in the previous chapter that involve inhibitory interactions under mixed environmental conditions to understand the biological aspects and experimental techniques better and answer the questions raised in the previous chapter.

- Perform a series of experiments involving the selected species before engaging them in competitions to determine their characteristic features.

- Examine inhibitory production and resistance evolution in invasion and competition under mixed conditions.

- Extend the duration of the interactions to investigate the behaviour of the evolved species.

- Perform a set of experiments involving the selected species after engaging them in the competitions to determine to what extent the interactions changed their characteristic features.

- Develop mathematical models to explain and simulate the behaviour of evolved species when cultured separately, as well as explain and simulate the dynamics of interactions under mixed conditions.

- Fit model parameters to experimental data.

- Perform numerical experiments to test and validate the three and four-variable model hypotheses.

3.2 An Overview of Species Used and Experiments Performed in This Chapter

Obtaining mathematical models capable of simulating the dynamics of these interactions, considering the differences in the conditions governing these interactions, must be achieved through a deep understanding of the biological aspects. Close observation of

Species	Strain identifications	Inhibitor
S. aureus	SH1000	Non-producing
S. epidermidis	B180	Uncharacterised antibiotic
S. epidermidis	B155	Epifadin [67]
S. epidermidis	TU3298	The lantibiotic epidermin [144]

Table 3.1: **Identification of strains used in this study.**

the nature of these interactions would provide the opportunity to produce a model that could be considered a reflection of the dynamic processes involved therein and in making practical predictions.

The experiment	Purpose of the experiment
Incubating replicates for each strain at $37°C$ for 24 h, and taking OD_{600} readings at 30-min intervals.	To determine the growth rate and generation time of bacteria.
Incubating replicates for each strain in Petri dishes at $37°C$ for 24 h, and taking the measurements of the spot in each strain before and after incubating.	To determine the rate of change in the spot size which is known as the diffusion coefficients.
The growth inhibition assay, experimental study of toxin-mediated inhibition, pre-interactions.	To determine the sensitivity of *S. aureus* strain against the toxins produced by *S. epidermidis* populations.
Interactions, (competitions and inhibitions)	To observe the dynamics of these interactions under different conditions.
The growth inhibition assay, after interactions	To evaluate the adaptations behaviour developed by *S. aureus* strain against the toxins produced by *S. epidermidis* populations.

Table 3.2: **A brief overview of experiments conducted in Dr Malcolm Horsburgh's laboratory.**

Here in this chapter, the possibilities of producing such a model by experimentally and theoretically defining such microbial interactions will be explored. In other words, both experimental and theoretical studies that cover different aspects of single and multi-species populations evolutions will be presented before presenting and introducing detailed explanations of these studies. (Table 3.1) presents an illustration of strains used in this study.

Furthermore, (Table 3.2), demonstrates a brief illustration and overview of experiments conducted and performed in Dr. Horsburgh's laboratory in the Institute of Integrative Biology, University of Liverpool.

3.3 Bacterial Growth Rate Dynamics

Bacteria were frequently cultured in $10\,ml$ Brain Heart Infusion (BHI) broth (LabM) in a $20\,ml$ glass universal tube. Cultures were grown at $37°C$, shaken at $200\,rpm$, revolutions per minute. Overnight cultures were typically grown for around $18 - 24\,h$. Exact details of the media can be found in (Table 3.3). Strain stocks were preserved by adding either $700\,\mu l$ of an overnight culture, or a single colony collected from a plate and resuspended in $700\,\mu l$ of BHI broth (LabM) to $300\,\mu l$ of 50 (v/v), volume per volume glycerol and freezing at $-80°C$. Duplicates were made of all freezer stocks.

Media / Buffers / Antibiotic	Composition
BHI agar plates	3.7% (w/v) BHI Broth (Lab M), 1.5% (w/v), weight per volume Agar-(Lab M), distilled water, $dd\,H_2O$
BHI broth	3.7% (w/v) BHI Broth (Lab M), $dd\,H_2O$
Mannitol salt agar	10.8% (w/v) Mannitol Salt Agar (labM), $dd\,H_2O$
PBS	0.8% (w/v) $NaCl$, 0.034% (w/v) KH_2PO_4, 0.12% (w/v) K_2HPO_4

Table 3.3: **Components for reagents used throughout this study.**

3.3.1 Experimental Techniques

Overnight cultures of each strain in Table (3.1) were incubated for 24 h in Growth Profiler 960 device, which generates growth curves of up to 960 microbial cultures in microtiter plates. Because oxygen-transfer rates are readily reached (at $225rpm/50mm$), exponential growth occurs up till OD_{600} values of $3 - 10$ (depending on the strain and its specific oxygen demand), which allows an accurate determination of maximal growth rates, see example curves at Fig (3.1). The shaker unit can be set to slow down (e.g.,

every 30 minutes) to $30 rpm$ for a few seconds. In these few seconds the culture comes temporarily to a rest (surface becomes close to horizontal), and the 10 cameras make photos of the bottom of the (transparent) wells. Image analysis software in this device quantifies the cell density, and produces growth curves for all 960 strains, in this case, the biomass levels are expressed in OD_{600} equivalents.

Eight replicates for each strain were incubated after fixing the conditions that might influence their growth. For instance, the initial density, the abundance of the resources, temperature, speed of the shaker unit, reading interval and run time. OD_{600} readings were taken at 30-min intervals for all the involved spices.

3.3.2 Experimental Results

As mentioned previously in the introductory chapter, also illustrated in Fig (3.2), the growth of bacterial communities entails four primary stages: lag phase, log phase, stable or stationary phase and death phase where the size of the population starts to decline.

(a)

(b)

(c)

(d)
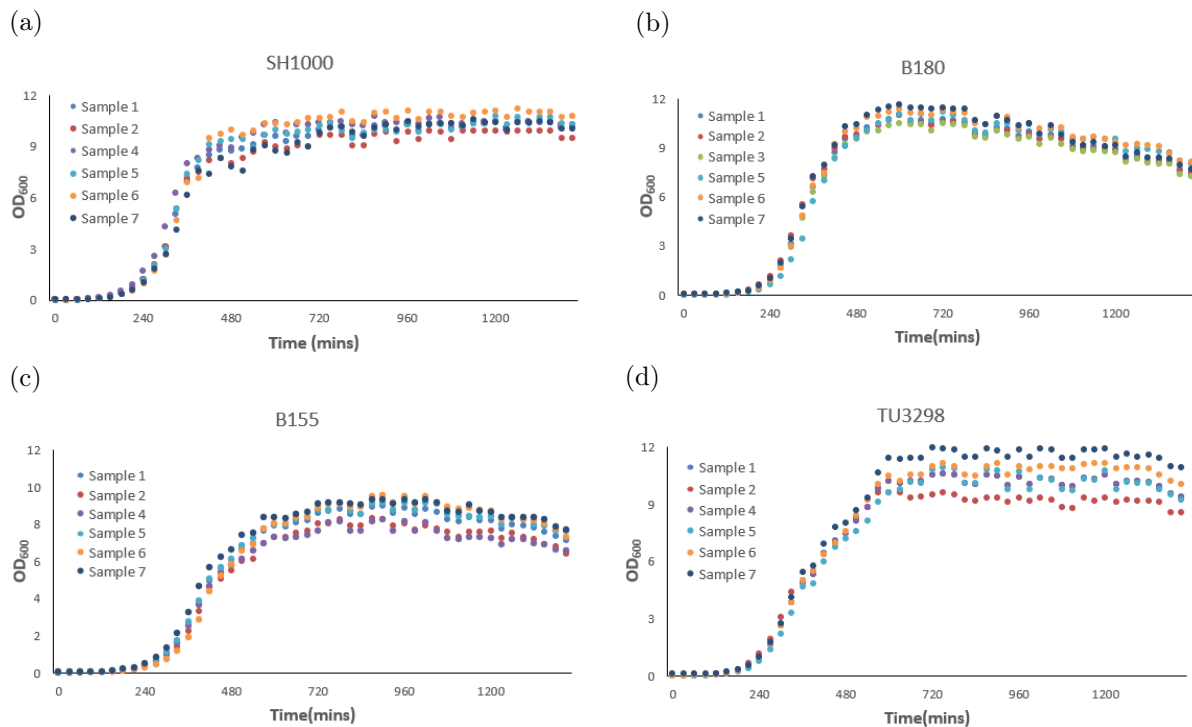
Figure 3.1: **Growth curves.** Experimental data on the dynamics of growing populations. Panel (a): growth curves of *S. aureus* (SH1000) are represented by the dotted lines. Panel (b): growth curves of *S. epidermidis* (B180) are represented by the dotted lines. Panel (c): growth curves of *S. epidermidis* (B155) are represented by the dotted lines. Panel (d): growth curves of *S. epidermidis* (TU3298) are represented by the dotted lines. Dots represent the OD_{600} readings, which were taken at 30-min intervals. The x-axis is the time in minutes, and the y-axis is the optical density at $600\,nm$ (OD_{600}). Data plotted in panels (a) to (d) will be provided in the appendix in Tables (6.1), (6.2), (6.3) and (6.4) respectively.

After liquid culture broths are inoculated for the involved species, the proliferation of bacteria does not start immediately but takes some time to proliferate. As stated

earlier, the time between inoculation and the beginning of multiplication is known as the lag phase. In this phase, the inoculated bacteria become familiar with the environment, activate various enzymes, and adapt to the environmental temperature and surrounding conditions. During this phase, there is an increase in the size of bacteria but no visible increase in the number of bacterial cells. The cells function metabolically. Since all the surrounding conditions for all the incubated species are fixed, the lag phase duration varies according to the bacterial species.

As shown in Fig (3.1), it can be determined that all inoculated species consumed approximately the same amount of time in this phase, which is four hours, taking into account that *S. aureus* population, SH1000, Fig (3.1a), were the fastest and *S. epidermidis* population, B155, Fig (3.1c) were the slowest.

Subsequently, the start of a new phase known as the log phase was noted, characterised by rapid exponential cell growth, where the bacterial population doubles during every generation. They increased at their maximum rate. The growth rates of B180, Fig (3.1b), and TU3298, Fig (3.1d), populations were the greatest during this phase, while B155 population scored the least growth rates at this phase. Since the rapidly dividing cultures were not provided with constant addition of nutrients and frequent removal of waste products, this phase was brief for all incubated species. As shown in Fig (3.2), the log phase appears as a steeply sloped straight line.

After the log phase, the bacterial growth almost stopped entirely, due to lack of necessary nutrients, lack of water and oxygen, changes in pH of the medium, and accumulation of their own toxic metabolic wastes. This phase is known as the stationary phase. It was during this phase that the cultures were at their greatest population density. However, the death rate of bacteria exceeded the rate of reproduction of bacteria, as is rapidly evident particularly in B180 population. The last phase in the growth curve is known as the decline phase. During this phase, the bacterial population declined due to the death of cells. The death rate of B180 populations was the greatest during this period, while SH1000 populations maintained their stability for a longer time.

3.3.3 Mathematical Analysis of The Obtained Results

From the graphs obtained in the laboratory of OD_{600} against time over 24 hours, the sampling time can be identified that occurred during the exponential phase of the growth curves and by using exponential curve fitting function, equations were generated. The equations take the form presented in (2.2). By re-arranging this equation, it was possible to estimate the doubling time, relaxation time, and growth rate for all the involved species per minute, hour, and day as follows:

$$\text{Relaxation time} = \frac{t_2 - t_1}{B},$$

87

$$\text{Growth rate} = \frac{1}{\text{Relaxation time}} = \frac{B}{t_2 - t_1},$$

$$\text{Doubling time} = \frac{\ln 2}{\text{Growth rate}},$$

where t_1 and t_2 are two consecutive time points throughout the bacterial growth, and B is a positive constant representing the relative growth rate.
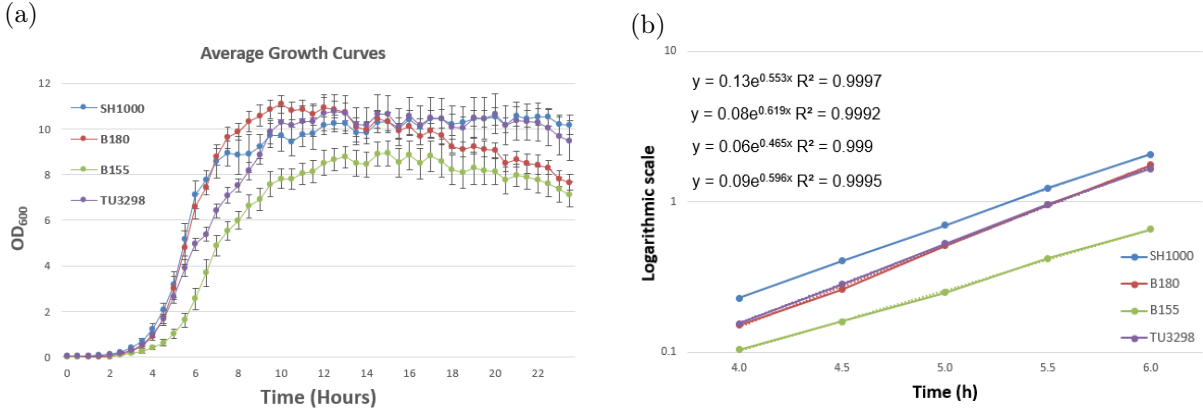
Figure 3.2: **Averaged growth curves of the involved strains.** Panel (a): illustrations of the bacterial growth curves after averaging the curves presented in Fig (3.1). The error bars show the standard deviation of the mean ($n = 6$). Panel (b): depicts the exponential phase used to calculate the doubling time of cultured populations. The y equations represent the line equations by changing the y-axis into logarithmic scale, R denotes the R-squared values. The x-axis is the time in hours, and the y-axis is the optical density at $600\,nm$ (OD_{600}).

Conducting these experiments enabled the obtaining of accurate data and readings regarding the growth rate and doubling time for the involved populations by using the logarithmic scale for the log phase for all evolved populations, as seen in Fig (3.2b). The averaged curve for each strain was obtained from the best six replicates results, Fig (3.2a). According to (Table 3.4), there is no significant difference in terms of the doubling times nor the growth rates between any of the S. epidermidis strains tested and the S. aureus strain SH1000 used in this study.

Species	Relative rate B	Doubling time			Relaxation time			Growth rate		
		Min	Hour	Day	Min	Hour	Day	Min	Hour	Day
SH1000	0.553	37.623	0.627	0.026	54.279	0.905	0.038	0.018	1.105	26.530
B180	0.619	33.583	0.560	0.023	48.450	0.807	0.034	0.021	1.238	29.722
B155	0.465	44.690	0.745	0.031	64.475	1.075	0.045	0.016	0.931	22.334
TU3298	0.596	34.884	0.581	0.024	50.327	0.839	0.035	0.020	1.192	28.613

Table 3.4: **Doubling times and growth rates of strains used in this study.** The doubling times were compared to SH1000 (S. aureus) as a control using a post hoc Dunnett's test [51].

3.3.4 Mathematical Models and Simulations

In the first chapter in (1.3.2) section, a very simple model for population evolution in

which the growth rates were independent and dependent of the size of the population was studied in detail. Population evolution growth rate can be independent of the size of the population. This only has a chance of being successful while the resources available to the population are unlimited. If these resources are finite and limited, as in the situation here, then there is a maximum population size that can be supported by the environment. This maximum population is often called the carrying capacity and it is proportional to the abundance of resources, $K \propto R$. In these circumstances, the growth rate must depend on the size of the population and specifically it must approach zero as the population approaches the carrying capacity. In this way it is possible to arrive at the logistic model for population growth:

$$\frac{dN}{dt} = r\,N\left(1 - \frac{N}{R}\right),$$

where r and R are positive constants representing the linear growth rate and the abundance of resources, respectively. For small N (compared with R) the growth rate $r(N)$ is close to the linear growth rate r. This is consistent with the fact that when the population is small, resources are plentiful and seemingly infinite. It is only when the population size enlarges that the effect of the finiteness of resources is noticeable. This model was first examined by the Belgian Mathematician, Pierre Francois Verhulst, in the middle of the 19th century, [204]. In this model, as in the exponential model, the only mechanisms for changing the population size are births and deaths; there is nothing to account for migration into or out of the population. However, by adding another variable that represents the resources as following:

$$\frac{dR}{dt} = (a - s\,R) - \ cN. \tag{3.1}$$

In the absence of N, the resource R is depleted due to natural factors at a rate $s\,R$, while it is replenished to a stable level a. At equilibrium, the rate of production equals the rate of depletion. Hence, the first term is equal to zero. When N is present, the resource is additionally depleted at a rate cN, where c is known to be the consumption rate of the existing population. The equation (3.1) represents the general case when a single population consumes a single resource [195]. However, as these experiments were incubated for only 24 hours, and during this period no food was introduced or added for the incubated populations besides the initial amount that was presented at the beginning of this experiment, this means that $a = 0$ and the reduction of the resources due to natural factors will not be significant when compared to the decline caused by population consumption.

Hence, only the population consumption will noticeably influence the evolution of the resource equation. This means the values of the first term in the resource equation, production, and depletion due to other reasons, will not be significant compared to the second

term, which represents the reduction of limited resources due to population consumption. Thus, the first term of this equation can be neglected, and the system of equations will take the form:

$$
\begin{cases}
\dfrac{dN}{dt} = r\,N\left(1 - \dfrac{N}{R}\right), \\
\dfrac{dR}{dt} = -\,cN,
\end{cases}
\tag{3.2}
$$

where $N = N(t)$ represents the densities of the populations and $R = R(t)$ represents the resource abundances at time t and c represents positive constant rates of consumption. Initial conditions $N(0)$ for all species were obtained and defined in the laboratory by defining the OD_{600}, which is an abbreviation indicating the optical density of a sample measured at a wavelength of $600\,nm$, before incubating the samples. Furthermore, growth rates r were determined for each incubated population from Table (3.4).
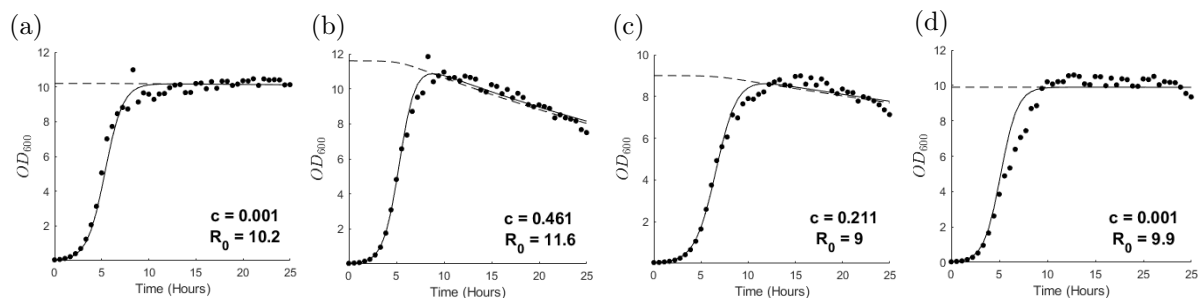
Figure 3.3: **Modelling the growth of bacterial populations.** The simulations of growth curves (solid lines) and resource evolution (dashed lines) generated from (3.2) plotted against the actual experimental data (black dots). Panel (a): represents SH1000. Panel (b): B180. Panel (c): B155. Panel (d): TU3298. Different values of c's indicate different rates of resource consumption, whereas different values of R_0 indicate different initial values of the limited resource. The x-axis is the time in hours, and the y-axis is the optical density at $600\,nm$ (OD_{600}).

According to the model (3.2) simulations, and as shown in Fig (3.3b), the highest rate of resource consumption was achieved by *S. epidermidis* population, B180, with $c = 0.461$ and initial resource density $R_0 = 11.6$, followed by *S. epidermidis* population, B155, Fig (3.3c), with $c = 0.211$ and initial resource density $R_0 = 9$. According to figures (3.3d) and (3.3a), both *S. epidermidis*, TU3298, and *S. aureus*, SH1000 populations ranked third with the same consumption rates $c = 0.001$ and initial resource density $R_0 = 9.9$, $R_0 = 10.2$, respectively.

3.3.5 Determining The Diffusion Coefficients of The Involved Species

To determine the diffusion coefficients, all strains involved were cultured on BHI agar plates before experiments. Bacteria were cultured for 24 h on $10\,cm$ diameter BHI agar

plates, and the lawns of *S. aureus* (SH1000) and *S. epidermidis* strains Table (3.1) were then scraped off the agar plates and suspended in $10\,mL$ of PBS by vortexing thoroughly. The cfu/mL in each tube was equalized by diluting the cell suspensions in PBS and comparing the OD_{600} of each suspension (approximately $5 \times 10^8\,cfu/mL$ for *S. aureus* and *S. epidermidis*, determined by viable count). All isolates were vortexed thoroughly before $50\mu L$ (containing approximately 2.5×10^6 cells) was plated onto $25mL$ BHI agar and incubated at $37°C$. Measurements of the cultured spots were taking for each plate prior to incubation and after, i.e., measurements of initial and incubated spots.
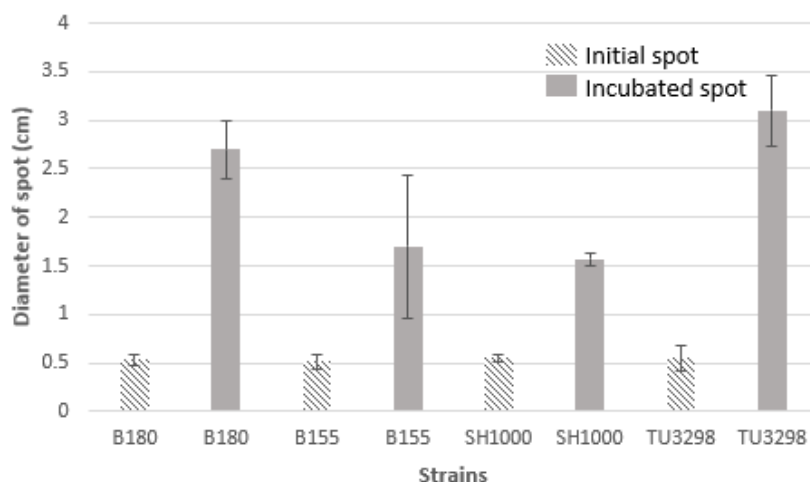
Figure 3.4: **Diagram showing the size of the spot diameter before and after the incubation.** Dashed bars indicate the average diameter of the bacterial spot before incubation; solid bars are the same indications after the incubation pointed out for B180, B155, SH1000, and TU3298, respectively in the x-axis. y-axis is the diameter of the spot in (cm). Error bars represent the standard error of the mean.

According to the diagram shown in Fig (3.4), the average size of the spot diameter for all the involved strains before incubating is approximately $0.5\,cm$, where the size of the diameter for the incubated spots varies from one strain to another. It is worth noting that *S. epidermidis* (TU3298) recorded the highest rate of diffusion while *S. aureus* (SH1000) ranked last in the rate of diffusion. Experimentally, it was possible to define the rate of change in the size of the incubated spots by finding the ratio between the average size of the diameter of incubated spots and initial spots, as follows:

$$\frac{B180(24)}{B180(0)} = 5.06, \ \frac{B155(24)}{B155(0)} = 3.29, \frac{SH1000(24)}{SH1000(0)} = 2.85, \ \frac{TU3298(24)}{TU3298(0)} = 5.64. \quad (3.3)$$

Mathematically, it was possible to estimate the diffusion coefficient for each strain by rescaling and adapting the actual sizes of medium and spots into the simulation. As noted previously, the size of Petri dishes used in the experiments is $10\,cm$ and the average size of the diameter of pre-incubated spots for all strains is $0.5\,cm$. Therefore, $L = 1$ was

91

chosen as the size of the medium; $hx = L/n$ as the space step size, where $n = 100$ the number of grid points. Furthermore, a column vector was constructed for each strain that represented the initial conditions. The initial vectors were divided into 100 grid points and the spot was introduced to these zero vectors as non-zero values in the middle where $a = 0.05$ indicates the diameter of the initial spots for all strains i.e., 5 space steps. Thus, the ratios between the length of the medium and the diameter of the initial spot were maintained the same in the simulations as in the actual experiments:

$$\frac{\text{Diameter of the initial spot}}{\text{Diameter of the medium}} = \frac{0.5}{10} = \frac{0.05}{1} = 0.05.$$

Since the diffusion coefficient for each strain was estimated by culturing them independently for a day, this can be represented mathematically by the logistic equation (1.3). In order to obtain the diffusion coefficients for the involved strains, it is necessary to define the proper values for D, which is the diffusion coefficients in simulations, that satisfy the actual experimental ratio between the average size of diameter of incubated spots and initial spots presented in (3.3).

The diffusion coefficient for each strain was obtained by considering the ratio between the initial spot and 24-hour incubated spot diameters obtained in (3.3) as conditions and by starting to introduce different values for the diffusion coefficient, using loops in MATLAB, it was possible to determine the diffusion coefficients for the involved strains that satisfy the obtained ratios in (3.3) with minimum error. Thus:

$$D_{B180} = 2 \times 10^{-5}, D_{B155} = 5 \times 10^{-6}, D_{SH1000} = 1.8 \times 10^{-6}, D_{TU3298} = 5 \times 10^{-5}. \quad (3.4)$$

where $D_{B180} = 2 \times 10^{-5}$ in our simulation space and time units corresponds to $D_{B180} = 2 \times 10^{-3} \frac{cm^2}{day}$ in the actual experimental units, and similarly for the diffusion coefficients of other strains.
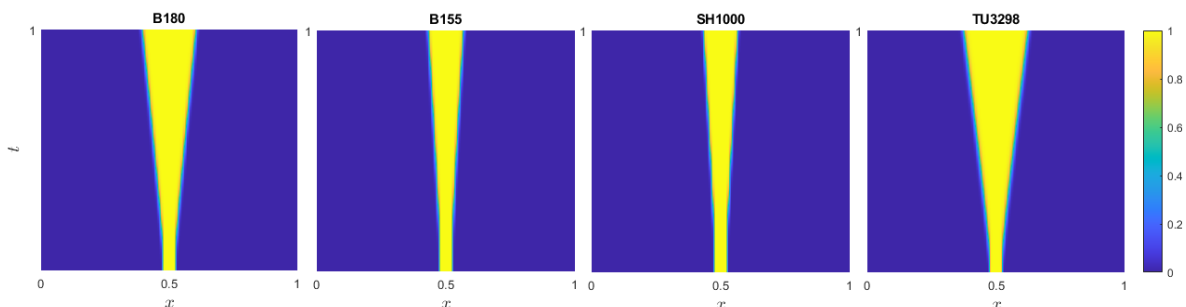
Figure 3.5: **Mathematical simulation of the incubated spot evolution.** Surface plots showing the one-day evolution of the incubated spots for the involved species, B180, B155, SH1000, and TU3298, respectively. The x-axis represents space ($10\,cm$), the y-axis represents time (1 day).

As demonstrated in Fig (3.5), which shows simulations obtained from (1.3) representing

the evolution of the incubated spots for the populations (B180), (B155), (SH1000), and (TU3298), respectively.

In terms of the toxins, according to [141], the characteristic diffusion constant for a molecule the size of a monomeric protein is $\approx 100 \mu m^2/s$ in water and is about ten-fold smaller, $\approx 10 \mu m^2/s$, inside a cell. Hence rescaling this coefficient to the units used in these simulations yields:

$$D_{\text{toxin}} = \frac{100 \times 10^{-8}}{1.16 \times 10^{-5}} = 8.6 \times 10^{-2} \frac{cm^2}{day} \Leftrightarrow 8.6 \times 10^{-4} \frac{s.s.u}{s.t.u}.$$

where $s.s.u$ is the simulation space unit and $s.t.u$ means the simulation time unit.

3.4 Study of Toxin-mediated Inhibition

As noted previously, the aims of these experiments were to determine the sensitivity of *S. aureus* strain against the toxins produced by *S. epidermidis* populations. Hence, this type of experiment was performed twice. Firstly, the parental isolate of all *S. epidermidis* species was used to determine and measure the effect of their toxins on the involved *S. aureus* populations before starting the invasions. Secondly, the parental isolate was used at the end of performed interactions, to investigate the evolution of resistance by the evolved populations of *S. aureus*. This was achieved when ancestral and evolved *S. aureus* strains were sprayed over ancestral and evolved *S. epidermidis*, toxin-producing residents.

3.4.1 Experimental Techniques

As indicated in (Table 3.1), three independent *S. epidermidis* isolates were selected, two of them from the previous study that sampled the anterior nares of 60 healthy volunteers (Libberton et al. 2014). The following method was adapted to test competitor strains with inhibitor- producing strains.

The inhibition spray assay was based on the protocol described previously in [143], by using SH1000 as the indicator strain. A $25 \mu l$ spot (approximately 10^8 cells) of an overnight bacterial culture was pipetted onto the centre of an agar plate containing $15 \, ml$ of BHI agar (lab M). The plates were incubated for $18 \, h$ at $37°C$ before $250 \, \mu l$ of a ten-fold diluted overnight culture of *S. aureus* SH1000 ($10^6 \, cfu$) was sprayed over the plate. The plates were incubated again for a further $18 \, h$, when the size of the inhibition zone produced by the central nasal isolate on SH1000 was assessed. As shown in Fig (3.6), the experiment was repeated 5 to 10 times to obtain accurate and consistent results.
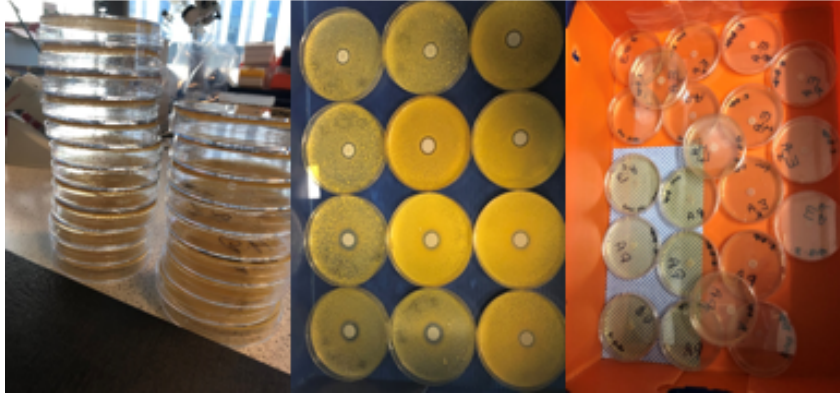
Figure 3.6: **Replicates of toxin-mediated inhibition experiments.**

The clarity of the inhibition zone was scored according to a simple scoring system of 1 to 4, 4 being completely clear and 1 being no detectable zone. The areas of any detectable zones were also recorded by measuring the diameter of the inhibition zone and the central colony. The area of both the zone and the colony were calculated using the equation:

$$Area = \pi r^2,$$

where r is the radius of the colony or the inhibition zone. The central colony area was then subtracted from the total zone area, leaving only the area of the zone around the perimeter of the central colony.

3.4.2 Experimental Results (Pre-invasions)

As shown in Fig (3.7a), all three isolates were toxin producers as revealed in a deferred inhibition assay by their killing of *S. aureus* [zone of clearing] when a lawn of *S. aureus* strain, SH1000, was sprayed over them.

Although one of the species, B180, produces an inhibition zone against *S. aureus*, in the study presented in this thesis, these particular isolates were considered non-toxin producers based on their not significantly reducing the viability of strain SH1000 when comparing the obtained zone of inhibition with the other isolates, B155 and TU3298, [see Fig (3.7b)].

Moreover, SH1000 displayed no growth inhibition activity against any of the selected *S. epidermidis* strains when performing the mutual deferred inhibition assay. Of the two toxin-producing *S. epidermidis* strains, TU3298 produced an inhibition area that was around two times greater than that of B155.

3.4.3 Experimental Results (After-invasions)

According to the performed competition outcomes, *Staphylococcus aureus* populations were able to restrict, inhibit, and invade communities of *S. epidermidis* under mixed conditions. To test whether the evolution of inhibitory toxin resistance by *S. aureus*

was responsible for the inhibition and invasion in a mixed environment, evolved *S. aureus* strains were sprayed over ancestral and evolved *S. epidermidis*, toxin-producing residents. In most cases, evolved *S. aureus* were resistant to the *S. epidermidis* toxins (see Fig 3.8).
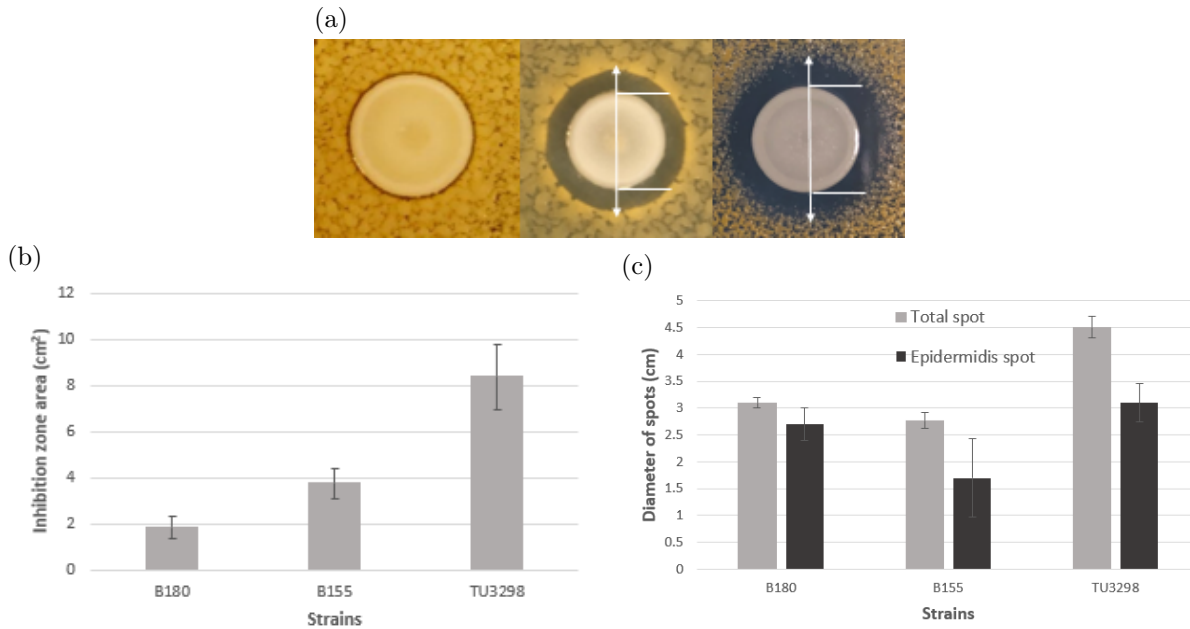
Figure 3.7: **Results of toxin-mediated inhibition, (pre-invasions).** Panel (a): examples of the actual inhibition zone produced by the ancestral *S. epidermidis* B180, B155, and TU3298 strains against the ancestral SH1000, respectively. Panel (b): the inhibition zone area (cm^2) produced by the ancestral inhibitor-producing *S. epidermidis* strains, pointed in the x-axis, against the ancestral SH1000. Panel (c): the diameters of both *S. epidermidis* spots and total spots, i.e., the inhibition circle + *S. epidermidis* spot, for all three strains. Error bars represent the standard error of the mean.

Furthermore, the size of the inhibition zones produced by ancestral and evolved TU 3298 against evolved *S. aureus* decreased, indicating that it is only a matter of time before the evolved *S. aureus* populations completely resist the toxins produced by this strain, as there is a positive association between the level of toxicity expressed by *S. epidermidis* and the time consumed by *S. aureus* populations to adapt to this toxicity.

Interestingly, as seen in Fig (3.8, solid bars), evolved *S. epidermidis* populations had greater inhibitory activity on ancestral SH1000, Fig(3.8b), than ancestral *S. epidermidis* populations, Fig(3.8a).

This supports the opinion that the toxin producer developed to overcome the survival challenges forced by increasingly resistant *S. aureus* populations. The evolved *S. epidermidis* may have increased the production of the inhibitory toxin or started the production of different toxins.

(a)

(b)

(c)
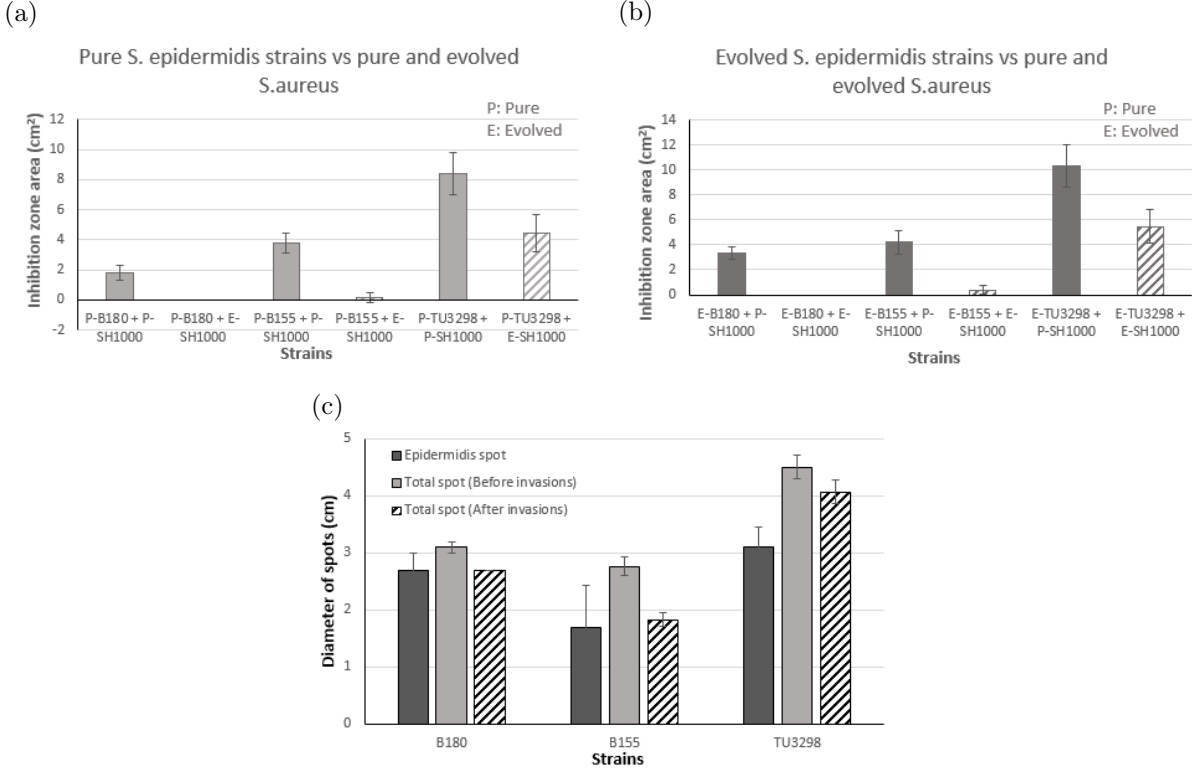
Figure 3.8: **Resistance of SH1000 before and after competing against *S. epidermidis* (B180, B155 and TU3298).** Panel (a): shows inhibition zones produced by pure *S. epidermidis* strains, and panel (b): by the evolved *S. epidermidis* strains against the pure SH1000 (P) and the evolved SH1000 (E). In both panels, the y-axis represents the inhibition zone area (cm^2). Panel (c): for each strain, a comparison of the diameter of the inhibition zone before (light solid bars) and after invasions (dashed bars), as well as the diameter of the *S. epidermidis* spot (dark solid bars). Error bars represent the standard error of the mean.

3.4.4   Mathematical Models and Simulations

Two bacterial populations in a one-dimensional domain are considered. One species, the 'producer,' produces an antimicrobial toxin that inhibits the other, the susceptible. Denoting the concentrations of susceptible, producer and toxin at position x and time t by $u(x,t)$, $v(x,t)$ and $T(x,t)$, this ecosystem is modelled via the equations:

$$\begin{cases} \dfrac{\partial u}{\partial t} = D_u \dfrac{\partial^2 u}{\partial x^2} + r_u\, u\, (1 - u - pT), \\[2mm] \dfrac{\partial v}{\partial t} = D_v \dfrac{\partial^2 v}{\partial x^2} + r_v\, v\, (1 - v), \\[2mm] \dfrac{\partial T}{\partial t} = D_T \dfrac{\partial^2 T}{\partial x^2} + f_1\, v - f_2\, T, \end{cases} \qquad (3.5)$$

where $u = u(x,t), v = v(x,t)$ and $T = T(x,t)$ are concentrations of *S. aureus*, *S. epidermidis* and toxic substance. p: inhibition coefficient, f_1: inhibitor production rate, f_2: inhibitor degradation rate.

96

Initial conditions:

$$u(x,0) = 0.1 \ , \ T(x,0) = 0 \ \forall \, x \ \in \ [0,L], \ \text{and} \ v(x,0) = \begin{cases} 1 & x \in [\dfrac{L}{2} - l, \dfrac{L}{2} + l], \\ 0 & \text{otherwise.} \end{cases}$$

Boundary condition;

Again, zero–flux boundary conditions are imposed for all variables.

$$u_x(0,t) = u_x(L,t) = v_x(0,t) = v_x(L,t) = T_x(0,t) = T_x(L,t) = 0 \quad \forall \, t > 0. \tag{3.6}$$

Since the solution $T(x,t)$ represents a travelling wave, the structure of the solution will be the same for all time and the speed of spread of this shape is a constant, denoted by c. If this wave is considered in a travelling form moving at speed c, it will appear stationary. Mathematically we can say that if the solution

$$T(x,t) = T(x - ct) = T(\zeta), \ \ \zeta = x - ct \tag{3.7}$$

then $T(x,t)$ is a travelling wave, and it moves at constant speed c in the positive x-direction. Rewriting the equation that represents the toxin substance in the system (3.5) by using the form of the solution presented in (3.7), gives:

$$\frac{\partial T}{\partial t} = D_T \frac{\partial^2 T}{\partial x^2} + f_1 \, v - f_2 \, T, \tag{3.8}$$

$$\frac{\partial T}{\partial t} = -cT', \ \frac{\partial T}{\partial x} = DT', \ \frac{\partial^2 T}{\partial x^2} = DT''.$$

Thus, the equation (3.8), takes this form:

$$DT'' + cT' - f_2 \, T = -f_1 \, v. \tag{3.9}$$

To be able to solve this equation certain assumptions should be made, such as that at equilibrium there is no movement, hence $c = 0$. Also, the value of v which represents the concentration of the producer is equal to one inside the cultured spot, whereas it equals zero everywhere else, thus the equation (3.9), takes the following form:

$$DT'' - f_2 \, T = \begin{cases} -f_1 & x \le |a|, \\ 0 & \text{otherwise.} \end{cases} \tag{3.10}$$

To find the general solution to the non-homogeneous differential equation (3.10), in this case the solution can be written in this form:

$$T(x,t) = T_{cf} + T_p, \tag{3.11}$$

where T_{cf} is the solution to the complementary function $DT'' - f_2 T = 0$, and T_p is the particular solution to the equation $DT'' - f_2 T = G(x)$. First we start by finding the solution for the complementary function, by setting:

$$T = e^{mx}, \quad T' = me^{mx}, \quad T'' = m^2 e^{mx}.$$

Inserting these values into the complementary function, yields:

$$Dm^2 e^{mx} - f_2 e^{mx} = 0 \rightarrow Dm^2 - f_2 = 0 \rightarrow m = \pm\sqrt{\frac{f_2}{D}}. \tag{3.12}$$

Thus:

$$T_{cf} = c_1 e^{mx} + c_2 e^{-mx}.$$

Now, it is necessary to find the specific solution to the equation (3.10), since the form of $G(x)$ is constant, meaning that $T_p = c$ and $T'' = 0$. Inserting these values into the equation (3.10), yields:

$$-f_2 c = -f_1 \rightarrow c = \frac{f_1}{f_2}.$$

Thus, the equation (3.11) becomes:

$$T(x,t) = c_1 e^{mx} + c_2 e^{-mx} + \frac{f_1}{f_2}.$$

Therefore,

$$T(x,t) = \begin{cases} c_1 e^{mx} + c_2 e^{-mx} + \dfrac{f_1}{f_2} & x \leq |a|, \\ c_3 e^{mx} + c_4 e^{-mx} & \text{otherwise.} \end{cases} \tag{3.13}$$

The values of the constants can be determined from the boundary conditions (3.6): $T_x(0,t) = 0$:

$$c_1 m e^{m(0)} - c_2 m e^{-m(0)} = 0 \rightarrow c_1 m - c_2 m = 0 \rightarrow c_1 = c_2.$$

$T_x(L,t) = 0$:

$$c_3 m e^{m(L)} - c_4 m e^{-m(L)} = 0 \rightarrow c_3 e^{mL} = c_4 m e^{-mL} \rightarrow c_3 = c_4 e^{-2mL}. \tag{3.14}$$

In order to define these constants, we need to add two more conditions as follows: $\lim_{x \to a^+} T(x,t) = \lim_{x \to a^-} T(x,t)$ and $\lim_{x \to a^+} T_x(x,t) = \lim_{x \to a^-} T_x(x,t)$. From these two conditions it is possible to obtain values of the constants c_1, c_3 and c_4.

$$c_1 e^{am} + c_1 e^{-am} + \frac{f_1}{f_2} = c_4 e^{-2Lm} e^{am} + c_4 e^{-am}.$$

Solving this equation for the constant c_1, yields:

$$c_1 = \frac{c_4\,\mathrm{e}^{-a\,m} + c_4\,\mathrm{e}^{-2\,L\,m}\,\mathrm{e}^{a\,m} - \frac{f_1}{f_2}}{\mathrm{e}^{a\,m} + \mathrm{e}^{-a\,m}}. \tag{3.15}$$

Applying the second condition, gives:

$$c_1\,m\,\mathrm{e}^{a\,m} - c_1\,m\,\mathrm{e}^{-a\,m} = c_4\,m\,\mathrm{e}^{-2\,L\,m}\,\mathrm{e}^{a\,m} - c_4\,m\,\mathrm{e}^{-a\,m}.$$

Again, solving this equation for the constant c_1, yields:

$$c_1 = \frac{c_4\,\mathrm{e}^{2\,L\,m} - c_4\,\mathrm{e}^{2\,a\,m}}{\mathrm{e}^{2\,L\,m} - \mathrm{e}^{2\,L\,m}\,\mathrm{e}^{2\,a\,m}}. \tag{3.16}$$

From equations (3.15) and (3.16), we have:

$$\frac{c_4\,\mathrm{e}^{-a\,m} + c_4\,\mathrm{e}^{-2\,L\,m}\,\mathrm{e}^{a\,m} - \frac{f_1}{f_2}}{\mathrm{e}^{a\,m} + \mathrm{e}^{-a\,m}} = \frac{c_4\,\mathrm{e}^{2\,L\,m} - c_4\,\mathrm{e}^{2\,a\,m}}{\mathrm{e}^{2\,L\,m} - \mathrm{e}^{2\,L\,m}\,\mathrm{e}^{2\,a\,m}}. \tag{3.17}$$

Solving the equation (3.17) for c_4, gives:

$$c_4 = -\frac{f_1\,\mathrm{e}^{2\,L\,m}\,\left(\mathrm{e}^{2\,a\,m} - 1\right)}{2\,f_2\,\left(\mathrm{e}^{a\,m} - \mathrm{e}^{m\,(2\,L+a)}\right)}.$$

Inserting the value of c_4 into the equation (3.14), yields:

$$c_3 = -\frac{f_1\,\left(\mathrm{e}^{2\,a\,m} - 1\right)}{2\,f_2\,\left(\mathrm{e}^{a\,m} - \mathrm{e}^{m\,(2\,L+a)}\right)}.$$

Similarly for the equation (3.16):

$$c_1 = \frac{f_1\,\left(\mathrm{e}^{2\,L\,m} - \mathrm{e}^{2\,a\,m}\right)}{2\,f_2\,\left(\mathrm{e}^{a\,m} - \mathrm{e}^{m\,(2\,L+a)}\right)}.$$

Thus, the solution (3.13) takes the following form:

$$T(x,t) = \begin{cases} \dfrac{f_1\,\left(\mathrm{e}^{2\,L\,m} - \mathrm{e}^{2\,a\,m}\right)}{2\,f_2\,\left(\mathrm{e}^{a\,m} - \mathrm{e}^{m\,(2\,L+a)}\right)}\left(\mathrm{e}^{mx} + \mathrm{e}^{-mx}\right) + \dfrac{f_1}{f_2} & x \le |a|, \\[3mm] -\dfrac{f_1\,\left(\mathrm{e}^{2\,a\,m} - 1\right)}{2\,f_2\,\left(\mathrm{e}^{a\,m} - \mathrm{e}^{m\,(2\,L+a)}\right)}\,\mathrm{e}^{mx} - \dfrac{f_1\,\mathrm{e}^{2\,L\,m}\,\left(\mathrm{e}^{2\,a\,m} - 1\right)}{2\,f_2\,\left(\mathrm{e}^{a\,m} - \mathrm{e}^{m\,(2\,L+a)}\right)}\,\mathrm{e}^{-mx} & \text{otherwise.} \end{cases} \tag{3.18}$$
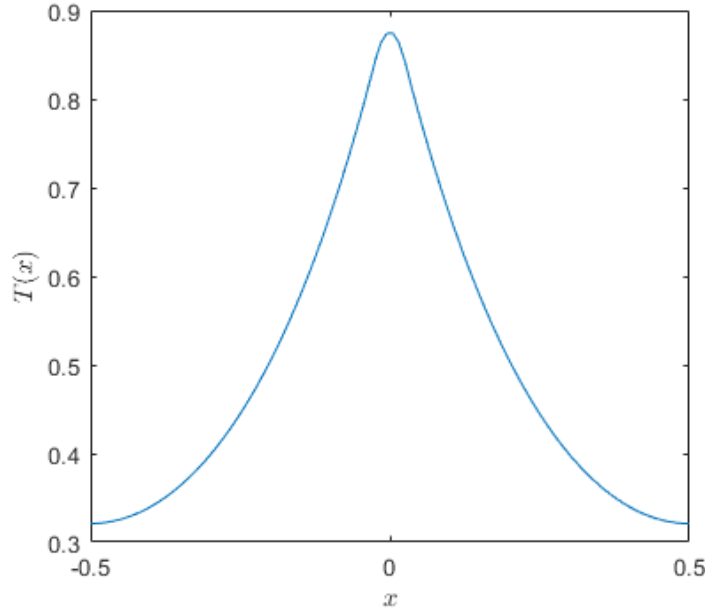
Figure 3.9: **Profile of toxin.** Illustration of the solution $T(x,t)$ in the equation (3.18). The x-axis represents space, and the y-axis represents toxin concentration. Parameters: $L = 0.5$, $a = 0.025$, $D = 0.086$, $f_1 = 1$, $f_2 = 0.1$.

After obtaining a graph of the solution $T(x,t)$ shown in Fig(3.9), the aim is to define a relationship between the parameters p, f_1 and f_2 which represent the inhibition coefficient, the production and the decaying of the toxin substance respectively. Since these parameters cannot be determined precisely, as in the case in determining the growth rate as well as the diffusion coefficients for the involved bacterial strains, the aim is to define a relationship between these coefficients based on what there is in the model (3.5). In order to achieve this, the first equation in the system (3.5) is considered, at equilibrium $\dot{u} = 0$, when $u = 0$ or $u = 1 - pT$, from (3.18) this can be written as following:

$$1 - p\left(-\frac{f_1\left(e^{2am} - 1\right)}{2f_2\left(e^{am} - e^{m(2L+a)}\right)}e^{mx} - \frac{f_1 e^{2Lm}\left(e^{2am} - 1\right)}{2f_2\left(e^{am} - e^{m(2L+a)}\right)}e^{-mx}\right) = u.$$

According to (3.18), this solution of T covers the area outside of S. epidermidis spots, where the inhibition zone occurs and beyond, which means that u has either vanished or is dying in this area. Therefore, for simplicity, we set $u = 0$, and this yields:

$$-\frac{f_1 p}{f_2}\left(\frac{e^{2am} - 1}{2\left(e^{am} - e^{m(2L+a)}\right)}e^{mx} + \frac{e^{2Lm}\left(e^{2am} - 1\right)}{2\left(e^{am} - e^{m(2L+a)}\right)}e^{-mx}\right) = 1,$$

$$f_1 p = \frac{-f_2}{\left(\frac{e^{2am}-1}{2\left(e^{am}-e^{m(2L+a)}\right)}e^{mx} + \frac{e^{2Lm}\left(e^{2am}-1\right)}{2\left(e^{am}-e^{m(2L+a)}\right)}e^{-mx}\right)}, \tag{3.19}$$

where a represents the radius of the S. epidermidis spot, and x is the radius of the total spot including the S. epidermidis spot plus the inhibition zone. As $f_1 p$ is a constant,

100

hence, for simplicity $f_1 = 1$ can be set to reduce the number of parameters when plotting the relationship between p and f_2.
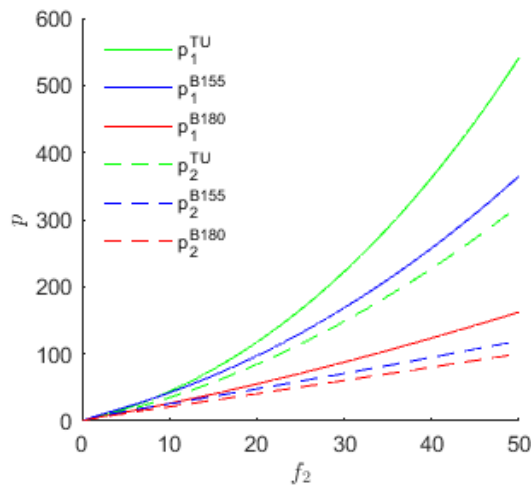
Figure 3.10: **Illustration of the relation between the inhibition coefficient p and decaying rate f_2, Eq** (3.19). Solid lines represent the association of the inhibitory coefficients between the toxins and the susceptible fraction of *S. aureus*, whereas the dashed lines represent the same associations with the adapted fraction of *S. aureus* populations. TU3298 in green, B155 in blue, and B180 in red. Parameters: in solid lines, (green) $a = 0.155$ and $x = 0.225$, (blue) $a = 0.085$ and $x = 0.138$, and (red) $a = 0.135$ and $x = 0.155$. In dashed lines, (green) $x = 0.203$, (red) $x = 0.135$, and (blue) $x = 0.092$.

According to Fig (3.7c), there are three different strains with three different values of a and x. To obtain a better understanding of the relationship between p and f_2, it was decided to plot p against different values of f_2, and not the other way around as the value of m in the equation (3.12) depends on the value of f_2.

As seen in Fig (3.8), the evolved population SH1000 mutated against the toxins produced by B180, as no inhibition zones were observed when applying evolved SH1000 on pure B180 nor evolved. As a result, when producing the red dashed line in Fig (3.10), which shows the relationship between the inhibition coefficient and the decaying rate in an evolved mixed population of *S. aureus* and *S. epidermidis* B180, $a = x$ was set in the equation (3.19), meaning that the radius of the total spot is equal to the radius of the B180 spot, zero inhibition zone, (See Fig 3.8c). Since it was not possible to quantify the inhibition coefficient and the decaying rates of the toxins produced by the involved *S. epidermidis* strains, i.e., the values of p and f_2, the equation (3.19) indicates the relationship between these factors. Therefore, whenever any of these values can be defined the other will lie within the lines plotted and shown in Fig (3.10).

3.5   Dynamics of Interacting Population

Before exploring and showing the materials and the methods of the competitions, several concepts need to be explained. These concepts are presented as follows:

Types of Interactions

1. Competition for resources.

   Competition for resources occurs when two or more species in a community compete for a shared resource. When one species consumes a finite resource, it leaves less available for other species and those that rely on it to suffer as a result. Species acting in their own best interests will utilise a finite resource until it is depleted, resulting in a population crash [79]. Competitors might avoid this disaster by using resources more slowly [112] or by using a different resource altogether, a phenomenon known as niche partitioning [168]. *S. aureus* and *Pseudomonas aeruginosa* compete for iron scavenging resources in vitro [80] and in vivo (rat infection model) [133]. However, in the nasal environment, this has yet to be proven.

2. Inhibition and competition for resources.

   When one organism produces a chemical that reduces the relative fitness of another organism in the community, it is referred to as toxin-mediated interference competition [145]. Toxin-mediated interference is popular in bacteria from the manufacture of bacteriocins [98], antibiotics [175], and secondary metabolites [115]. However, toxin-mediated interference has not been studied in connection to the nasal microbial population or colonisation. Although *Staphylococci* have a wide spectrum of bacteriocins capable of killing closely- related species [82]. *S. epidermidis* produces two bacteriocins that have been rigorously studied and have been shown to kill *S. aureus*. These are *epidermin* [59] and *gallidermin* in aureus [164].

Environmental Structure

Interference competition in bacterial communities is often induced by costly environmentally produced toxins and is thus likely to be influenced by spatial population structure [32].
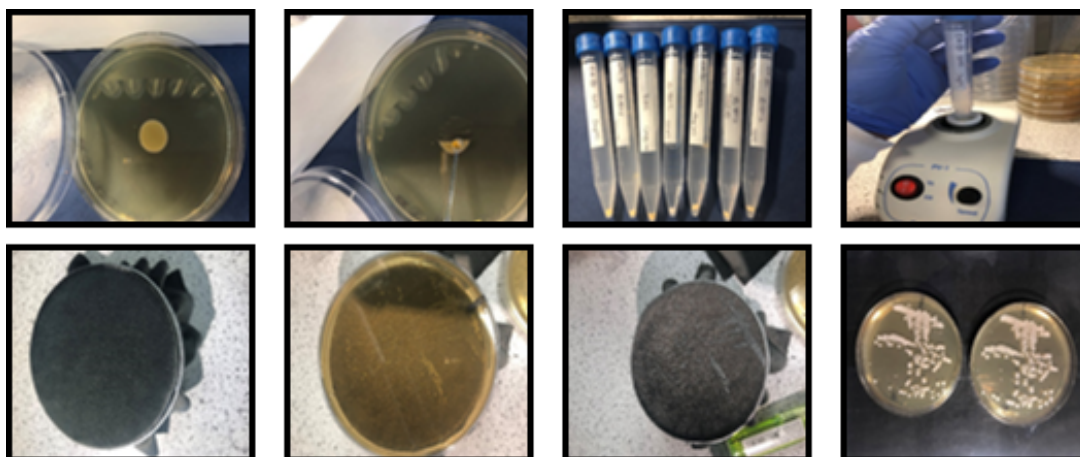
Figure 3.11: **Illustrations of different types of environmental structure.** Panels in the first row show the steps of the daily transfer process among the populations interacting under mixed conditions. In contrast, the second row shows the actions taken under structured conditions.

Based on this knowledge, the experiments were performed in two different environmental structures to investigate the influence of the environmental structure on the dynamics of interactions. These two structures were known as mixed and structured environments, and they were distinct in terms of transferring the populations, as shown in Fig (3.11). In a mixed environment, the competing populations were introduced into a new and fresh medium every day by scraping the entire bacterial lawn off before thoroughly vortexing and then pipetting onto a new plate. In contrast, in a structured environment, the transfers were made by replica, plating with velvet to maintain spatial structure.

Initial Frequencies

As illustrated previously, the initial frequency, along with the environmental structure, plays a significant role in determining the outcomes of these interactions and influencing the dynamics of interactions. Hence, different initial frequencies were considered to test this theory in the experiments in this study. Therefore, three different sets of experiments were performed. The first set concerned populations of toxin-producing *S. epidermidis* invading resident populations of susceptible *S. aureus* at a concentration of (0.01: 1). The second set involved what is defined as the mutual invasions, where populations of toxin-producing *S. epidermidis* were invaded by a susceptible population of *S. aureus* at a concentration of (1: 0.01). The third set involved performing these interactions from equal initial frequency (1:1).

Level of Toxicity

As shown in (Table 3.1), three different strains from the *S. epidermidis* family were used, distinguished by their level of toxicity, where (B180) is considered a low toxin strain, (B155) with a moderate level of toxicity and (TU3298) is a high toxin strain. These toxicity levels were determined as revealed in a deferred inhibition assay by their killing of *S. aureus* [zone of clearing when a lawn of *S. aureus* strain SH1000 was sprayed over them], (See Fig 3.7). Of the three toxin-producing *S. epidermidis* strains, B180 produced an inhibition area that was around three times smaller than that of B155. On the other hand, TU3298 produced an inhibition area that was around two times greater than that of B155.

Before the start of the invasion experiment, all nasal isolates were cultured on BHI agar plates. Bacteria were cultured for $18\,h$ on $100\,mm$ diameter BHI agar plates when the lawns of *S. aureus* (SH1000) and *S. epidermidis* strains (resident and invader – Table 3.1) were scraped from the agar plates and suspended in $10\,ml$ of PBS (Table 3.3), (containing approximately $5 \times 10^8 cfu/ml$ for *S. aureus* and *S. epidermidis*, determined with a colony count) by vortexing thoroughly. By diluting the cell suspensions in PBS and measuring the OD_{600} of each suspension, the cfu/ml in each tube was equalised. In a final volume of $10\,ml$ PBS, the two species were mixed with the invader at a different frequency

(ratio) to the resident (0.01 : 1). The mixtures were well-vortexed before plating $50\,\mu l$ (containing about 2.5×10^6 cells) on $25\,ml$ BHI agar and incubating at $37°C$. Five replicate communities were established at each starting frequency.

The communities were transferred to a new agar plate every day, the mixed environmental conditions explained in the previous section and shown in Fig (3.11). Furthermore, each isolate determined viable counts by scraping the bacterial lawn from the plate and transferring it to $10ml$ of sterile PBS. After thoroughly vortexing and then pipetting $50\mu l$ onto a new plate to complete the experiment, the competing populations were counted by using the serial dilution method ($100\mu l$ of the sample+$900\mu l$ PBS) (See Fig 3.12).

The colony-forming unit (CFU) is a microbiological counting unit used to quantify the number of viable microorganisms in a sample. The term 'viable' refers to microorganisms that can divide and are alive. Unlike other methods that count the number of cells regardless of viability, this approach counts just the living cells because this term reflects the number of bacteria capable of reproducing when colonies develop on the plate. A CFU calculation requires sampling [187]. The viable counts were accomplished on the structured plates by scraping the remaining bacterial lawn after duplicate plating and serial diluting in PBS. Colony counts were done on BHI plates, and colony morphology and colour were used to distinguish colonies.
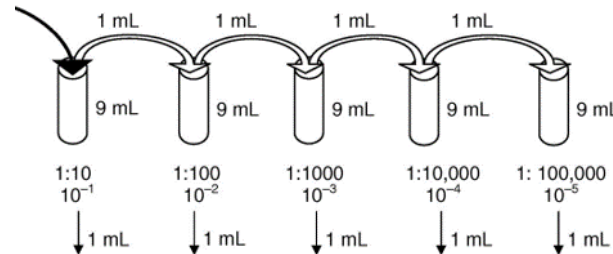
Figure 3.12: **Serial dilution method.** A serial dilution is used to dilute a microbial sample enough to obtain single colonies when plating. $100\mu l$ of liquid containing the bacteria is mixed with $900\mu l$ of PBS liquid in order to give the dilution a 1:10 ratio, and several dilutions are frequently recommended. Taken from [187].

After obtaining the experimental data, i.e., the number of colonies in the fraction of the population, the CFU calculation in the original sample can be achieved using the equation [187]:

$$\text{Number of CFU per } ml = \frac{\text{number of colonies} \times \text{dilution factor}}{\text{size of the sample}(ml)} \tag{3.20}$$

As explained earlier, there occurred two types of interactions. The first type involved resource competitions, interactions between *S. epidermidis* B180 and *S. aureus* SH1000, while the second type involved resource competitions and the produced toxins played a

significant role in the outcomes of these invasions, interactions between *S. epidermidis* B155, TU3298, and *S. aureus* SH1000.

As shown in Fig (3.13), the performed interactions lasted for varying periods until the change in the competing population density was no longer significant. Thus, the interactions between *S. aureus* strain, SH1000, and the inhibitor-producing *S. epidermidis* species, B155 and TU3298, were carried on for 28 days, which is longer than the interactions between SH1000 and the low-inhibitor-producing strain, B180 (17 days).

3.5.1 Experimental Results

When performing the interactions under mixed conditions, the following findings were obtained:

Regardless of the initial concentrations and the level of toxicity, *S. aureus* populations were always able to limit the presence of their opponents.

Under mixed conditions, the pathogenic species SH1000 dominated all interactions performed regardless of the manipulated factors imposed (level of toxicity and initial frequency). Such findings are consistent with those of the study presented in the previous chapter, as it was demonstrated that *S. epidermidis* was never able to successfully invade under mixed conditions, and that *Staphylococcus aureus* was only able to invade toxin-producing *S. epidermidis* under mixed conditions.

A positive association between the interaction level of toxicity and the time consumed by the *S. aureus* population to recover.

During the interactions, all developed isolates of *S. aureus* displayed similar behaviour, with a fall in growth level at the start of these competitions, followed by a rise, indicating the remarkable adaptability of pathogenic strain SH1000. The decrease in *S. aureus* density was related to the toxin level and growth rate of the respective species.

Furthermore, as shown in Fig (3.13), there was a significant link between the toxicity of the developed strain of *S. epidermidis* and the time required for *S. aureus* to adapt and mutate against these toxins. The most toxic species, TU3298, was able to inhibit SH1000 for a longer period.

A negative association between the initial density of the *S. aureus* population and their ability to recover.

Unlike that found in [122], invasion of *S. aureus* into a toxin-producing *S. epidermidis* resident was positively frequency-dependent with the highest initial frequencies invading the fastest and lower initial frequencies becoming extinct. The interactions in this study shown in Fig (3.13), revealed that the evolved *S. aureus* populations were able to recover faster when they started from lower initial frequencies (See figures 3.13c, 3.13f, and 3.13i). The evolved *S. aureus*, on the other hand, struggled when they started from higher initial

frequencies (resident), as shown in figures (3.13a), (3.13d), and (3.13g).
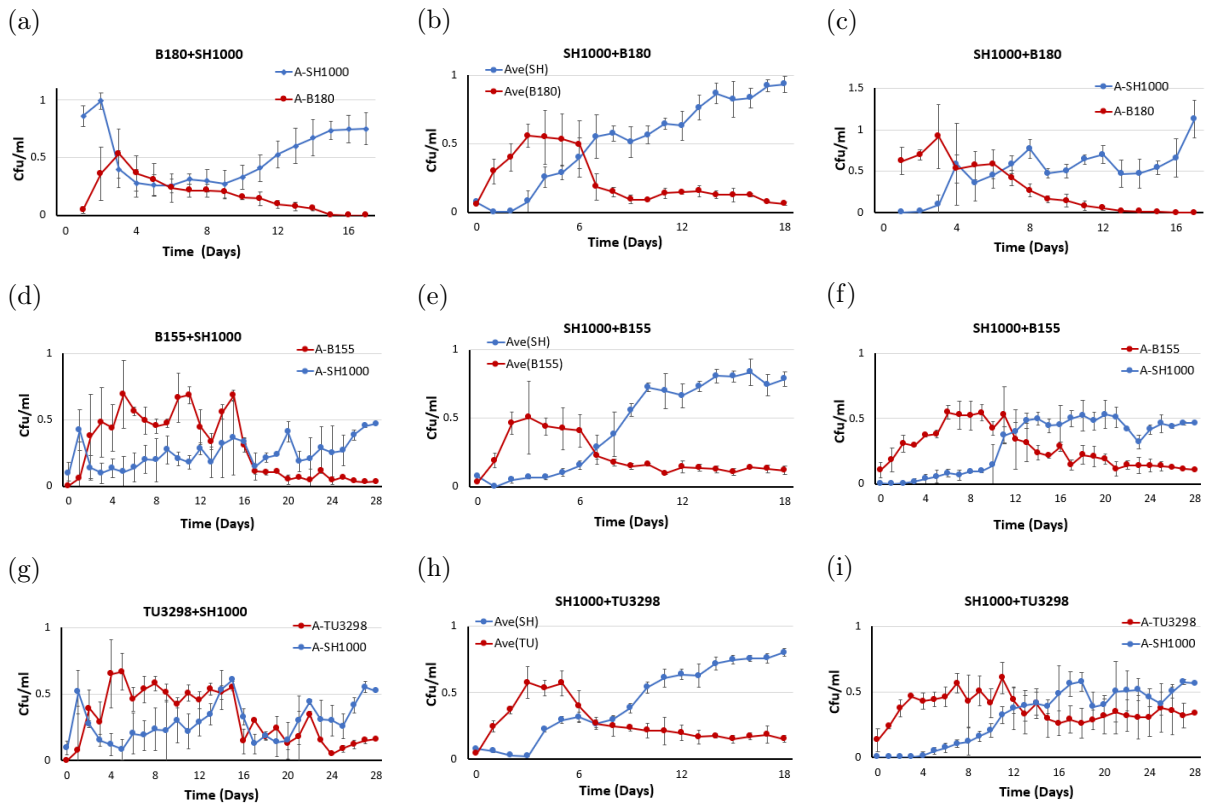
Figure 3.13: **The experimental data on the interaction dynamics of S. epidermidis and S. aureus species in mixed environments.** Panels (a), (b) and (c): show the interactions between low-toxin producing isolates of S. epidermidis (B180, red) and populations of S. aureus (SH1000, blue), starting from different initial concentrations. Panels (d), (e), and (f): reflect the interactions between moderate toxicity populations of S. epidermidis, (B155, red) and S. aureus, (SH1000, blue). Panels (g), (h), and (i): show the interactions between highly toxic populations of S. epidermidis (TU3298, red) and S. aureus (SH1000, blue). Panels in the first column, (a), (d), and (g): represent invasions of S. epidermidis (invaders) at initial ratios of (0.01: 1) to (resident) S. aureus populations. Panels in the second column, (b), (e) and (h): when the evolutions between the interacted populations started from equal initial frequencies. Panels in the third column, (c), (f) and (i): represent the mutual invasions performed between invaders of S. aureus at initial ratios of (0.01: 1) to resident populations of S. epidermidis. The x-axis is the time in days, and the y-axis is the colony-forming units (CFU) per plate. Error bars represent the standard error of the mean (n = 3).

A positive association between the level of toxicity produced by S. epidermidis populations and their ability to persist.

In all performed interactions, no eliminations or complete displacements were observed. All evolved populations coexisted. However, S. epidermidis was more likely to persist at low frequencies, as seen in Fig (3.13), and their chances of survival were positively associated with their level of toxicity.

The oscillations of the evolved population density were more evident when the interactions started from different initial concentrations.

As seen in Fig (3.13), the invasion scenarios, when the evolved populations started from different initial concentrations rather than equal initial frequencies, the fluctuations

in the density of evolving populations were more obvious and noticeable. Additionally, as seen in figures (3.13d, 3.13f, 3.13g, and 3.13i), the production of toxins contributed favourably to this phenomenon.

(a)

(b)

(c)

(d)

(e)

(f)

(g)

(h)

(i)
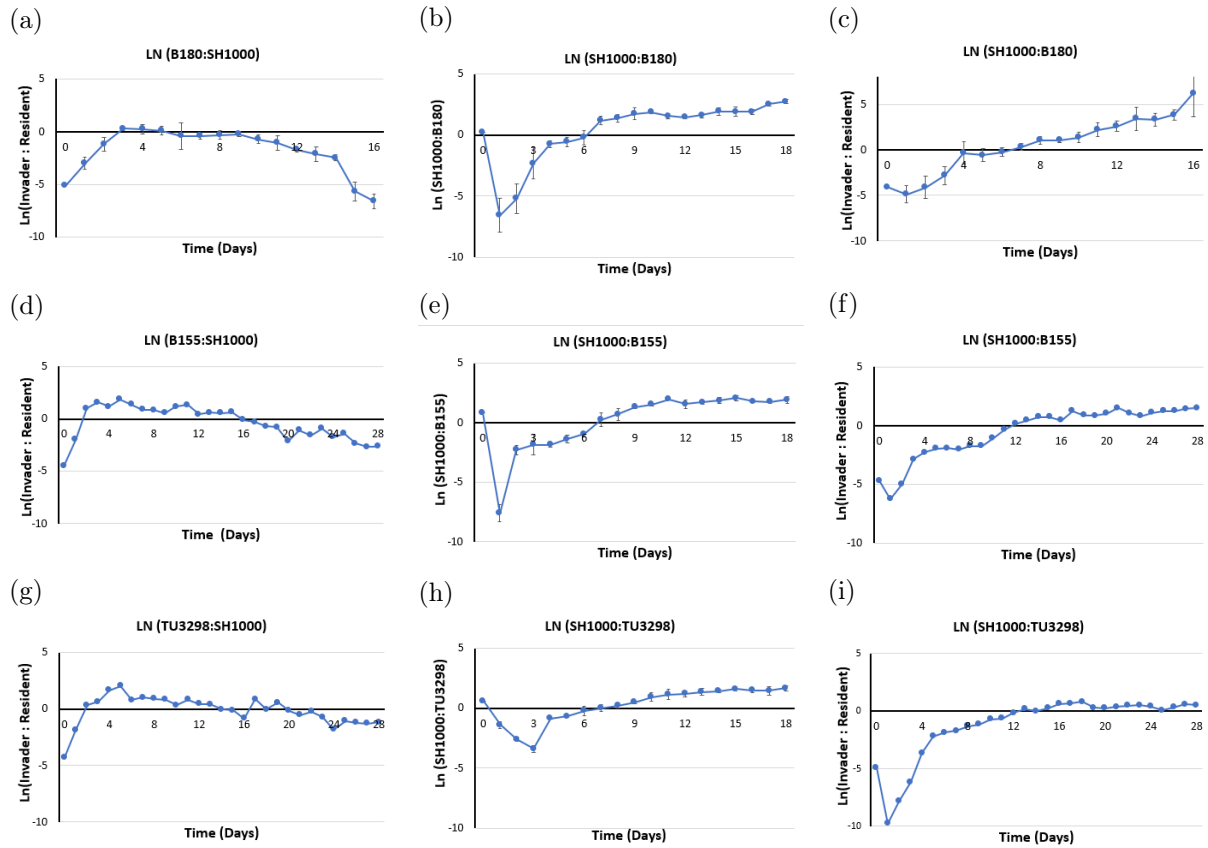
Figure 3.14: **Plots of the natural log of the evolved population ratio over time when interactions were conducted under mixed conditions.** Panels (a), (d) and (g): show the natural log of the invader to resident ratio, (B180: SH1000), (B155: SH1000) and (TU3298: SH1000) respectively. Panels (b), (e) and (h): display the natural log of the interacting population ratios, (SH1000: B180), (SH1000: B155), and (SH1000: TU3298), in that order, when starting from equal initial concentrations. Panels (c), (f), and (i): represent the natural log of the invader to resident ratio when performing reciprocal invasions. Again, the x-axis is the time in days. Error bars represent the standard error of the mean (n = 3).

3.5.2   Mathematical Models and Simulations

It is possible to expand on the spatially homogeneous *Lotka-Volterra* competition model to incorporate the diffusive terms of the respective species, u and v. This creates the (2.8) system. As shown in Fig (1.8), the interacted populations form a spot in the middle of the plate and expand symmetrically. Therefore, ideally, when modelling the interactions of microbial communities in Petri dishes, the Laplace operator in polar coordinates is used to express the space factor (1.34).

It should be noted that when scaling the space, larger r would mean smaller diffusion coefficients D and vice versa. Consequently, in any situation involving a small D, it is to

be expected that any simulations produced by (1.34) would be identical to simulations produced by (1.35). As shown in Fig (3.15a), after setting the time unit to $t = 1$, which is equivalent to one day, the growth rate for the evolved populations and the diffusion coefficients are defined as estimated in (3.4). Simulations obtained from (1.34), (blue), coincide with the (1.35) simulations, (red), when using the values found in the study presented in this thesis.
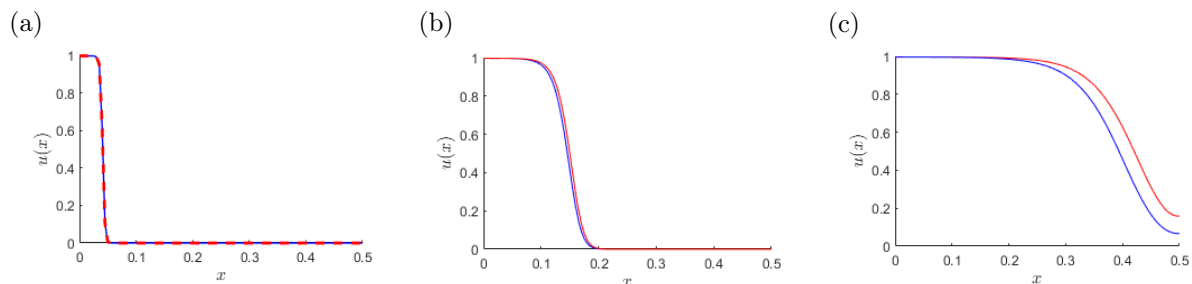
Figure 3.15: **A comparison of simulations produced by (1.34) and (1.35).** The profiles of u are plotted in space at time ($T = 10000 \approx 12$ hours), in the one-dimensional (red) and radially symmetric domains (blue). Panel (a): simulations obtained using the actual estimated diffusion coefficients in this study, $D_u = 1.8 \times 10^{-6}$. Panel (b): $D_u = 0.001$. Panel (c): $D_u = 0.01$. Parameters: $u_0 = 1$, $v_0 = 0.01$, $r_u = 26.5296$, $r_v = 28.613$, $b_1 = 0.1$ and $b_2 = 0.1$.

Further investigations were conducted to see if this added term would make a difference. Thus, the space step was fixed to ensure the accuracy and the time step was fixed to satisfy the stability conditions of all the simulations, with and without the first derivative, and the diffusion coefficients were manipulated in both variables. As previously stated, gradually increasing the diffusion coefficients for the evolved populations is equivalent to decreasing r. It was observed that the simulations obtained from (1.34) and (1.35) would differ slightly, as shown in Fig (3.15b), if the diffusion coefficients were significantly larger, (around 600 times larger), in comparison to the actual estimated values in this study. When the diffusion coefficients were increased about 6000 times more than the actuals, as seen in Fig (3.15c), it was observed that the speed of the right travelling waves of the 1-D model in (1.35), (red), was higher than the speed of the radially symmetric solutions, (blue). This delay was caused by the first derivative term in (1.34). The additional term in (1.34), which includes the first derivatives, makes a difference if the diffusion coefficients are significant, as illustrated in Fig (3.15a). Numerically distinguishing between the 1-D wave solution of (1.35) and the corresponding front solution of (1.34) poses a difficulty as they coincide when D is small. Furthermore, as shown in Fig (3.5) and determined in (3.4), when studying the diffusivities of the involved bacterial species, it is clear that all the bacterial species used diffuse weakly to the point that in many studies they are considered as non-motile species [28]. Thus, it is considered that for the given $D's$ the solutions of (1.34) will be well approximated by solutions of (1.35).

3.5.2.1 Modelling Non-inhibitory Interactions

As indicated previously in Chapter 2, simulations of the two-variable model concurred relatively with the actual experimental data in terms of the final stage of the competing populations. However, the dynamics of interaction were different. The non-monotonic behaviour of the competing populations when calculating the natural log of the invader to resident ratio was not obtained when producing the simulations using the two-variable model. The two-variable model simulations show a monotonic behaviour, meaning that the rate of change in population concentrations over time does not change the sign (i.e., if one of the competing populations is increasing, it is continuously increasing, and if it is decreasing it is continuously decreasing). Theoretically, to show that the two-variable model has a monotonic behaviour, the initial step was to define the expression $\frac{d}{dt}(ln(\frac{u}{v}))$, as follows:

$$\frac{d}{dt}\left(ln\left(\frac{u}{v}\right)\right) = \frac{v}{u} \cdot \frac{v.u^{'} - u.v^{'}}{v^2},$$

from (2.9), implanting the definition of u' and v' yields:

$$\frac{d}{dt}\left(ln\left(\frac{u}{v}\right)\right) = \frac{v}{u} \cdot \frac{v.r_u u(1 - u - b_1 v) - u.r_v v(1 - v - b_2 u)}{v^2}.$$

For simplicity, as the growth rate for both competing populations are positive and comparable to each other, it was decided to set $r_u = r_v = 1$, Hence:

$$\frac{d}{dt}\left(ln\left(\frac{u}{v}\right)\right) = \frac{\cancel{v}}{\cancel{u}} \cdot \frac{\cancel{v}.\cancel{u}(1 - u - b_1 v) - \cancel{u}.\cancel{v}(1 - v - b_2 u)}{\cancel{v}^{\cancel{2}}}.$$

Thus:

$$\frac{d}{dt}\left(ln\left(\frac{u}{v}\right)\right) = \left[(b_2 - 1)u + (1 - b_1)v\right].$$

Since all the competitions outcomes converge to the second equilibrium point $(u^*, v^*) = (1, 0)$ and according to the detailed analysis of Competitive *Lotka-Volterra* equations obtained in the first chapter, this equilibrium is stable if $b_1 < 1, b_2 > 1$. Hence:

$$\frac{d}{dt}\left(ln\left(\frac{u}{v}\right)\right) = a_1 u + a_2 v, \tag{3.21}$$

where a_1 and a_2 are positive constants and $u, v \in [0, 1]$. This means that rate of change in population concentrations, (SH1000: B180), over time is always positive, $\frac{d}{dt}\left(ln\left(\frac{u}{v}\right)\right) \geq 0$, and this contradicts the findings presented in Fig (3.14c), and Fig (3.14b).

On the other hand, when defining $\frac{d}{dt}(ln(\frac{v}{u}))$, as follows:

$$\frac{d}{dt}\left(ln\left(\frac{v}{u}\right)\right) = \frac{u}{v} \cdot \frac{u.v' - v.u'}{u^2}.$$

Following the previous steps, this expression was obtained:

$$\frac{d}{dt}\left(ln\left(\frac{v}{u}\right)\right) = \left[(1 - b_2)u + (b_1 - 1)v\right].$$

Again, applying the stability conditions gives:

$$\frac{d}{dt}\left(ln\left(\frac{v}{u}\right)\right) = -\left[a_1 u + a_2 v\right]. \qquad (3.22)$$

This signifies that rate of change in population concentrations, (B180: SH1000), over time is always negative, and this contradicts the findings presented in Fig (3.14a). From (3.21) and (3.22), it can be concluded that all possible simulations obtained from two-variable models that satisfy the stability conditions have monotonic behaviour. Such behaviour is inconsistent with the dynamics of interaction observed in the laboratory results.

Thus, the two-variable model failed to simulate the illustrated experimental dynamics. Hence, the use of a two-variable model to simulate the experimental data was discarded.

Modelling The Dynamics of Interactions Between Two Populations With Adaptation

According to the experimental data shown in figures (3.14a), (3.14c) and (3.14b), the evolved *S. aureus* exhibited a reduction in population size at the start of all interactions before recovering and becoming dominant. This reduction means that a large part of the interacted *S. aureus* population could not survive the competition and died. In contrast, a small part of the same population developed resistance against the opponent, which led to their success in achieving dominance. This dynamic of *S. aureus* population explains the non-monotonicity observed when plotting the natural logarithm of the competing population ratio. Mathematically, such a dynamic could be presented and generated if a third variable is added to represent the adapted part of the population. This part acts differently when interacting with *S. epidermidis*, as it is less sensitive to the effects of the opponent and competes more strongly to the point where it excludes its opponent. As a result, in the following section, a three-variable model is introduced. In this model, two variables represent the fractions of the *S. aureus* population known as susceptible, u_s, and adapted, u_a.

Two competing bacterial populations in a one-dimensional domain are considered. One species, the 'susceptible', has a fraction of cells capable of adapting to the fierceness of the competition, the 'adapted'. Denoting the concentrations of susceptible *S. aureus*,

adapted *S. aureus* and *S. epidermidis* at position x and time t by $u_s(x,t)$, $u_a(x,t)$ and $v_{(x,t)}$, this ecosystem is modelled via the equations:

$$\begin{cases} \dfrac{\partial u_s}{\partial t} = D_{u_s} \dfrac{\partial^2 u_s}{\partial x^2} + r_{u_s}\, u_s\, (1 - u_s - b_1\, v - (1 + \psi)\, u_a), \\[2mm] \dfrac{\partial u_a}{\partial t} = D_{u_a} \dfrac{\partial^2 u_a}{\partial x^2} + r_{u_a}\, u_a\, (1 - u_a - b_2\, v - (1 + \psi)\, u_s), \\[2mm] \dfrac{\partial v}{\partial t} = D_v \dfrac{\partial^2 v}{\partial x^2} + r_v\, v\, (1 - v - b_3\, u_s - b_4\, u_a), \end{cases} \qquad (3.23)$$

where D, r, b and ψ terms are all positive constants. D_{u_s}, D_{u_a} and D_v represent the respective diffusion coefficient of each population, r_{u_s}, r_{u_a} and r_v represent the linear birth rates of each species. The b terms measure the competitive effect of each population on the other, while $\psi \ll 1$ is a small value-added to the interaction coefficients between the susceptible and the adapted fractions of the *S. aureus* population to prevent obtaining zero as an eigenvalue when analysing the equilibrium points of this system.

Initial conditions:

$$v(x,0) \begin{cases} 1 & x \in [\tfrac{L}{2} - l, \tfrac{L}{2} + l], \\ 0 & \text{otherwise,} \end{cases}$$

$$u_s(x,0) + u_a(x,0) = 0.01 \times v(x,0) \text{ and } u_a/u_s = 0.01.$$

This can be presented the other way around when performing the mutual invasions.

Boundary conditions: Again, zero–flux boundary conditions are imposed for all variables.

Similarly, as shown in two-variable model, in the absence of spatial variation, the system (3.23) is considered as the three species food web model with the *Lotka-Volterra* type interaction between populations [148]. There are six physically relevant (i.e., real and non-negative) stationary homogeneous solutions $(u_s, u_a, v) = (u_s^*, u_a^*, v^*)$

- the trivial solution, $(u_s^*, u_a^*, v^*) = (0, 0, 0)$

- u_s excludes u_a and v, $(u_s^*, u_a^*, v^*) = (1, 0, 0)$

- u_a excludes u_s and v, $(u_s^*, u_a^*, v^*) = (0, 1, 0)$

- v excludes u_s and u_a, $(u_s^*, u_a^*, v^*) = (0, 0, 1)$

- u_s and v exclude u_a, $(u_s^*, u_a^*, v^*) = (\frac{1-b_1}{1-b_1\,b_3}, 0, \frac{1-b_3}{1-b_1\,b_3})$

- u_a and v exclude u_s, $(u_s^*, u_a^*, v^*) = (0, \frac{1-b_2}{1-b_2\,b_4}, \frac{1-b_4}{1-b_2\,b_4})$

The two equilibriums that indicate co-existence between *S. aureus* and *S. epidermidis* are only considered if $u_s^* \geq 0$, $u_a^* \geq 0$ and $v^* \geq 0$ are finite, in which case $b_1 \cdot b_3 \neq 1$ and

$b_2 . b_4 \neq 1$ respectively. To determine the stability of the steady states, the Jacobian of communities is needed:

$$J = \begin{bmatrix} r_1\left(-b_1\,v - u_s - u_a + 1\right) - r_1 u_s & -r_1 u_s & -r_1 b_1 u_s \\ -r_2 u_a & r_2\left(-b_2 v - u_s - u_a + 1\right) - r_2 u_a & -r_2 b_2 u_a \\ -r_3 b_3\,v & -r_3 b_4 v & r_3\left(-b_3 u_s - u_a b_4 - v + 1\right) - r_3 v \end{bmatrix}.$$

The first steady state $(0,0,0)$, is unstable. By implementing this point into the Jacobian matrix, the positive eigenvalues $\lambda_1 = r_1$, $\lambda_2 = r_2$ and $\lambda_3 = r_3$ are obtained.

$$\begin{bmatrix} \lambda_1 \\ \lambda_2 \\ \lambda_3 \end{bmatrix}_{(0,0,0)} = \begin{bmatrix} r_1 \\ r_2 \\ r_3 \end{bmatrix}.$$

Implementing the second equilibrium point, $(1,0,0)$, into the Jacobian matrix gives:

$$\begin{bmatrix} \lambda_1 \\ \lambda_2 \\ \lambda_3 \end{bmatrix}_{(1,0,0)} = \begin{bmatrix} -r_1 \\ -\frac{r_2}{10000} \\ -r_3\left(b_3 - 1\right) \end{bmatrix}.$$

The condition for this equilibrium to be stable is the following:

$$(u_s^*, u_a^*, v^*) = (1,0,0) \text{ is } \begin{cases} \text{stable,} & \text{if } b_3 > 1, \\ \text{unstable,} & \text{if } b_3 < 1. \end{cases}$$

The eigenvalues for the third equilibrium point, $(0,1,0)$, are:

$$\begin{bmatrix} \lambda_1 \\ \lambda_2 \\ \lambda_3 \end{bmatrix}_{(0,1,0)} = \begin{bmatrix} -r_3(b_4 - 1) \\ -r_2 \\ -\frac{r_1}{10000} \end{bmatrix}.$$

The condition for this equilibrium to be stable is the following:

$$(u_s^*, u_a^*, v^*) = (0,1,0) \text{ is } \begin{cases} \text{stable,} & \text{if } b_4 > 1, \\ \text{unstable,} & \text{if } b_4 < 1. \end{cases}$$

When implementing the fourth equilibrium point, $(0,0,1)$, into the Jacobian matrix, the following eigenvalues were obtained:

$$\begin{bmatrix} \lambda_1 \\ \lambda_2 \\ \lambda_3 \end{bmatrix}_{(0,0,1)} = \begin{bmatrix} -r_1(b_1 - 1) \\ -r_2(b_2 - 1) \\ -r_3 \end{bmatrix}.$$

The conditions for this equilibrium to be stable are the following:

$$(u_s^*, u_a^*, v^*) = (0,0,1) \text{ is } \begin{cases} \text{stable,} & \text{if } b_1, b_2 > 1, \\ \text{unstable,} & \text{if } b_1, b_2 < 1. \end{cases}$$

The eigenvalues for the equilibrium that indicates a co-existence between the susceptible *S. aureus* and *S. epidermidis* are:

$$
\begin{bmatrix} \lambda_1 \\ \lambda_2 \\ \lambda_3 \end{bmatrix}_{\left(\frac{1-b_1}{1-b_1 b_3},0,\frac{1-b_3}{1-b_1 b_3}\right)} = \begin{bmatrix} \frac{-r_1 b_1 - r_3 b_3 + r_1 + r_3 + \sqrt{r_1^2(-1+b_1)^2 + 4\left(b_1 b_3 - \frac{1}{2}\right)(-1+b_1)r_3(b_3-1)r_1 + r_3^2(b_3-1)^2}}{2b_1 b_3 - 2} \\ \frac{-r_1 b_1 - r_3 b_3 + r_1 + r_3 - \sqrt{r_1^2(-1+b_1)^2 + 4\left(b_1 b_3 - \frac{1}{2}\right)(-1+b_1)r_3(b_3-1)r_1 + r_3^2(b_3-1)^2}}{2b_1 b_3 - 2} \\ \frac{r_2(b_3-1)(b_1-b_2)}{b_1 b_3 - 1} \end{bmatrix}.
$$

For simplicity, as the growth rate for both competing populations are positive and comparable to each other, it was decided to set $r_{u_s} = r_{u_a} = r_v = 1$. Hence:

$$
\begin{bmatrix} \lambda_1 \\ \lambda_2 \\ \lambda_3 \end{bmatrix}_{\left(\frac{1-b_1}{1-b_1 b_3},0,\frac{1-b_3}{1-b_1 b_3}\right)} = \begin{bmatrix} -1 \\ \frac{(-1+b_3)(-1+b_1)}{b_1 b_3 - 1} \\ \frac{(-1+b_3)(b_1-b_2)}{b_1 b_3 - 1} \end{bmatrix}.
$$

The conditions for this equilibrium to be stable are the following:

$$
(u_s^*, u_a^*, v^*) = \left(\frac{1-b_1}{1-b_1 b_3}, 0, \frac{1-b_3}{1-b_1 b_3}\right) \text{ is } \begin{cases} \text{stable,} & \text{if} \quad b_1, b_3 < 1 \text{ and } b_2 > b_1, \\ \text{unstable,} & \text{if} \quad \text{otherwise.} \end{cases}
$$

$$
\begin{bmatrix} \lambda_1 \\ \lambda_2 \\ \lambda_3 \end{bmatrix}_{\left(0,\frac{1-b_2}{1-b_2 b_4},\frac{1-b_4}{1-b_2 b_4}\right)} = \begin{bmatrix} \frac{-r_2 b_2 - r_3 b_4 + r_2 + r_3 + \sqrt{r_2^2(b_2-1)^2 + 4(b_2-1)r_3\left(b_2 b_4 - \frac{1}{2}\right)(-1+b_4)r_2 + r_3^2(-1+b_4)^2}}{2b_2 b_4 - 2} \\ \frac{-r_2 b_2 - r_3 b_4 + r_2 + r_3 - \sqrt{r_2^2(b_2-1)^2 + 4(b_2-1)r_3\left(b_2 b_4 - \frac{1}{2}\right)(-1+b_4)r_2 + r_3^2(-1+b_4)^2}}{2b_2 b_4 - 2} \\ -\frac{r_1(-1+b_4)(b_1-b_2)}{b_2 b_4 - 1} \end{bmatrix}.
$$

Similarly, for simplicity, as the growth rate for both competing populations are positive and comparable to each other, it was decided to set $r_{u_s} = r_{u_a} = r_v = 1$. Hence:

$$
\begin{bmatrix} \lambda_1 \\ \lambda_2 \\ \lambda_3 \end{bmatrix}_{\left(0,\frac{1-b_2}{1-b_2 b_4},\frac{1-b_4}{1-b_2 b_4}\right)} = \begin{bmatrix} -1 \\ \frac{(-1+b_4)(-1+b_2)}{b_2 b_4 - 1} \\ \frac{(-1+b_4)(b_2-b_1)}{b_2 b_4 - 1} \end{bmatrix}.
$$

The conditions for this equilibrium to be stable are the following:

$$
(u_s^*, u_a^*, v^*) = \left(0, \frac{1-b_2}{1-b_2 b_4}, \frac{1-b_4}{1-b_2 b_4}\right) \text{ is } \begin{cases} \text{stable,} & \text{if} \quad b_2, b_4 < 1 \text{ and } b_1 > b_2, \\ \text{unstable,} & \text{if} \quad \text{otherwise.} \end{cases}
$$

From the previous equilibrium points, the only interest is in the third point, $(0, 1, 0)$, where the adapted fraction of the *S. aureus* population, u_a, exclude the susceptible fraction, u_s, and *S. epidermidis* population v. Thus, the stability of this particular point is

113

sought. By applying the stability condition $b_4 > 1$, better simulations are obtained that satisfy the obtained experimental data.

According to the actual experimental data shown in Fig (3.13), when isolates of *S. epidermidis* invaded the resident population of *S. aureus*, these invasions resulted in a decrease in the resident population density. However, the resident population recovered from the impact of these invasions and were able to increase production to reach population domination. This recovery started on the sixth day, when they reached the ratio (1: 1) with the *S. epidermidis* population and overcame their opponent afterwards. The extended model was able to capture these dynamics, and, as shown in Fig (3.16a), the evolved population intersected on day six. Furthermore, Fig (3.16b) displays the dynamic of interactions more clearly, where the increase of the invader, the red line, was at the expense of the collapse of the susceptible fraction of resident, blue line, resulting in the growth and emergence of resistance, (green line). The non-monotonicity appeared in the dynamics of interference when plotting the ratio between the evolved population, Fig (3.16c), which was mainly caused by the behaviour of the *S. aureus* population during the competition as it adapted after the majority of its population collapsed at the beginning of these invasions. The three-variable model successfully simulated such behaviour, (See Fig 3.16c).

Figure 3.16: **Three-variable model simulation when low-toxin-producing isolates of *S. epidermidis* (B**180**) invade populations of *S. aureus* (SH**1000**) at frequencies of** 0.01. Panel (a): simulations of interactions obtained from (3.23); (red) is *S. epidermidis*; (blue) is *S. aureus*, $(u_s + u_a)$. Panel (b): demonstration of the three variable dynamics where (red) is *S. epidermidis*, (blue) is the susceptible fraction of *S. aureus* population, and (green) is the adapted part. Panel (c): the solid line indicates the simulation of the natural log of the invader to resident ratio, black dots represent the natural log of the invader to resident ratio from the actual data. In all panels, the x-axis is the time in days. The y-axis in panels (a) and (b) represents the relative concentrations of the evolved populations, and in panel (c) the natural log of the evolved population ratio. Parameters: $D_u = 1.8 \times 10^{-6}$, $D_v = 2 \times 10^{-5}$, $r_u = 26.5296$, $r_v = 29.7216$, $b_1 = 1.1$, $b_2 = 0.89$, $b_3 = 0.82$ and $b_4 = 1.45$.

Likewise, as shown in Fig (3.17), the three-variable model was able to simulate the other directions of the invasions when *S. epidermidis* populations became residents. Regardless of the oscillation that appeared in the behaviour of the *S. aureus* population during the interactions, and such behaviour was also observed in controls (See Fig 6.3, dotted black lines), the obtained laboratory results showed that *S. aureus* was able to overcome its

opponent by the fourth day when they intersected, (See Fig 3.14c).

The dynamic of interactions when performing this direction of invasion is illustrated evidently in Fig (3.17b), as the resident population of *S. epidermidis* (red line) restricted and inhibited the invasion by susceptible *S. aureus* (blue line). This led to the emergence of resistance by the invader population of *S. aureus* (green line).

Evolution from equal initial frequencies

As shown in Fig (3.13b), and as previously noted, when the interaction between these two species, B180 and SH1000, started from equal initial concentration, it was observed that both populations tend to behave similarly when performing the invasions. The competing population of *S. epidermidis* diverged from the control experiment, where they were cultured independently, which indicates that the population was about to become extinct and vanish, and on the other hand the evolved *S. aureus* strain converged to its control experiment, from which it appears that their growth was no longer affected by the presence of the other competitor. However, the dynamic of the evolution seemed slower. As shown in Fig (3.18a), the competing population of *S. aureus* recovered and started to grow by day six, when they reached a (1: 1) ratio with *S. epidermidis* B180, (See Fig 3.18c), and continued to evolve to become the majority of the developed populations.

Figure 3.17: **Three-variable model simulation when low-toxin-producing isolates of *S. epidermidis* (B180) invaded by populations of *S. aureus* (SH1000) at frequencies of 0.01.** Panel (a): simulations of interactions obtained from (3.23); (red) is *S. epidermidis*; (blue) is *S. aureus*, $(u_s + u_a)$. Panel (b): demonstration of the three variable dynamics where (red) is *S. epidermidis*; (blue) is the susceptible fraction of *S. aureus* population; and (green) is the adapted part. Panel (c): the solid line indicates the simulation of the natural log of the invader to resident ratio; black dots represent the natural log of the invader to resident ratio from the actual data. In all panels, the x-axis is the time in days. The y-axis in panels (a) and (b) represents the relative concentrations of the evolved populations, and in panel (c) the natural log of the evolved population ratio. Parameters: $D_u = 1.8 \times 10^{-6}$, $D_v = 2 \times 10^{-5}$, $r_u = 26.5296$, $r_v = 29.7216$, $b_1 = 1.1$, $b_2 = 0.89$, $b_3 = 0.82$ and $b_4 = 1.45$.

A detailed overview of the interactions is demonstrated in Fig (3.18b), where the evolved population of B180 (red line) inhibited and restricted the evolution of the susceptible fraction of *S. aureus* population (blue line) causing them to develop a resistance against their competitor (green line) and grow exponentially to form the major component of the population sample.

Figure 3.18: **Three-variable model simulation when low-toxin-producing isolates of *S. epidermidis* (B**180**) compete with populations of *S. aureus* (SH**1000**) at frequencies of** $1:1.$ Panel (a): simulations of interactions obtained from (3.23); (red) is *S. epidermidis*; (blue) is *S. aureus*, $(u_s + u_a)$. Panel (b): demonstration of the three variable dynamics where (red) is *S. epidermidis*; (blue) is the susceptible fraction of *S. aureus* population; and (green) is the adapted part. Panel (c): the solid line indicates the simulation of the natural log of SH1000 to B180 ratio; black dots represent the natural log of this ratio from the actual data. In all panels, the x-axis is the time in days. The y-axis in panels (a) and (b) represents the relative concentrations of the evolved populations, and in panel (c) the natural log of the evolved population ratio. Parameters: $D_u = 1.8 \times 10^{-6}$, $D_v = 2 \times 10^{-5}$, $r_u = 26.5296$, $r_v = 29.7216$, $b_1 = 1.1$, $b_2 = 0.89$, $b_3 = 0.82$ and $b_4 = 1.45$.

Considering the simulations shown in Fig (3.16), Fig (3.17), and Fig (3.18), it can be concluded that the three-variable model could generate a demonstration of the interaction dynamics. However, this model was not able to create the oscillation observed in the experimental data.

3.5.2.2 Modelling Inhibitory Interactions

The aim of this study is to model the interactions involving toxin production, where one of the competing populations, *S. epidermidis*, produces toxin at a rate of f_1, while the other competing population, *S. aureus*, is well-known for its ability to adapt and mutate against these toxins. The concentrations of susceptible *S. aureus*, adapted S. aureus, producer *S. epidermidis*, and toxin at position x and time t are defined as $u_s(x,t)$, $u_a(x,t)$, $v(x,t)$, and $T(x,t)$.

Thus, this ecosystem is modelled via the equations:

$$\begin{cases} \dfrac{\partial u_s}{\partial t} = D\dfrac{\partial^2 u_s}{\partial x^2} + r_{u_s}\, u_s\left(1 - u_s - b_1\, v - (1+\psi)\, u_a - p_1\, T\right), \\[2mm] \dfrac{\partial u_a}{\partial t} = D\dfrac{\partial^2 u_a}{\partial x^2} + r_{u_a}\, u_a\left(1 - u_a - b_2\, v - (1+\psi)\, u_s - p_2\, T\right), \\[2mm] \dfrac{\partial v}{\partial t} = D\dfrac{\partial^2 v}{\partial x^2} + r_v\, v\left(1 - v - b_3\, u_s - b_4\, u_a\right), \\[2mm] \dfrac{\partial T}{\partial t} = D_T\dfrac{\partial^2 T}{\partial x^2} + f_1\, v - f_2\, T, \end{cases} \tag{3.24}$$

where r's represent the growth rates and b's are the competition coefficients, p: inhibition coefficient, f_1: inhibitor production rate, f_2: inhibitor degradation rate. While $\psi \ll 1$ is a

116

small value-added to the interaction coefficients between the susceptible and the adapted fractions of the *S. aureus* population to prevent obtaining zero as an eigenvalue when analysing the equilibrium points of this system.

Initial conditions:

$$v(x,0) \begin{cases} 1 & x \in [\frac{L}{2} - l, \frac{L}{2} + l], \\ 0 & \text{otherwise,} \end{cases}$$

$u_s(x,0) + u_a(x,0) = a \cdot v(x,0)$ where $a = 0.01$ and $u_a/u_s = 0.01$ and $T(x,0) = 0$.

This is also valid contrariwise when performing the mutual invasions.

Boundary conditions: Again, zero–flux boundary conditions are imposed for all variables. This model (3.24) represents the spatially extended *Lotka-Volterra* model when two species compete in one dimension.
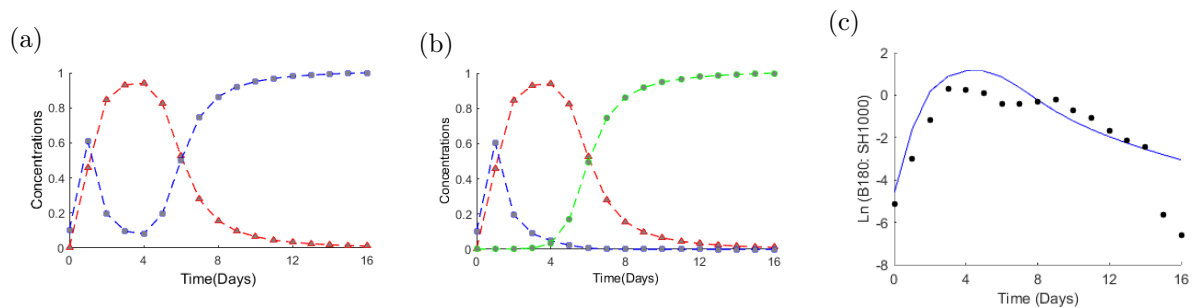

Figure 3.19: **Four-variable model simulation when toxin-producing isolates of *S. epidermidis* (B155) invade populations of *S. aureus* (SH1000) at frequencies of 0.01: 1.** Panel (a): simulations of interactions obtained from (3.24); (red) is *S. epidermidis*; (blue) is *S. aureus*, $(u_s + u_a)$. Panel (b): demonstration of the four variable dynamics where (red) is *S. epidermidis*; (blue) is the susceptible fraction of *S. aureus* population; (green) is the adapted part; and (black) is the toxin. Panel (c): the solid line indicates the simulation of the natural log of the invader to resident ratio; black dots represent the natural log of the invader to resident ratio from the actual data. In all panels, the x-axis is the time in days. The y-axis in panels (a) and (b) represents the relative concentrations of the evolved populations and toxins, and in panel (c) the natural log of the evolved population ratio. Parameters: $D_u = 1.8 \times 10^{-6}$, $D_v = 5 \times 10^{-6}$, $r_u = 26.5296$, $r_v = 22.3344$, $p_1 = 1.0091$, $p_2 = 0.9755$, $f_1 = 1$, $f_2 = 0.18$, $b_1 = 1.1$, $b_2 = 0.9$, $b_3 = 0.65$ and $b_4 = 0.96$.

The modifications were made to account for the production of toxins by one species to inhibit the other and the ability of the inhibited population to mutate against these toxins. This model has more parameters, as stated and defined previously, in compression with the other models. However, all the added parameters which represent inhibition coefficients, production, and decaying rate of the toxins can be estimated and defined by using the equation (3.19).

As illustrated in Fig (3.10), there is a positive association between the toxin production rate and the decaying rate. The same correlation is observed between the inhibition coefficients and the decaying rate.
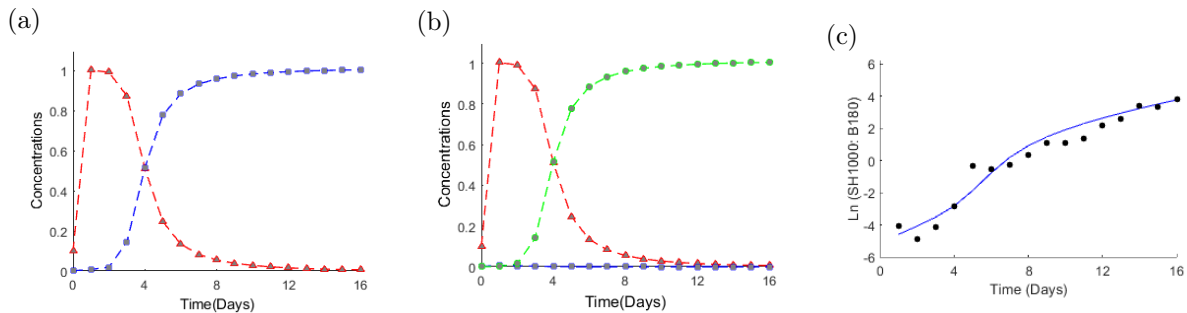
Figure 3.20: **Four-variable model simulation when toxin-producing isolates of *S. epidermidis* (B**155**) invaded by populations of *S. aureus* (SH**1000**) at frequencies of** $0.01 : 1$**.** Panel (a): simulations of interactions obtained from (3.24); (red) is *S. epidermidis*; (blue) is *S. aureus*, $(u_s + u_a)$. Panel (b): demonstration of the four variable dynamics where (red) is *S. epidermidis*; (blue) is the susceptible fraction of *S. aureus* population; (green) is the adapted part; and (black) is the toxin. Panel (c): the solid line indicates the simulation of the natural log of the invader to resident ratio; black dots represent the natural log of the invader to resident ratio from the actual data. In all panels, the x-axis is the time in days. The y-axis in panels (a) and (b) represents the relative concentrations of the evolved populations and toxins, and in panel (c) the natural log of the evolved population ratio. Parameters: $D_u = 1.8 \times 10^{-6}$, $D_v = 5 \times 10^{-6}$, $r_u = 26.5296$, $r_v = 22.3344$, $p_1 = 1.0091$, $p_2 = 0.9755$, $f_1 = 1$, $f_2 = 0.18$, $b_1 = 1.1$, $b_2 = 0.9$, $b_3 = 0.65$ and $b_4 = 0.96$.

When different values of f_2 were tested in the model (3.24), it was discovered that higher values of the declining rate, f_2, imply higher values of the production rate, f_1, as the results of these *S. aureus* populations would not have a chance to successfully invade the *S. epidermidis* populations, which contradicts the experimental findings of this study. See figures (3.13d), (3.13e), and (3.13f).

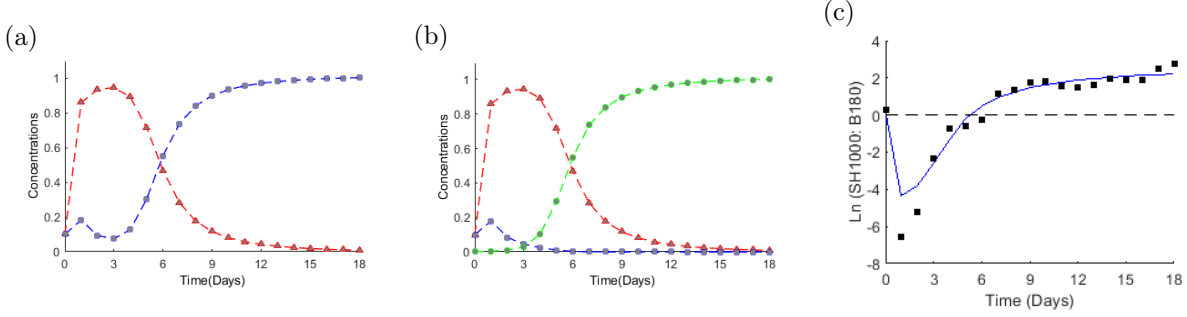Figure 3.21: **Four-variable model simulation when toxin-producing isolates of *S. epidermidis* (B**155**) compete with populations of *S. aureus* (SH**1000**) at initial frequencies of** $1 : 1$**.** Panel (a): simulations of interactions obtained from (3.24); (red) is *S. epidermidis*; (blue) is *S. aureus*, $(u_s + u_a)$. Panel (b): demonstration of the four variable dynamics where (red) is *S. epidermidis*; (blue) is the susceptible fraction of *S. aureus* population; (green) is the adapted part; and (black) is the toxin. Panel (c): the solid line indicates the simulation of the natural log of SH1000 to B155 ratio; black dots represent the natural log of this ratio from the actual data. In all panels, the x-axis is the time in days. The y-axis in panels (a) and (b) represents the relative concentrations of the evolved populations and toxins, panel (c) the natural log of the evolved population ratio. Parameters: $D_u = 1.8 \times 10^{-6}$, $D_v = 5 \times 10^{-6}$, $r_u = 26.5296$, $r_v = 22.3344$, $p_1 = 1.0091$, $p_2 = 0.9755$, $f_1 = 1$, $f_2 = 0.18$, $b_1 = 1.1$, $b_2 = 0.9$, $b_3 = 0.65$ and $b_4 = 0.96$.

Furthermore, small values of f_2 mean that *S. aureus* will invade rapidly. Hence, it is necessary to choose the proper value that will satisfy the experimental data in this study. Thus, when the production rate is fixed at $f_1 = 1$, selecting the appropriate value of f_2 gives the corresponding values for p_1 and p_2, which are the inhibition coefficients

of the toxins produced by B155 on the susceptible and adapted fractions of *S. aureus*, respectively. Four variable model simulations were fitted to the actual experimental data by using the least square method. It was possible to obtain the best values, with the minimum error, for the interaction coefficients as well as the inhibitory reduction rate after defining the inhibition coefficients p_1 and p_2 with respect to f_2, as presented in equation (3.19).

Regardless of the oscillations observed in the dynamics of interactions when starting from different initial concentrations, figures (3.13d) and (3.13f), the four-variable model successfully simulated the experimental data that reflect interactions between toxin-producing *S. epidermidis* and *S. aureus* populations in terms of the intersection point between the competing populations as well as the final state of the evolved species, as seen in Fig (3.19).
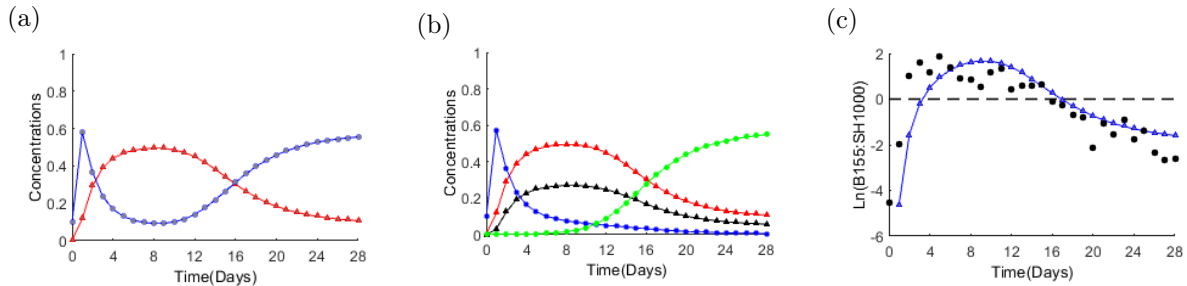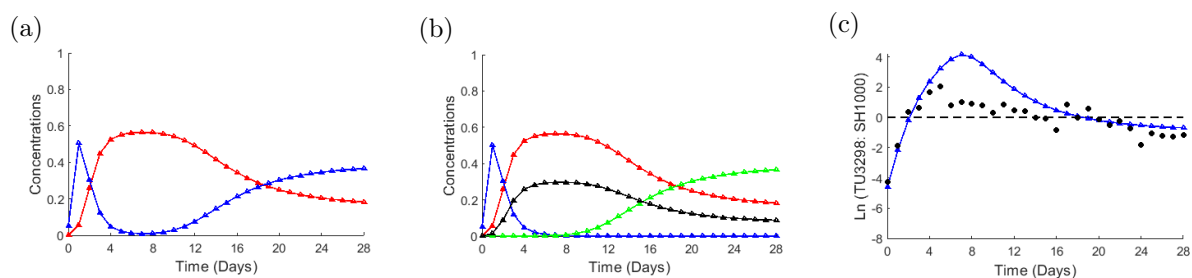

Figure 3.22: **Four-variable model simulation when toxin-producing isolates of *S. epidermidis* (TU**3298**) invade populations of *S. aureus* (SH**1000**) at frequencies of** $0.01 : 1$**.** Panel (a): simulations of interactions obtained from (3.24); (red) is *S. epidermidis*; (blue) is *S. aureus*, $(u_s + u_a)$. Panel (b): demonstration of the four variable dynamics where (red) is *S. epidermidis*; (blue) is the susceptible fraction of *S. aureus* population; (green) is the adapted part; and (black) is the toxin. Panel (c): the solid line indicates the simulation of the natural log of the invader to resident ratio; black dots represent the natural log of the invader to resident ratio from the actual data. In all panels, the x-axis is the time in days. The y-axis in panels (a) and (b) represents the relative concentrations of the evolved populations and toxins, and in panel (c) the natural log of the evolved population ratio. Parameters: $D_u = 1.8 \times 10^{-6}$, $D_v = 5 \times 10^{-5}$, $r_u = 26.5296$, $r_v = 28.613$, $p_1 = 0.7746$, $p_2 = 0.7623$, $f_1 = 1$, $f_2 = 0.24$, $b_1 = 0.9$, $b_2 = 0.84$, $b_3 = 0.9$ and $b_4 = 1.09$.

When populations of the toxin-producing strain B155 were introduced to the resident population of *S. aureus*, SH1000, as a result the density of the resident population decreased and struggled until it was able to develop a resistance mechanism and raise its concentration back to the ratio of (1: 1) with its opponent by day $16-17$. Similarly, when the invasion was carried out in the opposite direction, the resident population of B155 restricted and inhibited the invasions by *S. aureus* up to day 8, after which the invader *S. aureus* mutated against the inhibitory produced by B155 and began to recover to the point where it coincided with B155 on day 12 and eventually dominated the interactions.

The model simulations presented in figures (3.19), (3.20), and (3.21) captured these sort of behaviours when simulating the invasions. When using the four-variable model to simulate the interaction outcomes between B155 and SH1000, all parameters were fixed

regardless of the initial concentrations of the competing populations.

Likewise, when using a four-variable model to produce simulations of the interactions between populations of *S. aureus* and *S. epidermidis*, TU3298, the production, decaying and inhibition coefficients were fixed regardless of the initial concentrations of the competing populations.

According to Fig (3.7a), *S. epidermidis* strain TU3298 produced a larger inhibition zone in comparison with the other involved strains. However, according to [196], there are many technical factors influencing the size of the zone in the disc diffusion method. For instance, the density of inoculum, the inhibition zones will be larger if the inoculum is too light, even if the organism's sensitivity remains unchanged. Relatively resistant strains can be considered as susceptible strains. If the inoculum is too heavy, the zone size is reduced, and susceptible strains may be reported as resistant.
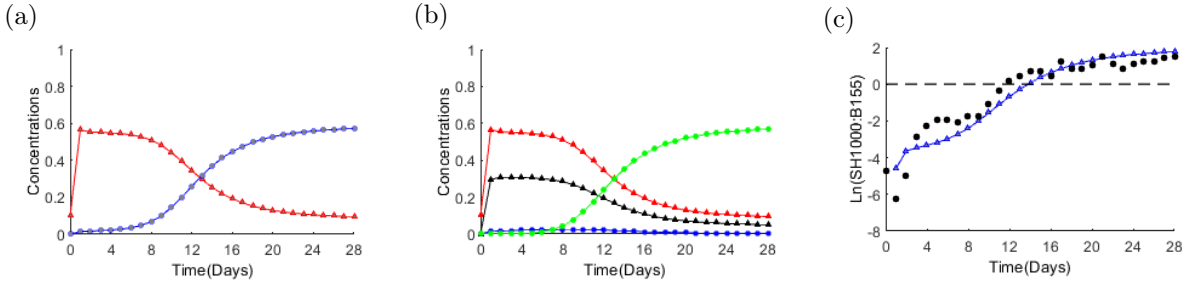
(a) (b) (c)
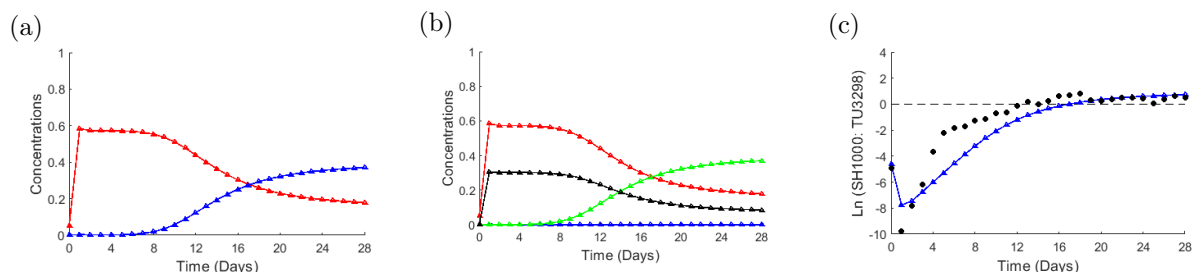
Figure 3.23: **Four-variable model simulation when toxin-producing isolates of *S. epidermidis* (TU3298) invaded by populations of *S. aureus* (SH1000) at frequencies of** $0.01 : 1.$ Panel (a): simulations of interactions obtained from (3.24); (red) is *S. epidermidis*; (blue) is *S. aureus*, $(u_s + u_a)$. Panel (b): demonstration of the four variable dynamics where (red) is *S. epidermidis*; (blue) is the susceptible fraction of *S. aureus* population; (green) is the adapted part; and (black) is the toxin. Panel (c): the solid line indicates the simulation of the natural log of the invader to resident ratio; black dots represent the natural log of the invader to resident ratio from the actual data. In all panels, the x-axis is the time in days. The y-axis in panels (a) and (b) represents the relative concentrations of the evolved populations and toxins, and in panel (c) the natural log of the evolved population ratio. Parameters: $D_u = 1.8 \times 10^{-6}$, $D_v = 5 \times 10^{-5}$, $r_u = 26.5296$, $r_v = 28.613$, $p_1 = 0.7746$, $p_2 = 0.7623$, $f_1 = 1$, $f_2 = 0.24$, $b_1 = 0.9$, $b_2 = 0.84$, $b_3 = 0.9$ and $b_4 = 1.09$.

Furthermore, the production rate of the producer can positively contribute to the size of the inhibition zone. As stated in [143], a growth inhibition experiment evaluates one bacterium's ability to inhibit the growth of another by producing antimicrobial chemicals or competing for resources. Thus, the clear zone around the spot possibly signifies that it does not contain food, as it is consumed by the producer, and that it is no longer suitable for the growth of the other competing bacteria.

As demonstrated in Table (3.4), *S. epidermidis* strain TU3298 has a higher growth rate than its opponent, *S. aureus* SH1000 and in the model (3.24), the production rate of the toxins is positively associated with the growth rate of the producer. As it was decided to set the toxin production rate to $f_1 = 1$, it is necessary to define the minimum inhibitory coefficients p_1 and p_2 to allow *S. aureus* to invade and satisfy the experimental findings,

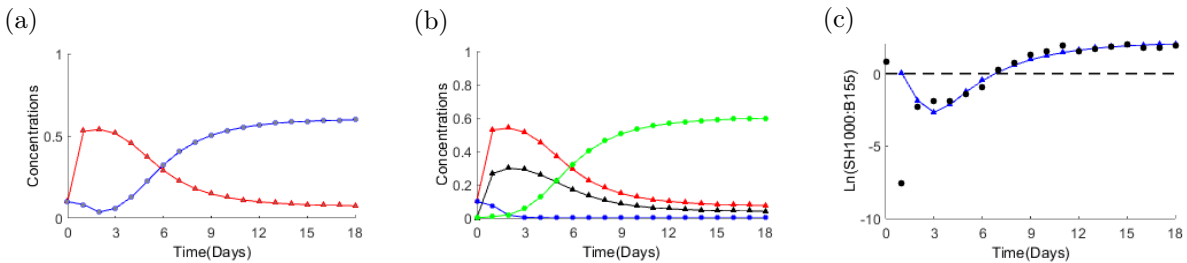as shown in figures (3.22), (3.23) and (3.24).

(a)

(b)

(c)
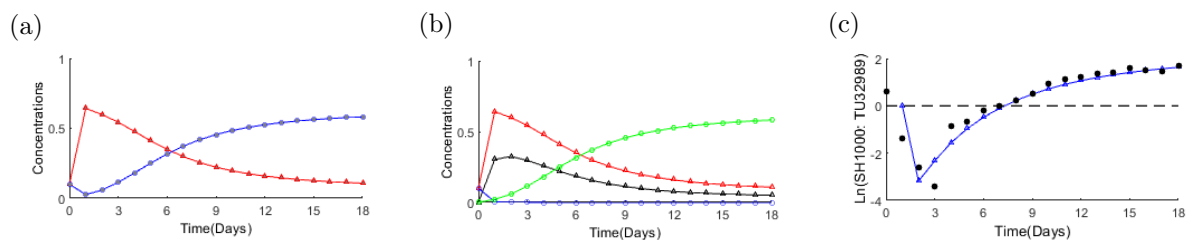
Figure 3.24: **Four-variable model simulation when toxin-producing isolates of *S. epidermidis* (TU**3298**) compete with populations of *S. aureus* (SH**1000**) at initial frequencies of** $1:1$. Panel (a): simulations of interactions obtained from (3.24); (red) is *S. epidermidis*; (blue) is *S. aureus*, $(u_s + u_a)$. Panel (b): demonstration of the four variable dynamics where (red) is *S. epidermidis*; (blue) is the susceptible fraction of *S. aureus* population; (green) is the adapted part; and (black) is the toxin. Panel (c): the solid line indicates the simulation of the natural log of SH1000 to TU3298 ratio; black dots represent the natural log of this ratio from the actual data. In all panels, the x-axis is the time in days. The y-axis in panels (a) and (b) represents the relative concentrations of the evolved populations and toxins, and in panel (c) the natural log of the evolved population ratio. Parameters: $D_u = 1.8 \times 10^{-6}$, $D_v = 5 \times 10^{-5}$, $r_u = 26.5296$, $r_v = 28.613$, $p_1 = 0.7746$, $p_2 = 0.7623$, $f_1 = 1$, $f_2 = 0.24$, $b_1 = 0.9$, $b_2 = 0.84$, $b_3 = 0.9$ and $b_4 = 1.09$.

The values of the coefficients p_1 and p_2, the inhibiting factors, and the corresponding decay rate f_2 that satisfy the observed behaviour of the evolved *S. aureus* are determined using the fitting technique.

The best fit to the experimental data with the minimum error was obtained when $p_1 = 0.7746$, $p_2 = 0.7623$ and $f_2 = 0.24$ and the ratio between these factors were defined and illustrated in equation (3.19) and plotted in Fig (3.10). The consequences of choosing slightly higher inhibition coefficients, that fit the ratio presented in Fig (3.10), is an acceleration of the interference mechanism because the toxin-producing population will inhibit and restrict the susceptible fraction of the population faster. According to the model produced in this study, the decline of the susceptible fraction leads to the emergence of the resistance population. Thus, the whole mechanism will be accelerated. On the contrary, choosing slightly lower inhibition coefficients would delay the dynamics of interaction. For the same purposes, a lower inhibition coefficient allows the susceptible fraction of the population to sustain for a longer period which leads to a delay in the emergence of resistance. Illustrations of the effect of different values of p_1 and p_2 will be shown in the appendix Fig (6.4).

3.6 Mathematical Investigation of Resistance Evolution

This section aims to test the 3-4 variable model hypotheses generated as set out in the previous sections. According to the interaction outcomes, regardless of the initial concentrations of the evolved populations, *S. aureus* was able to dominate in every sin-

gle interaction, meaning that *S. aureus* populations had developed resistance against the toxins produced by *S. epidermidis*, which explains the decline in their frequencies. These findings were also confirmed by results presented in section (3.2.3), as most of the evolved populations of *S. aureus* showed no inhibition zones when spread over the evolved populations of *S. epidermidis*.

However, some replicates showed smaller inhibition zones against the toxins produced by B155 and TU3298 compared to the initial inhibition zones (before interactions), indicating that the evolved isolates had not yet entirely mutated against these toxins and that isolates still contained a sensitive fraction of populations.

Since the size of post-interaction inhibition zones is positively correlated with the level of toxicity of the evolved *S. epidermidis*, the author of this thesis considers that it is only a matter of time before the whole developed population of *S. aureus* becomes resistant to these toxins. It is also worth noting that all evolved strains of *S. epidermidis* maintain their existence at lower frequencies than *S. aureus*, and the chances of their survival are positively correlated with their level of toxicity.

Thus, the final ratio between the evolved populations differs, *S. aureus* grew approximately ten times larger than B180, almost five times larger than B155, and approximately three times larger than TU3298. The three and four-variable model predictions could be tested in silico by changing the initial conditions, which assumed that the adapted fraction of *S. aureus* represented only 1% of the population. The proportions of the adapted fraction of *S. aureus* SH1000 were gradually increased. Thus, a family of population curves (shown in Fig 3.25) was produced, and plotted against the simulations fitted to the experimental data for illustration purposes.

Since all initial conditions have led to approximately the same ratio in each strain, the decision was made to produce the curves when *S. aureus* populations represented the resident populations in the numerical experiments in this study. This decision was based on two reasons. First, in this situation, SH1000 struggled the most to develop resistance. As previously indicated by the results of the interactions, negative correlations were observed between the initial density of the evolved *S. aureus* and its ability to recover and gain control over its opponents. Second, in this situation, when varying the ratio of the adapted SH1000, it is more evident when the resident populations can restrict and inhibit the invasions by *S. epidermidis* than under any other initial conditions.

The models in this study predict that the final sample of evolved isolates of SH1000 will become resistant to the toxins produced by *S. epidermidis*, meaning that if samples were taken from the evolved SH1000 and engaged again in interactions with the same toxin-producing strains, the initial decline in SH1000 density would not be observed.
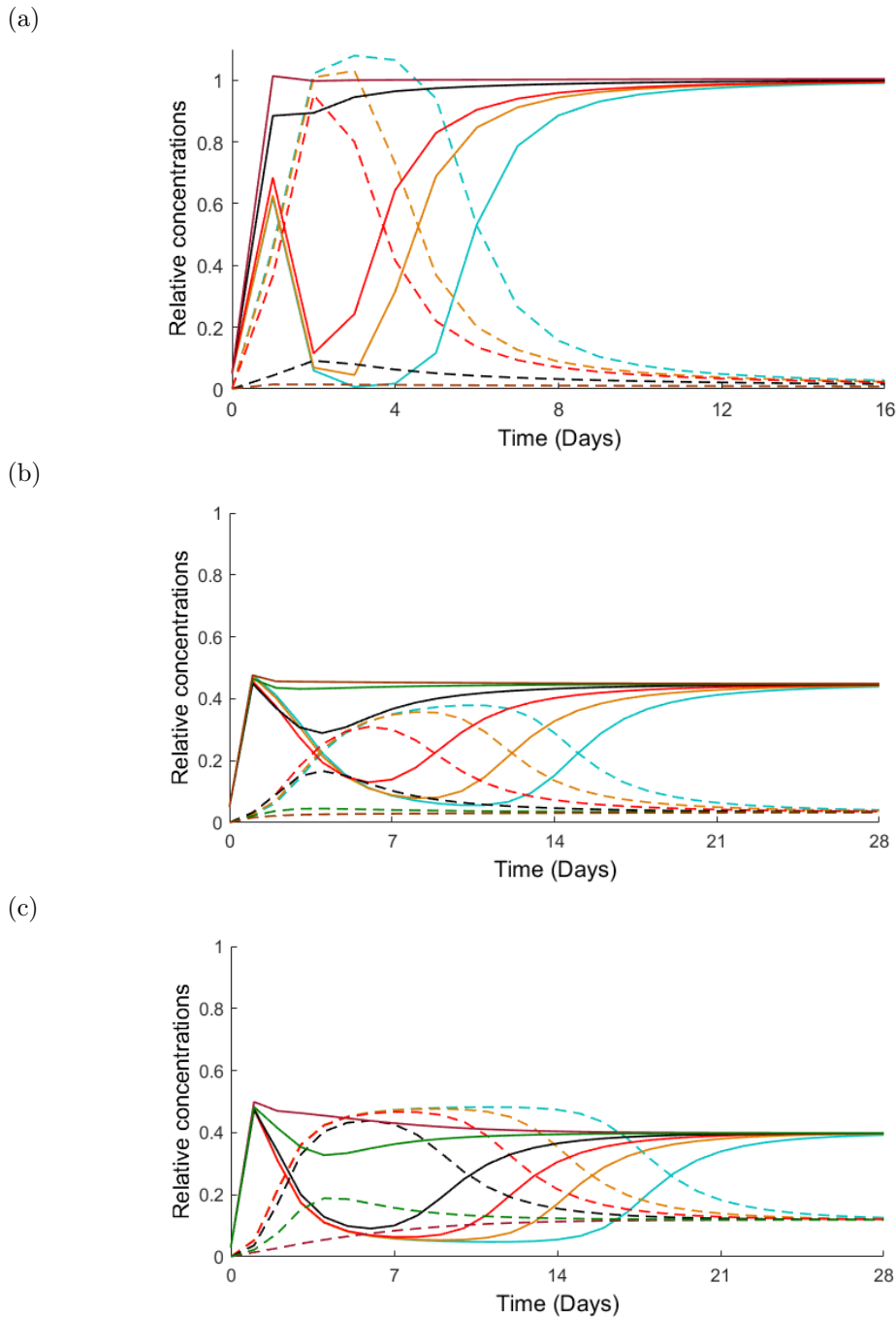
Figure 3.25: **Results of numerical experiments conducted to evaluate the modelling predictions and estimate the proportion of the adapted S. aureus SH1000.** Panel (a): Different simulations were generated from the three-variable model (3.23), representing the interactions between *S. epidermidis* B180 (invader) and *S. aureus* SH1000 (resident) when the ratios of adaptive (u_a) and susceptible (u_s) *S. aureus* fractures were varied. Panels (b) and (c): different simulations were generated from the four-variable model (3.24), representing the interactions between *S. epidermidis* B155 (invader) and *S. aureus* SH1000 (resident), and between *S. epidermidis* TU3298 (invader) and *S. aureus* SH1000 (resident), when the ratios of adaptive (u_a) and susceptible (u_s) *S. aureus* fractures were varied. Dashed lines represent *S. epidermidis*; solid lines represent *S. aureus* $(u_s + u_a)$. Different colours of lines indicate different ratios of the adapted fractures of SH1000, 70% dark red, 60% dark green, 50% black, 30% red, 10% orange, and 1% (initial assumption) light blue lines. The x-axis represents the time in days, and the y-axis is the relative concentrations of the evolved populations. The parameters used in panels (a), (b), and (c) were the same as the parameters in figures (3.16), (3.19), and (3.22), respectively.

Thus, performing these numerical experiments aims to validate the model hypothesis

of this study and to determine the proportion of evolved *S. aureus* SH1000 which must adapt to the toxins produced by *S. epidermidis* strains to be able to inhibit and restrict their invasions.

The numerical experiments were begun by assuming the reverse ratio between the fractions of *S. aureus* populations, i.e., the susceptible fraction represents 1% of the evolved SH1000. Then the proportion of adaptive to susceptible was gradually reduced at a rate of ten percent until arriving at the initial assumption (light blue lines). However, only the following $(u_a : u_s)$ ratios are shown in Fig (3.25): 1% light blue lines, 10% orange lines, 30% red lines, 50% black lines, 60% green lines, and 70% dark red lines, for illustration purposes only. The rest of the ratios can be seen in the appendix in Fig (6.7).

The outcomes of the numerical experiments, shown in Fig (3.25a), revealed that for the evolved *S. aureus* to restrict the invasions by B180 and recover, at least 50% of *S. aureus* must mutate (black lines).

According to Fig (3.16b), mutation occurred at approximately day 4. Furthermore, when the ratio of the adaptive fraction of the *S. aureus* population was gradually reduced, the initial decline in the curves representing the density of *S. aureus* was observed, signifying that the evolved isolates of SH1000 were still sensitive to the toxins produced by B180, which contradicts the experimental findings. According to the results obtained from the deferred inhibition assay, in Fig (3.8b), performed between the evolved populations of B180 and SH1000, B180 displayed no growth inhibition activity against the selected *S. aureus* SH1000. This indicates that by the end of interactions performed between SH1000 and B180 (day 17), the entire population of SH1000 changed and became resistant to the toxins produced by B180.

Similarly, as illustrated in Fig (3.25b), the numerical experiments demonstrated that when the interactions were conducted between SH1000 and B155, at least 60% or above of the evolved SH1000 had to adapt against the toxins produced by B155 before the evolution of the resistance became evident and recognised, which explains the delay in the process. According to Fig (3.19b), this occurred between days 11 and 12. Also, as shown in Fig (3.19b), by the end of interactions performed between SH1000 and B155 (day 28), the majority of the evolved SH1000 changed and became resistant to the toxins produced by B155. This was also confirmed by the experimental outcomes obtained in Fig (3.8b).

According to the results obtained from the deferred inhibition assay performed between the evolved populations of B155 and SH1000, B155 displayed no growth inhibition activity against the selected *S. aureus* SH1000 in some replicates. At the same time, it showed minor inhibition activity against the evolved SH1000 compared to the initial inhibition zones between the ancestral populations of B155 and SH1000 in other replicates. Likewise,

124

as displayed in Fig (3.25b), when the ratio of the adaptive fraction of *S. aureus* was reduced to under 60%, the initial decline in the curves representing the density of *S. aureus* was observed. This contradicts the experimental findings illustrated in Fig (3.13d), which indicate that the change in the evolved population density is no longer significant regardless of the maintained oscillations.

Finally, as depicted in Fig (3.25c), the numerical experiments demonstrated that almost 70% or above of the evolved SH1000 adapted against the toxins produced by TU3298 before the evolution of the resistance became evident (70%-dark red, 80%-yellow, 90%-green, and 99%-gray lines). According to Fig (3.22b), this happened approximately on days 9 and 10. According to the results obtained from the deferred inhibition assay performed between these evolved populations at day 28, some replicates showed no growth inhibition activity against the selected *S. aureus* SH1000.

The numerical experiments demonstrated a positive correlation between the toxicity level of the reactions and the required resistance ratio. Furthermore, an inverse relationship was also noticed between the time required for the adaptive fraction of *S. aureus* to overcome the susceptible ratio and the growth rate of their opponent strain of *S. epidermidis*, i.e., the faster the evolved *S. epidermidis* strain grew, the more they provoked their opponent to transform. According to (Table 3.4), B180 had the highest growth rate out of the selected *S. epidermidis* strains, and as shown in Fig (3.17b), they were able to achieve the required ratio for the beginning of the resistance around the fourth day. In contrast, the most extended period consumed by the evolved SH1000 to reach the required ratio for the beginning of the resistance to evolve was when it participated in competitions with B155, which had the lowest growth rate.

Remarkably, while high toxin interactions urged their competitors from SH1000 to develop a higher resistance ratio, some of their evolved isolates showed minor inhibition activity against the evolved isolates of SH1000 at the end of interactions and maintained their existence at a higher ratio than the low-toxin strains. Such findings imply that the toxin-producer strains of *S. epidermidis* co-evolved in response to the survival challenges raised by increasingly resistant *S. aureus* populations. The evolved *S. epidermidis* may have increased the production of the inhibitory toxin or initiated the production of other toxins. However, this remains undetermined in the absence of an understanding of the inhibition mechanism.

3.7 Conclusions

In this chapter, a comprehensive study was presented that dealt with biological and mathematical aspects of the nature of the interactions in bacterial communities and the implications and consequences of these interactions. Several factors were considered when

performing these experiments that could affect the dynamics of these interferences, for instance, the initial concentrations of the competing populations and the level of toxicity of the involved populations. Laboratory experiments were conducted where populations of the pathogenic strain *S. aureus*, SH1000, were engaged in competitions with different species of *S. epidermidis* that were distinguished by their level of toxicity.

The primary purpose of conducting these experiments was to investigate a hypothesis. Several studies confirm that the interactions between bacterial communities limit the colonisation of pathogenic bacteria [122]. Moreover, studies have demonstrated that manipulating some of the environmental factors surrounding these interactions may contribute to the inhibition of pathogenic bacteria. Thus, several experiments were conducted to explore these hypotheses.

Three of the species used in this study were selected from a previous study presented in Chapter 2. Another species with a high toxicity level was added. A series of experiments (Table 3.2) was conducted prior to the competition to gain a better understanding of the nature, characteristics, and features of these species, as well as to determine the extent of the change that may occur as a result of the competition.

It was possible to accurately determine the production rate for each involved strain by incubating several replicates of each strain overnight and taking the OD_{600} readings every 30 minutes. Inhibition assay experiments enabled the quantifying of the effect of bacteria-derived antimicrobials on competition. Incubating many replicates of the ($50\mu l$) spot for each strain overnight allowed for the determination of the diffusion coefficients for all the involved strains.

The principal component of this study was achieved by conducting competitions between the selected *S. epidermidis* species and the pathogenic *S. aureus* strain. Some factors were manipulated to ascertain their impact on the nature of these interactions, for example, the level of toxicity and the initial concentrations. These competitions were achieved from different initial concentrations, i.e., 0.01 : 1 and vice versa. These interactions were known as invasions, and they were also conducted from equal initial concentrations. These interactions lasted for different periods until the change of the competing population density was no longer significant.

The most important results that were obtained through the study presented in this chapter is that the pathogenic species, SH1000, managed to dominate in all the competitions that were conducted in mixed environments, regardless of the toxicity of the competitor or the initial concentrations. This is consistent with the findings of the study presented in Chapter 2, in which it is stated that *Staphylococcus aureus* was only able to invade toxin-producing *S. epidermidis* under mixed conditions.

The findings revealed the high adaptability of the pathogenic strain, SH1000, as it showed a decrease in its growth level at the beginning of these competitions. This de-

crease was positively proportional to the level of toxicity and the growth rate of the corresponding species. There is also a positive correlation between the level of toxicity of the competing strain of *S. epidermidis* and the time required for *S. aureus* to adapt and mutate against these toxins. The species with the highest toxicity was able to inhibit this species for a more extended period.

Additionally, when conducting competitions with bacteria with a low level of toxicity, B180, toxins did not play a significant role in the outcomes of these interactions, when the interaction dynamics between SH1000 and B180 were compared with the interaction dynamics between the same species and another non-toxic *S. epidermidis* species, (from a previous study [122]).

Furthermore, a difference in the dynamics of these interferences was noticed when starting from different concentrations, as they showed clear and intense fluctuations during these competitions than when starting from equal concentrations (See Fig 3.13).

None of the invasions and competitions performed and presented in this chapter resulted in any exclusions or total eliminations of the competitors, which differs from the findings in the study cited in Chapter 2. The evolved *S. epidermidis* coexisted with the opponent and was able to survive and maintain its presence at low concentrations.

To determine whether the emergence of genetic mutations is the reason behind the survival of this pathogenic species, a final experiment was conducted to measure the level of sensitivity of the evolved *S. aureus* populations when applied upon pure and evolved populations of *S. epidermidis*. This experiment showed that the pathogenic species were no longer affected by the toxins secreted by their opponents. In addition, it was noticed that the change was not limited to the pathogenic species but also affected the species that secrete toxins, as they became more ferocious when tested against pure samples of the pathogenic species (See figures 3.8a and 3.8b), signifying that both evolved species developed to suit the surrounding conditions and used all the tools that enable them to survive.

Mathematically, different models were designed to analyse and simulate each experiment performed. The first mathematical model was to simulate growth curves, and this model was based on the logistic equation where a single population consumes a single and limited resource. From this model, it was possible to estimate the consumption rate of each population along with their carrying capacity. In addition, the use of the logarithmic scale of the log phase in the obtained growth curves of the involved strains, (See Fig 3.2), made it possible to accurately define doubling and relaxation times along with the growth rate for each population in minutes, hours, and days. By scaling the time in the MATLAB simulations to $t = 1$ is one day in our time unit, the findings helped to define the daily growth rate (Table 3.4) for the evolved species.

The outcomes of toxin-mediated inhibition experiments, which were performed to test

the sensitivity of the pathogenic species to toxins secreted by other competing species, were modelled. Through this system of equations (3.5), it was possible to solve the toxin variable equation, (3.18), and obtain a toxin profile, Fig (3.9), as well as a mathematical term, (3.19), that links the rate of secretion of toxins and the rate of their decrease, f_1 and f_2, with the inhibition coefficients, p_1 and p_2, that affect the susceptible and resistant fractions of *S. aureus* species. Such an approach was useful as there was no other way to estimate or determine the exact values for these parameters.

The research presented in this chapter principally concerns modelling the interference between bacterial communities. These interactions were divided into two types. The first type was a competition for resources only, performed between B180 and SH1000, where toxicity did not play a significant role in the outcomes of these competitions; the other type was concerned with modelling the inhibitory interactions performed between samples of B155, TU3298 on the one hand, and SH1000 on the other.

In the first type of these interactions, competition for resources, a three-variable model was developed to simulate the dynamics of interference. This model (3.23) was an expansion of the spatially homogeneous *Lotka-Volterra* competition model to include the diffusive terms of the evolved species. Observing the interactions between *S. aureus* and *S. epidermidis* a repeated pattern was detected where the pathogenic bacteria community begins to decline at the start of each competition and then persists to increase its population size. It was possible to replicate the non-monotonic behaviour seen in the interaction dynamics by assuming that the pathogenic bacteria, SH1000, comprises two fractions of the population. The susceptible fraction represents most of the population, and its inability to resist its opponents causes its decrease at the start of all interactions.

In contrast, the resistant fraction represents only one per cent of the total population and can restructure the pathogen species, allowing it to increase production and dominate. Thus, a three-variable model was presented to consider the adapted fraction of *S. aureus* populations and its influence on the dynamics of interactions. A three-variable model was able to improve the simulations of the interference dynamics. However, this model could not produce the oscillations occurring in both populations during the competitions.

A mathematical model was also developed to simulate the inhibitory interaction dynamics in bacterial communities, considering the toxicity factor and its impact on the course of this dynamic. A four-variable model (3.24) was introduced, where the toxin variable was added to the previous model and linked to the producers. The associated inhibition coefficients with the toxin variable on the *S. aureus* community with both parts were added. This model was more complex than the previous models due to its many parameters. However, the existence of a relationship between these parameters (3.19) allowed the programming obstacle to be overcome in which the secretion factor, f_1, was set to one. Simultaneously, after defining the inhibition coefficients using their connection

to f_2, the least square method was utilised to obtain the values with the least error for each interference coefficient and the rate of toxin dissolution.

When modelling the interactions between *S. aureus* and *S. epidermidis* populations, the models predict the disappearance and demise of the B180 species after a period. At the same time, the competing communities that possess the toxic factors, B155 and TU3298, can survive at low rates if the resources are replenished. Moreover, the appropriate environment is maintained for their survival.

In addition, according to the numerical experiments performed to test the modelling predictions, the final sample of evolved isolates of SH1000 become resistant to the toxins produced by *S. epidermidis*. There is a positive correlation between the toxicity level of the interactions and the required resistance ratio. Also, an inverse relationship was observed between the time required for the adaptive fracture of *S. aureus* to overcome the susceptible ratio and the growth rate of their opponent strain of *S. epidermidis*, i.e., the faster the evolved *S. epidermidis* strain grew, the more it provoked its opponent to develop the resistance.

From the numerical experiments, also indicated in Fig (3.8b), all the evolved populations of *S. epidermidis* changed to keep up with *S. aureus* species. This change was evident and observed in the evolved populations when they produced larger inhibition zones against the ancestral SH1000 compared to the inhibition zones created by the ancestral populations.

Such findings may motivate and inspire future work, as it may be possible to expand the models in this study to consider the alterations in the evolved *S. epidermidis* populations, which are possibly the leading cause of the observed oscillations during the interference process. For example, another variable could be added to represent and express the change in these populations. Thus, both competing species can mutate and co-evolve to address the survival difficulties presented by their opponents.

Chapter 4

Study of The Dynamics of Interacting Populations in Spatially Structured Environments

4.1 Introduction

Competitions in bacterial communities are common due to limited resources such as food and space, and catalysts are frequently used to increase the intensity of these interactions, such as the secretion of toxins to reduce the colonisation of competing species [17]. As a result, spatial population structure is likely to have an impact.

A previous study was performed [32], to test the effect of spatial structure on invasions conducted between *E. coli* strains that produce bacteriocin, which is a protein produced by bacteria of one strain and active against those of a closely related strain, and populations of susceptible *E. coli* strains. The outcomes of these experiments indicated that bacteriocin producers could successfully invade susceptible populations starting from low initial concentrations (frequency of 0.001) in spatially-structured environments (agar plates). However, on the contrary, it required considerably higher initial concentrations of the producers (frequency of 0.1) to enable successful invasion when performed in the absence of spatial structure (shaken liquid broth).

Spatial clustering contributed positively to toxin producers when the invasions were carried out in spatially-structured environments, as toxins reached higher concentrations once the effects of toxins were localised (confined to a small area) [131].

In spatially-structured environments, the effects of toxins are evident and beneficial, even when produced by a minority [131]. However, spreading toxins away from generating cells in spatially-unstructured situations requires producers to reach a higher frequency before the advantages of the toxin are realised [32, 76, 173]. This study [32] suggests that, unlike the case in mixed environments, the production of toxins by *S.epidermidis* in spatially-structured environments enhances the outcomes of these invasions in their favour and contributes to the full achievement of the role of toxins.

The ecological theory describes environments that involve aggressive interactions as

black-hole sinks [88], based on the ability of the resident populations to exclude and inhibit invasions by susceptible populations, as the inhibitors eliminate their existence [2]. In such an environment, invaders are unable to maintain a sustainable population. However, a vulnerable species can develop resistance, which has not often been addressed in the framework of interference competition [32, 88].

Several theoretical models predict the existence of a positive correlation between the population's ability to adapt and their initial concentration [70]. This association arises because higher initial concentrations increase the probability that populations transmit advantageous mutations able to survive the conditions of black-hole sinks [88, 163]. As a result, when invading from higher initial densities, S. aureus populations have a higher probability of possessing mutants resistant to S. epidermidis toxins.

On the other hand, the production of these advantageous resistance mutations is expected to be inhibited in highly spatially-organised situations as competition for the mutant may occur only at the colony's edge. As the colony expands, a small fraction of the mutant population competes with the pure genotype [76]. These findings imply that non-inhibitory communities are more vulnerable to invasion.

With consideration of the above, a study was conducted [122], to test several predictions, perhaps the most prominent of which is the following: inhibitor-producing strains of S. epidermidis are able to infiltrate S. aureus populations better than non-producing strains, which was even more evident when the interactions were conducted under structured conditions.

In an unstructured medium, the invasion will be feasible only above a threshold frequency [32, 76, 173]. Non-inhibitor-producing strains of S. epidermidis will not limit S. aureus invasions to the same extent as inhibitor-producing strains. The evolved populations of S. aureus are more likely to develop resistance to inhibitors generated by S. epidermidis when starting at a high frequency [70, 122].

These predictions were confirmed when performing a set of experiments between different populations of S. epidermidis, toxin-producing and non-toxin producing, and susceptible populations of S. aureus. These experiments were carried out in structured environments. Also, different initial frequencies when performing these interactions were considered to test these predictions [122].

However, the author of this study maintains that such findings were concluded before the optimum time for confirmation, especially since the behaviour of the pathogenic strain SH1000 was not stable and did not demonstrate complete exclusion in most of the reported cases.

Thus, it was decided to re-perform the interactions under structured conditions and extend the period of interactions to either confirm the findings obtained earlier in [122] or to reveal new findings.

Indeed, manipulating the nasal microbial community contributed to limiting the transmission and infection rates associated with the colonisation of *S. aureus*; this was more effectively achieved under structured environmental conditions and high toxicity levels. However, unlike that reported in [122], this study found that the nasal microbiota has only a moderate influence on the colonisation state of *S. aureus*, meaning the evolved *S. aureus* was never permanently removed or displaced.

Furthermore, when the interactions were conducted under structured conditions, several patterns were observed on the formed bacterial spots, where the clusters of the evolved *S. aureus* populations appeared in different positions. This phenomenon evokes interest in further investigating the effect on interference dynamics.

Thus, in the study presented in this chapter, the aim is to:

- Re-perform the experiments presented in Chapter 2 that involve inhibitory interactions under structured environmental conditions to better understand the biological aspects and experimental techniques and answer the questions raised in the second chapter.

- Examine inhibitory production and resistance evolution in invasion and competition under structured conditions.

- Extend the duration of the interactions to investigate the behaviour of the evolved species.

- Perform a set of experiments involving the evolved species to determine the extent to which the interactions changed their characteristic features.

- Develop mathematical models to explain and simulate the dynamics of interactions under structured conditions.

- Fit model parameters to experimental data.

- Investigate the initial position of resistance in the evolved populations of *S. aureus* when performing the interactions under structured conditions and its influence on the interaction dynamics.

4.2   Competition Experiments

The principal goal of this study, as stated previously, is to understand the nature of these interferences in bacterial populations and to reach an understanding of how external factors will influence the dynamics of these interactions to determine if manipulating these reduces the colonisation and spread of the pathogenic bacteria. In this chapter all the interaction experiments that were presented in the previous chapter were re-conducted,

using the same species previously selected in (Table 3.1). However, when transferring the communities every day, the performed ecological structure was preserved through a procedure known as velvet duplicate plating shown in Fig (2.3). The purpose of this was to determine the effect of this factor on the outcomes and progress of these competitions. As in a previous study, [122], it was indicated that the preservation of the environmental structure contributed positively to reducing colonisation by harmful bacteria. In this chapter, the aim is to investigate this hypothesis.

4.2.1 Materials and methods

When performing the interactions under spatially-structured conditions, the same material and methods were used as described in the previous chapter, presented in section (3.5). However, it should be emphasised that the transfers in this set of experiments were performed using velvet duplicate plating, as shown in Fig (3.11). The approach of transplanting interacting populations was utilised to recreate the original colonial spatial pattern. The method entails pressing the velvet disc into the original plate, then imprinting duplicate plates with bacterial cells attached to the material.

After obtaining the replicas, the remains were scraped to calculate the Cfu/ml for the evolved populations every day. On other BHI plates, colonies were counted and classified based on colony form and colour.

In some cases, the *S. aureus* colonies may lose their usual colour and identification and selection presents a challenge, so a product known as MSA is used (Table 3.3). In this medium, *S. aureus* develops and ferments mannitol to create yellow colonies. Most coagulase-negative *Staphylococci* and *Micrococci* do not ferment mannitol and propagate as tiny red colonies. The pigment of the colonies and media is caused by phenol's red reaction to the pH of the medium. According to [33], phenol is red at pH 8.4 and yellow at pH 6.8.

4.2.2 Results

The results of the experiments conducted in this chapter are presented in three sections: firstly, when isolates of *S. epidermidis* strains invaded populations of *S. aureus* (SH1000) at initial concentrations of (0.01:1); the second stage of results occurring when the competitions were conducted, starting from equal initial concentrations, and the third stage, the mutual invasions, when susceptible populations of *S. aureus* invaded *S. epidermidis* populations.

First: the invasion of *S. epidermidis* into resident populations of *S. aureus*

Under structured conditions, the invasions lasted 28 days. Invasions were performed until the difference in concentrations of the interacting populations became insignificant.

As shown in figures (4.1a), (4.1d), (4.1g), (4.2a), (4.2d), and (4.2g) *S. epidermidis* was never able to invade successfully under structured conditions, which contradicts the findings obtained in [122]. The evolved *S. aureus* populations were able to dominate and force their opponents to persist at low concentrations. In addition, there is a positive association between the level of toxicity and the time required for the emergence of resistance in the resident populations of *S. aureus* (SH1000). In other words, *S. aureus* populations took longer to recover when competing against (TU3298) than (B180).
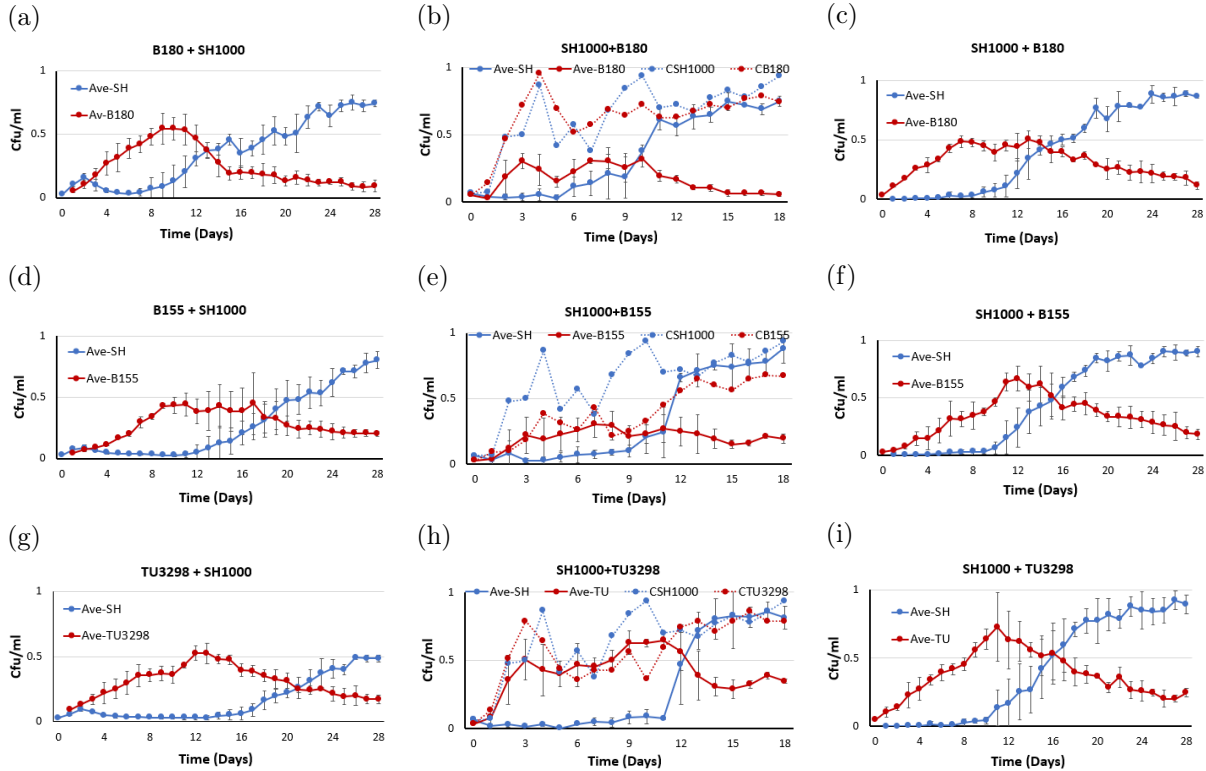
Figure 4.1: **The experimental data on the interaction dynamics of *S. epidermidis* and *S. aureus* species in structured environments.** Panels (a), (b) and (c): show the interactions between low-toxin producing isolates of *S. epidermidis* (B180, red) and populations of *S. aureus* (SH1000, blue), starting from different initial concentrations. Panels (d), (e), and (f): reflect the interactions between moderate toxicity populations of *S. epidermidis*, (B155, red) and *S. aureus*, (SH1000, blue). Panels (g), (h), and (i): show the interactions between highly toxic populations of *S. epidermidis* (TU3298, red) and *S. aureus* (SH1000, blue). Panels in the first column, (a), (d), and (g): represent invasions of *S. epidermidis* (invaders) at initial ratios of (0.01: 1) to (resident) *S. aureus* populations. Panels in the second column, (b), (e) and (h): when the evolutions between the interacted populations started from equal initial frequencies, dotted lines represent the controls. Panels in the third column, (c), (f) and (i): represent the mutual invasions performed between invaders of *S. aureus* at initial ratios of (0.01: 1) to resident populations of *S. epidermidis*. The *x*-axis is the time in days, and the *y*-axis is the colony-forming units (CFU) per plate. The error bars represent the standard error of the mean (n = 3). Data plotted in panels (a-i) will be provided in the appendix in Tables (6.19)-(6.28).

The interactions between *S. epidermidis* (B180) and *S. aureus* (SH1000) were categorised as competition for the resource, given the fact that the toxin secreted by the *S. epidermidis* population did not contribute to the outcomes of these interactions. As reported in [122], the (B180) strain behaved like the non-toxin strain (B115) when per-

forming interactions with *S. aureus* populations (SH1000). On the other hand, competitions between populations of *S. aureus* (SH1000) and isolates of *S. epidermidis* (B155) and (TU3298) were considered as inhibition.

As shown in figures (4.1d), (4.1f), (4.1g), and (4.1i), it is worth noting that when performing the inhibitory interactions, as *S. aureus* populations started from a higher initial concentration in comparison to their opponents (i.e., when *S. aureus* populations were residents), the evolved *S. aureus* struggled to develop resistance for a more extended period than when they were invaders.

Furthermore, positive correlations were noticed between the level of toxicity and the improved chances of survival of the producers. This is possibly only a question of time, since an inverse relationship between the degree of toxicity and the speed of the interference dynamics was discovered.

The three invading strains of *S. epidermidis* exhibited similar dynamics over time under structured conditions, as shown in figures (4.2a), (4.2d), and (4.2g). (B180) increased until day 12, after which it decreased. Increases in (B155) occurred until day 18 and approached a 1: 1 invader to resident ratio, after which they decreased. (TU3298) invader populations maintained control until day 21 when both populations reached a 1:1 ratio and began to decline.

Second: evolution from equal initial frequencies

The second stage of the results occurred when the competitions were conducted, starting from equal initial concentrations. Three replicates were obtained for these competitions. The initial frequencies of the involved strains were equal to (1:1) and the controls, where each competing strain was cultured independently. These competitions and controls were conducted under spatially-structured environmental conditions and lasted 18 days.

Once again, as shown in figures (4.1b), (4.1e), (4.1h), (4.2b), (4.2e), and (4.2h), the evolved *S. aureus* populations dominated and forced their opponents to persist at low concentrations. Similarly, these competitions did not result in the disappearance or extinction of one of the competitor strains. However, (B180) maintained its survival at low rates.

According to figures (4.1b), (4.1e) and (4.1h), the populations of *S. epidermidis* that possessed a high degree of toxicity were more efficient in inhibiting the susceptible *S. aureus*. However, when the susceptible populations of *S. aureus* were exposed to high levels of toxicity, they became more aggressive, as shown in Fig (4.1h), where the concentration of *S. aureus* jumped nearly eight times within two days when performing the interactions with (TU3298) and four times when the interactions were carried out with (B155), Fig (4.1e), before stabilising, after which, the increase of *S. aureus* populations

became monotonous.
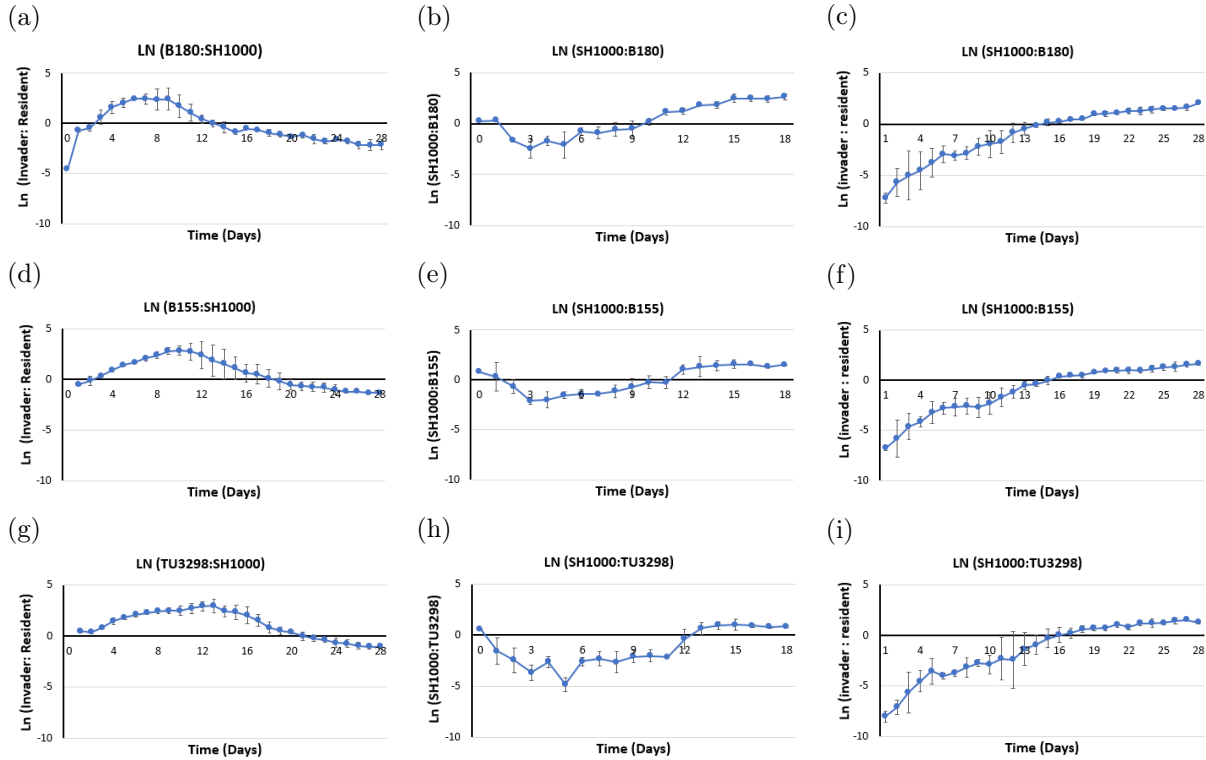
Figure 4.2: **Plots of the natural log of the evolved population ratio over time when interactions were conducted under structured conditions.** Panels (a), (d) and (g): show the natural log of the invader to resident ratio, (B180: SH1000), (B155: SH1000) and (TU3298: SH1000) respectively. Panels (b), (e) and (h): display the natural log of the interacting population ratios, (SH1000: B180), (SH1000: B155), and (SH1000: TU3298), in that order, when starting from equal initial concentrations. Panels (c), (f), and (i): represent the natural log of the invader to resident ratio when performing reciprocal invasions. Again, the x-axis is the time in days. Error bars represent the standard error of the mean (n = 3).

Furthermore, as shown in figures (4.2b), (4.2e) and (4.2h), *S. aureus* populations grew to nearly 14 times the population of (B180), about five times the population of (B155), and twice the population of (TU3298).

Third: the invasion of *S. aureus* into *S. epidermidis* resident populations.

To determine whether resident *S. epidermidis* populations may inhibit *S. aureus* invasion, *S. aureus* was reciprocally invaded into inhibitor-producing *S. epidermidis* populations. According to figures (4.1c), (4.1f) and (4.1i), *S. aureus* was able to invade all the resident population of *S. epidermidis*. However, there was a positive association between the time required for *S. aureus* to invade and the level of toxicity of the resident populations of *S. epidermidis*. *S aureus* invaded into (B180) by day 14, Fig (4.2c), into B155 by day 15, Fig (4.2f), and by day 17 into TU3298, Fig (4.2i). In all instances, evolved *S. aureus* was resistant to the toxins produced by *S. epidermidis* populations, indicating that successful *S. aureus* invasion is a consequence of resistance evolution.

In general, *S. epidermidis* was never able to invade successfully. However, *S. epidermidis*

was more likely to persist and avoid extinction when toxins were involved. A spray assay method was used to determine if the decline in *S. epidermidis* populations was driven by resistance evolution in the *S. aureus* population.

S. aureus strains, both pure and evolved, were sprayed onto pure and evolved *S. epidermidis* populations. These tests demonstrate that *S. aureus* developed resistance to the toxins produced by *S. epidermidis* populations. Mutations did not appear simultaneously even when interactions were performed with the same species in other replicates. Still, it can be stated that *S. aureus* was able to fully mutate against toxins produced by (B180) and partially against toxins produced by (B155) and (TU3298), as shown in graph (3.8b). After the emergence of resistance, the evolved *S. aureus* populations increased monotonously.

4.3 Modelling The Dynamics of Interacting Populations

As explained previously, interference experiments were conducted in two types of environments: a mixed environment where the resulting structure was destroyed daily when transferring the populations into a new medium, and in the other type, a structured environment where the resulting structure was preserved. It is worth noting that the interactions in both environments began in the same way. The difference between the two environments arose by the end of the first 24 hours when different methods were employed to relocate the interacted communities.

4.3.1 Structured vs. Mixed in Two-variable Model

Mathematically, the two-variable model that was presented earlier in (2.8) will be used to illustrate the difference between conducting interactions in mixed environments and structured environments. As previously stated, interactions in both environments have the same initial conditions, so in 1-D, the first step was to define a zero-column vector that obtains specific values in the middle, representing the initial spot, and the ratio between the total space steps; the space steps occupied by the initial values is equivalent to the ratio between the diameter of the Petri dish and the diameter of the initial spot:

$$\frac{\text{The diameter of the initial spot}}{\text{The diameter of the Petri dish}} = \frac{0.5cm}{10cm} = \frac{5 \, \text{space unit}}{100 \, \text{space unit}} \qquad (4.1)$$
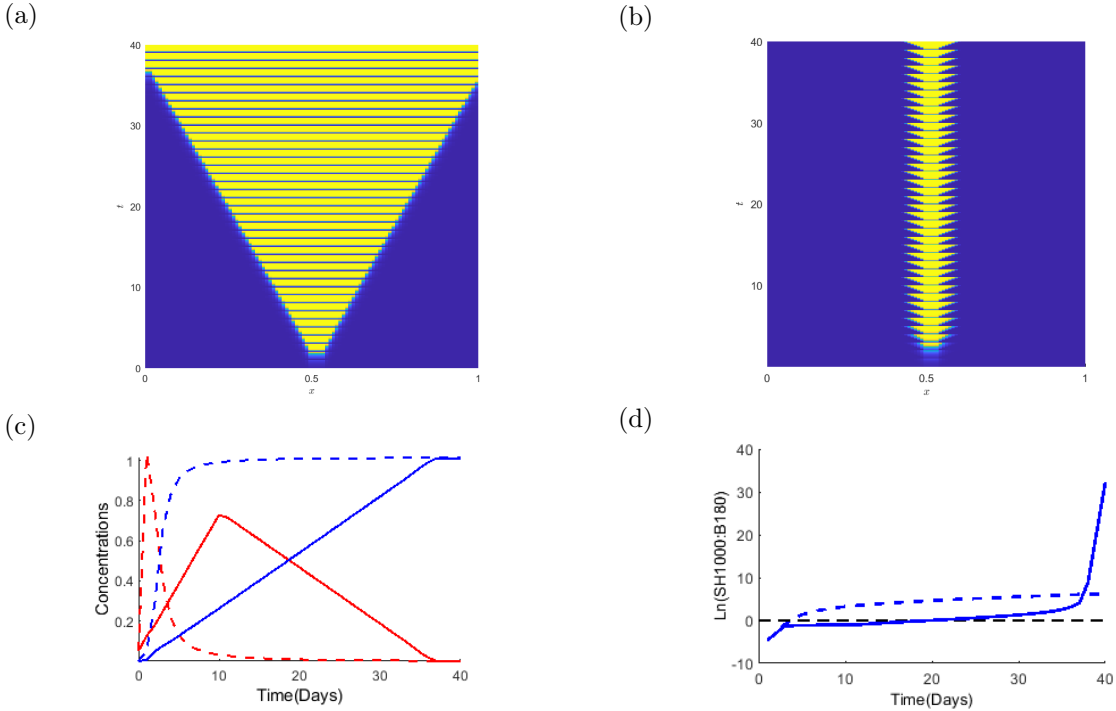
Figure 4.3: **A comparison between the evolution of interacted populations under mixed and structured conditions when using the two-variable model** (2.8)**.** Panel (a): a surface image shows the development of the interacted populations under structured conditions where the mixture is daily diluted while maintaining the structure. Panel (b): a surface image shows the development of the interacting populations under mixed conditions where the mixture is daily destroyed, diluted, and cultured as a spot for the next day. Panel (c): illustrations of interaction dynamics; solid lines under structured conditions, dashed lines under mixed conditions; (blue) lines represent invader *S. aureus* populations (SH1000), (red) lines represent resident *S. epidermidis* populations (B180), and the initial concentration ratio is (0.01:1). Panel (d): simulation of the natural log of the invader-to-resident ratio. In panels (a) and (b), the x-axis represents space, the y-axis represents time in days. In panels (c) and (d), the x-axis is the time in days, and the y-axis represents the relative concentrations of the evolved populations. Parameter: $D_u = 1.8 \times 10^{-6}$, $D_v = 2 \times 10^{-5}$, $r_u = 26.5296$, $r_v = 29.7216$, $b_1 = 0.92$ and $b_2 = 1.5$.

As illustrated in Fig (4.3b), under mixed environmental conditions, the structure of the spot was destroyed at the end of each day. Thus, the obtained values in the column were added and divided by the number of space units occupied by the spot to obtain the average. Subsequently, that value was multiplied by the dilution rate. In the laboratory experiments, after diluting the spot in $10 \, ml$ of PBS liquid, (Table 3.3), a new spot was cultured at a volume of $50 \, \mu l$. Thus, the dilution rate is calculated as follows:

$$d = \frac{50 \mu l}{10000 \mu l} = 0.005$$

However, as shown in Fig (4.3a), under structured environmental conditions, after each day, all values in the column were multiplied by the dilution factor without adding them to get the average to maintain the spatial structure, as in the case of the laboratory experiments. As shown in Fig (4.3), the difference appeared clearly between the two environments. Fig (4.3c) shows the evolution of both competing strains under both envi-

ronmental conditions. In a structured environment, the population concentrations (solid lines) were relative to the total plate size, whereas in mixed conditions the population concentrations (dashed lines) were proportional to the spot size. As seen in Fig (4.3a), when the structure was preserved, the resulting spot covered the entire plate when reaching day 37.

4.3.2   Structured vs. Mixed in Three-variable Model

As stated in the preceding chapter, all simulations generated by the two-variable model exhibit monotonic behaviour, regardless of whether they begin with differing or equal initial concentrations. This indicates that the rate of change in population concentrations over time does not change the sign, i.e., the natural logarithms of the competing population ratios are either growing or decreasing. On the other hand, some of the experimental outcomes in both environments show non-monotonic behaviour. Since this type of behaviour cannot be produced by a two-variable model, it was decided to expand this model to include an extra variable representing the susceptible fracture of a population in *S. aureus*, as seen in (3.23), to justify and simulate the drop of *S. aureus* populations at the beginning of the interactions. This model considers two competing bacterial populations in a one-dimensional domain. One species, the 'susceptible', has a number of cells capable of adapting to the fierceness of the competition, the 'adapted'. This ecosystem is modelled using (3.23) equations. Further information on this model regarding the boundary and initial conditions is given and explained in detail in the previous chapters.

As shown in Fig (4.1) and Fig (4.3), when the interactions were conducted in structured environments, the emergence of resistance slowed, meaning that *S. epidermidis* populations with different levels of toxicity had the advantage at the beginning of these interactions and continued for a more extended period compared to the interactions performed in mixed environments, i.e., preservation of the structure and the accumulation of toxins contributed positively to inhibiting the emergence of resistance for a longer period. However, the conservation of the structure and the accumulation of toxins did not prevent the emergence of resistance, as the evolved populations of *S. aureus* were able to form mutations that were able to resist the secreted toxins, reappear again, and invading successfully.

When the structured environmental conditions were applied to a two-variable model, the obtained simulations indicate that the outcomes of these interactions are similar regardless of the ecological structure. As shown in Fig (4.3c), blue lines, solid and dashed, which represent *S. aureus* concentrations in structured and mixed environments respectively, converged to the same outcomes. Similarly, red lines, which represent *S. epidermidis* concentrations, tended to have the same outcomes in both types of environments.

The only difference noted was the time it took to reach these results.
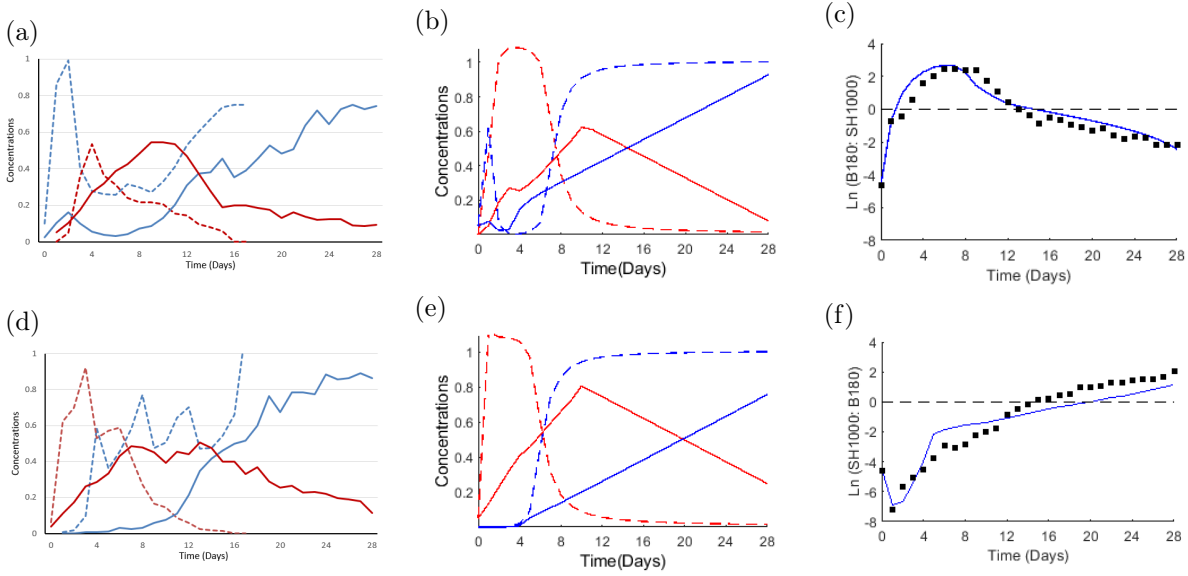
Figure 4.4: **A comparison between the evolution of interacted populations of _S. aureus_ (SH1000) and _S. epidermidis_ (B180) under mixed and structured conditions using a three-variable model** (3.23). Panel (a): illustration of the experimental data showing the dynamics of interactions where _S. epidermidis_ (red) invades resident populations of _S. aureus_ (blue). Panel (d) depicts the mutual invasions. Panels (b) and (e): show the three-variable model simulations that represent the dynamics of the interactions reported in panels (a) and (d), respectively. In all panels, the initial concentration ratio (0.01: 1), dashed lines when the interactions were conducted under mixed conditions, and solid lines under structured conditions. Panels (c) and (f): (3.23) model simulations of the natural log of the invader to resident ratios (solid lines) plotted against the experimental data (black dots) that represents these ratios under structured conditions. The x-axis in all panels is the time in days, and the y-axis in panels (a), (b), (d), and (e) represents the relative concentrations of the evolved populations, and in panels (c) and (f) represents the natural log of the evolved populations. Parameter: $D_u = 1.8 \times 10^{-6}$, $D_v = 2 \times 10^{-5}$, $r_u = 26.5296$, $r_v = 29.7216$, $b_1 = 1.1$, $b_2 = 0.89$, $b_3 = 0.82$, and $b_4 = 1.45$.

This suggests that preserving the environmental structure will not inhibit the existence of _S. aureus_; it will only delay the emergence of resistance in both directions of invasions. To test this hypothesis, simulations of the interactions between populations of _S. aureus_ (SH1000) and low-toxin producing populations of _S. epidermidis_ (B180) were produced using the three-variable model after applying the structured environmental conditions in terms of transferring the evolved populations at the end of each day.

In Fig (4.4), the simulations were produced that represent interactions between _S. aureus_ (SH1000) and the low-toxin producing strain, _S. epidermidis_ (B180), under mixed environmental conditions (dashed lines). The simulations representing the same interactions under structural environmental conditions (solid lines) were added. These interactions were classified as competitions for resources as the toxin factor did not significantly impact the outcomes. The first direction of invasions is shown in Fig (4.4b), where populations of _S. epidermidis_ invade resident populations of _S. aureus_ at an initial frequency of (0.01:1), whereas Fig (4.4e) illustrates the other direction of invasions. The purpose of adding these simulations is to demonstrate and prove that when the rate of toxin pro-

duction is low, these interactions achieve the same results regardless of the environmental conditions.

The results emphasise the importance of spatial structure in delaying the dynamics of interference competition. If the spatial structure is preserved, *S. epidermidis* (B180) will better prevent *S. aureus* invasions for an extended period, indicating that retaining the spatial structure contributes to boosting the role of toxins more effectively. On the other hand, unstructured environments do not usually promote the formation of inhibitory toxins. Also, the findings may support the initial assumptions that there are mutations within the susceptible populations of *S. aureus* and that their presence and evolution contribute to the survival of the *S. aureus* population, as the sensitive fracture of the populations died at the beginning of the interactions.

Simulations of the natural logarithm of the invader to resident ratios were plotted against the experimental data that represented these ratios in figures (4.4c) and (4.4f). It is worth noting that when producing the structured simulations shown in Fig (4.4), the same parameters were used to generate the mixed simulations.

4.3.3 Structured vs. Mixed in Four-variable Model

The simulations obtained from the three-variable model after applying the structured conditions concurred with the experimental data presented in the research conducted for this thesis in terms of delaying the emergence of the resistance. This delay was justified biologically by the fact that the structured environment enhanced the role of the toxins, and mathematically by explaining that under structured conditions, the spot size is proportional to the plate size. Although the parameters used to produce the structured simulations were the exact same parameters as for the mixed simulations, the simulations concurred relatively with the experimental findings. As indicated in the previous chapter, the interactions between populations of *S. aureus* (SH1000) and low toxin-producing populations of *S. epidermidis* (B180) were classified as competition for resources because the produced toxins did not significantly affect the dynamics of interactions. This conclusion was made after comparing the dynamics of interactions between (SH1000) and (B180) with another non-inhibitor producing strain of *S. epidermidis* (B115, Libberton et al. (2014)). However, maintaining the structure contributed positively to promoting the role of toxins produced.

Experimentally, as shown in Fig (3.13) and Fig (4.1), it was possible to show that when performing interactions between susceptible populations of *S. aureus* (SH1000) and other populations of *S. epidermidis* (B180), (B155), and (TU3298), the evolved *S. aureus* populations showed a strong ability to adapt, coexist, and eventually dominate, regardless of the toxins secreted by their opponents, environmental structures, and initial

concentrations.

Figure 4.5: **Four variable model simulations of the dynamics of interactions between populations of *S. aureus* (SH1000) and inhibitory producing *S. epidermidis* (B155) under mixed and structured conditions using** (3.24) **with the mixed environment parameters.** Panel (a): four-variable model simulations that represent the dynamics of interactions; solid lines under structured conditions, dashed lines under mixed conditions; (blue) lines represent the resident *S. aureus*, $(u_s + u_a)$, (red) lines represent the invader *S. epidermidis* populations (B155), and the ratio of initial concentrations is (0.01:1). Panel (b): a demonstration of the four-variable model dynamics, where (red) represents *S. epidermidis*, v, (blue) represents the susceptible fraction of the *S. aureus* population, u_s, and (green) represents the adapted fraction, u_a. Panel (c): extension of the dynamics introduced in (b). Panels (d), (e) and (f): four-variable model simulations of the mutual invasion where populations of *S. aureus* invaded into resident populations of *S. epidermidis*. The x-axis is the time in days. The y-axis represents the relative concentrations of the evolved populations. Parameters: $D_u = 1.8 \times 10^{-6}$, $D_v = 5 \times 10^{-6}$, $r_u = 26.5296$, $r_v = 22.3344$, $p_1 = 1.0091$, $p_2 = 0.9755$, $f_1 = 1$, $f_2 = 0.18$, $b_1 = 1.1$, $b_2 = 0.9$, $b_3 = 0.65$ and $b_4 = 0.96$.

Furthermore, it was possible to demonstrate mathematically that in the absence of a significant effect of toxins when performing interactions between (B180) and (SH1000), similar results were obtained without the need to change the parameters, implying that the only difference was the time delay of the dynamics when the interactions were performed under structured conditions. Structured environments favoured the producer for a more extended period than mixed environmental conditions, resulting in a delay in the dynamics of interactions. Retaining the environmental structure contributed to the accumulation of toxins. This privilege was not possible under mixed conditions.

In this section, the hypothesis of this thesis will continue to be tested in the presence of the toxins. This hypothesis proposes that preserving the environmental format will not prevent *S. aureus* from existing; rather, it will only delay the emergence of resistance in both directions of invasion. In addition, the test is to determine whether the application of the previous settings that were used in mixed simulations in a structured environment will result in obtaining simulations that are consistent with those observed

experimentally, as in the last case with the three-variable model. This means that either toxin accumulations under structured environmental conditions will not alter the dynamics, or the inhibitory interactions under regulated environment conditions will necessitate changing the parameters to obtain simulations that are more consistent and compatible with our findings.

The interactions that involve toxin production were modelled by assuming that one of the competing populations, *S. epidermidis*, produces toxin at a rate of f_1. In contrast, the other competing population, *S. aureus*, is well-known for its ability to adapt and mutate against these toxins. At position x and time t, the concentrations of susceptible *S. aureus*, adapted *S. aureus*, producer *S. epidermidis*, and toxin are defined as $u_s(x,t)$, $u_a(x,t)$, $v(x,t)$, and $T(x,t)$. Thus, this ecosystem is modelled via the (3.24) equations. Further details and information regarding the initial and boundary conditions can be found in Chapter 3.

As shown in Fig (4.5), when producing the four-variable model simulations under structured environmental conditions (solid lines), using the previous parameters used in mixed environments (dashed lines), the obtained simulations indicate that the toxin-producing species dominates when interactions are conducted in organised environments. Using mixed environment parameters to generate structured environment simulations reveals that preserving the spatial structure facilitates invasions by inhibitor-producing *S. epidermidis* strains, Fig (4.5a), and toxin-producing *S. epidermidis* strains resist and prevent invasion by *S. aureus* strains, Fig (4.5d).

As indicated in several studies, when conducting microbial interactions while maintaining spatial structure, especially in an *E. coli* evolution experiment in conditions with different degrees of spatial structure [32], the findings highlight that the rate of invasion and the dynamics of interactions are determined by the degree of mixing, as the daily mixing results in the rapid invasion, whereas a tight spatial population structure significantly slows the invasion process. Furthermore, bacterial populations developed in a spatially-organised environment with preserved population structure have a lower rate of adaptation and higher sustained diversity than populations formed in a mixed environment [77]. Spatial structure has also been considered as an important element in the persistence of species, mostly in non-transitive competitions [110, 173]. Thus, the associated slower dynamics that are observed here are possibly the reason for the delay in the emergence of resistance. In order to verify that the findings were stable and did not alter later as a consequence of the delay caused by performing these interactions in structured environments, as is the case in the three-variable model, simulations were extended, and, as seen in Fig (4.5c), and Fig (4.5f), the mutations did not appear.
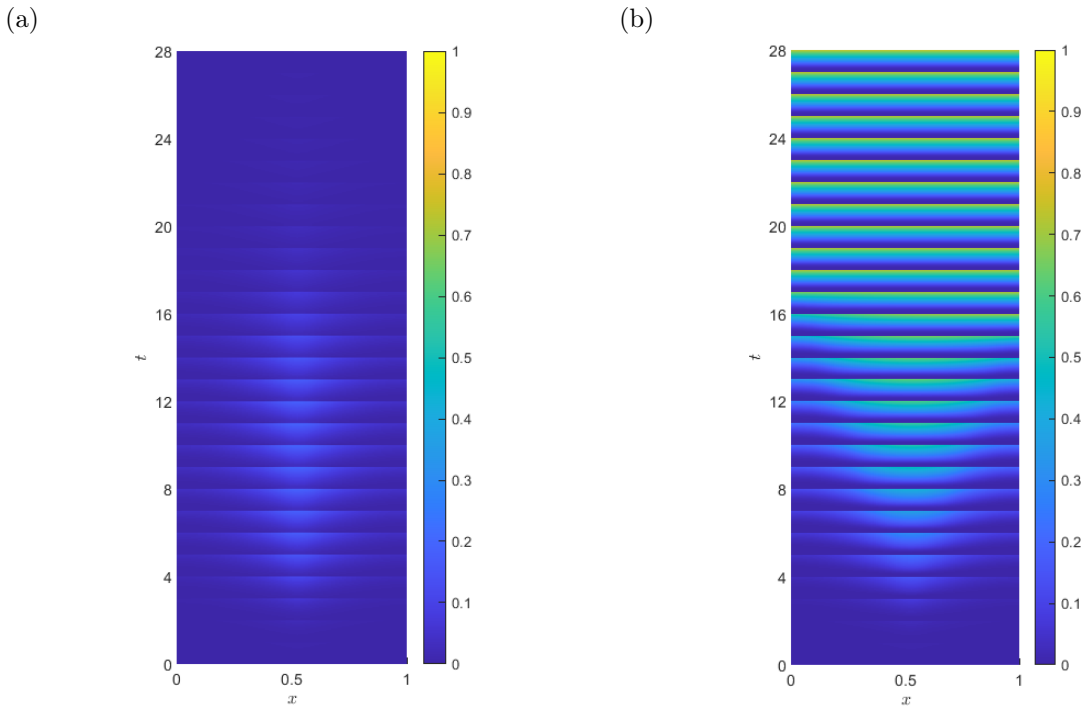
Figure 4.6: **Numerical simulations of the toxin evolution using model** (3.24) Surface images of the toxin concentration secreted by *S. epidermidis* populations (B155) when populations of *S. epidermidis* (the producer) invade resident population of *S. aureus* SH1000. Panel (a): under mixed conditions. Panel (b): under structured conditions. The x-axis represents space, and the y-axis represents time in days. Parameters: $D_u = 1.8 \times 10^{-6}$, $D_v = 5 \times 10^{-6}$, $r_u = 26.5296$, $r_v = 22.3344$, $p_1 = 1.0091$, $p_2 = 0.9755$, $f_1 = 1$ and $f_2 = 0.18$.

Such findings concur with the study previously presented and discussed in Chapter 2 of this thesis [122]. However, the experimental results, Fig (4.2), illustrate that even when the interactions were conducted under structured conditions, the evolution of resistance by *S. aureus* impeded/promoted the invasions by/of toxin-producing populations of *S. epidermidis*.

Unlike the three-variable model case, applying the parameters that were used when performing the mixed inhibitory interactions in the four-variable model did not result in obtaining simulations that concur relatively with the experimental findings under structured conditions as can be seen in Fig (4.5). This indicates that the presence of the toxicity factor can alter the course of interactions under structured conditions, which indicates that changing the prior parameters is required to generate simulations that are compatible with the laboratory data.

Experimentally, it was observed that structured environments enabled the inhibitory-producing populations of *S. epidermidis* to compete better and more effectively than in mixed habitats; this can be justified by the knowledge that interference competition in bacteria is primarily controlled and mediated by toxins produced in the environment and thus likely to be influenced by environmental spatial structure. According to [32], when performing experiments with *Escherichia coli*, the outcomes revealed that in spatially-

structured medium (agar plates), inhibitory-producing populations were able to invade sensitive populations starting from low initial concentrations. However, in the lack of spatial structure (shaken liquid broth), to achieve successful invasions substantially higher starting concentrations of the producers were required.
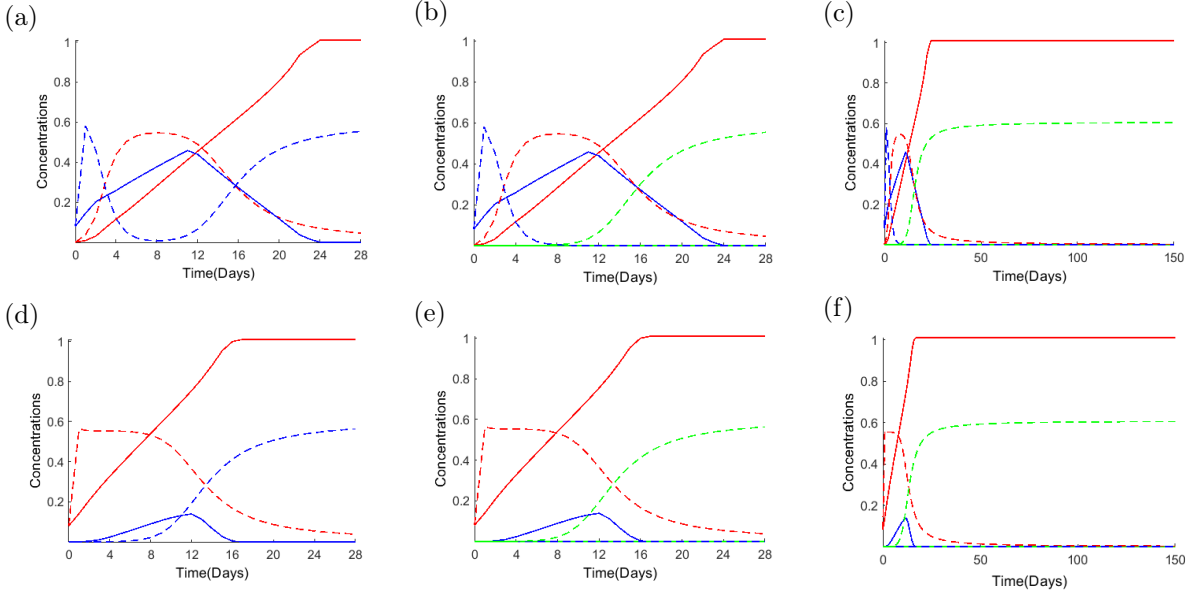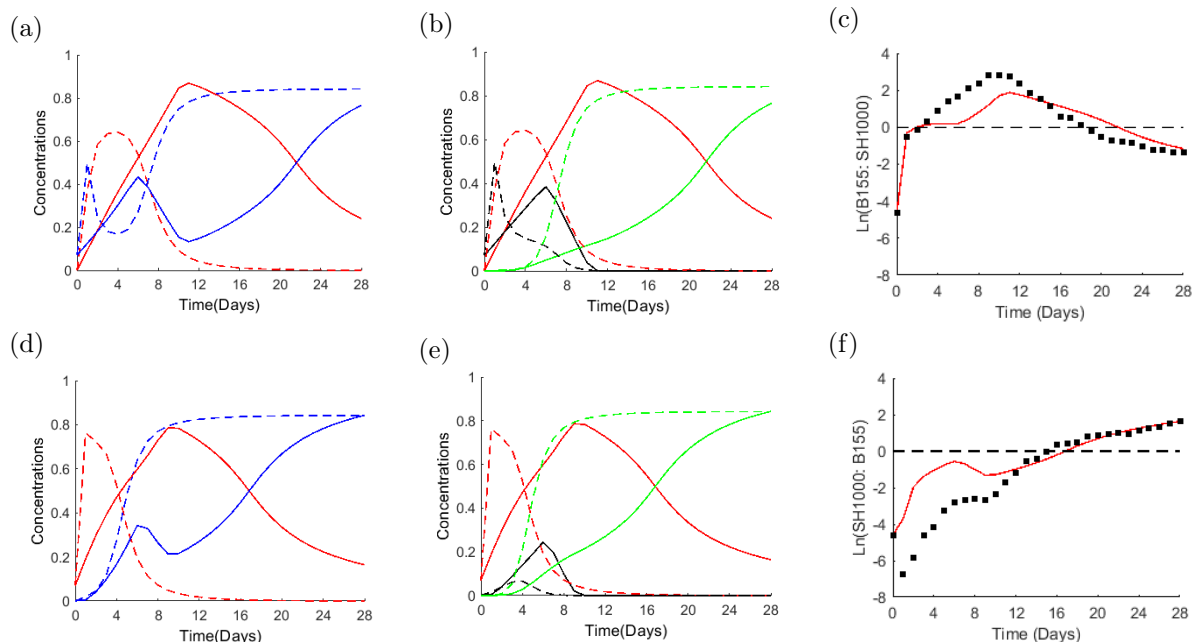

Figure 4.7: **Four variable model simulations of the dynamics of interactions between populations of _S. aureus_ (SH1000) and inhibitory producing _S. epidermidis_ (B155) under mixed and structured conditions using** (3.24) **with different inhibitory coefficients.** Panel (a): show the four-variable model simulations that represent the dynamics of interactions under structured and mixed conditions after changing the inhibitory coefficients; solid lines under structured conditions, dashed lines under mixed conditions; (blue) lines represent the resident _S. aureus_, $(u_s + u_a)$, (red) lines represent the invader _S. epidermidis_ populations (B155), and the ratio of initial concentrations is (0.01:1). Panel (b): a demonstration of the four-variable model dynamics, where (red) represents _S. epidermidis_, v, (black) represents the susceptible fraction of the _S. aureus_ population, u_s, and (green) represents the adapted fraction, u_a. Panel (c): a simulation of the natural log of the invader to resident ratio (red line) plotted against the actual experimental ratio under structured conditions (black dots). Panels (d), (e) and (f): show the four-variable model simulations of the mutual invasion where populations of _S. aureus_ invaded resident populations of _S. epidermidis_. In all panels, the x-axis is the time in days. The y-axis in panels (a), (b), (d), and (e) represents the relative concentrations of the evolved populations, and in panels (c) and (f), the natural log of the evolved population ratio. Parameters: $D_u = 1.8 \times 10^{-6}$, $D_v = 5 \times 10^{-6}$, $r_u = 26.5296$, $r_v = 22.3344$, $p_1 = 0.2613$, $p_2 = 0.2590$, $f_1 = 1$, $f_2 = 0.045$, $b_1 = 1.1$, $b_2 = 0.9$, $b_3 = 0.65$ and $b_4 = 0.96$.

Several studies have focused on understanding the reason for the difference in the performance of the toxins according to the type of incubating environment. These studies found that maintaining the spatial structure when conducting the inhibitory interactions gives the inhibitory-producing populations a chance to form clusters that would support the secreted toxins to achieve the highest possible concentrations [131]. As a result, as seen in Fig (4.6b) the advantages of the secreted toxins can be observed in tiny founder populations. Thus, spatially-structured habitats have been suggested to encourage toxin-producer invasions. In contrast, as seen in Fig (4.6a), continuous diffusion and

destruction of the formed structure of the evolved populations in mixed environments requires producers to reach a much higher concentration so that the role of the secreted toxins becomes evident [32].
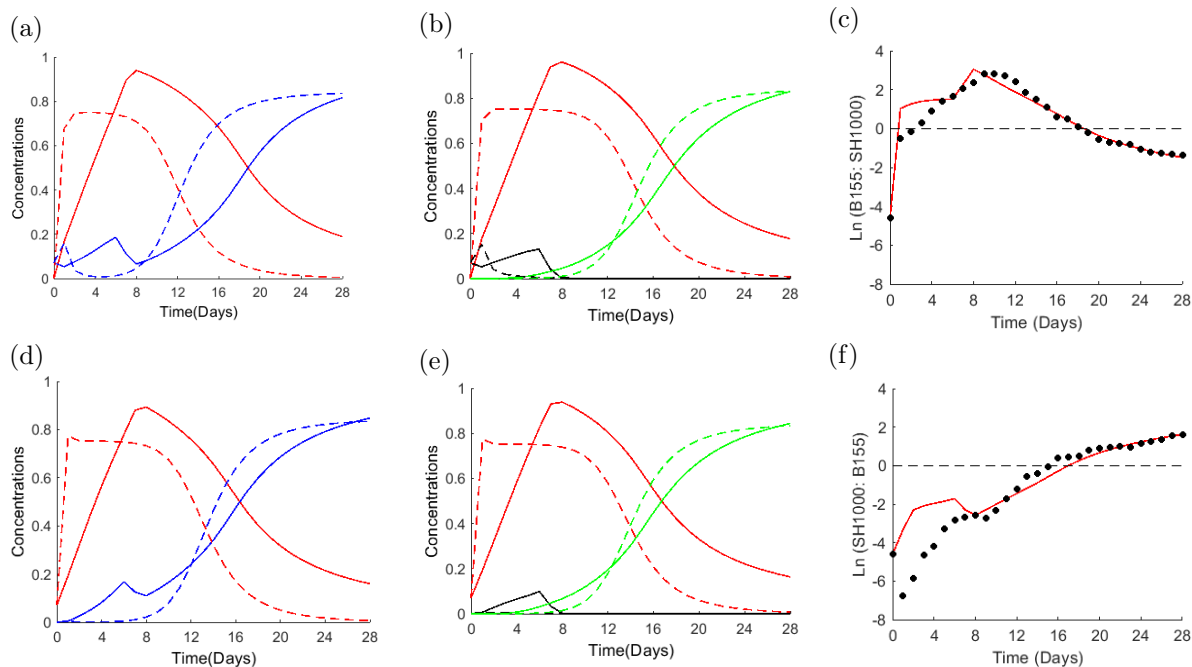
Figure 4.8: **Four variable model simulations of the dynamics of interactions between populations of S. aureus (SH1000) and inhibitory producing S. epidermidis (B155) under mixed and structured conditions using** (3.24) **with different inhibitory and interaction coefficients.** Panel (a): show the four-variable model simulations that represent the dynamics of interactions under structured and mixed conditions after changing the inhibitory coefficients; solid lines under structured conditions, dashed lines under mixed conditions; (blue) lines represent the resident S. aureus, $(u_s + u_a)$, (red) lines represent the invader S. epidermidis populations (B155), and the ratio of initial concentrations is (0.01:1). Panel (b): a demonstration of the four-variable model dynamics, where (red) represents S. epidermidis, v, (black) represents the susceptible fraction of the S. aureus population, u_s, and (green) represents the adapted fraction, u_a. Panel (c): a simulation of the natural log of the invader to resident ratio (red line) plotted against the actual experimental ratio under structured conditions (black dots). Panels (d), (e) and (f): show the four-variable model simulations of the mutual invasion where populations of S. aureus invaded resident populations of S. epidermidis. In all panels, the x-axis is the time in days. The y-axis in panels (a), (b), (d), and (e) represents the relative concentrations of the evolved populations, and in panels (c) and (f), the natural log of the evolved population ratio. Parameters: $D_u = 1.8 \times 10^{-6}$, $D_v = 5 \times 10^{-6}$, $r_u = 26.5296$, $r_v = 22.3344$, $b_1 = 1$, $b_2 = 0.9$, $b_3 = 0$ and $b_4 = 0.96$. Toxin parameters under mixed conditions: $f_1 = 1$, $f_2 = 0.18$, $p_1 = 1.0091$, $p_2 = 0.9755$. Toxin parameters under structured conditions: $f_1 = 1$, $f_2 = 0.045$, $p_1 = 0.2613$, $p_2 = 0.2590$.

Since it has been concluded that when the interactions are conducted under structured conditions the toxicity factor plays an essential role in terms of changing the outcomes of these interactions, the following section describes several attempts made to obtain the best simulation consistent with the experimental results of this thesis by using the four-variable model.

Changing Toxicity Parameters

Through laboratory observations and the presented studies, it becomes clear that regulated environments boost toxin concentrations. Hence, manipulating the parameters that

govern the toxins may result in improved four-variable model simulations to concur with the results.

As stated in the previous chapter, the parameters that control toxicity performance cannot be identified. However, through the combined experimental and theoretical study presented earlier in Chapter 3, it was possible to define a relationship (3.19) that associates these factors under mixed conditions.
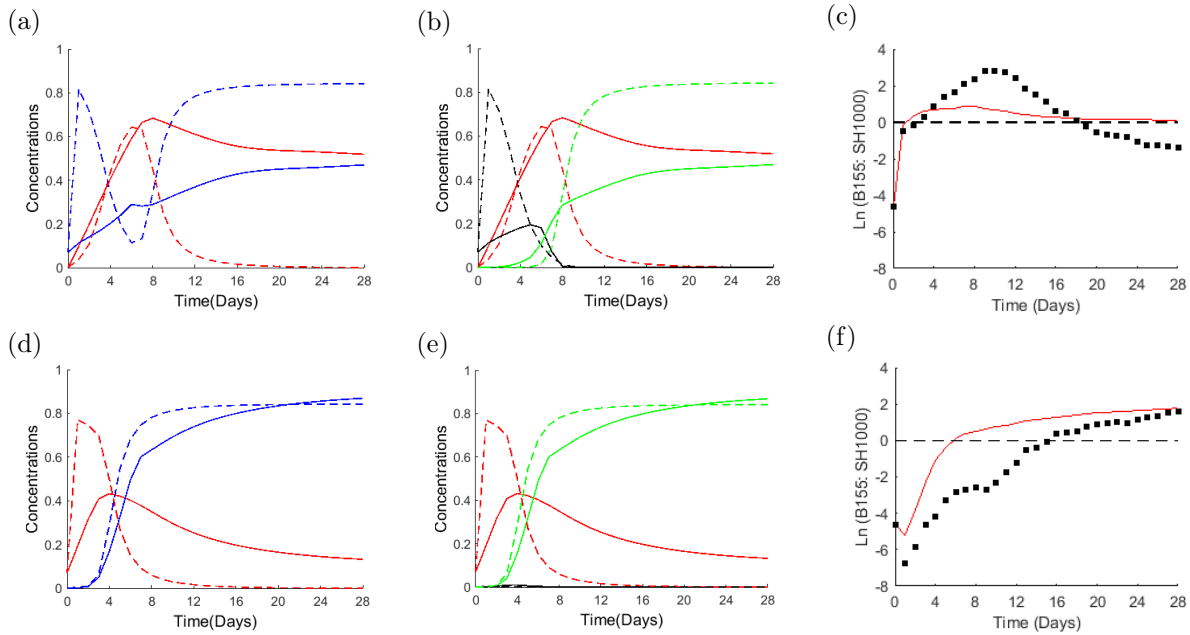
Figure 4.9: **Four variable model simulations of the dynamics of interactions between populations of *S. aureus* (SH1000) and inhibitory producing *S. epidermidis* (B155) under mixed and structured conditions using** (3.24) **with different** p_2**.** Panel (a): show the four-variable model simulations that represent the dynamics of interactions under structured and mixed conditions after changing the inhibitory coefficients; solid lines under structured conditions, dashed lines under mixed conditions; (blue) lines represent the resident *S. aureus*, $(u_s + u_a)$, (red) lines represent the invader *S. epidermidis* populations (B155), and the ratio of initial concentrations is (0.01:1). Panel (b): a demonstration of the four-variable model dynamics, where (red) represents *S. epidermidis*, v, (black) represents the susceptible fraction of the *S. aureus* population, u_s, and (green) represents the adapted fraction, u_a. Panel (c): a simulation of the natural log of the invader to resident ratio (red line) plotted against the actual experimental ratio under structured conditions (black dots). Panels (d), (e) and (f): show the four-variable model simulations of the mutual invasion where populations of *S. aureus* invaded resident populations of *S. epidermidis*. In all panels, the x-axis is the time in days. The y-axis in panels (a), (b), (d), and (e) represents the relative concentrations of the evolved populations, and in panels (c) and (f), the natural log of the evolved population ratio. Parameters: $D_u = 1.8 \times 10^{-6}$, $D_v = 5 \times 10^{-6}$, $r_u = 26.5296$, $r_v = 22.3344$, $p_1 = 1.0091$, $p_2 = 0.37$, $f_1 = 1$, $f_2 = 0.18$, $b_1 = 1.1$, $b_2 = 0.9$, $b_3 = 0.65$ and $b_4 = 0.96$.

As seen in this equation, there is an association between four variables that govern the influence of the toxins on the dynamics of interactions. These variables are f_1, f_2, p_1, and p_2, which donate inhibitor production rate, inhibitor degradation rate, inhibition rate on the susceptible fraction of the population, and inhibition rate on the adapted fraction of the population, respectively, as shown in (3.24). To reduce the number of parameters in this equation, the production rate, f_1 was fixed to be equal to 1. Thus, the best-fit

simulations can be produced with the minimum errors by defining the proper value for f_2 by using the least square method. Consequently, it was possible to find the corresponding values of the inhibition coefficients.

As previously indicated, the equation (3.19) shows the positive relationship between the decaying rate of toxins and the inhibition parameters, meaning that reducing f_2 will lead to reducing both inhibition coefficients. Since the decaying coefficient with the lowest error rate was lower than the one determined when simulating the interaction under mixed conditions, this denotes that p_1, which represents the effect of the toxins on the susceptible fraction of the evolved *S. aureus* population, will decrease.

As a result of reducing the effectiveness of toxins secreted by (B155) on the sensitive part of (SH1000), the initial drop in the evolved *S. aureus* population was no longer observed when simulating the natural logarithm of the ratio between the invader *S. aureus* and the resident population of *S. epidermidis*, as shown in Fig (4.7f). Therefore, another attempt at the simulation was necessary to obtain a more accurate simulation consistent with the laboratory results, shown as black dots in the figures (4.7c) and (4.7f).

Changing Intensity of Interactions

Although reducing the effect of the toxins when performing the interactions under structured conditions contributed to achieving comparable and more realistic simulations, it may be possible to improve these simulations by changing the parameters that govern the intensity of the interactions between *S. epidermidis* and the susceptible fraction of the *S. aureus* population.

Supposing that this change results in significantly improved and more accurate simulations, these new parameters will be used to produce simulations under mixed conditions to determine if the new parameters could be adopted in the simulations of both environments.

Changing the parameters b_1 and b_3, which control the level of interaction intensity between u_s and v, as shown in Fig (4.8), improved the simulations produced by the four-variable model under structured conditions. Furthermore, when implementing these new parameters while producing mixed simulations, as seen in Fig (4.8a) and Fig (4.8d), the results concurred to a certain extent with that experimentally obtained when performing these interactions under mixed conditions. However, the goal of this stage, which was to observe the initial decrease in *S. aureus* population density when invading the resident population of the inhibitory producing *S. epidermidis*, was not entirely achieved.

Increase in the strength of the competition between the producer and the sensitive fraction of the *S. aureus* population was not sufficient to observe such a pattern.

Thus, considering the characteristic features of this species, as it has a low growth rate as well as a low diffusion rate compared to *S. aureus* (SH1000), the only way to observe this pattern is to keep the effect of the toxins high on the sensitive part of the evolved *S.*

aureus populations.

Changing p_2

Before conducting the interactions between *S. aureus* and all other strains of *S. epidermidis* under different conditions, deferred inhibition spray assays were performed to determine the sensitivity of a pure population of *S. aureus* against the toxins produced by pure populations of *S. epidermidis* strains.

Also, another deferred inhibition spray assay was performed after the interactions to determine whether the evolved *S. aureus* clones had developed resistance to the toxins produced by *S. epidermidis* strains. These experiments were referred to and the results reviewed in detail in the previous chapter. However, the purpose of mentioning these experiments at this point is to indicate that the results of the first experiment (pre-invasions), where the sensitivity of pure isolates of *S. aureus* was determined against the toxins produced by pure isolates of *S. epidermidis*, can also be adopted when carrying out invasions in both environments. From the results of the pre-invasions inhibition spray assay, it was possible to define a mathematical expression that associates the decaying rate of the toxins produced by the evolved *S. epidermidis* populations f_2 and the inhibition rate of the susceptible fracture of the evolved *S. aureus* populations p_1. These values are the same in both environments.

From the second experiment, the mathematical expression that associates the decaying rate of the toxins with the parameter p_2 was defined, which measures the effect of the produced toxins on the adapted part of the evolved *S. aureus* population. On the other hand, this value, p_2, can vary greatly from one encounter to the next, not least when performed under different circumstances.

Furthermore, as shown in Fig (4.8), changing the toxicity parameters as well as the parameters that control the intensity of interactions between v and u_s resulted in more accurate simulations. However, considering the characteristic features of this species (B155), as it has a low growth rate as well as a low diffusion rate compared to *S. aureus* (SH1000), the non-monotonic behaviour when simulating the natural log of (SH1000: B155) ratio, presented in Fig (4.2f), cannot be observed with this particular strain unless the effect of the toxins on the sensitive part of the evolved *S. aureus* populations remains high. Therefore, in another attempt to achieve more accurate simulations consistent with laboratory results, it was decided to break the associations between p_2 and f_2, which means only the coefficient that controls the effect of the toxins on the adopted fraction of the evolved *S. aureus* population was reduced.

Although the desired pattern was reached through this attempt, as seen in Fig (4.9f), it can be stated that this attempt was unsuccessful and did not yield results more consistent with that achieved in the laboratory, as reducing the effect of toxins on the adapted part of the evolved *Staphylococcus aureus* contributed to the faster emergence of resistance,

which led to the rapid inhibition of the toxin-producing invaders, as shown in Fig (4.9c). Nevertheless, from this attempt, it was proven that to obtain a non-monotonous pattern, the role of toxins must be maintained more effectively on the sensitive part of the *S. aureus* population.

Introducing Mutations

As noted earlier, when the role of toxins was not significantly recognised, as was the case when populations of low-toxin producing *S. epidermidis* B180 interacted with *S. aureus* (SH1000), it was possible to obtain simulations from the three-variable model that were commensurate with the results when performing the interactions under both environmental structures. As shown in Fig (4.4), when the conditions of the structure environments were imposed on the three-variable model, the obtained simulations concurred with the experimental findings without the need to change the parameters. Thus, it was concluded that when the toxicity level was low, the organised environment differed from the mixed environment only in timing. The dynamics of interactions were slower when preserving the structure. This delay was justified by the fact that retaining the spatial structure contributed to boosting the role of toxins more effectively.

(a)   (b)
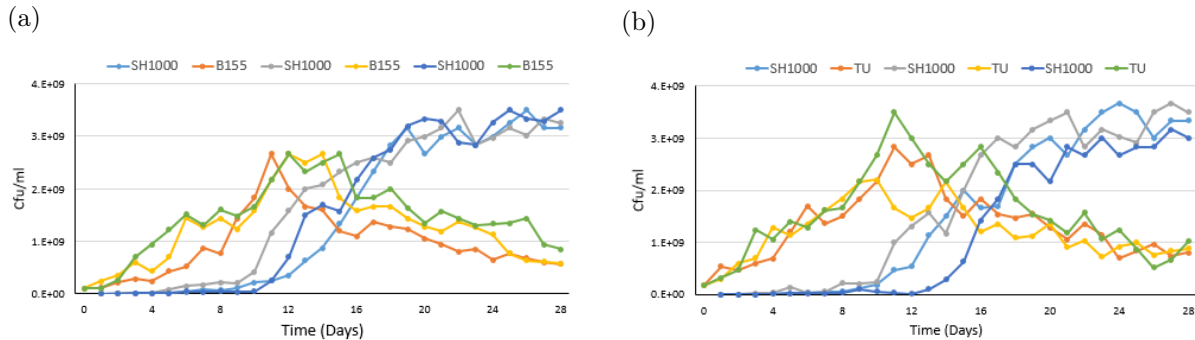
Figure 4.10: **The experimental data showing the evolution of *S. aureus* populations when invading into inhibitory-producing *S. epidermidis* populations at a frequency of 0.01.** *S. aureus* (SH1000) populations were introduced into two different toxin-producing *S. epidermidis* populations. Panel (a): B155 were the resident population. Panel (b): TU3298 were the resident populations. Invasions were carried out under spatially structured conditions. The x-axis is the time in days, and the y-axis is the colony-forming units (cfu) per plate.

According to [131], clustering of toxin producers enables toxins to reach higher local concentrations, hence spatially-organised habitats were considered to facilitate toxin producer invasion. Therefore, it was concluded that the difference that was observed when performing the inhibitory interactions under structured and mixed conditions, see Fig (4.5), was due to the involvement of a significant level of toxicity, [see Fig (4.6)], which had an influential role in altering the dynamics of interactions. Accordingly, several attempts were made to simulate the obtained experimental data when conducting the inhibitory interactions under structured conditions. Although satisfactory results were achieved in several of these attempts, the author of this thesis upholds that a more re-

alistic scenario should be imposed to simulate the laboratory findings. As illustrated in Fig (4.5b) and Fig (4.5e), the assumption previously adopted when producing all simulations, that the initial *S. aureus* population contains 1% of beneficial resistance mutations, which was not adequate in this case, particularly given the presence of both structure and inhibition factors.

This assumption was based on an evolutionary theory that proposes that increased initial concentrations of the susceptible *S. aureus* population increases the possibility that these isolates contain viable mutations that have been pre-adapted to overcome the circumstances of the black hole sink [88, 163]. The term, the black hole sink, is often used in population ecology to represent the hostility of a toxic environment when invaded by a susceptible population. The secreted toxins kill the susceptible immigrants, making the invaders unable to survive and sustain a viable population [88].

In addition to the evolutionary theory, several theoretical models suggest that the initial concentration of immigrants from the source population enhances the possibility of adaption in an inhibitory environment [70, 89]. As a result, when *S. aureus* populations invade from higher starting frequencies, they are more likely to have mutants that are resistant to *S. epidermidis* toxins.

The evolutionary theory and the theoretical models were taken into consideration when it was assumed that the initial isolate of the evolved *S.aureus* contains a fraction pre-adapted to the toxins produced by *S. epidermidis* and that this fraction represents one percent of the total population size, signifying that the evolutionary theory and the theoretical models are valid, producing outcomes commensurate with those expected.

The propagation of these advantageous resistance mutations, on the other hand, is likely to be restricted and delayed in more highly spatially-organised ecosystems. This is since competition for the advantageous mutant may emerge only at the colony's edge, and as the colony develops and expands, a smaller fraction of the mutant population will be involved in competitions with the ancestral genotype [76].

On the one hand, such findings can be considered as sufficient justification for the simulation that was reached in Fig (4.5), and maybe a logical explanation for the resistance disappearance illustrated in figures (4.5b, 4.5e), (solid green line) when imposing the conditions and parameters of the mixed environment on the interferences carried out under the structured conditions. On the other hand, according to figures (4.1, 4.2), the results showed that evolved *S. aureus* populations were able to maintain their existence and adapt to the structured environmental circumstances.

From this point of view, it can be stated that the resistance that appeared when conducting competitions in organised environments was not based on assumptions about the presence of mutations in the initial samples, as they would be unable to survive in these challenging conditions. Rather, these mutations are formed within the course of

interactions.
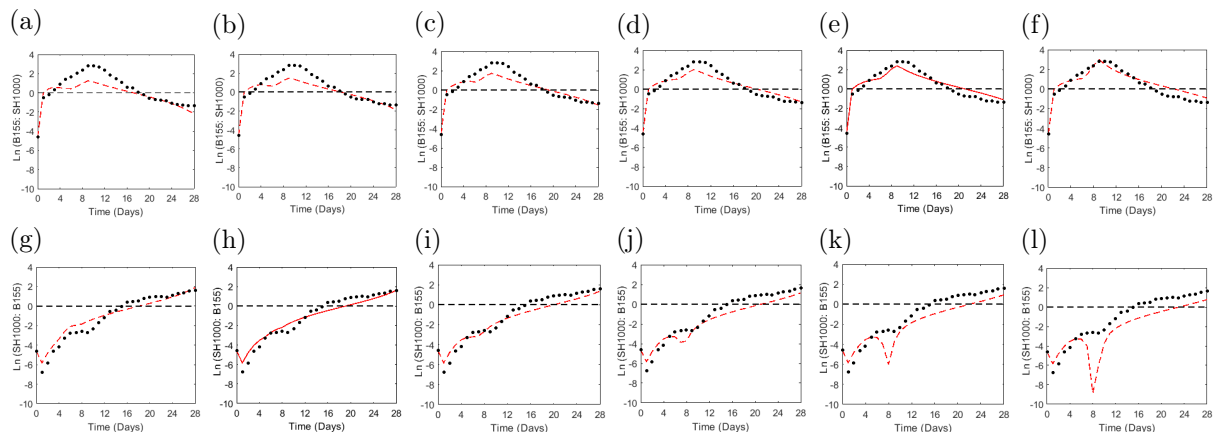
Figure 4.11: **Plots of the natural log of the invader to resident ratio simulations when mutations were introduced on different days.** Panels in the first row depicts four-variable model simulations of the ratios (dashed red lines) plotted against the ratio of the actual data (black dots) when populations of toxin-producing *S. epidermidis* (B155) invaded populations of *S. aureus* (SH1000) at a frequency of 0.01. Panels (a) → (f): represent simulations with mutations assumed to appear on (day 2) → (day 7), respectively. Panels in the second row exhibit simulations of mutual invasions using a four-variable model. The solid red lines indicate when simulations had the lowest error rate. The x-axis is the time in days. The y-axis is the natural log of the evolved population ratio. Parameters: $D_u = 1.8 \times 10^{-6}$, $D_v = 5 \times 10^{-6}$, $r_u = 26.5296$, $r_v = 22.3344$, $p_1 = 1.0091$, $p_2 = 0$, $f_1 = 1$, $f_2 = 0.18$, $b_1 = 1.1$, $b_2 = 0.9$, $b_3 = 0.65$ and $b_4 = 0.96$.

In mixed environments, several factors assisted the survival of the evolved *S. aureus* populations during competitions involving high toxicity levels, possibly the most important of which is that the secreted toxins did not reach their maximum effectiveness due to the rapid diffusion of the bacteriocin and the daily destruction of the formed colonies.

On the contrary, as shown in Fig (4.6), the toxins showed maximum effectiveness when conducting interferences in structured environments. Since the experimental findings showed that evolved *S. aureus* populations presided and persisted under such severe conditions, the emergence of mutations during interactions may be the logical explanation for this phenomenon.

Therefore, in this attempt it was decided to introduce the mutations later during the process of interactions instead of assuming their initial presence. As noted in Chapter 3, all previous parameters that were used when producing the mixed environments simulations were imposed in this scenario, except the value of p_2 as it was assumed it would be equal to zero.

In the beginning, several assumptions were made, as it was difficult to detect when the resistance occurred. According to the laboratory observations, [see Fig (4.10)], the resistance appeared on different days when performing the same experiment, but in other replications. Considering the figures (4.1d, 4.1f), it can be stated that the resistance began prior to the eleventh day. As indicated in Fig (4.11), the range of days was narrowed down by fitting the natural log of the invader to resident ratio simulations to actual

experimental data, using the fitting method to determine which day had the least error.

Figure 4.12: **The dynamics of interactions between populations of *S. aureus* (SH1000) and inhibitory producing *S. epidermidis* (B155) under structured conditions when mutations were introduced on different days.** Panel (a): illustration of the experimental data showing the dynamics of interactions when toxin-producing *S. epidermidis* (B155, red) invades resident populations of *S. aureus* (blue) under structured conditions at an initial concentration of (0.01: 1). Panel (b): show the four-variable model (3.24) simulations that represent the dynamics of the interactions reported in panel (a) when mutations were introduced on day 6. Panel (c): a demonstration of the four-variable model dynamics under structured conditions, with (red) representing *S. epidermidis*, v, (black) the susceptible fraction of the *S. aureus* population, u_s, and (green) the adapted fraction, u_a. Panels (d), (e), and (f) showed reciprocal invasions when mutations were introduced on day 3. The x-axis is the time in days. The y-axis represents the relative concentrations of the evolved populations. Parameters: $D_u = 1.8 \times 10^{-6}$, $D_v = 5 \times 10^{-6}$, $r_u = 26.5296$, $r_v = 22.3344$, $p_1 = 1.0091$, $p_2 = 0$, $f_1 = 1$, $f_2 = 0.18$, $b_1 = 1.1$, $b_2 = 0.9$, $b_3 = 0.65$ and $b_4 = 0.96$.

The outcomes of the final attempt to produce simulations from the four-variable model that satisfy the experimental findings when performing the invasions under spatially-structured conditions were more accurate, more realistic, more consistent, and compatible with the other studies that have been presented. As illustrated in Fig (4.11), simulations indicated that mutations evolved on day six when *S. aureus* populations were the residents, see Fig (4.11e). In contrast, mutations appeared on the third day when *S. aureus* populations were the invaders, see Fig (4.11h).

This suggests the presence of a negative correlation between *S. aureus* population density and the emergence of the adapted generations. Such a correlation can be explained and justified by the presence of what is known as intraspecific competition within the *S. aureus* strain.

The primary distinction between interspecific and intraspecific competition is that interspecific competition involves members of different species competing for common resources. In contrast, the intraspecific competition involves members of the same species competing. Thus, when the initial size of the population is larger, the competition will continue for a more extended period, and accordingly, the emergence of resistance is

delayed, and vice versa.
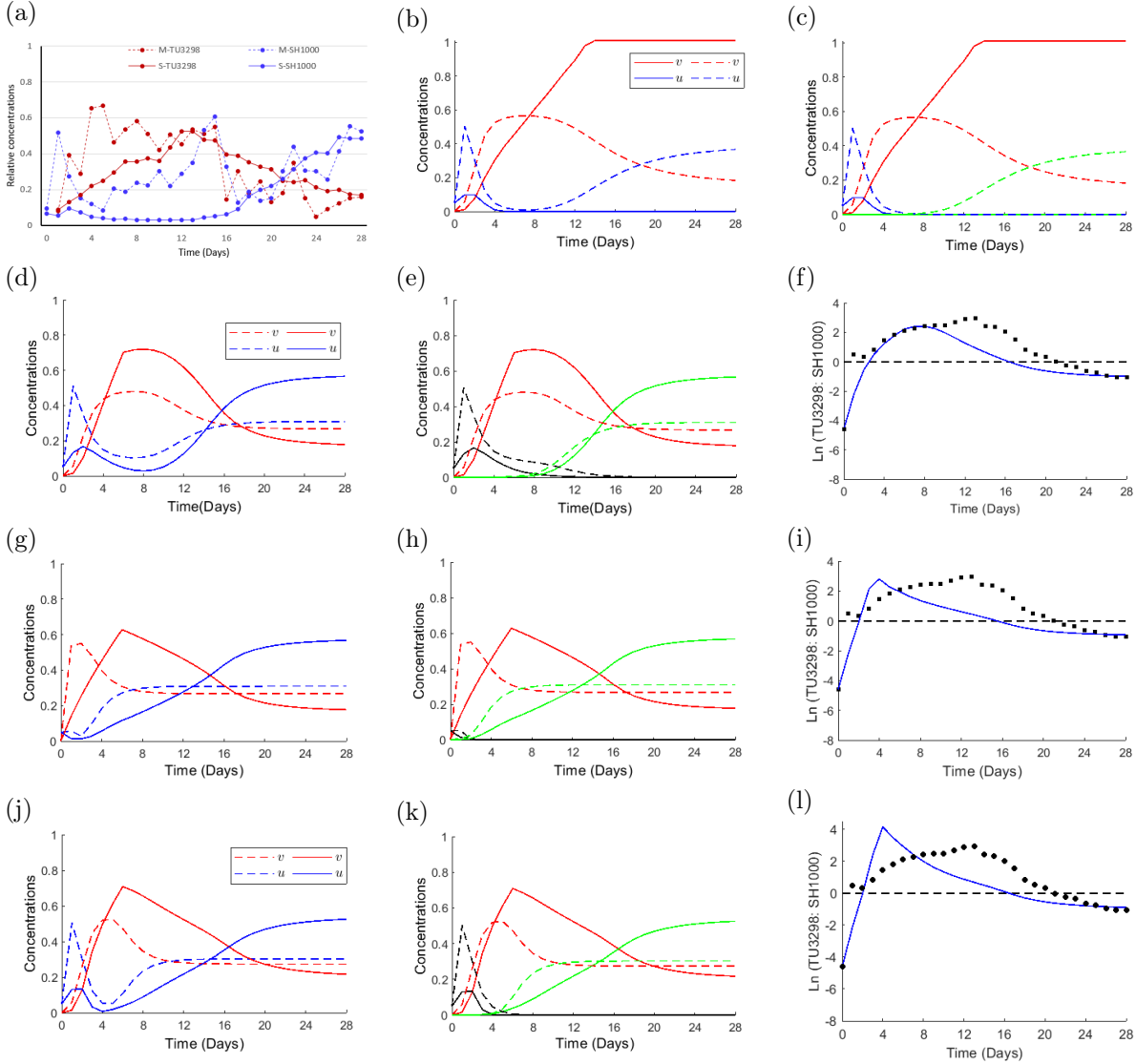
Figure 4.13: **The effect of applying improvement attempts on the dynamics of interactions when toxin-producing populations of *S. epidermidis* (TU3298) invade populations of *S. aureus* (SH1000) at a frequency of 0.01.** Panel (a): illustration of the experimental data showing the dynamics of interactions when toxin-producing populations of *S. epidermidis* (TU3298, red) invade resident populations of *S. aureus* (SH1000, blue) under mixed (dashed lines) and structured (solid lines) conditions. Panels (b) and (c) show the four-variable model (3.24) simulations when applying the mixed environment parameters. The blue line represents the whole *S. aureus* population, whereas blue and green represent the susceptible and adapted fractures of the *S. aureus* population, respectively. Parameters: $D_u = 1.8 \times 10^{-6}$, $D_v = 5 \times 10^{-5}$, $r_u = 26.5296$, $r_v = 28.613$, $p_1 = 0.7746$, $p_2 = 0.7623$, $f_1 = 1$, $f_2 = 0.24$, $b_1 = 0.9$, $b_2 = 0.84$, $b_3 = 0.9$ and $b_4 = 1.09$. Panels (d) and (e): show the influence of reducing the toxicity effect, $f_2 = 0.07$, $p_1 = 0.2258$ and $p_2 = 0.2247$. Panels- (g) and (h): show the influence of reducing the toxicity effect and increasing the intensity of the interactions between v and u_s, $b_1 = 1.1$ and $b_3 = 0$. Panels (j) and (k) demonstrate the resulting simulations when changing $p_2 = 0.26$, while all other parameters remain unchanged. Panels (f), (i) and (l): show simulations of the natural log of the invader-to-resident ratio (solid lines) plotted against the experimental data (black dots). The x-axis in all panels is the time in days, and the y-axis in panels (f), (i), and (l) represents the natural log of the evolved populations, whereas it represents the relative concentrations of the evolved populations in all other panels.

Similarly, when modelling the interactions between *S. aureus* and *S. epidermidis* (TU3298),

the same attempts were made to reach and obtain the best four-variable model simulations that matched the experiments.

It should also be noted that when applying the mixed conditions setting to the interactions that were performed under structured conditions, simulations were obtained that were similar in terms of outputs to those previously obtained with the other toxin-producing strain (B155), where the toxin-producing *S. epidermidis* species (TU3298) dominated entirely in both directions of the invasions, as shown in Fig (4.13b) and Fig (4.13c).
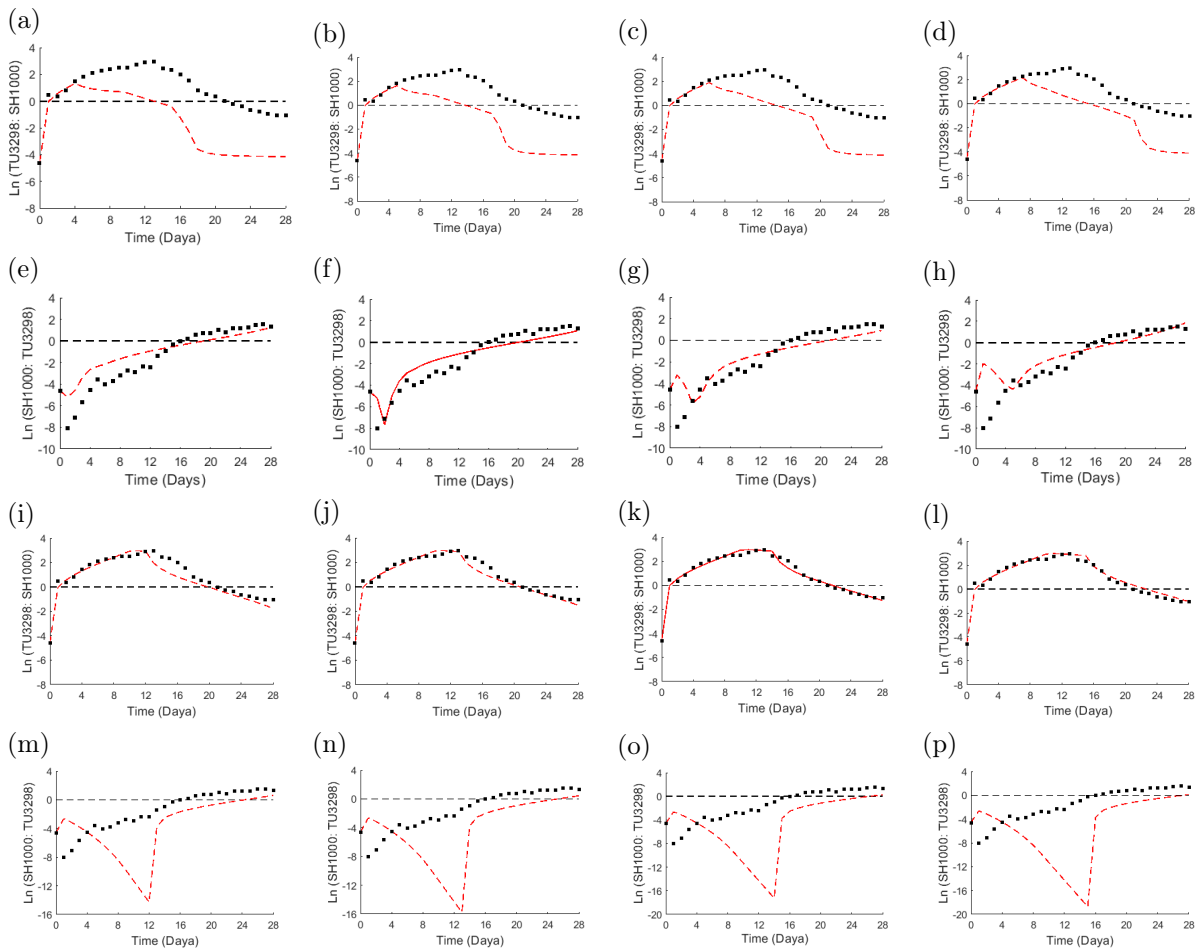
Figure 4.14: **Plots of the natural log of the invader to resident ratio simulations when mutations were introduced on different days.** Panels in the first and third rows display four-variable model simulations of the ratios (red lines) plotted against the ratio of the actual data (black dots) when populations of toxin-producing *S. epidermidis* (TU3298) invaded populations of *S. aureus* (SH1000) at a frequency of 0.01. Panels (a) $\rightarrow$ (d): represent simulations with mutations assumed to appear on (day 4) $\rightarrow$ (day 7), whereas (i) $\rightarrow$ (l) represent simulations with mutations that appear on (day 12) $\rightarrow$ (day 15), respectively. Panels in the second and fourth rows demonstrate the corresponding ratio of reciprocated invasions. Solid red lines in (g) and (k) indicate the lowest error rate of simulations. The x-axis is the time in days. The y-axis is the natural log of the evolved population ratio. Parameters: $D_u = 1.8 \times 10^{-6}$, $D_v = 5 \times 10^{-5}$, $r_u = 26.5296$, $r_v = 28.613$, $p_1 = 0.7746$, $p_2 = 0$, $f_1 = 1$, $f_2 = 0.24$, $b_1 = 0.9$, $b_2 = 0.84$, $b_3 = 0.9$ and $b_4 = 1.09$.

Since, as previously indicated, it is already known that this occurred because of the toxins, their role was more evident and effective when preserving the spatial structure

during the interactions. Accordingly, applying the mixed environment parameters led to displacement and the disappearance of the evolved *S. aureus* populations in both parts (sensitive as well as adaptive). Therefore, the same process must be followed in order to obtain a more realistic simulation representing the laboratory results of this thesis.

When modelling the interactions involving toxins in structured environments began, the interactions between (B155) and (SH1000), all the trials were presented in detail, with varying degrees of accuracy and consistency of their outputs compared with actual data. However, in this case, when modelling the interactions between (TU3298) and (SH1000), a brief presentation, as seen in Fig (4.13), shows the outcomes of all the attempts in only one direction of the invasions: when a toxin-producing population of *S. epidermidis* (TU3298) invades a resident population of *S. aureus* (SH1000). However, Fig (6.6) in the appendix, illustrates the consequences of these attempts in the other direction of invasions.

Figures (4.13) and (6.6) illustrate outcomes of the four-variable model when simulating the mutual interactions between populations of inhibitory-producing *S. epidermidis* (TU3298) and susceptible populations of *S. aureus* (SH1000). The first row in both figures shows the actual experimental data that reflects the dynamics of interactions and the four-variable model simulations (dashed lines) when performing the interactions under mixed conditions (solid lines) under structured conditions.

Panels (4.13b) and (4.13c) illustrate the inability of mixed environment parameters to produce compatible simulations in both environments, i.e., maintaining the parameters used when simulating the interactions under mixed conditions did not create sufficient simulations that reflect the dynamics of interactions under structured conditions. On consideration of this issue, it was decided to perform the previous processes and manipulate the toxins factors again to obtain comparable simulations that agree with the dynamics of interactions under both conditions.

Each row in figures (4.13) and (6.6) reflects the output of each process. Panels (4.13d) $\rightarrow$ (4.13f) illustrate when the effect of toxicity was reduced on both fractions of the *S. aureus* population by choosing the appropriate inhibition degradation rate, $f_2 = 0.07$ that has the lowest error value, and based on that, the corresponding inhibition coefficients, $p_1 = 0.2258$ and $p_2 = 0.2247$, were determined. Panels (4.13g) $\rightarrow$ (4.13i) illustrate when the effect of toxicity was reduced and the intensity of interactions between v and u_s was increased in favour of *S. epidermidis* strain, $b_1 = 1.1$ and $b_3 = 0$. However, the process performed in the last row, as seen in panels (4.13j) $\rightarrow$ (4.13l), aimed to keep all the previous parameters and only change $p_2 = 0.26$, which controls the inhibition degree of the adaptive part of the *S. aureus* population. Reducing this parameter preserves the dynamics observed at the beginning of the interactions when the inhibitory-producing *S.*

156

epidermidis could only restrict and inhibit the growth of susceptible *S. aureus* fractions. In contrast, the adapted fracture u_a will have a better chance of survival.
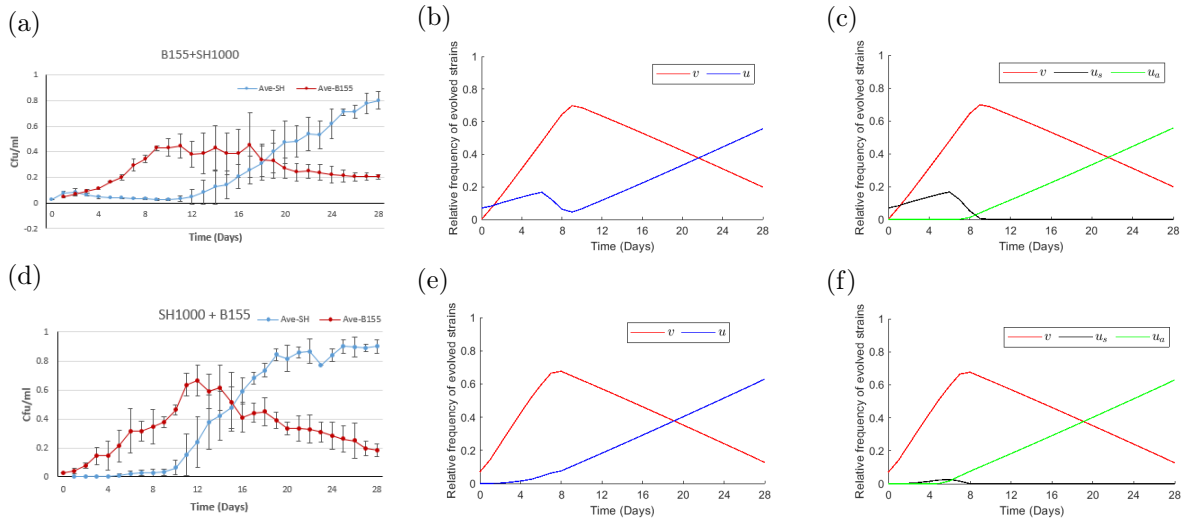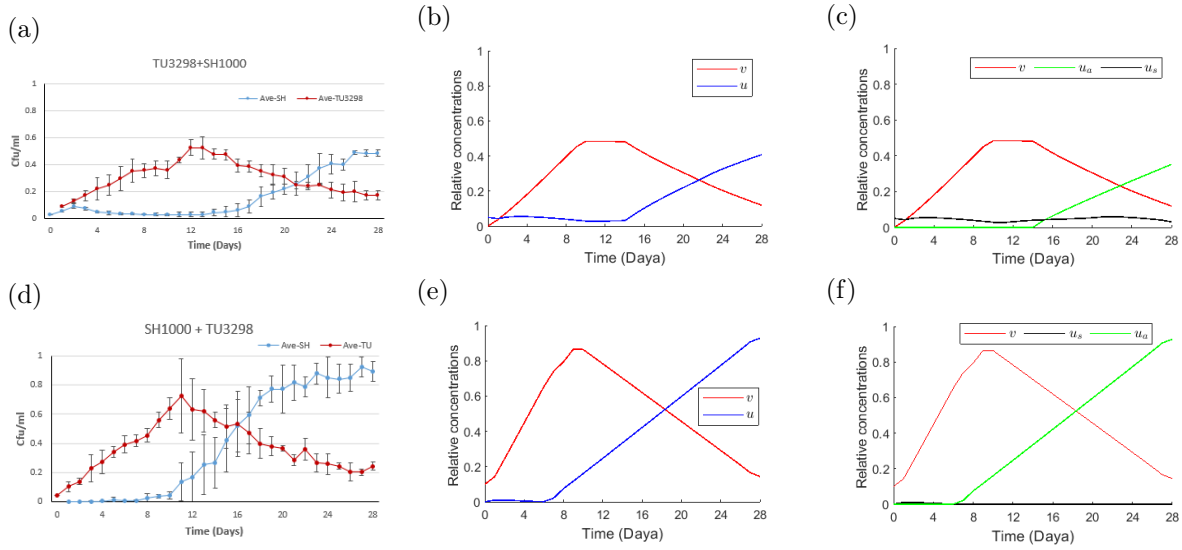

Figure 4.15: **The dynamics of interactions between populations of *S. aureus* (SH1000) and inhibitory producing *S. epidermidis* (TU3298) under structured conditions when mutations were introduced on different days.** Panel (a): illustration of the experimental data showing the dynamics of interactions when toxin-producing *S. epidermidis* (TU3298, red) invades resident populations of *S. aureus* (blue) under structured conditions at an initial concentration of (0.01: 1). Panel (b): show the four-variable model (3.24) simulations that represent the dynamics of the interactions reported in panel (a) when mutations were introduced on day 14. Panel (c): a demonstration of the four-variable model dynamics under structured conditions, with (red) representing *S. epidermidis*, v, (black) the susceptible fraction of the *S. aureus* population, u_s, and (green) the adapted fraction, u_a. Panels (d), (e), and (f) showed reciprocal invasions when mutations were introduced on day 6. The x-axis is the time in days. The y-axis represents the relative concentrations of the evolved populations. Parameters: $D_u = 1.8 \times 10^{-6}$, $D_v = 5 \times 10^{-5}$, $r_u = 26.5296$, $r_v = 28.613$, $p_1 = 0.7746$, $p_2 = 0$, $f_1 = 1$, $f_2 = 0.24$, $b_1 = 0.9$, $b_2 = 0.84$, $b_3 = 0.9$ and $b_4 = 1.09$.

The obtained results of some of these processes could better simulate the dynamics of interactions observed in the experiments. However, no single attempt at the process was able to achieve a better simulation of both directions of invasions.

Applying the settings of the first attempt, as illustrated in Fig (4.13f), resulted in obtaining better simulations in the first direction of the invasions, i.e., when toxin isolates of *S. epidermidis* (TU3298) invaded resident populations of *S. aureus* (SH1000), whereas the best simulations of mutual invasion, as shown in Fig (6.6i), were obtained when the second attempt was made. Thus, it was decided to further investigate the obtained behaviour by expanding the process to include introducing the mutations at a later stage of the interactions rather than assuming that the initial population contains beneficial resistance mutations.

As shown in Fig (4.14), when performing this process, all the previous parameters used to simulate the interactions under mixed conditions were preserved. However, since the findings indicated that the engaged *S. aureus* populations evolved and proliferated, they did not disappear. Hence, it was assumed that the adapted fracture of the evolved *S.*

aureus populations was no longer affected by the toxins produced by the *S. epidermidis* strain. The only connection that associated the producer with the resistant part of *S. aureus* populations was the competition for resources, which favoured and promoted resistance as it competed more successfully for resources. In fact, the presence of this link, both populations competing for joint resources, and the rapid growth rate of the producers (TU3298) contributed to establishing a state of coexistence between the evolved populations.

(a)   (b)
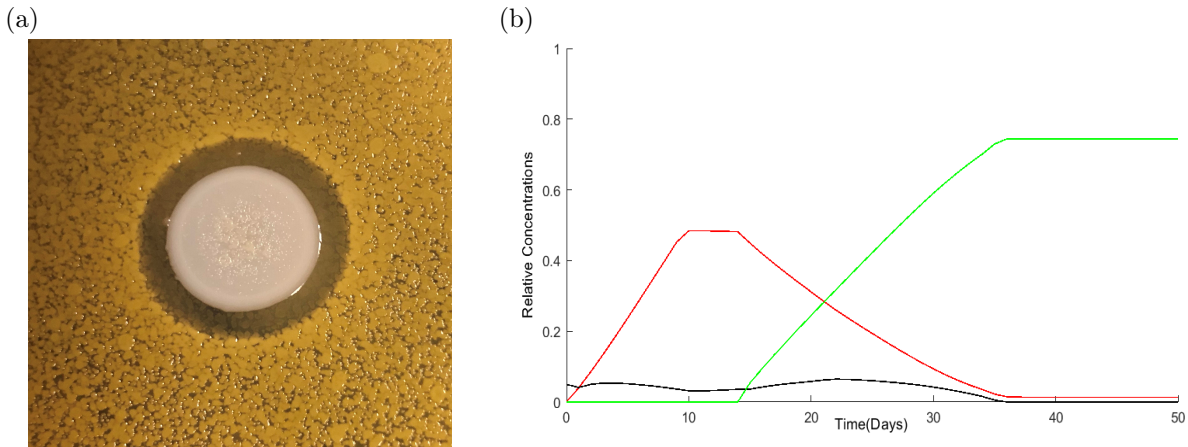
Figure 4.16: **Experimental and theoretical illustrations of the coexistence phenomenon between susceptible and adapted fractures of the population within the same evolved isolate of *S. aureus*.** Panel (a): the experimental demonstration of the qualitative result obtained from the deferred growth inhibition assay performed on the evolved populations shows partial inhibition, which can be a result of promoting the growth of the mutant or surviving bacteria in the inhibition zone once the inhibitor has diffused away [66, 143]. Panel (b): an extension of the dynamics introduced in (4.15c), which was generated by simulating the inhibitory interactions with the (3.24) model.

Several possibilities regarding the point at which the resistance would occur were assumed during this process. Initially, the possibilities of their appearance were expanded to include the period from the second day of interactions until the concentration of *Staphylococcus aureus* was retrieved. The range was then limited to precisely the period with the lowest error values when fitting the experimental data to the model simulations using the least square approach, which was from the fourth day until the seventh day when *S. aureus* invaded, while the period ranged from the twelfth day until the fifteenth day when the mutual invasion occurred.

Considering the outcomes shown in Fig (4.15), the best simulations that concur with the experimental outcomes were obtained when it was assumed that the adapted fraction of the evolved *S. aureus* populations was no longer affected by the toxins produced by the engaged *S. epidermidis* populations. However, according to the results obtained from the deferred inhibition assays demonstrated in the previous chapter in Fig (3.8b), which were performed to determine the sensitivity of the ancestral and evolved SH1000 populations against the toxins produced by the evolved *S. epidermidis* populations, the evolved *S. epidermidis* (TU3298) showed inhibitory activity on the evolved *S. aureus* (SH1000).

The only possibility to obtain a logical explanation that would justify the existence of these contradictions is by proving that, unlike that which occurs when competitions are conducted in a mixed environment, performing the competitions under structured conditions contributes to maintaining the susceptible fraction of the evolved *S. aureus* for a more extended period, which justifies the existence of the inhibition zone produced by the evolved *S. epidermidis* against the evolved *S. aureus*, despite the assumption that *S. aureus* clones develops complete resistance to the toxin-producing *S. epidermidis* strains.

This can be clearly seen when examining the laboratory results presented in Fig (4.16a), which illustrates the inhibition zone produced by the evolved *S. epidermidis* strain (TU3298) against the evolved SH1000. Several replicates of the same experiments were obtained, showing a different resistance level, which enables bacteria to grow at an inhibitory concentration that would otherwise prevent growth. These outcomes revealed a potential for resistance or regrowth. A radius that appears to have been cleared was observed. However, several colonies were growing within this radius. This was possibly colonies of resistant bacteria or bacteria that develop after the antimicrobial agent breaks down.

In a previous study, this type of coexistence was observed as populations living in spatially-structured habitats were composed of semi-isolated sub-populations. The study investigated the rate of invasion of advantageous mutations of *Escherichia coli* that were spread to varying degrees in a spatially-organised environment across 40 generations [76]. The outcomes highlighted the relationship between the spatial structure and the rate of beneficial mutation invasions. It was also indicated that the interactions that occurred while maintaining the spatial structure slowed the rate of invasion, causing a temporary coexistence of superior and inferior genotypes. This can be explained as follows: When an advantageous mutant invades from a single spot, competition with the ancestral occurs exclusively along the boundaries of the colony patch. As the colony doubles in size, the mutant's fitness will fall as the proportion of the mutant that actively competes with the surrounding ancestor decreases. Both simulations and experimental data indicate that as diffusion becomes more limited, the rate of invasion decreases. As a result, the mutant may not be able to take over quickly because of local competition and limited spread. This allows ancestral genotypes and mutants to coexist for a short time, although the mutant has a higher capacity to compete.

To verify that this coexistence is for a limited period only, the simulation presented in Fig (4.15c) was extended, which confirms the presence and survival of the susceptible fraction of the evolved *S. aureus* population (black line) until the last day of the competition, explaining the emergence of the inhibition zone when performing the post-invasion inhibition assays. It should be noted that, according to simulations demonstrated in Fig (4.16b), the mutant fraction of the evolved *S. aureus* population was able to overcome

159

the susceptible by the end of the thirty-seventh day, which confirms that this coexistence was not permanent in this case.

4.4 The Position of Resistance Emergence and its Influence on The Interaction Dynamics

When the interactions were conducted under structured conditions, several patterns were observed, where the clusters of the evolved *S. aureus* populations appeared in different positions. As demonstrated in Fig (4.17), these clusters were identified as being *S. aureus* based on their colour.

(a)   (b)
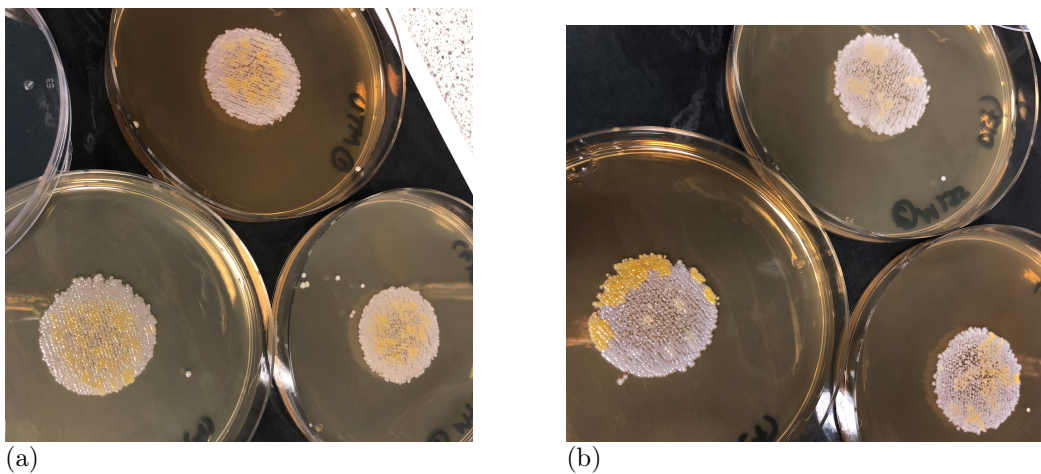
Figure 4.17: **Fifteen-day-old colonies of the interacted populations under structured conditions.** Panel (a): when the interactions were performed between isolates of *S. aureus* (SH1000) and toxin-producing *S. epidermidis* (TU3298). Panel (b): isolates of *S. aureus* (SH1000) and toxin-producing *S. epidermidis* (B155).

Many different features can characterise *S. aureus*. As shown in Fig (4.18a), after 24 hours of incubation at $37°C$, *S. aureus* colonies develop pigmented, smooth, complete, slightly elevated colonies measuring approximately $2 - 3\,mm$ in diameter.

However, the absence of the golden pigment inside the spot that contains the evolved populations does not necessarily mean the absence of *S. aureus*. During interactions, non-pigment colonies of *S. aureus* were found. These colonies were detected by using a special medium known as MSA, a Mannitol Salt Agar medium that is used to isolate and identify *Staphylococcus aureus* [22].

When the identity of the colonies is uncertain, a sample is taken from all these colonies and categorised by specific numbers as shown in Fig (4.18b). The reason for taking this step is to make it easier to track them later, and these samples will be cultured in MSA mediums and incubated overnight. Coagulase-positive *Staphylococci* (e.g., *Staphylococcus aureus*) generate yellow colonies and a yellow medium around them (see Fig (4.18c)).

In contrast, coagulase-negative *Staphylococci* (e.g., *Staphylococcus epidermidis*) form red colonies, and the red phenol indicator remains unchanged.

(a)   (b)   (c)
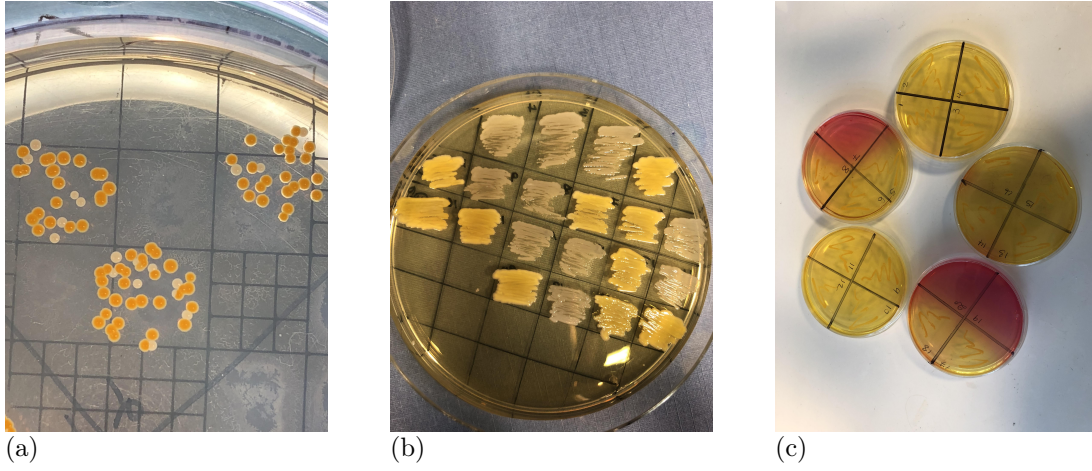
Figure 4.18: **Illustrations of pigmented and non-pigmented *Staphylococcus aureus.*** Panel (a): colonies of *Staphylococcus aureus* and *Staphylococcus epidermidis* on Brain Heart Infusion Agar (BHI). Panel (b): collecting and sorting samples from incubated colonies for simple tracking and identification processes. Panel (c): Mannitol Salt Agar (MSA) plates with cultures for mannitol fermentation, both positive (*S. aureus*) and negative (*S. epidermidis*).

When investigating the reasons behind the disappearance of the golden pigment during the interaction process, several were found, perhaps the most prominent of which is that producing this pigment by *S. aureus* is energy-consuming while the evolved *S. aureus* populations aim to conserve energy in any way possible in order to survive. Also, it could be an indication of virulence reduction in evolved *S. aureus* isolates [224]. *Staphyloxanthin* is a golden carotenoid pigment produced by *S. aureus* strains that functions as a significant virulence component. Restriction of *STX* production was used as an indicator of virulence reduction. It is unknown, however, whether non-pigmented *S. aureus* isolates are less virulent than pigmented isolates [50, 218, 224].

Thus, the disappearance of the golden pigment is not sufficient evidence to confirm the absence of *Staphylococcus aureus*. Despite this fact, it is not possible to determine when or where the mutations will appear.

Therefore, the model in this section was extended to the 2D n-species competition-diffusive model for the densities of evolved populations of the species $u_s(t, x, y)$, $u_a(t, x, y)$, and $v(t, x, y)$ and toxins $T(t, x, y)$ depending on time t and spatial variable (x, y) states as in the following:

$$
\begin{cases}
u_{s_t} = D_u \left(u_{s_{xx}} + u_{s_{yy}} \right) + r_{u_s} u_s \left(1 - u_s - b_1 v - (1 + \psi) u_a - p_1 T \right), \\
u_{a_t} = D_u \left(u_{a_{xx}} + u_{a_{yy}} \right) + r_{u_a} u_a \left(1 - u_a - b_2 v - (1 + \psi) u_s - p_2 T \right), \\
v_t = D_v \left(v_{xx} + v_{yy} \right) + r_v v \left(1 - v - b_3 u_s - b_4 u_a \right), \\
T_t = D_T \left(T_{xx} + T_{yy} \right) + f_1 v - f_2 T,
\end{cases}
\tag{4.2}
$$

where $(x, y) \in \Omega \subseteq \mathbb{R}^2$ for some set Ω. Here an extension of the work in Chapters 2 and 3 is presented since certain effects are only manifested and realised in two dimensions.

Boundary conditions:

Again, zero-flux boundary conditions are imposed.

Initial conditions:

The first step is to define the square grid coordinates, where the number of grid points in the x direction equals to the number of grid points in the y direction $= n$. X is a matrix in which each row duplicates the previous row, and Y is a matrix in which each column duplicates the previous column.

$$\text{Center } X = \text{Center } Y = \frac{n}{2}.$$

According to (4.1):

$$r = 0.025 \times L,$$

where L is the size of the medium,

$$\Theta = (\bar{X} - \frac{n}{2})^2 + (\bar{Y} - \frac{n}{2})^2 \leq r^2.$$

Thus:

$$u_s(x, y, 0) = \begin{cases} 1 & \text{if } [x, y] \in \Theta, \\ 0 & \text{otherwise,} \end{cases}$$

$$v(x, y, 0) = 0.01 \times u_s(x, y, 0).$$

This can be presented the other way around when performing the mutual invasions.

$$T(x, y, 0) = u_a(x, y, 0) = 0$$

Numerical Schemes:

As indicated Chapter 1, explicit numerical techniques were adopted to integrate the equations in (4.2). The diffusion terms in (4.2) were discretised using (1.38) approach, which as shown in Fig (4.19), the simulations produced using this approach were much more isotropic than those generated using the standard scheme [16, 205].

Different assumptions were made regarding the positions of the initial appearance of mutations, i.e., by introducing the mutations at the centre of the spot, fifteen space steps away from the centre of the spot, and at the spot's edge, as shown in the figures (4.19a), (4.20a), and (4.21a) respectively.

The purpose of these assumptions was to determine whether the location of the mutations impacts the dynamics and evolution of the competing populations, and, if there is an effect, the possibility of it being defined and linked to the experimental outcomes.
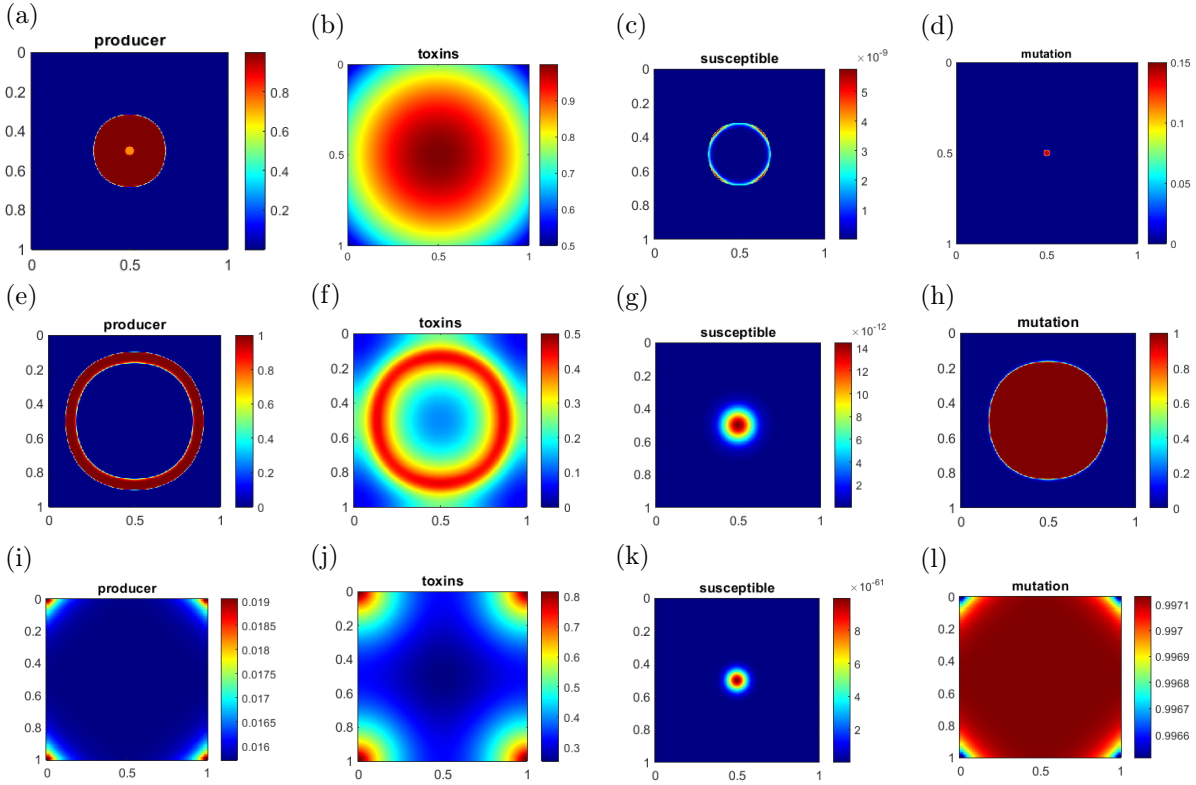
Figure 4.19: **Surface plots generated from** (4.2) **demonstrate the evolution of the interacting populations with central mutations.** Panel (a): the spot represents the toxin-producing *S. epidermidis* population (TU3298) one day after introducing the mutations presented in panel (d) at the centre of the spot. Panels (b) and (c): represent the evolution of the toxins produced by the evolved *S. epidermidis* population and the susceptible fraction of the evolved *S. aureus* population, respectively. Panels (a) → (d): depict the model (4.2) 2D simulations at day 15. Panels (e) → (h): at day 28, which corresponds to the actual duration of the experiments represented in (4.1g). Panels (i) → (l): at day 50. In all panels, the x and y axes represent the space coordinates.

The figures (4.19), (4.20), and (4.21) display 2D simulations of the four-variable model (4.2); figures in the first row, (4.19a→ 4.19d), show surface simulations of the components of the Petri dish on the fifteenth day, i.e., one day after introducing the mutations, and since these mutations were no longer affected by the toxins produced by *S. epidermidis* Fig (4.19b), it became clear from the second day. The figures presented in the second row, (4.19e→ 4.19h), simulate the ingredients of the dish on the last day of the experiment, which is the twenty-eighth as reported in Fig (4.1g). At the same time, the figures displayed on the third row, (4.19i→ 4.19l), are only an extension of these simulations until the fiftieth day to see if coexistence will continue when the spot covers the entire area of the Petri dish.

Evidently the initial place or position of the mutations has an impact on the dynamics of interactions.

According to Fig (4.22), when the mutation appeared in the middle of the spot (solid lines), it was more effective and showed more ability to recover. In contrast, the appearance of the mutation away from the centre of the spot (dashed and dotted lines) led to

163

a delay in the recovery process. Thus, the associations between the positions of initial mutations and the dynamics of interactions can be defined as a positive correlation between the appearance of mutations in a place far from the centre of the spot and the time required for *S. aureus* populations to recover. The farther the mutations are from the centre of the spot, the longer it takes them to be able to dominate and control because the diffusion coefficient is weak.
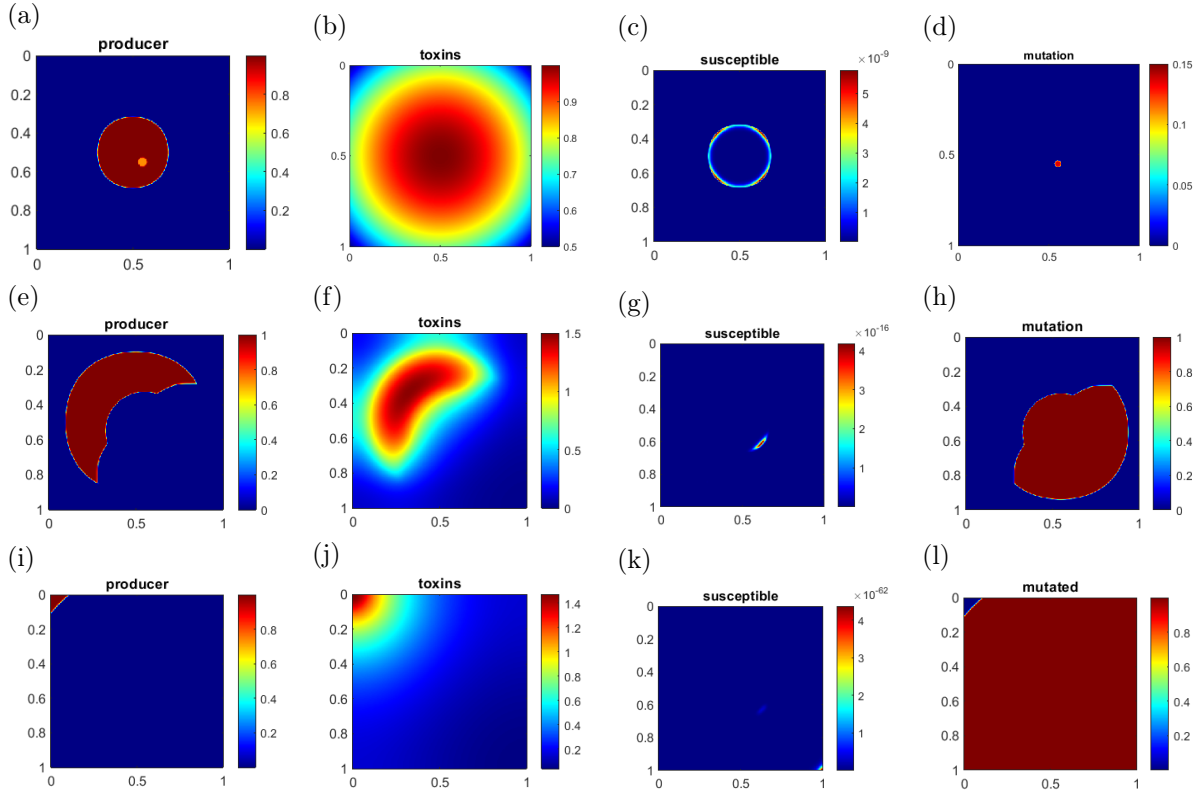
Figure 4.20: **Surface plots generated from** (4.2) **demonstrate the evolution of the interacting populations when mutations are introduced fifteen space steps away from the centre of the spot.** Panel (a): the spot represents the toxin-producing *S. epidermidis* population (TU3298) one day after introducing the mutations presented in panel (d) at the centre of the spot. Panels (b) and (c): represent the evolution of the toxins produced by the evolved *S. epidermidis* population and the susceptible fraction of the evolved *S. aureus* population, respectively. Panels (a) → (d): depict the model (4.2) 2D simulations at day 15. Panels (e) → (h): at day 28, which corresponds to the actual duration of the experiments represented in (4.1g). Panels (i) → (l): at day 50. In all panels, the x and y axes represent the space coordinates.

Since all the evolved populations have a relatively low motility rate, it took the adapted *S. aureus* some time to cover the whole bacterial lawn if they were introduced in the middle of the spot, and an even a longer time when introduced further away from the centre. On the other hand, for the evolved *S. apidermidis* populations, the further they were from the mutations, the better their chances of survival. However, regardless of the mutation positions, all evolved populations will converge eventually towards the same equilibrium.

Another justification is that if the mutations are introduced further away from the spot centre, their opponents have a better chance to proliferate and reproduce. Thus,

the mutations will compete for resources and nutrients with a higher concentration of *S. epidermidis*, which slows down their growth and vice versa.
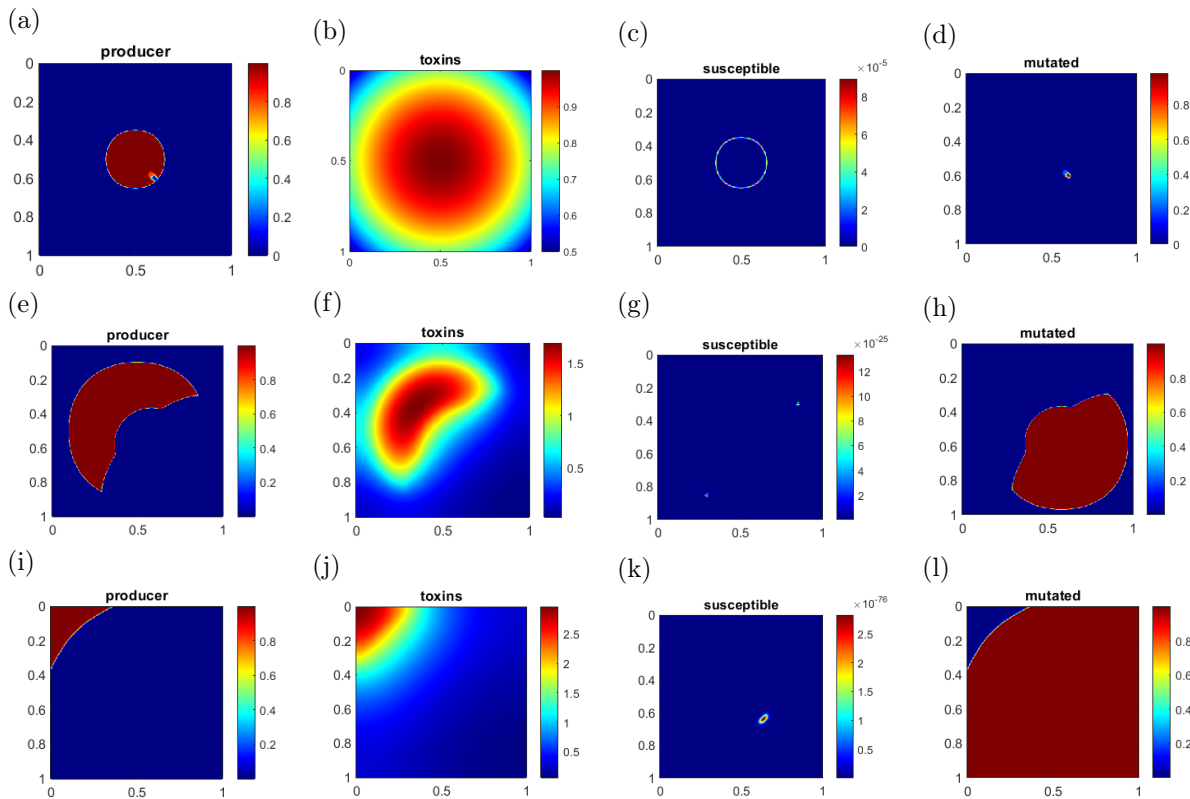
Figure 4.21: **Surface plots generated from** (4.2) **demonstrate the evolution of the interacting populations when mutations are introduced at the edge of the spot.** Panel (a): represents the toxin-producing *S. epidermidis* population (TU3298) one day after introducing the mutations presented in panel (d) at the edge of the spot. Panels (b) and (c): represent the evolution of the toxins produced by the evolved *S. epidermidis* population and the susceptible fraction of the evolved *S. aureus* population, respectively. Panels (a) → (d): depict the model (4.2) 2D simulations at day 15. Panels (e) → (h): at day 28, which corresponds to the actual duration of the experiments represented in (4.1g). Panels (i) → (l): at day 50. In all panels, the x and y axes represent the space coordinates.

This can be justified and explained biologically: When mutations appear in the middle of the spot, they are adjacent to a larger number of cells and this facilitates the transfer of immunity, while the appearance of mutations in another place, for example, on the edges of the spot, means they are in contact with a relatively smaller number of cells, which may negatively affect the process of transmission. Consequently, mutation appearance away from the middle of the spot slows down the dynamics of the spread of immunity.

The surface plots are demonstrations to show the distribution of the population on specific days based on where the mutation appeared. In contrast, figures (4.22c), (4.22d), (4.22g), and (4.22h) indicate the corresponding relative concentrations of the population overall days. The solid lines in figures (4.22c), (4.22d), (4.22g), and (4.22h) show the concentrations of the evolved populations when mutations appear in the middle of the bacterial lawn.
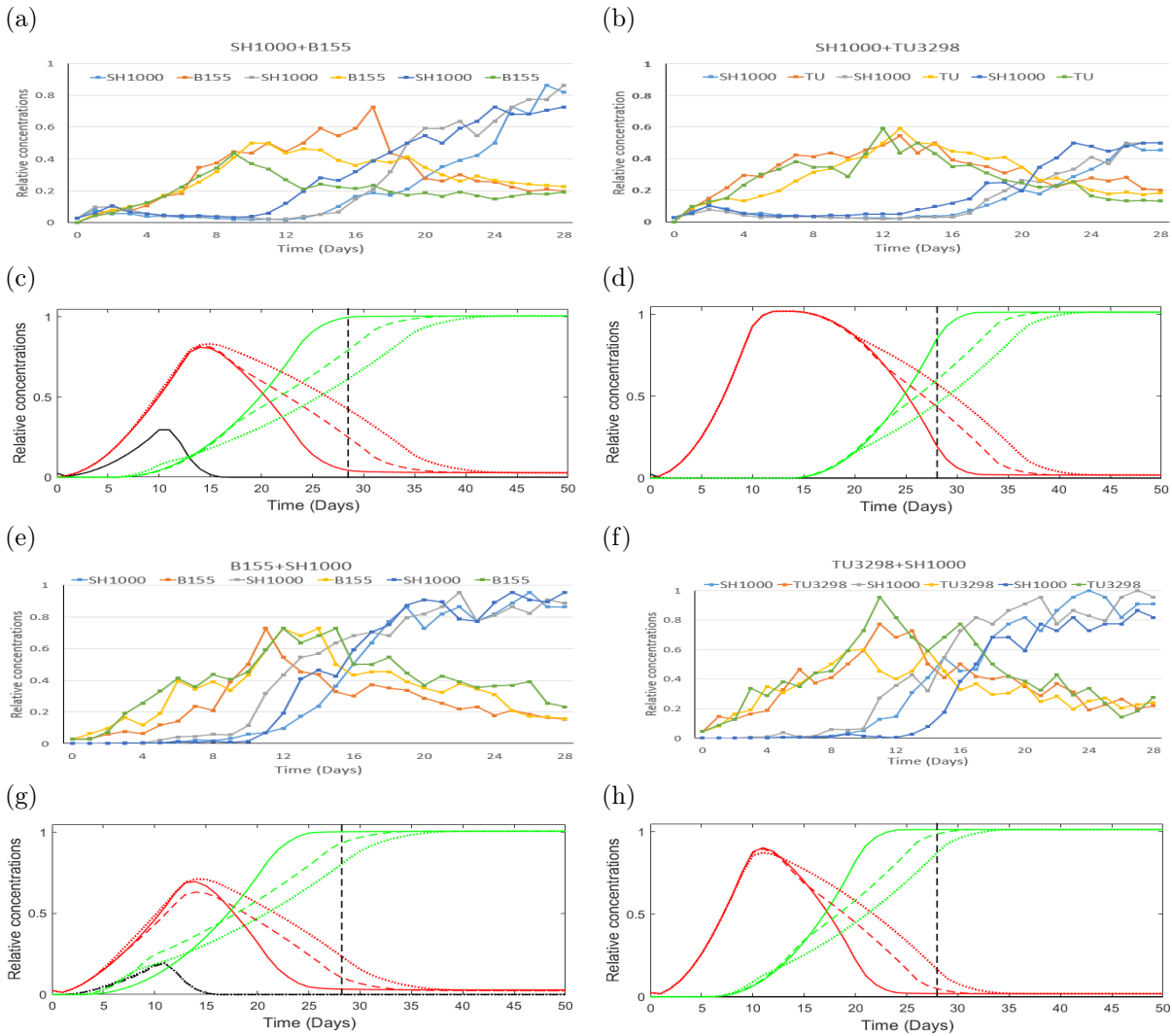
Figure 4.22: **Illustrations of the dynamics of interactions observed in the experiments and model simulations when manipulating the positions of the initial mutations.** The first and third rows are representations of the actual data (three replicates). Panel (a): toxin-producing isolates of *S. epidermidis* (B155) invade populations of *S. aureus* (SH1000). Panel (b): toxin-producing isolates of (TU3298) invading populations of (SH1000). Panels (e) and (f): represent the opposite directions of invasion, respectively. Panels (c), (d), (g), and (h): the model (4.2) simulations of data presented in (a), (b), (e), and (f), respectively, when mutations are introduced at the centre of the cultured spot (solid lines); fifteen space steps away from the centre of the spot (dashed lines); at the edge of the spot (dotted lines). The vertical dashed lines specify the end time of the experiments. In model simulations, red is *S. epidermidis*, v, black is the susceptible fraction of the *S. aureus* population, u_s, and green is the adapted fraction, u_a. The x-axis is the time in days. The y-axis represents the relative concentrations of the evolved populations.

In contrast, the dashed and dotted lines indicate the relative concentrations of the population when the mutations appear in places farther from the lawn centre. It can be noted from this figure that the concentrations of the evolved species converge in one way or another to the same equilibrium. However, it is the location of the initial emergence of mutations which controls the speed of these evolved strains to reach this equilibrium. When mutations initially form in the middle of the incubated bacterial lawn, the lines representing the concentrations intersect earlier than when mutations initially appeared

somewhere else around the spot.

To summarise, it can be stated that, based on mathematical simulation, it was concluded that the initial location of mutations impacts the dynamics of the evolved populations. The more mutations arise closer to the centre of the spot, the faster the dynamics of the interactions, and vice versa.

As shown in Fig (4.22a) and Fig (4.22b), the actual data illustrates different behaviours of interaction dynamics when toxin-producing populations of *S. epidermidis* invade populations of *S. aureus* at an initial concentration of (0.01: 1). These differences are usually associated with the impact of the toxins produced, the diffusion properties, the strength of competition, and the growth rates of the involved populations [148].

Despite all these differences, the evolved populations intersected in a period ranging between day 13, when *S. aureus* populations competed against *S. epidermidis* (B155) as shown in Fig (4.22a) (the third replica), and day 23, when *S. aureus* competed against *S. epidermidis* (TU3298), as shown in Fig (4.22b), (first replica).

From the mathematical findings of this thesis, it can be concluded that there is no possibility for the mutations to initially form at the edges of the spot. According to Fig (4.22), if the mutation arises at the edges of the spot, then the intersection point between the evolved populations will occur shortly before or after day 28, which contradicts the laboratory results. When conducting all inhibitory interactions, the evolved populations converged to an equilibrium state before reaching day 28. In fact, by this time, the change in the evolved population concentrations was no longer significant; hence, the decision was made to halt the experiments.

4.5 Conclusions

This chapter provides a detailed and combined biological and mathematical study of interactions in natural bacterial communities and their implications and outcomes. All the previous experiments, in which populations of *S. aureus* competed against different species of *S. epidermidis* under different settings in terms of the initial concentrations of the interacted populations and in terms of the level of toxicity of *S. aureus* opponents, were performed again in structured environments to produce the research in this chapter. As previously stated, several microbial evolution studies suggest that manipulating environmental factors surrounding these interactions may inhibit the pathogenic species. Thus, these factors were considered when re-performing these experiments in addition to the preservation factor. During these competitions, the environmental structure of the evolved populations was maintained.

The primary purpose of preserving the structure when re-performing all the experiments is as follows: to investigate how far this step contributes to limiting the spread

of the pathogenic strain (SH1000) and eliminating its colonisation; to determine the extent to which the preservation of the environmental structure contributes to altering and changing the dynamics of the interactions; to record the results of these interferences and compare them with the outcomes of interactions conducted under mixed conditions.

All the involved bacterial strains in the experiments presented in this chapter were the same species used previously when performing the interactions under mixed conditions [See Chapter 3]. When investigating these species, several characteristic features that determine the behaviour of these species before and after interactions were highlighted, i.e., growth rates, doubling times, diffusion coefficients, and their ability to inhibit the ancestral and evolved populations of *S. aureus* (SH1000). The purpose of the study was to establish a better understanding of the nature of these species and evaluate the degree to which these species may alter because of competition.

The focus of this study was the competition between the selected *S. epidermidis* species and the pathogenic *S. aureus* strain under structured conditions, in which the populations were diluted daily and transferred into a new medium while maintaining the environmental structure of the cultured spot using the velvet replica method [see Fig (3.11)]. Also performed was that referred to earlier as invasions, when the initial concentrations of the evolved populations differ, in addition to the interactions established by equal concentrations.

All interaction experiments were performed in Dr Horsburgh's laboratory in the Institute of Integrative Biology at the University of Liverpool. These interactions lasted until the change in the evolved population density was no longer significant.

From a biological perspective, the findings emphasise the critical role of spatial structure in altering and changing the course of interactions, especially if these interactions involve a high degree of toxicity. Maintaining spatial structure enables inhibitor-producing *S. epidermidis* to better prevent and promote invasions from and into the evolved *S. aureus* populations, since structured environments typically favour the manufacture of inhibitory toxins. As toxin producer clustering allows toxins to reach more significant local concentrations, spatially-structured habitats were postulated to facilitate the invasion by toxin producers.

As a result, small populations may profit from the high cost of toxin generation. In contrast, rapid diffusion and destruction of the bacteriocin lawn require bacteriocin producers to achieve a higher threshold frequency in order to acquire the advantages of bacteriocin synthesis in spatially unstructured environments. Nevertheless, the evolved populations of *S. aureus* (SH1000) overcame these complex and difficult conditions.

Mathematically, the models based on logistic equations presented in the previous chapter were used, considering the environmental conditions when simulating these interactions. As seen in Fig (4.3a), the mathematical translation of this biological concept

involves reducing the concentrations at the end of each day without compromising the dimensions of the formed spots.

From a mathematical perspective, the findings presented in this thesis indicated two different results when the interactions were conducted under structured conditions. The first type was associated with the low-toxin interactions between *S. aureus* (SH1000) and *S. epidermidis* (B180) populations. The second type of outcome was observed in interactions involving a high toxicity level, conducted between *S. aureus* and the other two species of *S. epidermidis*.

As explained earlier, the *S. epidermidis* strain (B180) is considered a toxin-producing strain. Yet, the interactions were controlled by other factors that contributed to the survival of this strain during competitions, such as the strength of competition and having a relatively high proliferation rate compared to other species. The toxins produced did not significantly affect the dynamics of interactions. Hence, when simulating these interactions, the three-variable model was used, which assumes that the non-inhibitory population contains an adaptive part representing one percent of the total population. In this model, the first variable represents the proportion of the susceptible population of *S. aureus*, while the second variable represents adaptive fraction and the third variable represents *S. epidermidis* B180 without considering the toxicity variable.

When applying the structured conditions to a three-variable model to simulate the interactions between SH1000 and B180, simulations were obtained that were relatively in agreement with that experimentally obtained without the need to change any of the mixed environment parameters. The competition dynamics under structured conditions were slower than those under mixed environments. In the absence of the significant roles of the toxins, the initial assumption that the sample contained an adapted fragment was enough to produce a simulation consistent with the laboratory results. Thus, if the toxins do not significantly drive the interactions, both environments lead to a similar evolution regardless of the timing factor.

On the other hand, producing mathematical simulations in line with the laboratory results was challenging when toxins played an active role in these interactions. When simulating the inhibitory interactions, the four-variable model was used. The fourth variable was added to represent the toxins as their role was no longer marginalised. In this model, as seen in (3.24), a direct proportionality was imposed between the toxins and the producer and an indirect one between the toxins and both fractions of *S. aureus* population.

As noted earlier, preserving the structure during the interactions enhanced and improved the effectiveness of the toxins. Therefore, as seen in Fig (4.5), the initial hypothesis of the existence of an adaptive part of the population failed to produce a simulation that simulates laboratory interactions.

Mathematically, the inability of the initial adaptive part to recover in the presence of toxins can be justified since it became negatively attached to all variables. The adaptive fraction of *S. aureus* (u_a) competed with susceptible populations of *S. aureus* (u_s) and the producer (v), and was also influenced by toxins (T) produced during these interactions.

Several attempts were made to obtain model simulations that coincided with the reported experimental data. In the first place, it was assumed that by manipulating the parameters that govern the toxicity in this model, it would be possible to simulate the experimental data. It was then decided to change inhibitory parameters because the interaction parameters did not alter the outcomes as seen in the three-variable model. Thus, by considering the defined relationship between these parameters (3.19), it was possible to determine different sets of toxic parameters. The outcome of this process reduced the effects of the toxins on both fractions of the *S. aureus* populations, which led to eliminating the non-monotonicity behaviour observed in the evolved *S. aureus* populations. In order to enhance the production of this process, another attempt was made. In this attempt, the aim was to increase the intensity of the interactions between the susceptible fraction of the evolved *S. aureus* and the producer *S. epidermidis*. The simulation results from adding up this stage were promising. However, other attempts were needed to produce better simulations.

When performing the deferred inhibition assays on the evolved populations to test the sensitivity of the evolved populations of *S. aureus* towards the toxins produced by the evolved *S. epidermidis*, and to determine whether *S. aureus* clones developed resistance to the toxin-producing *S. epidermidis* strains, the inhibition zones produced by (B155) and (TU3298), presented with different areas, despite the standardisation of the optical density of the competitors.

Such a difference can be justified in different ways:
Suppose this difference is associated with the producing populations. In this case, it is possible that the same species may possess more than one inhibitor or that this same inhibitor is multifaceted in terms of its impact on vulnerable populations [122]. However, if this variation is due to evolved populations of *S. aureus*, it is possibly because of the degree of resistance varying from one competition to the next, i.e., it presented entirely in some replicates and was still being established in other replicates. Alternatively, this difference may be due to different proportions of the susceptible fractions within the evolved populations of *S. aureus*, as seen in Fig (4.16). According to the model simulations, there is a temporary coexistence relationship between the susceptible and resistant fractions of the evolved *S. aureus* populations.

Regardless of the reason for these differences, it should be noted that by calculating the average inhibition zones from all replicates, it was possible to define a relationship between the level of decomposition of toxins f_2 and p_2, which controls the effect of toxins

on the resistant part of the evolved *S. aureus* populations.

Given the possibility that these inhibition zones were caused by the temporary survival of the susceptible fraction within the evolved sample of *S. aureus* and not by inhibiting the adaptive fraction of *S. aureus*, u_a, the third attempt at the process, shown in Fig (4.9), was established to achieve simulations consistent with the laboratory results. The goal of this attempt was to keep all parameters the same as the simulations under mixed conditions while only changing the parameter (p_2).

The simulations obtained from this attempt yielded better results concerning the non-monotonous pattern, as seen in Fig (4.9f). However, the emergence of this behaviour through this attempt was at the expense of the accuracy and quality of the model simulation, as illustrated in Fig (4.9).

All the attempts to produce simulations consistent with laboratory findings when invasions were conducted under structured conditions did not yield results entirely consistent with both directions of invasions. For example, the first attempt, reducing the effect of toxins, resulted in satisfactory results to some extent when simulating the invasions of toxin-producing (TU3298) into a resident population of *S. aureus*, as seen in Fig (4.13f). In contrast, the simulations from this attempt, illustrated in Fig (6.6f), did not concur with the dynamics observed in the mutual invasion. Fig (6.6i) shows how close the second attempt simulation came to the experimental data describing this direction of invasion. As a result of this attempt, the mutual simulation, Fig (4.13i), was less accurate.

All these attempts assume the presence of an adaptive fraction in the initial isolates of *S. aureus*. As explained earlier, numerous theoretical models suggest that as the frequency of immigrants from the source population increases, the chance of adaptation to an aggressive environment also increases. Consequently, when *S. aureus* populations invade at a greater initial frequency, they are more likely to have mutants resistant to *S. epidermidis* toxins [88, 70, 163, 89]. However, as previously stated, the development of these mutations is expected to be suppressed in ecosystems with a high degree of spatial structure because competitions for the advantageous mutant may arise only at the colony's edge, and as the colony grows and expands, a smaller fraction of the mutant population will be engaged in competitions with the ancestral genotype [76]. Thus, the initial assumption of this thesis was insufficiently adequate to produce simulations in agreement with the experimental findings. Furthermore, to create more realistic simulations, different assumptions should be made. Therefore, in this attempt, it was decided to introduce the mutations at a later stage of the process of interactions rather than assume their initial existence.

All mixed environment parameters were imposed when producing the simulations under structured conditions except the value of p_2. It was assumed that the fraction of the population introduced later was fully mutated against the inhibitory produced by the

evolved *S. epidermidis* populations.

Different assumptions were made to estimate the optimal day for mutation emergence since determining when and where resistance forms are challenging. Fig (4.11) and Fig (4.14) show how the range of days with the minor error was narrowed down by fitting the natural log of the invader to resident ratio simulations to actual experimental data using the least square method.

As seen in Fig (4.12) and Fig (4.15), the outcomes of the final attempt to produce simulations from the four-variable model are commensurate with the experimental findings when performing the invasions under spatially-structured conditions and were more accurate, realistic, consistent, and compatible with the studies presented.

In the final section of this chapter, the way in which the initial location of resistance in the evolved spot impacts the interference dynamics by extending the model to the 2D n-species competition-diffusive model was examined. The simulations in figures (4.19), (4.20), and (4.21) were carried out by explicitly solving the reaction-diffusion differential equations (4.2) using an FTCS integration technique, after specifying the appropriate parameters to guarantee and meet the explicit integration scheme's stability requirement described in (1.28).

From this analysis, it was concluded that the farther the mutations are formed from the centre of the spot, the longer it takes to be able to recover and eventually dominate because the diffusion coefficient is weak. Biologically, this phenomenon is justified, as the appearance of the mutation on the edges of the spot signifies that it will be adjacent and in contact with a relatively smaller number of cells, which contributes to slowing down the process of spreading these mutations and vice versa. The findings in this regard can be seen in Fig (4.22), which illustrates the association between the initial position of mutations and the interference dynamics.

Chapter 5

Discussion

For many years, the medical profession and pharmaceutical companies have witnessed and warned of the consequences of the continuous and rapid growth of bacterial resistance to antibiotics. The role of antibiotics in saving lives is now at risk of being undermined by this bacterial phenomenon [7, 127].

One of the most well-known bacterial species that has developed resistance is *Staphylococcus aureus*. *S. aureus* is a significant opportunistic pathogen that colonises nearly 50% of individuals [4]. Furthermore, it shares the human anterior nares with other populations and must survive to carry the infection successfully.

The process of producing new antibiotics is an energy-consuming and financially burdensome process [29, 97, 101, 169]. When considering the antibiotic discoveries and the resistance timeline presented in Fig (1.1), it can be stated that the need for different approaches and alternatives to antibiotics has become urgent [128].

Several studies, research, and approaches have been conducted to limit the spread of the pathogenic bacteria (Table 1.1). According to some of these studies, the opportunistic pathogen *Staphylococcus aureus* is suppressed by other microbial populations, which also inhabit the human nasal airway [122, 96]. It can be hypothesised that this suppression is due to competition and inhibition between bacterial species.

Shared resources such as food and shelter may cause *S. aureus* populations to be engaged in constant competition and interference with their neighbours. This competition influences the distribution of *S. aureus* either by inhibiting and preventing colonization. In the most extreme cases, the result may be complete elimination [124, 198].

5.1 An Overview of The Research Presented in This Thesis

In this thesis, the focus was the study presented in [122], which suggests that interference competition between bacteria shapes the distribution of the opportunistic pathogen *Staphylococcus aureus* in the lower nasal airway of humans, which in addition to the

host variables influence colonisation. Thus, this study tested the role of toxin-mediated interference competition in structured and unstructured environments by performing mutual invasions between *S. aureus* on the one hand and toxin-producing or non-producing *Staphylococcus epidermidis* nasal isolates on the other.

According to the findings of this study, toxin-producing *S. epidermidis* invaded *S. aureus* populations more successfully than non-producers, and invasions were promoted by spatial structure. In addition, the evolution of toxin resistance by the evolved populations of *S. aureus* prevented the complete displacement in some cases. Furthermore, when performing mutual invasions, toxin-producing *S. epidermidis* strains resist invasion, especially in structured environments. The findings of this study also emphasise that the evolved *S. aureus* populations were only able to invade toxin-producing *S. epidermidis* when starting from a high initial frequency and in a low spatial structure environment, and this ability resulted from the evolution of toxin resistance. It was also indicated that these interactions led to an improvement in the performance of toxins produced by the evolved B180, as it showed greater inhibitory activity on ancestral SH1000 than the ancestral B180 genotype.

Finally, the findings suggest limiting the transmission and infection rates that are associated with the colonisations of *S. aureus* could be achieved by manipulating the nasal microbial community.

Throughout the second chapter, a comprehensive overview of the experiments reported in [122] was presented. Based on this reported data, we introduced two different mathematical models. At first, the classic two-species *Lotka-Volterra* competition was used in a one-dimensional spatial dimension model. Although this model was able to simulate the final states of the competing populations, the two-variable model was unable to simulate the non-monotonic behaviour of the evolved populations. Thus, it was decided to model this phenomenon by extending the classic two-species *Lotka-Volterra* to incorporate the adaptation by one species.

The three-variable model was able to simulate the dynamics presented in the experimental data. However, although the attempt was made to further expand the model to include toxin production by one species to model the inhibitory interactions, the model was unable to generate simulations that satisfied both invasion directions. Furthermore, many aspects were not clear, and further investigation was required. Thus, it was decided to model the inhibitory interactions after re-performing these experiments and gaining an understanding of different biological aspects.

Chapter 3 featured a combined study that examined the mathematical and biological elements of the nature of interactions in bacterial communities and their implications. In laboratory experiments, populations of the pathogenic strain *S. aureus*, SH1000, competed against several species of *S. epidermidis*.

Numerous variables affecting the dynamics of these interferences were taken into account while conducting these studies. The studies were conducted primarily to test the hypothesis stated in the previous chapter, which suggests that adjusting some of the environmental parameters affecting the interactions between bacterial communities will restrict the colonisation of pathogenic bacteria [122].

All the experiments presented in Chapters 3 and 4 were conducted under the supervision of Dr Malcolm Horsburgh in the Institute of Integrative Biology- University of Liverpool. A brief illustration and overview of experiments conducted are seen in Table (3.2).

Biologically, the findings from the experiments performed for this thesis concur with the findings obtained in [122], in terms of:

- Under mixed conditions, *S. epidermidis* populations were never able to invade or prevent invasions by *S. aureus* SH1000 successfully.

- Invasions were impeded or promoted by the evolution of resistance by *S. aureus*.

- *S. epidermidis* was more likely to persist at low frequencies and avoid extinction in mixed environments.

- High-toxin-producing *S. epidermidis* strains were more resistant to invasion than low-producing strains, as a positive correlation between the level of toxicity of the competing strain of *S. epidermidis*, and the time required for *S. aureus* to adapt and mutate against these toxins was found.

- Structured environments favour the production of inhibitory toxins.

- Evolved *S. epidermidis* strains, as shown in (Fig 3.8b), produced larger inhibition zones against susceptible *S. aureus* than the ancestral *S. epidermidis* strains.

Thus, the *S. epidermidis* populations that co-evolved with *S. aureus* could be enhanced and utilised in the future as nasal probiotics to lower the risk of severe *S. aureus* infection.

As mentioned previously, the author of this thesis maintains that the interactions reported in [122] did not last for the adequate amount of time required to determine the behaviour of the evolved populations, especially since the dynamics did not converge to a specific point, so when performing the interactions for a more extended period, this resulted in altering and changing the states of the interacted populations. Consequently, several of the findings of this thesis contradict the conclusions of [122]. Therefore, unlike that found in [122], the findings of the author of this thesis indicate the following:

- Regardless of the initial concentrations, the level of toxicity and the environmental structure, *S. aureus* populations were always able to limit the presence of their opponents.

- In all invasions, no eliminations were observed.

- In all invasions, the evolved populations of *S. aureus* exhibit similar behaviour: they decrease at the beginning of the interactions, after which they increase. Such behaviour was never observed in the evolved populations of *S. epidermidis*.

- Negative associations were observed between the initial frequencies of *S. aureus* and their ability to invade and recover. Invader populations of *S. aureus* were able to recover and gain control faster than the resident populations, which conflicts with the findings obtained in [122], as they found that invasion of *S. aureus* into a toxin-producing *S. epidermidis* was positively frequency-dependent, with the highest initial frequencies invading the fastest and lower initial frequencies going to extinction.

Furthermore, according to [70, 88], higher immigration rates increase the likelihood that immigrants carry beneficial mutations pre-adapted to the toxins produced, which means invading *S. aureus* populations from higher starting frequencies are more likely to contain toxin-resistant mutants. Consequently, *S. aureus* should be better at preventing and promoting invasions when starting from higher initial concentrations than when starting from lower initial concentrations. Nevertheless, as shown in Fig (3.13) and Fig (4.1), the findings indicate that the evolved *S. aureus* populations struggled the most to outcompete *S. epidermidis* populations when starting from a higher initial frequency (residents) in both environments. Taken together, it is hypothesised that the evolved *S. epidermidis* may have upregulated the production of the inhibitory toxin or initiated the production of alternative toxins. However, in the absence of knowledge of the mechanism of inhibition, this remains unclear.

In general, manipulating the nasal microbial community temporarily limited the transmission and infection rates associated with the colonisation of *S. aureus*. This inhibition was more effectively achieved under structured environmental conditions and high toxicity levels. However, unlike that reported in [122], this research showed that the nasal microbiota has only a moderate influence on the colonisation state of *S. aureus*, which means that the evolved *S. aureus* was only inhibited for a limited period that was positively associated with the level of toxicity of their competitor and was never permanently removed or displaced.

In addition to the above, the research presented in this thesis revealed that when conducting competitions with a low level of toxicity strain, (B180), toxins did not play a significant role in the outcomes of these interactions, as the behaviour of this strain during the interactions was similar to the behaviour observed with the non-toxin producing *S. epidermidis* (B115) [122].

Also, when the interactions started from different concentrations, precise and intense fluctuations in the dynamics were noticed compared to interactions initiated from equal concentrations. Competition for resources and adaptability to the medium may impact the outlined dynamics and contribute to triggering such behaviour, yet these factors would need additional investigation to be fully understood [203, 195].

Mathematical modelling is crucial for analysing and investigating the underlying phenomena and associating the diverse scales at which these systems act. In fact, in the study for this thesis, it was only possible to understand the nature of interaction dynamics reported in the data by giving several hypotheses, and by testing these hypotheses mathematically. Some were excluded and ideas explored that provide the best logical explanation for the course of events. Thus, continuous models represented by differential equations are a suitable approach that can effectively offer and deliver descriptions and illustrations of the outcomes from microscopic behaviours [11, 134, 147].

Therefore, different models were designed to analyse and simulate each experiment performed. The first mathematical model was to simulate the experimental growth curves of the involved species. This model was based on the logistic equation where a single population consumes a single limited resource. The outcomes of this model enabled the estimation of the consumption rate and carrying capacity of each population after accurately defining the doubling and relaxation times, and the growth rate for each population by using the logarithmic scale of the log phase in the obtained growth curves.

Furthermore, the outcomes of toxin-mediated inhibition experiments were modelled. Solving the equation (3.18) in the system (3.5) enabled the definition of a relationship (3.19) that associate and link the parameters that govern the inhibitory during the interactions. Such an approach was useful as there was no other way in which to estimate or determine the exact values for these parameters.

When modelling the interactions, they were divided into two types. The first was competition for resources, performed between (B180) and (SH1000); the other type was concerned with modelling the effect of toxicity on competing communities and was conducted between populations of (B155), (TU3298), on the one hand, and (SH1000), on the other hand.

In the first type of these interactions, competition for resources, a three-variable model (3.23) was able to replicate the non-monotonic behaviour, seen in the interaction dynamics, by assuming that the pathogenic bacteria, (SH1000), comprises two fractures of the population.

The susceptible fracture represents the vast majority, and its inability to resist causes the drop observed at the start of all interactions, whereas the resistant fracture represents only one per cent of the total population density and can restructure the pathogen species and eventually dominate. Furthermore, a four-variable model (3.24) was intro-

duced, where the effect of toxins was considered during the inhibitory interactions. The complexity of this model, caused by a large number of parameters, was overcome by the existence of the relationship between inhibitory parameters (3.19). Thus, when fixing the inhibitory production rate to equal one, it is only necessary to define the proper value for the decaying rate through the fitting technique, consequently determining the corresponding inhibitory coefficients from this term.

The models predict the disappearance and demise of the (B180) species. At the same time, the competing communities that possess the toxic factors, (B155) and (TU32980), are able to survive at low rates if the resources are kept replenished.

In addition, the numerical experiments in Section (3.6) enabled the validation of the model predictions and conclude a positive correlation between the reactions' toxicity level and the required resistance ratio to allow the evolved *S. aureus* to dominate the interactions. Furthermore, from these numerical experiments, an inverse relationship was noticed between the time required for the adaptive fracture of *S. aureus* to overcome the susceptible ratio and the growth rate of their opponent strain of *S. epidermidis*, i.e., the faster the evolved *S. epidermidis* strain grows, the more they provoke their opponent to transform. This was also confirmed under structured conditions, as shown in Fig (4.22). When the interactions between SH1000 and B155 were performed in panels (4.22c) and (4.22g), it can be seen that the susceptible fraction of *S. aureus* (black line) has the advantage of a relatively low growth rate and toxicity level compared to the other *S. epidermidis* strain (TU3298), which, as shown in panels (4.22d) and (4.22h), immediately inhibited the susceptible population in *S. aureus*. However, when performing the interactions under structured conditions, the accumulations of the toxins restrict the evolution of the resistance for more extended periods of time.

In Chapter 4, all previous experiments provided in Chapter 3 were repeated under structured conditions to assess the stability of the reported results and to determine the extent to which this step led to restricting the spread of the pathogenic strain (SH1000).

Additionally, the question was posed as to what degree would environmental structure preservation add to modifying and changing the dynamics of interactions and, subsequently, the consequences of these interferences compared to the outcomes of interactions carried under mixed conditions.

Under structured conditions, the evolved populations were diluted daily and transferred into a new medium while maintaining the environmental structure of the cultured spot using the velvet replica method [see Fig (3.11)]

The findings emphasise the critical role of spatial structure in altering and changing the course of interactions, especially if these interactions involve a high degree of toxicity. Maintaining spatial structure enables inhibitor-producing *S. epidermidis* to better prevent and promote invasions from and into the evolved *S. aureus* populations. The evolved *S.*
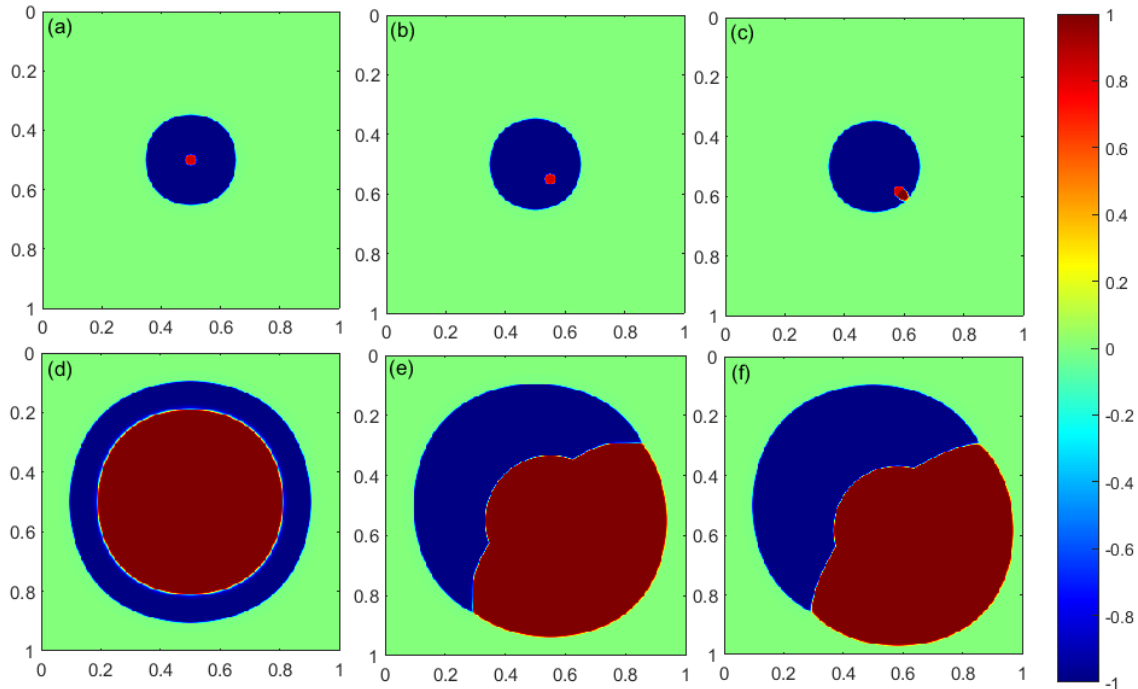
Figure 5.1: **Surface plots generated from** (4.2) **demonstrate the evolution of the interacting populations when mutations are introduced into different locations around the cultured bacterial spot.** The surface plots reflect the evolution of the interacted bacterial populations when inhibitory producing populations of *S. epidermidis* (TU3298, blue) invaded resident populations of *S. aureus* (SH1000, red). Panels (a), (b), and (c): show the simulated bacterial spot one day after introducing the mutations (day 14). Panels (d), (e), and (f): were on the last day of the conducted experiment (day 28). In all panels, the *x* and *y* axes represent the space coordinates.

aureus populations (SH1000) were able to survive and dominate in these complicated and hostile environments.

The prior models based on logistic equations provided in the previous chapter to simulate these interactions were utilised, considering the environmental settings. The mathematical translation of this biological concept, as shown in Fig (4.3a), involves decreasing concentrations at the end of each day without affecting the dimensions of the created spots.

From a mathematical point of view, the findings indicated two different results when the interactions were conducted under structured conditions. The first type was associated with low-toxin interactions. The competition dynamics under structured conditions were slower than those under mixed environments. Thus, if the toxins do not significantly drive the interactions, both environments lead to a similar evolution regardless of the timing factor.

The second type of outcome was associated with inhibitory interactions. Preserving the structure during the interactions enhanced and improved the effectiveness of the toxins. Therefore, as seen in Fig (4.5), the initial hypothesis of the existence of an adaptive part of the population failed to produce proper simulations. This concurs with the study presented in [76], suggesting that the spread of these beneficial resistance mutations

179

is likely to be restricted in spatially-structured environments. On the one hand, this is considered justification for what was observed when imposing mixed environmental conditions to generate structured simulations; on the other hand, the experimental data showed that evolved *S. aureus* populations were able to successfully invade even under structured environmental conditions.

Hence, several attempts were made to obtain model simulations that coincided with the reported experimental data. However, no attempts yielded results that are entirely consistent with both directions of invasions. The best simulations were obtained when introducing the mutations at a later stage of the interactions rather than assuming their initial existence.

(a)   (b)
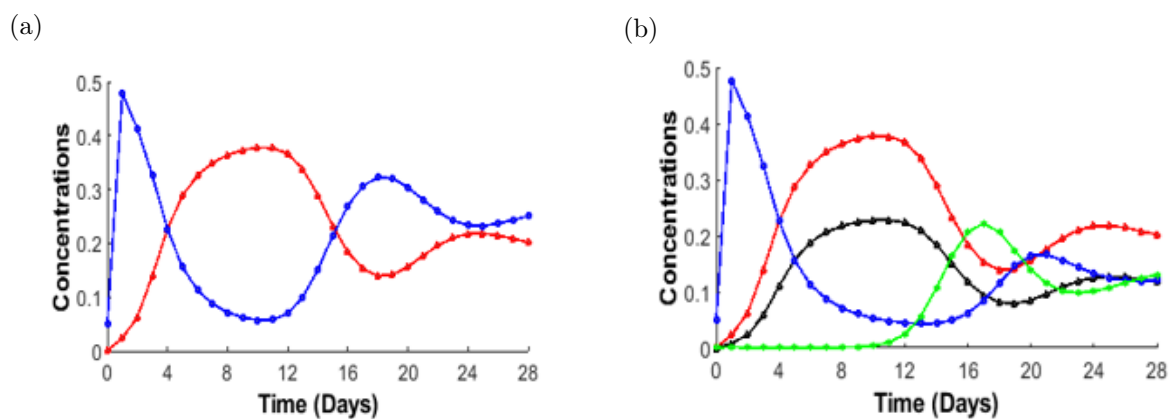
Figure 5.2: **Four-variable model simulation obtained from** (3.24) **after manipulating the values of** ψ, **the association between both susceptible and adapted fractures of S. aureus.** Simulations of interactions when toxin-producing isolates of *S. epidermidis* (B155) invade populations of *S. aureus* (SH1000) at frequencies of 0.01 : 1. Panel (a): red is *S. epidermidis*; blue is *S. aureus*; $(u_s + u_a)$ after adjusting the ψ values to be -0.1 in $\dot{u}_s$ and 0.1 in $\dot{u}_a$. Panel (b): demonstration of the four variable dynamics where (red) is *S. epidermidis*, (blue) is the susceptible fraction of *S. aureus* population, (green) is the adapted part, and (black) is the toxin. The x-axis is the time in days. The y-axis represents the relative concentrations of the evolved populations and toxins. Parameters: $D_u = 1.8 \times 10^{-6}$, $D_v = 5 \times 10^{-6}$, $r_u = 26.5296$, $r_v = 22.3344$, $p_1 = 1.0091$, $p_2 = 0.9755$, $f_1 = 1$, $f_2 = 0.18$, $b_1 = 1.1$, $b_2 = 0.9$, $b_3 = 0.65$ and $b_4 = 0.96$.

In the last section of this chapter, there is an investigation of the impact of initial resistance locations in the evolved spot on the interference dynamics by extending the model to the 2D n-species competition-diffusive model. As seen in figures (4.22), and (5.1), the results suggest that the farther the mutations are created from the centre of the spot, the longer it takes to recover and finally dominate.

5.2   Future Work

As previously stated, and shown in Fig (3.8), all the evolved populations of *S. epidermidis* changed to survive during the interaction with *S. aureus* species, as they generated

greater inhibition zones against the ancestral SH1000 when compared to the inhibition zones produced by the initial populations.

Such results may stimulate and inspire future research, as it may be possible to extend the models produced in this thesis to account for the mutations developed in *S. epidermidis* populations, which may be the primary source of the observed oscillations during the interference process.

Furthermore, the aim was to investigate the associations between the observed oscillations and the coexistence of susceptible and adapted fractures in the evolved *S. aureus* populations. As shown in Fig (5.2), the competition relationship between susceptible and adapted fractures of the evolved *S. aureus* populations and the producer follows the principle of the Red Queen hypothesis [86]. The producer limits the existence of the susceptible *S. aureus*. The adapted evolves to inhibit the growth of the producer, and once inhibited, the susceptible evolves to restore their normal distribution. According to [31], *Staphylococcus aureus* is naturally susceptible to virtually every antibiotic that has been developed. This evolution is constant; if one of the three were to stop evolving, it would become extinct.

Chapter 6

Appendix
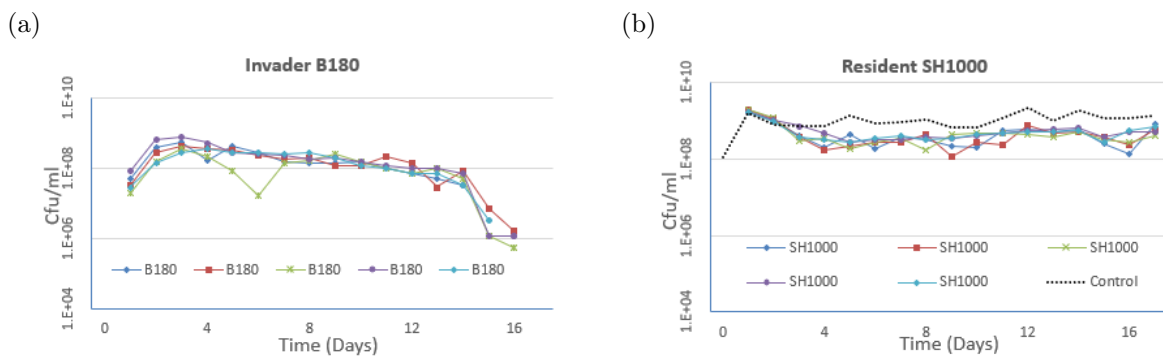
Figure 6.1: **Low-toxin-producing isolates of *S. epidermidis* (B**180**) invading populations of *S. aureus* (SH**1000**) at frequencies of** 0.01. These invasions were carried under a mixed regimen. Panel (a): shows the initial data obtained from five replicates, representing the behaviour of the invader population B180. Panel (b): the behaviour of the resident populations SH1000, along with the control (dotted line), where the population was cultured independently. The x-axis is the time in days. The y-axis in panels is the colony-forming units (cfu) per plate. Data plotted in panels (a) and (b) will be provided in the appendix in Tables (6.5), (6.6) and (6.7).

(a)

(b)
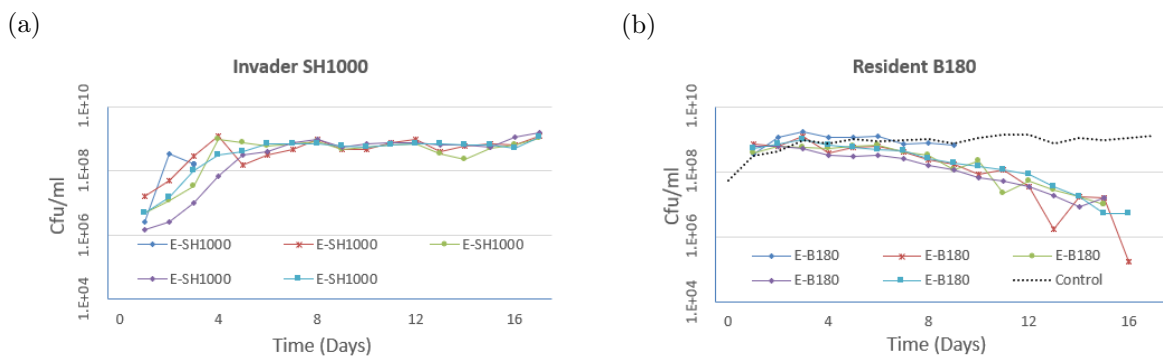
Figure 6.2: **Isolates of *S. aureus* (SH**1000**) invading populations of low-toxin-producing *S. epidermidis* (B**180**) at frequencies of** 0.01. These invasions were carried under a mixed regimen. Panel (a): shows the initial data obtained from five replicates, representing the behaviour of the invader population SH1000. Panel (b): the behaviour of the resident populations B180, along with the control (dotted line), where the population was cultured independently. The x-axis is the time in days. The y-axis is the colony-forming units (cfu) per plate. Data plotted in panels (a) and (b) will be provided in the appendix in Tables (6.5), (6.8) and (6.9).
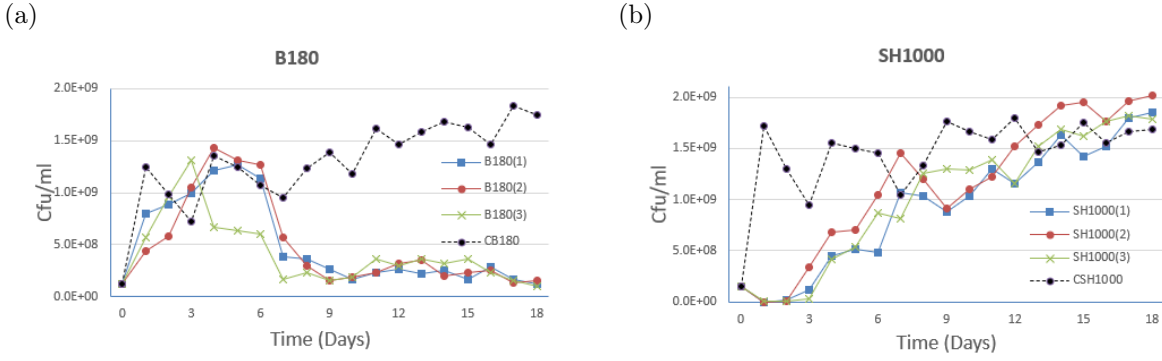
Figure 6.3: **Isolates of *S. aureus* (SH**1000**) competing with populations of low-toxin-producing *S. epidermidis* (B**180**) at initial frequencies of** 1 : 1. Panel (a): shows the initial data obtained from three replicates, representing the behaviour of the evolved populations B180. Panel (b): the behaviour of the evolved populations SH1000, along with the controls (dotted line), where the populations were cultured independently. The x-axis is the time in days, and the y-axis is the colony-forming units (cfu) per plate. Data plotted in panels (a) and (b) will be provided in the appendix in Tables (6.10) and (6.11).
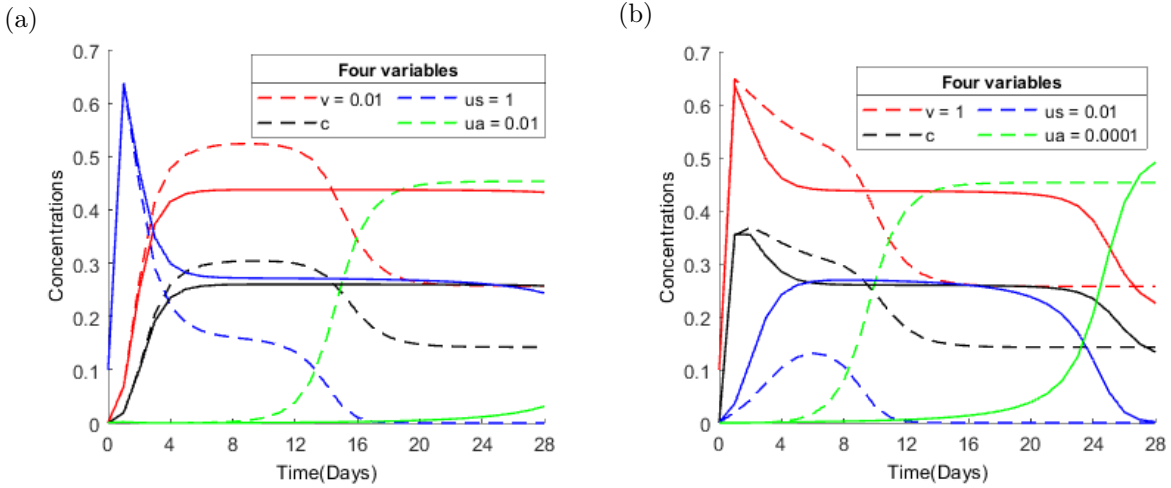
Figure 6.4: **The effect of different inhibition coefficients on the dynamics of interactions.** (a). Simulations of interactions when a toxin-producing population of *Staphylococcus epidermidis* TU3298 invades a resident population of *Staphylococcus aureus* SH1000 at a concentration of 0.01 : 1. (b). Simulations of interactions in the opposite direction. Solid lines indicate when the inhibition coefficients are lower than the dashed lines. Common parameters: $D_u = 1.8 \times 10^{-6}$, $D_v = 5 \times 10^{-5}$, $r_u = 26.5296$, $r_v = 28.613$, $b_1 = 0.9$, $b_2 = 0.82$, $b_3 = 0.9$ and $b_4 = 0.999$. Solid lines parameters: $p_1 = 0.0968$, $p_2 = 0.0966$, $f_1 = 1$, $f_2 = 0.03$. Dashed lines parameters: $p_1 = 0.2258$, $p_2 = 0.2247$, $f_1 = 1$, $f_2 = 0.07$.

183

TIME	Sample 1	Sample 2	Sample 3	Sample 4	Sample 5	Sample 6	Sample 7	Sample 8
0	0.035	0.025	0.002	0.018	0.030	0.039	0.045	0.067
30	0.035	0.027	0.002	0.018	0.032	0.037	0.050	0.060
60	0.048	0.038	0.021	0.026	0.038	0.060	0.063	0.059
90	0.073	0.066	0.045	0.074	0.063	0.069	0.072	0.059
120	0.129	0.118	0.099	0.148	0.115	0.117	0.122	0.060
150	0.228	0.233	0.181	0.269	0.189	0.188	0.208	0.064
180	0.404	0.398	0.313	0.517	0.373	0.347	0.349	0.060
210	0.698	0.710	0.575	0.918	0.649	0.562	0.616	0.067
240	1.238	1.242	1.031	1.681	1.190	0.995	1.079	0.068
270	2.066	2.078	1.794	2.591	2.071	1.765	1.851	0.069
300	3.128	3.146	2.554	4.271	3.051	2.652	2.746	0.075
330	5.055	5.379	3.312	6.263	5.389	4.678	4.149	0.091
360	7.011	7.145	4.669	7.971	7.423	6.912	6.152	0.144
390	7.722	7.553	5.392	8.277	8.193	7.177	7.589	0.208
420	8.459	8.211	5.743	8.787	9.111	9.503	7.411	0.325
450	8.821	8.349	6.254	9.037	9.305	9.724	8.319	0.563
480	8.727	8.004	6.219	8.927	9.475	10.015	7.871	0.980
510	8.840	8.323	6.323	9.516	9.457	9.718	7.617	1.590
540	9.132	8.703	6.555	9.789	8.935	9.926	8.802	2.561
570	9.655	9.235	7.325	10.292	9.676	10.363	9.065	4.250
600	9.582	9.042	7.489	10.416	10.010	10.363	8.772	5.439
630	9.283	8.871	7.348	9.758	9.758	10.322	8.615	6.662
660	9.592	9.050	7.512	10.285	9.847	10.431	9.280	8.129
690	9.619	9.034	7.859	10.295	10.016	10.705	9.019	9.222
720	9.955	9.698	8.254	10.427	10.263	10.657	9.829	10.634
750	10.102	9.667	8.274	10.397	10.346	10.732	10.101	11.281
780	10.132	9.700	8.355	10.459	9.921	11.019	10.156	11.939
810	9.670	9.088	8.263	10.268	9.512	10.485	9.876	12.002
840	9.680	9.057	8.362	10.222	9.814	10.438	9.649	12.124
870	10.193	9.730	8.767	10.746	10.001	10.974	10.105	12.873
900	10.221	9.891	8.888	10.407	9.992	11.044	10.285	12.903
930	9.894	9.338	8.688	10.408	9.861	10.682	10.006	12.166
960	10.302	9.886	9.329	10.394	10.297	11.097	10.480	12.887
990	9.919	9.449	8.768	10.331	9.900	10.587	10.174	12.132
1020	10.330	9.934	9.409	10.679	10.286	11.065	10.326	12.884
1050	10.322	9.873	9.077	10.703	10.322	11.059	10.371	12.476
1080	10.088	9.443	8.895	10.370	10.022	10.808	10.380	12.134
1110	10.160	9.927	8.920	10.345	10.164	10.729	10.278	12.116
1140	10.351	9.947	9.430	10.474	10.368	10.971	10.640	12.456
1170	10.340	9.953	9.172	10.461	10.349	11.063	10.410	12.429
1200	10.464	9.946	9.420	10.460	10.814	11.119	10.434	12.366
1230	10.085	9.884	9.053	9.969	10.308	10.762	10.001	12.084
1260	10.458	9.934	9.487	10.404	10.751	11.255	10.452	12.159
1290	10.393	9.954	9.460	10.440	10.374	11.058	10.455	11.957
1320	10.417	9.935	9.532	10.457	10.753	11.079	10.477	11.946
1350	10.399	9.935	9.517	10.437	10.738	11.068	10.451	11.900
1380	10.115	9.514	9.166	10.296	10.347	10.745	10.038	11.221
1410	10.128	9.489	9.180	10.278	10.331	10.775	10.040	10.946

Table 6.1: **Data presented in figure (3.1a).** Eight replicates for SH1000 strain were incubated at $37°C$ for 24 h, after fixing the conditions that might influence their growth. And OD_{600} readings were taken at 30-min intervals.

TIME	Sample 1	Sample 2	Sample 3	Sample 4	Sample 5	Sample 6	Sample 7	Sample 8
0	0.020	0.002	0.000	0.000	0.103	0.040	0.045	0.056
30	0.025	0.026	0.001	0.001	0.103	0.028	0.049	0.059
60	0.031	0.028	0.047	0.002	0.103	0.048	0.060	0.059
90	0.049	0.054	0.047	0.002	0.103	0.060	0.066	0.045
120	0.078	0.105	0.061	0.004	0.103	0.076	0.103	0.058
150	0.152	0.176	0.135	0.005	0.103	0.127	0.161	0.046
180	0.262	0.293	0.231	0.004	0.175	0.233	0.274	0.057
210	0.511	0.612	0.480	0.010	0.320	0.443	0.547	0.059
240	0.955	1.159	0.892	0.012	0.611	0.868	1.009	0.061
270	1.759	2.109	1.630	0.013	1.159	1.641	1.933	0.066
300	3.087	3.626	2.917	0.044	2.126	2.947	3.410	0.070
330	4.828	5.485	4.710	0.054	3.446	4.799	5.409	0.085
360	6.572	7.091	6.277	0.119	5.717	6.683	7.212	0.120
390	7.360	7.670	7.244	0.192	7.002	7.409	7.913	0.165
420	8.710	8.917	8.395	0.378	8.295	9.168	9.139	0.307
450	9.521	9.617	9.170	0.723	9.102	9.966	10.273	0.553
480	9.765	9.764	9.537	1.348	9.558	10.178	10.436	0.958
510	10.199	10.031	9.935	2.234	10.011	10.854	10.948	1.731
540	10.407	10.338	10.022	3.984	10.447	10.920	11.294	2.789
570	10.745	10.670	10.372	5.654	10.656	11.138	11.461	4.858
600	10.957	10.973	10.501	7.089	11.047	11.356	11.602	6.247
630	10.606	10.491	10.414	8.010	10.663	11.117	11.427	7.406
660	10.643	10.454	10.379	9.085	11.014	11.125	11.406	9.101
690	10.461	10.362	10.036	9.743	10.631	10.975	11.354	10.342
720	10.727	10.514	10.497	10.513	11.170	11.309	11.447	11.818
750	10.653	10.505	10.436	10.986	10.978	11.137	11.383	12.371
780	10.554	10.450	10.359	11.626	10.648	11.111	11.335	12.669
810	9.937	9.760	9.659	11.196	10.016	10.468	10.652	12.427
840	9.824	9.628	9.578	11.185	9.922	10.382	10.404	12.647
870	10.237	10.046	10.033	12.103	10.441	10.895	10.897	13.920
900	10.141	10.044	9.758	12.116	10.489	10.834	10.649	13.921
930	9.721	9.610	9.534	11.082	10.005	10.202	10.328	13.050
960	9.966	9.777	9.642	11.740	10.389	10.484	10.439	13.794
990	9.487	9.501	9.176	10.653	9.772	10.173	9.847	12.660
1020	9.746	9.635	9.558	11.164	10.069	10.200	10.315	13.224
1050	9.511	9.493	9.222	11.014	9.941	10.198	9.776	13.267
1080	9.100	8.943	8.904	10.436	9.540	9.619	9.330	12.647
1110	8.979	8.801	8.739	10.061	9.486	9.514	9.120	12.440
1140	9.086	8.907	8.812	10.485	9.616	9.612	9.320	13.090
1170	8.990	8.798	8.761	10.390	9.513	9.523	9.099	12.494
1200	8.884	8.731	8.681	10.374	9.494	9.347	9.106	12.640
1230	8.342	8.158	8.137	9.753	8.773	9.115	8.413	12.293
1260	8.517	8.323	8.307	10.045	8.955	9.209	8.696	12.491
1290	8.342	8.137	8.041	9.922	8.890	9.121	8.397	12.389
1320	8.271	8.027	8.010	9.929	8.748	9.076	8.379	12.350
1350	8.166	8.035	7.990	9.764	8.679	8.658	8.316	12.355
1380	7.671	7.551	7.381	9.534	8.172	8.194	7.913	11.475
1410	7.501	7.388	7.242	9.516	7.994	8.123	7.662	11.615

Table 6.2: **Data presented in figure (3.1b).** Eight replicates for B180 strain were incubated at $37°C$ for 24 h, after fixing the conditions that might influence their growth. And OD_{600} readings were taken at 30-min intervals.

TIME	Sample 1	Sample 2	Sample 3	Sample 4	Sample 5	Sample 6	Sample 7	Sample 8
0	0.025	0.017	0.000	0.011	0.002	0.023	0.034	0.095
30	0.032	0.014	0.000	0.011	0.020	0.024	0.035	0.096
60	0.040	0.020	0.000	0.021	0.034	0.033	0.041	0.097
90	0.049	0.035	0.000	0.030	0.037	0.039	0.049	0.109
120	0.073	0.043	0.061	0.062	0.062	0.060	0.068	0.145
150	0.104	0.071	0.061	0.092	0.094	0.068	0.125	0.180
180	0.160	0.119	0.109	0.148	0.147	0.101	0.206	0.249
210	0.249	0.193	0.153	0.233	0.243	0.169	0.294	0.376
240	0.419	0.350	0.253	0.396	0.408	0.283	0.513	0.593
270	0.658	0.591	0.407	0.615	0.661	0.429	0.845	0.872
300	1.065	0.922	0.653	1.023	1.113	0.726	1.349	1.375
330	1.651	1.425	0.968	1.601	1.715	1.150	2.119	2.082
360	2.594	2.269	1.601	2.505	2.731	1.906	3.251	3.129
390	3.755	3.298	2.401	3.660	3.849	2.883	4.657	4.442
420	4.929	4.586	3.629	4.664	5.054	4.403	5.658	5.310
450	5.594	5.076	4.358	5.384	5.678	5.230	6.227	6.045
480	6.061	5.497	4.746	5.762	6.146	5.851	6.619	6.559
510	6.674	5.997	5.584	6.149	6.859	6.579	7.394	7.165
540	6.973	6.146	6.031	6.545	7.247	6.934	7.525	7.538
570	7.647	6.940	6.630	6.963	7.772	7.754	8.353	8.197
600	7.899	7.310	6.885	7.278	7.999	8.047	8.380	8.452
630	7.870	7.288	7.165	7.241	8.000	8.040	8.334	8.387
660	8.103	7.541	7.220	7.319	8.268	8.393	8.521	8.658
690	8.218	7.629	7.318	7.403	8.372	8.399	8.674	8.922
720	8.576	8.012	8.025	7.658	8.763	8.906	9.114	9.096
750	8.698	8.008	8.073	8.084	8.778	9.087	9.165	9.137
780	8.802	8.250	8.157	8.130	9.080	9.099	9.181	9.128
810	8.556	7.916	8.105	7.669	8.709	8.926	9.127	9.088
840	8.516	7.906	8.065	7.654	8.528	8.921	9.062	9.125
870	8.960	8.340	8.460	8.148	9.098	9.481	9.321	9.449
900	8.990	8.283	8.429	8.239	9.160	9.538	9.311	9.490
930	8.592	7.904	8.160	7.638	8.741	9.144	9.097	9.139
960	8.895	8.010	8.452	8.171	9.158	9.508	9.324	9.300
990	8.544	7.675	8.095	7.654	8.756	9.083	9.133	9.089
1020	8.838	7.904	8.188	8.088	9.153	9.472	9.318	9.204
1050	8.636	7.769	8.142	7.624	9.085	9.175	9.166	9.135
1080	8.273	7.566	7.536	7.260	8.523	8.922	8.708	8.787
1110	8.136	7.299	7.553	7.213	8.403	8.794	8.680	8.560
1140	8.359	7.574	8.052	7.311	8.405	8.904	9.059	9.051
1170	8.212	7.608	7.567	7.278	8.396	8.752	8.709	8.631
1200	8.183	7.613	7.596	7.249	8.411	8.713	8.671	8.541
1230	7.780	7.238	7.293	6.885	7.957	8.253	8.354	8.088
1260	7.990	7.540	7.536	7.209	8.309	8.361	8.392	8.199
1290	7.914	7.301	7.572	7.208	8.284	8.266	8.355	8.141
1320	7.790	7.219	7.525	6.950	7.991	8.211	8.352	8.108
1350	7.600	6.909	7.300	6.902	7.928	8.052	8.286	7.619
1380	7.359	6.772	7.210	6.604	7.656	7.777	7.878	7.555
1410	7.131	6.398	6.950	6.574	7.629	7.306	7.698	7.271

Table 6.3: **Data presented in figure (3.1c).** Eight replicates for B155 strain were incubated at $37°C$ for 24 h, after fixing the conditions that might influence their growth. And OD_{600} readings were taken at 30-min intervals.

TIME	Sample 1	Sample 2	Sample 3	Sample 4	Sample 5	Sample 6	Sample 7	Sample 8
0	0.027	0.011	0.000	0.013	0.003	0.021	0.093	0.069
30	0.029	0.012	0.000	0.014	0.004	0.025	0.090	0.064
60	0.033	0.020	0.000	0.020	0.011	0.026	0.091	0.067
90	0.053	0.041	0.000	0.037	0.019	0.042	0.102	0.064
120	0.083	0.082	0.000	0.066	0.042	0.077	0.130	0.065
150	0.155	0.176	0.000	0.135	0.093	0.158	0.204	0.066
180	0.283	0.336	0.000	0.246	0.202	0.284	0.332	0.067
210	0.527	0.643	0.000	0.509	0.402	0.520	0.559	0.067
240	0.962	1.163	0.000	0.948	0.778	0.961	0.998	0.068
270	1.658	1.926	0.000	1.656	1.342	1.684	1.776	0.096
300	2.619	3.092	0.010	2.657	2.191	2.634	2.759	0.099
330	3.849	4.389	0.020	3.827	3.308	3.843	4.126	0.112
360	4.884	4.963	0.062	4.747	4.671	4.969	5.403	0.175
390	5.331	5.494	0.134	5.437	4.818	5.478	5.740	0.247
420	6.388	6.355	0.309	6.437	6.001	6.345	6.932	0.400
450	7.060	6.976	0.581	6.987	6.755	6.984	7.762	0.691
480	7.440	7.511	1.093	7.298	7.197	7.544	8.014	1.187
510	8.092	8.286	1.824	7.923	7.554	8.397	8.658	1.965
540	8.852	8.818	2.894	8.753	8.139	9.207	9.320	3.103
570	9.829	9.595	4.350	9.953	9.092	10.034	10.637	4.705
600	10.207	9.605	5.313	10.470	9.608	10.493	11.380	5.844
630	10.080	9.597	6.607	10.034	9.745	10.203	11.346	7.393
660	10.209	9.345	7.557	10.369	10.127	10.502	11.401	8.759
690	10.210	9.353	8.355	10.351	10.101	10.509	11.421	9.475
720	10.546	9.509	9.185	10.422	10.801	10.976	11.926	10.995
750	10.588	9.601	9.775	10.410	10.884	11.103	11.902	11.581
780	10.507	9.495	10.735	10.400	10.834	10.981	11.851	12.397
810	10.087	9.197	10.692	9.851	10.074	10.505	11.446	12.289
840	10.037	9.141	10.912	9.666	10.075	10.482	11.442	12.439
870	10.501	9.342	11.825	10.385	10.782	10.974	11.887	13.841
900	10.487	9.341	11.820	10.348	10.729	11.104	11.808	14.025
930	9.982	9.092	11.130	9.670	9.771	10.509	11.436	13.781
960	10.410	9.343	11.840	10.056	10.679	10.976	11.822	14.307
990	10.028	9.129	11.169	9.665	9.753	10.811	11.456	13.858
1020	10.369	9.322	11.821	10.062	10.337	10.969	11.913	14.339
1050	10.324	9.215	11.440	10.063	10.273	10.978	11.820	14.060
1080	9.963	8.799	11.120	9.670	9.741	10.861	11.381	13.773
1110	9.947	8.787	11.113	9.621	9.715	10.830	11.406	13.179
1140	10.365	9.324	11.447	10.029	10.308	11.098	11.829	14.037
1170	10.329	9.133	11.415	10.064	10.263	11.107	11.828	13.842
1200	10.511	9.309	11.364	10.365	10.753	11.118	11.914	13.975
1230	10.035	9.088	10.899	9.686	9.764	10.852	11.480	13.016
1260	10.213	9.190	11.321	10.013	10.118	10.934	11.612	13.909
1290	10.176	9.162	10.948	10.020	10.104	10.898	11.457	13.294
1320	10.151	9.160	11.113	9.866	10.103	10.848	11.579	13.072
1350	9.901	9.100	10.850	9.645	9.731	10.505	11.414	13.055
1380	9.545	8.548	10.184	9.335	9.476	10.185	10.983	12.428
1410	9.350	8.540	9.769	8.797	9.204	10.052	10.922	12.357

Table 6.4: **Data presented in figure (3.1d).** Eight replicates for TU3298 strain were incubated at $37°C$ for 24 h, after fixing the conditions that might influence their growth. And OD_{600} readings were taken at 30-min intervals.

Days	Controls	
	SH1000/ml	B180/ml
0	110000000	53333333.33
1	1633333333	300000000
2	800000000	433333333.3
3	733333333.3	950000000
4	733333333.3	733333333.3
5	1383333333	983333333.3
6	866666666.7	833333333.3
7	950000000	900000000
8	1050000000	1000000000
9	683333333.3	716666666.7
10	666666666.7	1050000000
11	1133333333	1350000000
12	2183333333	1366666667
13	1033333333	750000000
14	1900000000	1066666667
15	1216666667	950000000
16	1150000000	1116666667
17	1350000000	1250000000

Table 6.5: **Data presented in figures (6.1b)** and (6.2b)

1		2	
Cfu/ml SH1000	Cfu/ml B180	Cfu/ml SH1000	Cfu/ml B180
1766666667	50000000	1933333333	33333333.33
1066666667	383333333.3	1100000000	283333333.3
416666666.7	550000000	366666666.7	416666666.7
200000000	166666666.7	166666666.7	350000000
450000000	416666666.7	216666666.7	333333333.3
183333333.3	266666666.7	266666666.7	233333333.3
366666666.7	150000000	283333333.3	183333333.3
316666666.7	133333333.3	450000000	200000000
216666666.7	133333333.3	116666666.7	116666666.7
200000000	150000000	283333333.3	116666666.7
566666666.7	100000000	233333333.3	216666666.7
600000000	66666666.67	766666666.7	133333333.3
500000000	50000000	483333333.3	28333333.33
600000000	33333333.33	500000000	83333333.33
250000000	1666666.667	383333333.3	6666666.667
133333333.3	1666666.667	233333333.3	1666666.667
816666666.7	550000	600000000	0

Table 6.6: **Data presented in figures (6.1a) and (6.1b)**

3		4		5	
Cfu/ml SH1000	Cfu/ml B180	Cfu/ml SH1000	Cfu/ml B180	Cfu/ml SH1000	Cfu/ml B180
2000000000	20000000	1633333333	83333333.33	1700000000	28333333.33
1200000000	150000000	1033333333	633333333.3	1000000000	133333333.3
300000000	350000000	733333333.3	750000000	366666666.7	283333333.3
350000000	216666666.7	483333333.3	516666666.7	316666666.7	350000000
183333333.3	83333333.33	283333333.3	266666666.7	283333333.3	266666666.7
283333333.3	16666666.67	316666666.7	250000000	350000000	283333333.3
350000000	133333333.3	316666666.7	233333333.3	400000000	250000000
166666666.7	166666666.7	383333333.3	183333333.3	316666666.7	266666666.7
450000000	250000000	350000000	200000000	350000000	200000000
466666666.7	150000000	416666666.7	150000000	433333333.3	116666666.7
483333333.3	100000000	466666666.7	116666666.7	483333333.3	100000000
433333333.3	66666666.67	550000000	100000000	516666666.7	66666666.67
383333333.3	100000000	616666666.7	100000000	533333333.3	66666666.67
533333333.3	50000000	666666666.7	66666666.67	566666666.7	33333333.33
333333333.3	1116666.667	366666666.7	1116666.667	283333333.3	3333333.333
266666666.7	550000	516666666.7	1116666.667	566666666.7	0
400000000	0	500000000	0	700000000	0

Table 6.7: **Data presented in figures (6.1a) and (6.1b)**

1		2		3	
E-SH1000	E-B180	E-SH1000	E-B180	E-SH1000	E-B180
2500000	333333333.3	16666666.67	700000000	5000000	366666666.7
333333333.3	1166666667	50000000	583333333.3	11666666.67	583333333.3
166666666.7	1666666667	283333333.3	1216666667	33333333.33	566666666.7
0	1166666667	1233333333	383333333.3	933333333.3	516666666.7
0	1150000000	150000000	550000000	716666666.7	600000000
0	1250000000	316666666.7	600000000	566666666.7	666666666.7
0	683333333.3	466666666.7	400000000	666666666.7	400000000
0	766666666.7	916666666.7	233333333.3	800000000	316666666.7
0	666666666.7	466666666.7	166666666.7	466666666.7	116666666.7
		450000000	83333333.33	550000000	216666666.7
		766666666.7	116666666.7	650000000	21666666.67
		933333333.3	33333333.33	700000000	50000000
		383333333.3	1666666.667	333333333.3	26666666.67
		566666666.7	16666666.67	233333333.3	16666666.67
		700000000	15000000	500000000	10000000
		616666666.7	166666.6667	650000000	0
		1183333333	0	1000000000	0

Table 6.8: **Data presented in figures (6.2a) and (6.2b).**

4		5	
E-SH1000	E-B180	E-SH1000	E-B180
1500000	616666666.7	5000000	500000000
2500000	583333333.3	15000000	700000000
10000000	500000000	100000000	950000000
66666666.67	316666666.7	316666666.7	650000000
300000000	283333333.3	400000000	566666666.7
400000000	316666666.7	700000000	483333333.3
733333333.3	250000000	666666666.7	433333333.3
950000000	150000000	683333333.3	250000000
550000000	116666666.7	583333333.3	183333333.3
666666666.7	66666666.67	533333333.3	141666666.7
733333333.3	50000000	650000000	116666666.7
750000000	33333333.33	666666666.7	83333333.33
650000000	18333333.33	683333333.3	33333333.33
633333333.3	8166666.667	633333333.3	16666666.67
533333333.3	15000000	633333333.3	5000000
1083333333	0	516666666.7	5000000
1583333333	0	1150000000	0

Table 6.9: **Data presented in figures (6.2a) and (6.2b).**

	CSH1000	CB180	CB155	CTU3298
0	150000000	116666666.7	66666666.67	83333333.33
1	1716666667	1250000000	383333333.3	1300000000
2	1300000000	983333333.3	350000000	1033333333
3	950000000	716666666.7	416666666.7	1216666667
4	1550000000	1350000000	900000000	1016666667
5	1500000000	1250000000	800000000	1200000000
6	1450000000	1066666667	500000000	1683333333
7	1050000000	950000000	1066666667	1833333333
8	1333333333	1233333333	1333333333	2016666667
9	1766666667	1383333333	1216666667	1500000000
10	1666666667	1183333333	1033333333	1433333333
11	1583333333	1616666667	1166666667	1350000000
12	1800000000	1466666667	1233333333	1550000000
13	1466666667	1583333333	1283333333	1783333333
14	1533333333	1683333333	1133333333	1666666667
15	1750000000	1663333333	1350000000	1633333333
16	1550000000	1466666667	1533333333	1683333333
17	1666666667	1833333333	1316666667	1850000000
18	1683333333	1750000000	1466666667	1950000000

Table 6.10: **Data representing controls, where isolates of the involved strains were cultured independently to compare and measure the influence of the interactions. This data is plotted in figures (6.3a) and (6.3b).**

(B180:SH1000)	(1: 1)				
SH1000(1)	SH1000(2)	SH1000(3)	B180(1)	B180(2)	B180(3)
316666.6667	466666.6667	3500000	800000000	433333333.3	566666666.7
16666666.67	3000000	1666666.667	883333333.3	583333333.3	966666666.7
116666666.7	333333333.3	33333333.33	1000000000	1050000000	1316666667
450000000	683333333.3	416666666.7	1216666667	1433333333	666666666.7
516666666.7	700000000	533333333.3	1266666667	1316666667	633333333.3
483333333.3	1050000000	866666666.7	1133333333	1266666667	600000000
1066666667	1450000000	816666666.7	383333333.3	566666666.7	166666666.7
1033333333	1200000000	1250000000	366666666.7	300000000	233333333.3
883333333.3	916666666.7	1300000000	266666666.7	150000000	150000000
1033333333	1100000000	1283333333	166666666.7	183333333.3	183333333.3
1300000000	1216666667	1383333333	233333333.3	233333333.3	366666666.7
1150000000	1516666667	1150000000	266666666.7	316666666.7	300000000
1366666667	1733333333	1516666667	216666666.7	350000000	366666666.7
1633333333	1916666667	1683333333	250000000	200000000	316666666.7
1416666667	1950000000	1616666667	166666666.7	233333333.3	366666666.7
1516666667	1766666667	1766666667	283333333.3	250000000	233333333.3
1800000000	1966666667	1816666667	166666666.7	133333333.3	150000000
1850000000	2016666667	1783333333	116666666.7	150000000	100000000

Table 6.11: **Data presented in figures (6.3a) and (6.3b).**
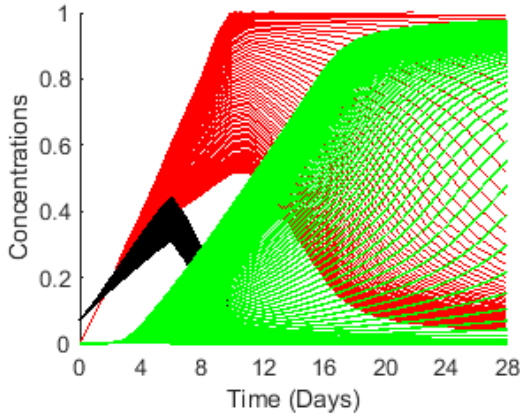
(a) Appendix-toxins1   (b)
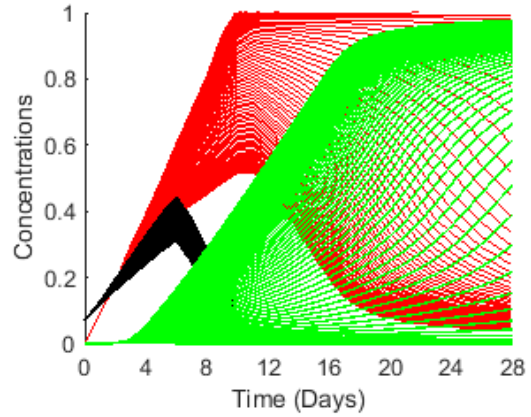
Figure 6.5: **Four variable model simulations of the dynamics of interactions between popula-tions of *S. aureus* (SH1000) and inhibitory producing *S. epidermidis* (B155) under mixed and structured conditions using different inhibitory coefficients.** (a). Four-variable model simu-lations that represent the dynamics of interactions; solid lines under structured conditions, dashed lines under mixed conditions; (blue) lines represent the resident *S. aureus*, $(u_s + u_a)$, (red) lines represent the invader *S. epidermidis* populations (B155), and the ratio of initial concentrations is (0.01:1). (b) A demonstration of the four-variable model dynamics, where (red) represents *S. epidermidis*, v, (blue) represents the susceptible fraction of the *S. aureus* population, u_s, and (green) represents the adapted fraction, u_a. (c) A simulation of the natural log of the invader to resident ratio (red line) plotted against the actual experimental ratio (black dots). (d), (e) and (f). Four-variable model simulations of the mutual invasion where populations of *S. aureus* invaded into resident populations of *S. epidermidis*. Pa-rameters: $D_u = 1.8 \times 10^{-6}$, $D_v = 5 \times 10^{-6}$, $r_u = 26.5296$, $r_v = 22.3344$, $p_1 = 0.2613$, $p_2 = 0.2590$, $f_1 = 1$, $f_2 = 0.045$, $b_1 = 1.1$, $b_2 = 0.9$, $b_3 = 0.65$ and $b_4 = 0.96$.

Days	Controls		
	1 ML	1 ML	1 ML
	C-B155	C-SH1000	C-TU3298
0	333333333.3	350000000	500000000
1	766666666.7	1883333333	1050000000
2	1133333333	2833333333	1633333333
3	1166666667	3666666667	1866666667
4	1266666667	2533333333	1633333333
5	1200000000	2000000000	1766666667
6	2000000000	1333333333	2333333333
7	1333333333	1033333333	2500000000
8	1666666667	1833333333	2166666667
9	1833333333	1500000000	2833333333
10	3166666667	3000000000	3833333333
11	1666666667	1616666667	2833333333
12	2083333333	3333333333	3666666667
13	2666666667	2833333333	1833333333
14	2550000000	2633333333	2300000000
15	2333333333	2716666667	2533333333
16	1666666667	2000000000	1450000000
17	2000000000	1333333333	1333333333
18	2033333333	1500000000	1416666667
19	2183333333	2216666667	1250000000
20	1833333333	1333333333	1000000000
21	1500000000	1666666667	1333333333
22	2166666667	2000000000	1733333333
23	1250000000	1566666667	1500000000
24	1500000000	1666666667	1116666667
25	1550000000	2033333333	1666666667
26	1666666667	2666666667	1666666667
27	1833333333	2016666667	1500000000
28	2166666667	2333333333	1833333333

	1		2		3	
Days	SH1000	B155	SH1000	B155	SH1000	B155
0						
1	1900000000	83333333.33	1433333333	166666666.7	1300000000	300000000
2	3333333333	2166666667	316666666.7	900000000	50000000	500000000
3	1833333333	2666666667	83333333.33	833333333.3	250000000	1066666667
4	666666666.7	1500000000	633333333.3	500000000	166666666.7	2166666667
5	666666666.7	2333333333	333333333.3	1583333333	166666666.7	2666666667
6	166666666.7	1500000000	1000000000	1166666667	383333333.3	2700000000
7	666666666.7	1500000000	1166666667	1500000000	366666666.7	1666666667
8	1166666667	1333333333	500000000	1166666667	500000000	1800000000
9	1166666667	1666666667	333333333.3	1333333333	1500000000	1500000000
10	833333333.3	2000000000	1100000000	2166666667	333333333.3	2166666667
11	833333333.3	2000000000	666666666.7	2833333333	450000000	1700000000
12	833333333.3	1333333333	1083333333	1633333333	1200000000	1250000000
13	666666666.7	666666666.7	833333333.3	1000000000	500000000	1500000000
14						
15	1166666667	2333333333	2333333333	2166666667	500000000	2000000000
16	1000000000	866666666.7	2333333333	950000000	333333333.3	1100000000
17	666666666.7	333333333.3	500000000	516666666.7	450000000	200000000
18	1000000000	300000000	333333333.3	400000000	1000000000	283333333.3
19	833333333.3	383333333.3	1000000000	266666666.7	750000000	366666666.7
20	1500000000	166666666.7	1500000000	133333333.3	1500000000	166666666.7
21	616666666.7	166666666.7	433333333.3	116666666.7	1000000000	333333333.3
22	833333333.3	133333333.3	1000000000	166666666.7	450000000	116666666.7
23	500000000	166666666.7	1666666667	250000000	1000000000	666666666.7
24	500000000	66666666.67	666666666.7	166666666.7	1600000000	183333333.3
25	416666666.7	116666666.7	700000000	216666666.7	1833333333	300000000
26	1000000000	83333333.33	1400000000	133333333.3	1833333333	133333333.3
27	1500000000	100000000	1716666667	100000000	1783333333	100000000
28	1666666667	100000000	1750000000	116666666.7	1750000000	111666666.7

Table 6.12: **Data presented in figure (3.13d).**

Days			Aureus invading			
	1		2		3	
	SH1000	B155	SH1000	B155	SH1000	B155
0						
1	333333.3333	666666666.7	3333333.333	366666666.7	150000	716666666.7
2	50000	650000000	18333333.33	1116666667	4500000	1166666667
3	33333333.33	700000000	50000000	1083333333	100000000	1000000000
4	200000000	1200000000	50000000	1166666667	166666666.7	1166666667
5	150000000	1200000000	91666666.67	1250000000	350000000	1166666667
6	200000000	1833333333	183333333.3	1666666667	500000000	1700000000
7	216666666.7	1666666667	166666666.7	1833333333	366666666.7	1500000000
8	300000000	1333333333	216666666.7	2000000000	500000000	1633333333
9	350000000	1833333333	383333333.3	1333333333	333333333.3	2000000000
10	500000000	500000000	583333333.3	1500000000	500000000	1416666667
11	2000000000	1500000000	1166666667	1833333333	916666666.7	1666666667
12	1666666667	333333333.3	1533333333	1666666667	1200000000	1250000000
13	1833333333	500000000	2000000000	1833333333	1500000000	666666666.7
14	1700000000	433333333.3	2083333333	1283333333	1700000000	550000000
15	1500000000	500000000	1833333333	833333333.3	1566666667	716666666.7
16	1833333333	833333333.3	1666666667	916666666.7	1466666667	966666666.7
17	2333333333	333333333.3	1916666667	500000000	1250000000	550000000
18	1666666667	583333333.3	2000000000	833333333.3	2083333333	666666666.7
19	1500000000	416666666.7	2250000000	700000000	1533333333	866666666.7
20	2166666667	833333333.3	1666666667	333333333.3	2000000000	616666666.7
21	1833333333	333333333.3	1500000000	250000000	2283333333	500000000
22	1666666667	666666666.7	1750000000	333333333.3	1216666667	366666666.7
23	1166666667	333333333.3	1166666667	500000000	1166666667	500000000
24	1666666667	666666666.7	1300000000	316666666.7	1600000000	350000000
25	1583333333	583333333.3	1666666667	416666666.7	1833333333	283333333.3
26	1833333333	333333333.3	1350000000	333333333.3	1666666667	533333333.3
27	1666666667	333333333.3	1666666667	366666666.7	1783333333	366666666.7
28	1666666667	333333333.3	1750000000	333333333.3	1700000000	333333333.3

Table 6.13: **Data presented in figure (3.13f).**

Days	1		2		3	
	SH1000	TU	SH1000	TU	SH1000	TU
0						
1	2100000000	266666666.7	1750000000	333333333.3	1833333333	316666666.7
2	1166666667	2666666667	333333333.3	1666666667	1500000000	166666666.7
3	500000000	1500000000	666666666.7	1333333333	500000000	500000000
4	633333333.3	2833333333	366666666.7	2833333333	333333333.3	1833333333
5	166666666.7	2166666667	100000000	1833333333	666666666.7	3666666667
6	1000000000	1166666667	450000000	2000000000	800000000	2150000000
7	1333333333	1666666667	500000000	2333333333	250000000	2166666667
8	1333333333	2000000000	733333333.3	2016666667	533333333.3	2666666667
9	1333333333	1833333333	966666666.7	2200000000	166666666.7	1833333333
10	1666666667	1666666667	1533333333	1833333333	133333333.3	1333333333
11	833333333.3	2000000000	1416666667	2000000000	166666666.7	1833333333
12	1366666667	1550000000	1300000000	1666666667	500000000	2000000000
13	1500000000	2333333333	1500000000	1833333333	833333333.3	2000000000
14						
15	2833333333	2000000000	1833333333	2000000000	2000000000	2333333333
16	1166666667	500000000	1250000000	666666666.7	1200000000	500000000
17	333333333.3	1166666667	716666666.7	800000000	333333333.3	1500000000
18	533333333.3	666666666.7	1000000000	733333333.3	533333333.3	666666666.7
19	400000000	1000000000	500000000	966666666.7	633333333.3	833333333.3
20	333333333.3	500000000	333333333.3	833333333.3	1000000000	166666666.7
21	666666666.7	500000000	1666666667	750000000	1000000000	833333333.3
22	2000000000	833333333.3	2000000000	2166666667	833333333.3	1000000000
23	1166666667	500000000	1050000000	583333333.3	1166666667	666666666.7
24	1333333333	166666666.7	500000000	233333333.3	1500000000	166666666.7
25	1000000000	333333333.3	500000000	333333333.3	1333333333	366666666.7
26	1566666667	483333333.3	1166666667	366666666.7	1833333333	566666666.7
27	1833333333	583333333.3	2000000000	700000000	2250000000	450000000
28	1750000000	516666666.7	2000000000	666666666.7	2000000000	666666666.7

Table 6.14: **Data presented in figure (3.13g).**

Days	Aureus invading					
	1		2		3	
	SH1000	TU	SH1000	TU	SH1000	TU
0						
1	33333.33333	533333333.3	16666.66667	1000000000	100000	1166666667
2	500000	1383333333	833333.3333	1433333333	333333.3333	1500000000
3	6666666.667	1500000000	3333333.333	2000000000	833333.3333	1833333333
4	33333333.33	1616666667	83333333.33	1666666667	5000000	1633333333
5	116666666.7	1416666667	300000000	1833333333	116666666.7	1833333333
6	166666666.7	1633333333	366666666.7	1666666667	266666666.7	2000000000
7	383333333.3	2333333333	500000000	2333333333	250000000	1833333333
8	500000000	1383333333	500000000	1600000000	300000000	1950000000
9	366666666.7	1500000000	366666666.7	1500000000	1033333333	2833333333
10	666666666.7	1333333333	666666666.7	1333333333	916666666.7	2083333333
11	1200000000	2166666667	1000000000	2000000000	1366666667	2800000000
12	1633333333	1616666667	1300000000	1250000000	1166666667	2166666667
13	2000000000	1166666667	1500000000	916666666.7	833333333.3	1666666667
14	1883333333	1400000000	1616666667	1133333333	1033333333	2200000000
15	1783333333	1533333333	1333333333	666666666.7	1166666667	1200000000
16	2000000000	1266666667	1666666667	366666666.7	1666666667	1350000000
17	1666666667	1433333333	2966666667	716666666.7	1533333333	1150000000
18	1850000000	1200000000	2500000000	533333333.3	2000000000	1250000000
19	1116666667	1516666667	1500000000	650000000	1633333333	1116666667
20	1000000000	1333333333	1666666667	866666666.7	1750000000	1400000000
21	2000000000	1633333333	2000000000	733333333.3	1533333333	1633333333
22	1500000000	1666666667	2833333333	483333333.3	1250000000	1500000000
23	2500000000	1500000000	1816666667	633333333.3	1366666667	1366666667
24	2000000000	1416666667	1366666667	450000000	1666666667	1633333333
25	1750000000	1800000000	1250000000	800000000	1500000000	1733333333
26	1466666667	1683333333	2016666667	550000000	2033333333	1850000000
27	2333333333	1633333333	2000000000	416666666.7	2000000000	1600000000
28	2133333333	1500000000	2000000000	883333333.3	2066666667	1500000000

Table 6.15: **Data presented in figure (3.13i).**

(B155:SH1000)	(1: 1)				
SH1000(1)	SH1000(2)	SH1000(3)	B155(1)	B155(2)	B155(3)
133333.3333	150000	333333.3333	500000000	350000000	300000000
150000000	66666666.67	83333333.33	1050000000	1000000000	750000000
166666666.7	116666666.7	133333333.3	400000000	1250000000	1400000000
166666666.7	100000000	150000000	900000000	750000000	1000000000
266666666.7	166666666.7	183333333.3	1033333333	500000000	1033333333
383333333.3	266666666.7	283333333.3	1000000000	550000000	916666666.7
383333333.3	616666666.7	733333333.3	566666666.7	450000000	333333333.3
833333333.3	416666666.7	1066666667	300000000	366666666.7	400000000
1133333333	1033333333	1216666667	350000000	283333333.3	266666666.7
1516666667	1400000000	1466666667	300000000	333333333.3	333333333.3
1333333333	1700000000	1200000000	183333333.3	216666666.7	183333333.3
1283333333	1533333333	1200000000	216666666.7	266666666.7	383333333.3
1550000000	1466666667	1400000000	283333333.3	316666666.7	216666666.7
1700000000	1666666667	1516666667	216666666.7	233333333.3	316666666.7
1650000000	1533333333	1683333333	266666666.7	183333333.3	183333333.3
1750000000	1833333333	1466666667	283333333.3	283333333.3	283333333.3
1616666667	1316666667	1550000000	316666666.7	200000000	266666666.7
1683333333	1466666667	1600000000	233333333.3	300000000	183333333.3

Table 6.16: **Data presented in figure (3.13e).**

(TU3298:SH1000)	(1: 1)				
SH1000(1)	SH1000(2)	SH1000(3)	TU(1)	TU(2)	TU(3)
100000000	133333333.3	133333333.3	516666666.7	566666666.7	400000000
50000000	66666666.67	50000000	683333333.3	750000000	800000000
33333333.33	50000000	33333333.33	1400000000	1166666667	916666666.7
416666666.7	433333333.3	500000000	966666666.7	1050000000	1200000000
533333333.3	800000000	766666666.7	750000000	700000000	1000000000
716666666.7	666666666.7	783333333.3	400000000	483333333.3	533333333.3
483333333.3	516666666.7	600000000	633333333.3	533333333.3	283333333.3
566666666.7	666666666.7	566666666.7	466666666.7	666666666.7	366666666.7
766666666.7	850000000	700000000	516666666.7	466666666.7	433333333.3
1016666667	1066666667	1183333333	450000000	533333333.3	316666666.7
1266666667	1350000000	1083333333	666666666.7	350000000	266666666.7
1350000000	1300000000	1200000000	533333333.3	316666666.7	333333333.3
1316666667	1416666667	1066666667	450000000	266666666.7	283333333.3
1466666667	1533333333	1350000000	316666666.7	350000000	383333333.3
1516666667	1566666667	1433333333	366666666.7	300000000	250000000
1566666667	1483333333	1533333333	366666666.7	383333333.3	283333333.3
1483333333	1500000000	1616666667	516666666.7	283333333.3	300000000
1600000000	1566666667	1683333333	316666666.7	350000000	250000000

Table 6.17: **Data presented in figure (3.13h).**
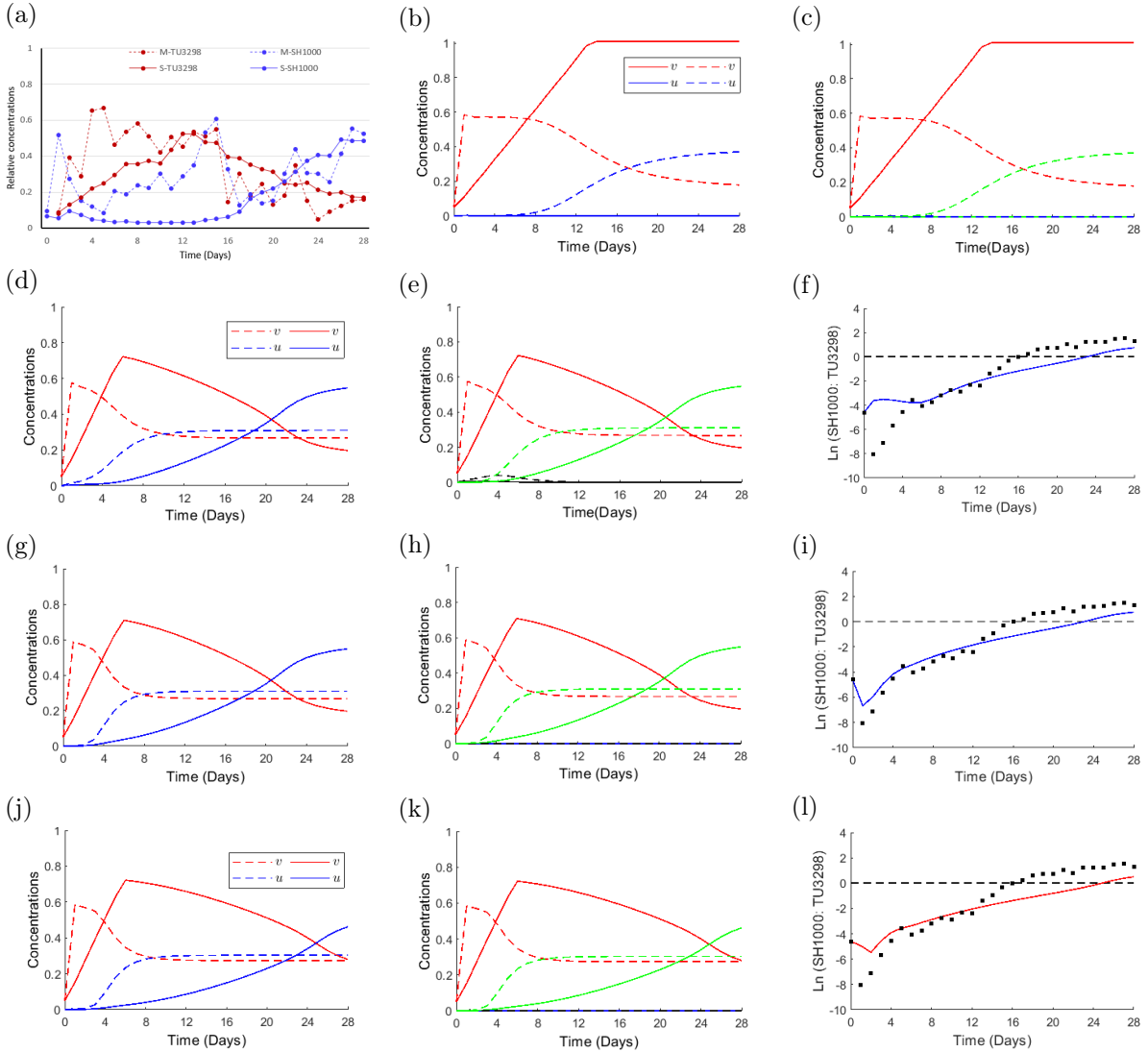
Figure 6.6: **The effect of applying improvement attempts on the dynamics of interactions when toxin-producing populations of *Staphylococcus epidermidis* (TU3298) invaded by populations of *S. aureus* (SH1000) at a frequency of 0.01.** (a). Illustrations of the experimental data show the dynamics of interactions when isolates of *S. epidermidis* (red) invaded by susceptible populations of *S. aureus* (blue) at an initial concentration ratio of 0.01:1, dashed lines when the interactions were conducted under mixed conditions, and solid lines under structured conditions. (b) and (c) show the four-variable model simulations when applying the mixed environment parameters. The blue line represents the whole *S. aureus* population, whereas green and black represent both fractures of the *S. aureus* population. Parameters: $D_u = 1.8 \times 10^{-6}$, $D_v = 5 \times 10^{-5}$, $r_u = 26.5296$, $r_v = 28.613$, $p_1 = 0.7746$, $p_2 = 0.7623$, $f_1 = 1$, $f_2 = 0.24$, $b_1 = 0.9$, $b_2 = 0.84$, $b_3 = 0.9$ and $b_4 = 1.09$. (d) and (e) show the influence of reducing the toxicity effect on both fractions of the *S. aureus* population by choosing the appropriate inhibition degradation rate, $f_2 = 0.07$ that has the lowest error value, and based on that, the corresponding inhibition coefficients, $p_1 = 0.2258$ and $p_2 = 0.2247$, were determined. (g) and (h) show the influence of reducing the toxicity effect on both fractions of the *S. aureus* population and increasing the intensity of the interactions between v and u_s. $b_1 = 1.1$ and $b_3 = 0$. (j) and (k) demonstrations of the resulting simulations when changing $p_2 = 0.26$, which controls the inhibition degree of the adaptive part of the *S. aureus* population, while all other parameters remain unchanged. (f), (i) and (l). Simulations of the natural log of the invader-to-resident ratio.

(a)
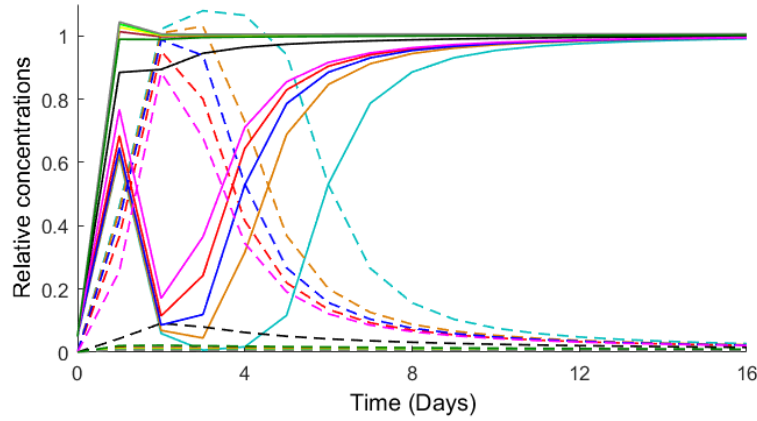
(b)
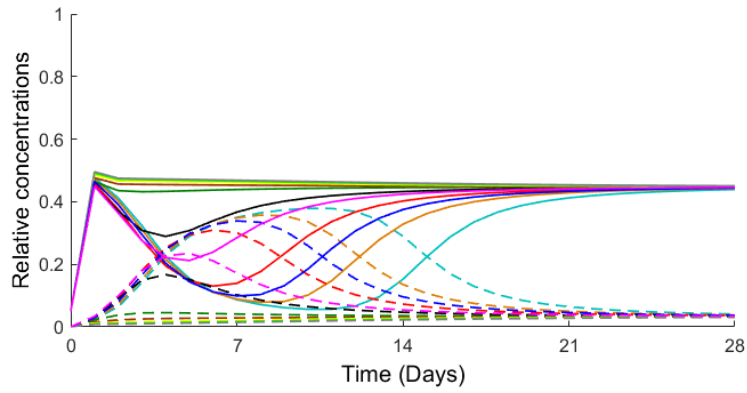
(c)
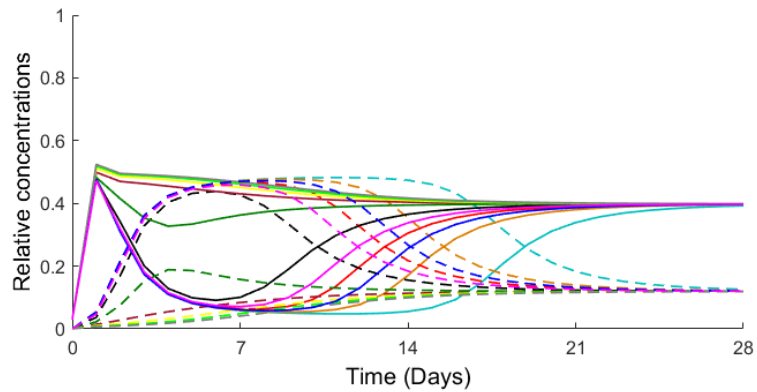
Figure 6.7: **Results of numerical experiments conducted to evaluate the modelling predictions and estimate the proportion of the adapted *S. aureus* SH1000.** Panel (a): different simulations were generated from the three-variable model (3.23), representing the interactions between *S. epidermidis* B180 and *S. aureus* SH1000 when varying the ratio between adaptive (u_a) and susceptible (u_s) fractures of *S. aureus*. Panels (b) and (c): different simulations were generated from the four-variable model (3.24), representing the interactions between *S. epidermidis* B155 and *S. aureus* SH1000 and between *S. epidermidis* TU3298 and *S. aureus* SH1000, respectively, when varying the ratio between adaptive (u_a) and susceptible (u_s) fractures of *S. aureus*. Dashed lines represent *S. epidermidis*; solid lines represent *S. aureus* ($u_s + u_a$). Different colours of lines indicate different ratios of the adapted fractures of SH1000, 99% grey, 90% green, 80% yellow, 70% dark red, 60% dark green, 50% black, 40% magenta, 30% red, 20% blue, 10% orange, and 1% (initial assumption) light blue lines. The x-axis represents the time in days, and the y-axis is the relative concentrations of the evolved populations. The parameters used in panels (a), (b), and (c) were the same as the parameters in figures (3.16), (3.19), and (3.22), respectively.

199

Days	Controls			
	1 ML	1 ML	1 ML	1 ML
	C-B180	C-B155	C-TU3298	C-SH1000
0	133333333.3	100000000	166666666.7	100000000
1	183333333.3	300000000	366666666.7	183333333.3
2	466666666.7	683333333.3	800000000	283333333.3
3	783333333.3	533333333.3	1366666667	500000000
4	1266666667	1100000000	1566666667	750000000
5	1366666667	1200000000	1433333333	1200000000
6	1666666667	1566666667	1500000000	1333333333
7	1666666667	1333333333	1666666667	1533333333
8	1666666667	1550000000	1750000000	1833333333
9	2166666667	1833333333	2000000000	2166666667
10	2333333333	2166666667	2166666667	2333333333
11	1833333333	2000000000	2500000000	1833333333
12	2083333333	2166666667	2083333333	2666666667
13	2500000000	2333333333	1833333333	2833333333
14	2550000000	2550000000	2300000000	2966666667
15	2333333333	2333333333	2366666667	3050000000
16	2500000000	2250000000	2166666667	3166666667
17	2166666667	2500000000	3000000000	3000000000
18	2083333333	2666666667	3083333333	3166666667
19	2566666667	2850000000	2916666667	3216666667
20	3000000000	3000000000	2666666667	3000000000
21	3000000000	3166666667	3000000000	3166666667
22	3166666667	2833333333	2900000000	3500000000
23	3500000000	2916666667	3166666667	3233333333
24	3166666667	3166666667	2783333333	2833333333
25	3666666667	3216666667	2666666667	3200000000
26	3333333333	3333333333	2333333333	3166666667
27	3000000000	2833333333	3166666667	2833333333
28	3500000000	2833333333	2833333333	3166666667

Table 6.18: **Data presented in figures (4.1).** The controls, where the populations were cultured independently.

1		2		3	
SH1000	B180	SH1000	B180	SH1000	B180
100000000		100000000		100000000	
400000000	233333333.3	316666666.7	133333333.3	433333333.3	200000000
583333333.3	516666666.7	466666666.7	283333333.3	716666666.7	350000000
233333333.3	883333333.3	566666666.7	533333333.3	316666666.7	533333333.3
155000000	1383333333	183333333.3	883333333.3	266666666.7	733333333.3
136666666.7	1366666667	150000000	700000000	150000000	1450000000
126666666.7	1600000000	95000000	1083333333	146666666.7	1600000000
283333333.3	1833333333	83333333.33	1400000000	103333333.3	1433333333
633333333.3	2000000000	73333333.33	1533333333	96666666.67	1766666667
800000000	2500000000	80000000	1833333333	91666666.67	1666666667
1016666667	1666666667	155000000	2333333333	266666666.7	2000000000
1266666667	1466666667	600000000	2333333333	383333333.3	2083333333
1233333333	1550000000	883333333.3	2166666667	1266666667	1433333333
1483333333	1216666667	1116666667	1633333333	1533333333	1283333333
1483333333	600000000	1200000000	1433333333	1516666667	1016666667
1533333333	483333333.3	1833333333	816666666.7	1666666667	800000000
800000000	516666666.7	1600000000	850000000	1483333333	850000000
1183333333	583333333.3	1516666667	700000000	1600000000	900000000
1200000000	366666666.7	2000000000	650000000	1833333333	1016666667
1466666667	483333333.3	2166666667	533333333.3	2166666667	933333333.3
1500000000	350000000	1833333333	466666666.7	2000000000	633333333.3
1433333333	366666666.7	1666666667	683333333.3	2500000000	716666666.7
2333333333	316666666.7	2000000000	650000000	2666666667	550000000
2666666667	333333333.3	2500000000	500000000	2750000000	483333333.3
2000000000	383333333.3	2500000000	466666666.7	2583333333	516666666.7
2500000000	383333333.3	2833333333	400000000	2666666667	600000000
3000000000	250000000	2666666667	283333333.3	2583333333	466666666.7
2833333333	166666666.7	2500000000	350000000	2666666667	433333333.3
2833333333	200000000	2666666667	300000000	2666666667	516666666.7

Table 6.19: **Data presented in figures (4.1a).** The experimental data reports the interactions between low-toxin producing isolates of *Staphylococcus epidermidis* (B180), the invader, and populations of *S. aureus* (SH1000), the resident.

1		2		3	
SH1000	B155	SH1000	B155	SH1000	B155
100000000		100000000		100000000	
283333333.3	166666666.7	350000000	183333333.3	216666666.7	150000000
200000000	283333333.3	366666666.7	283333333.3	383333333.3	216666666.7
200000000	266666666.7	283333333.3	366666666.7	233333333.3	350000000
133333333.3	383333333.3	200000000	433333333.3	200000000	450000000
150000000	600000000	143333333.3	633333333.3	163333333.3	600000000
113333333.3	666666666.7	160000000	716666666.7	148333333.3	816666666.7
120000000	1266666667	128333333.3	933333333.3	160000000	1066666667
90000000	1366666667	143333333.3	1166666667	130000000	1250000000
70000000	1633333333	111666666.7	1500000000	115000000	1600000000
63333333.33	1600000000	101666666.7	1833333333	133333333.3	1350000000
68333333.33	1833333333	80000000	1816666667	216666666.7	1233333333
60000000	1633333333	76666666.67	1600000000	433333333.3	983333333.3
100000000	1833333333	133333333.3	1700000000	716666666.7	766666666.7
183333333.3	2166666667	183333333.3	1666666667	1033333333	883333333.3
366666666.7	2000000000	233333333.3	1433333333	966666666.7	816666666.7
600000000	2166666667	533333333.3	1316666667	1166666667	783333333.3
683333333.3	2666666667	766666666.7	1433333333	1416666667	850000000
633333333.3	1600000000	1166666667	1383333333	1616666667	700000000
766666666.7	1483333333	1833333333	1516666667	1833333333	633333333.3
1033333333	1016666667	2166666667	1266666667	2000000000	683333333.3
1283333333	950000000	2166666667	1100000000	1833333333	600000000
1433333333	1100000000	2333333333	950000000	2166666667	700000000
1550000000	950000000	2000000000	1066666667	2333333333	616666666.7
1833333333	933333333.3	2333333333	966666666.7	2666666667	533333333.3
2666666667	816666666.7	2666666667	916666666.7	2500000000	600000000
2500000000	716666666.7	2833333333	883333333.3	2500000000	666666666.7
3166666667	766666666.7	2833333333	850000000	2583333333	650000000
3000000000	716666666.7	3166666667	833333333.3	2666666667	700000000

Table 6.20: **Data presented in figures (4.1d).** The experimental data reports the interactions between moderate toxicity isolates of *Staphylococcus epidermidis* (B155), the invader, and populations of *S. aureus* (SH1000), the resident.

1		2		3	
SH1000	TU	SH1000	TU	SH1000	TU
100000000		100000000		100000000	
233333333.3	300000000	183333333.3	333333333.3	200000000	350000000
366666666.7	550000000	283333333.3	433333333.3	383333333.3	466666666.7
300000000	783333333.3	233333333.3	550000000	283333333.3	550000000
183333333.3	1083333333	150000000	483333333.3	200000000	850000000
200000000	1050000000	100000000	600000000	150000000	1100000000
150000000	1316666667	110000000	716666666.7	128333333.3	1216666667
146666666.7	1550000000	118333333.3	950000000	136666666.7	1400000000
111666666.7	1516666667	113333333.3	1150000000	126666666.7	1266666667
106666666.7	1600000000	90000000	1233333333	151666666.7	1266666667
96666666.67	1483333333	91666666.67	1433333333	146666666.7	1050000000
91666666.67	1666666667	71666666.67	1516666667	183333333.3	1583333333
96666666.67	1783333333	65000000	1833333333	183333333.3	2166666667
68333333.33	2000000000	80000000	2166666667	183333333.3	1600000000
130000000	1600000000	98333333.33	1833333333	283333333.3	1833333333
126666666.7	1833333333	105000000	1800000000	350000000	1583333333
150000000	1433333333	108333333.3	1633333333	433333333.3	1283333333
266666666.7	1350000000	200000000	1600000000	533333333.3	1316666667
383333333.3	1283333333	516666666.7	1466666667	900000000	1133333333
533333333.3	1133333333	716666666.7	1500000000	916666666.7	966666666.7
733333333.3	1266666667	966666666.7	1266666667	716666666.7	900000000
650000000	966666666.7	933333333.3	966666666.7	1266666667	800000000
850000000	816666666.7	1116666667	1016666667	1483333333	833333333.3
1050000000	933333333.3	1216666667	900000000	1833333333	933333333.3
1216666667	1016666667	1500000000	733333333.3	1750000000	600000000
1433333333	950000000	1350000000	650000000	1633333333	516666666.7
1833333333	1033333333	1816666667	683333333.3	1750000000	483333333.3
1666666667	766666666.7	1833333333	633333333.3	1833333333	500000000
1666666667	733333333.3	1833333333	666666666.7	1833333333	483333333.3

Table 6.21: **Data presented in figures (4.1g).** The experimental data of the interactions between high-toxicity isolates of *Staphylococcus epidermidis* (TU3298), the invader, and populations of *S. aureus* (SH1000), the resident.

1		2		3	
SH1000	B180	SH1000	B180	SH1000	B180
	133333333.3		133333333.3		133333333.3
333333.3333	416666666.7	500000	433333333.3	150000	366666666.7
833333.3333	650000000	10000000	616666666.7	1166666.667	633333333.3
500000	1033333333	50000000	916666666.7	10000000	933333333.3
1666666.667	1250000000	50000000	1100000000	16666666.67	800000000
6666666.667	1300000000	91666666.67	1183333333	35000000	1183333333
50000000	1533333333	233333333.3	1716666667	50000000	1466666667
50000000	1666666667	150000000	2000000000	66666666.67	1666666667
116666666.7	1866666667	183333333.3	1783333333	50000000	1616666667
183333333.3	1550000000	383333333.3	1566666667	83333333.33	1833333333
383333333.3	1166666667	416666666.7	1500000000	50000000	1666666667
366666666.7	1500000000	750000000	1833333333	83333333.33	1650000000
866666666.7	1166666667	1200000000	1666666667	283333333.3	2000000000
1083333333	1666666667	2000000000	1716666667	733333333.3	2166666667
1533333333	1600000000	1666666667	1616666667	1366666667	2000000000
1500000000	1383333333	2000000000	1166666667	1566666667	1833333333
1833333333	1333333333	2000000000	1416666667	1666666667	1633333333
2000000000	1200000000	1916666667	1166666667	1750000000	1266666667
2333333333	1416666667	2166666667	1216666667	2083333333	1416666667
2666666667	1083333333	2583333333	1033333333	3166666667	1066666667
2166666667	833333333.3	2333333333	666666666.7	2916666667	1300000000
2333333333	800000000	3166666667	916666666.7	3116666667	1216666667
2833333333	666666666.7	2916666667	716666666.7	2883333333	1100000000
2833333333	666666666.7	2833333333	650000000	2883333333	1233333333
3500000000	633333333.3	2966666667	650000000	3266666667	1133333333
3250000000	583333333.3	3000000000	750000000	3166666667	816666666.7
3000000000	616666666.7	3016666667	666666666.7	3500000000	800000000
3333333333	533333333.3	3166666667	533333333.3	3283333333	900000000
3166666667	333333333.3	3133333333	550000000	3200000000	383333333.3

Table 6.22: **Data presented in figures (4.1c).** The experimental data represents the mutual invasions of the data presented in Table (6.19) when isolates of *S. aureus* (SH1000) invaded resident populations of *S. epidermidis* (B180) at starting concentrations of 0.01:1.

1		2		3	
SH1000	B155	SH1000	B155	SH1000	B155
	100000000		100000000		100000000
150000	116666666.7	333333.3333	233333333.3	83333.33333	100000000
183333.3333	216666666.7	8333333.333	350000000	333333.3333	266666666.7
666666.6667	283333333.3	16666666.67	600000000	10000000	700000000
2000000	233333333.3	10000000	433333333.3	16666666.67	933333333.3
15000000	433333333.3	83333333.33	700000000	16666666.67	1216666667
33333333.33	516666666.7	150000000	1450000000	50000000	1516666667
83333333.33	866666666.7	166666666.7	1266666667	33333333.33	1316666667
66666666.67	766666666.7	216666666.7	1433333333	50000000	1600000000
116666666.7	1433333333	200000000	1233333333	33333333.33	1483333333
216666666.7	1833333333	416666666.7	1583333333	50000000	1666666667
250000000	2666666667	1166666667	2166666667	250000000	2166666667
350000000	2000000000	1583333333	2666666667	700000000	2666666667
633333333.3	1666666667	2000000000	2500000000	1500000000	2333333333
866666666.7	1600000000	2083333333	2666666667	1700000000	2500000000
1333333333	1200000000	2333333333	1833333333	1566666667	2666666667
1833333333	1100000000	2500000000	1583333333	2166666667	1833333333
2333333333	1366666667	2583333333	1666666667	2583333333	1833333333
2833333333	1283333333	2500000000	1666666667	2750000000	2000000000
3166666667	1233333333	2916666667	1433333333	3200000000	1633333333
2666666667	1050000000	3000000000	1283333333	3333333333	1350000000
3000000000	933333333.3	3166666667	1183333333	3283333333	1566666667
3166666667	800000000	3500000000	1383333333	2883333333	1433333333
2833333333	850000000	2833333333	1266666667	2833333333	1300000000
3000000000	650000000	2966666667	1133333333	3266666667	1333333333
3250000000	766666666.7	3166666667	766666666.7	3500000000	1350000000
3500000000	683333333.3	3016666667	633333333.3	3333333333	1433333333
3166666667	600000000	3333333333	616666666.7	3283333333	933333333.3
3166666667	566666666.7	3250000000	583333333.3	3500000000	850000000

Table 6.23: **Data presented in figures (4.1f).** The experimental data represents the mutual invasions of the data presented in Table (6.20) when isolates of *S. aureus* (SH1000) invaded resident populations of *S. epidermidis* (B155) at starting concentrations of 0.01:1.

1		2		3	
SH1000	TU	SH1000	TU	SH1000	TU
	166666666.7		166666666.7		166666666.7
100000	533333333.3	166666.6667	300000000	100000	316666666.7
500000	466666666.7	833333.3333	600000000	166666.6667	466666666.7
1666666.667	600000000	20000000	700000000	666666.6667	1233333333
10000000	683333333.3	33333333.33	1283333333	3333333.333	1050000000
20000000	1200000000	133333333.3	1133333333	16666666.67	1400000000
30000000	1700000000	33333333.33	1350000000	16666666.67	1283333333
38333333.33	1366666667	50000000	1616666667	25000000	1616666667
50000000	1500000000	216666666.7	1833333333	30000000	1666666667
116666666.7	1833333333	200000000	2166666667	100000000	2166666667
183333333.3	2166666667	233333333.3	2200000000	50000000	2666666667
466666666.7	2833333333	1000000000	1666666667	33333333.33	3500000000
533333333.3	2500000000	1300000000	1466666667	11666666.67	3000000000
1133333333	2666666667	1566666667	1666666667	100000000	2500000000
1500000000	1833333333	1166666667	2166666667	283333333.3	2166666667
2000000000	1500000000	2000000000	1666666667	633333333.3	2500000000
1666666667	1833333333	2666666667	1200000000	1416666667	2833333333
1700000000	1533333333	3000000000	1350000000	1833333333	2333333333
2500000000	1466666667	2833333333	1083333333	2500000000	1833333333
2833333333	1550000000	3166666667	1116666667	2500000000	1533333333
3000000000	1283333333	3333333333	1350000000	2166666667	1416666667
2666666667	1050000000	3500000000	900000000	2833333333	1183333333
3166666667	1350000000	2833333333	1033333333	2666666667	1566666667
3500000000	1150000000	3166666667	716666666.7	3000000000	1066666667
3666666667	700000000	3033333333	916666666.7	2666666667	1233333333
3500000000	833333333.3	2916666667	1000000000	2833333333	866666666.7
3000000000	966666666.7	3500000000	750000000	2833333333	516666666.7
3333333333	733333333.3	3666666667	833333333.3	3166666667	666666666.7
3333333333	800000000	3500000000	883333333.3	3000000000	1016666667

Table 6.24: **Data presented in figures (4.1i).** The experimental data represents the mutual invasions of the data presented in Table (6.21) when isolates of *S. aureus* (SH1000) invaded resident populations of *S. epidermidis* (TU3298) at starting concentrations of 0.01:1.

Days	CSH1000	CB180	CB155	CTU3298
0	150000000	116666666.7	66666666.67	83333333.33
1	166666666.7	333333333.3	216666666.7	316666666.7
2	1116666667	1083333333	233333333.3	1200000000
3	1166666667	1666666667	433333333.3	1833333333
4	2016666667	2233333333	900000000	1500000000
5	966666666.7	1616666667	733333333.3	1016666667
6	1333333333	1200000000	616666666.7	833333333.3
7	883333333.3	1333333333	1000000000	1000000000
8	1583333333	1600000000	500000000	1000000000
9	1966666667	1500000000	583333333.3	1316666667
10	2183333333	1683333333	766666666.7	850000000
11	1633333333	1466666667	1050000000	1383333333
12	1683333333	1466666667	1300000000	1733333333
13	1566666667	1566666667	1516666667	1833333333
14	1800000000	1683333333	1400000000	1666666667
15	1933333333	1633333333	1316666667	1833333333
16	1816666667	1783333333	1516666667	2000000000
17	2000000000	1833333333	1583333333	1833333333
18	2183333333	1733333333	1566666667	1833333333

Table 6.25: **Data presented in figures (4.1b), (4.1e) and (4.1h).** The controls, where the populations were cultured independently.

SH1000(1)	SH1000(2)	SH1000(3)	B180(1)	B180(2)	B180(3)
150000000	150000000	150000000	116666666.7	116666666.7	116666666.7
100000000	66666666.67	83333333.33	83333333.33	50000000	50000000
133333333.3	66666666.67	33333333.33	733333333.3	416666666.7	150000000
150000000	83333333.33	16666666.67	816666666.7	733333333.3	566666666.7
233333333.3	100000000	33333333.33	833333333.3	533333333.3	300000000
16666666.67	133333333.3	33333333.33	350000000	250000000	450000000
200000000	450000000	133333333.3	616666666.7	666666666.7	283333333.3
233333333.3	566666666.7	166666666.7	716666666.7	750000000	666666666.7
200000000	1000000000	283333333.3	600000000	833333333.3	666666666.7
150000000	833333333.3	300000000	616666666.7	833333333.3	333333333.3
1000000000	833333333.3	800000000	583333333.3	800000000	833333333.3
1216666667	1500000000	1566666667	450000000	550000000	350000000
1333333333	1133333333	1483333333	366666666.7	466666666.7	333333333.3
1600000000	1233333333	1600000000	250000000	200000000	283333333.3
1466666667	1400000000	1666666667	233333333.3	300000000	183333333.3
1833333333	1566666667	1833333333	116666666.7	216666666.7	116666666.7
1666666667	1683333333	1666666667	166666666.7	100000000	166666666.7
1666666667	1500000000	1666666667	100000000	166666666.7	166666666.7
1666666667	1833333333	1733333333	116666666.7	100000000	166666666.7

Table 6.26: **Data presented in figures (4.1b).** The obtained experimental data reflects the evolution between the interacting populations of SH1000 and B180, starting from equal initial frequencies.

SH1000(1)	SH1000(2)	SH1000(3)	B155(1)	B155(2)	B155(3)
150000000	150000000	150000000	66666666.67	66666666.67	66666666.67
58333333.33	85000000	83333333.33	216666666.7	23333333.33	33333333.33
116666666.7	11666666.67	450000000	133333333.3	50000000	666666666.7
33333333.33	50000000	100000000	366666666.7	300000000	883333333.3
33333333.33	18333333.33	150000000	133333333.3	333333333.3	866666666.7
100000000	50000000	216666666.7	366666666.7	350000000	883333333.3
83333333.33	100000000	333333333.3	533333333.3	450000000	850000000
200000000	100000000	233333333.3	650000000	516666666.7	966666666.7
266666666.7	166666666.7	200000000	400000000	783333333.3	883333333.3
366666666.7	183333333.3	166666666.7	266666666.7	583333333.3	633333333.3
566666666.7	166666666.7	733333333.3	450000000	433333333.3	733333333.3
466666666.7	183333333.3	1066666667	500000000	483333333.3	916666666.7
1533333333	1616666667	1466666667	350000000	550000000	850000000
2000000000	1500000000	1500000000	166666666.7	616666666.7	833333333.3
1833333333	1750000000	1683333333	250000000	533333333.3	566666666.7
1666666667	2166666667	1333333333	283333333.3	350000000	433333333.3
1850000000	2016666667	1500000000	366666666.7	433333333.3	333333333.3
1633333333	1833333333	2000000000	516666666.7	450000000	516666666.7
1833333333	2333333333	2000000000	366666666.7	516666666.7	500000000

Table 6.27: **Data presented in figures (4.1e).** The obtained experimental data reflects the evolution between the interacting populations of SH1000 and B155, starting from equal initial frequencies.

SH1000(1)	SH1000(2)	SH1000(3)	TU(1)	TU(2)	TU(3)
150000000	150000000	150000000	83333333.33	83333333.33	83333333.33
83333333.33	33333333.33	16666666.67	150000000	100000000	333333333.3
66666666.67	116666666.7	33333333.33	833333333.3	416666666.7	1250000000
16666666.67	83333333.33	16666666.67	1316666667	1433333333	783333333.3
50000000	50000000	116666666.7	500000000	1316666667	1200000000
3333333.333	13333333.33	8333333.333	900000000	1166666667	733333333.3
83333333.33	83333333.33	66666666.67	666666666.7	1350000000	1250000000
116666666.7	50000000	183333333.3	900000000	1150000000	1150000000
33333333.33	83333333.33	200000000	1333333333	1183333333	1000000000
150000000	116666666.7	316666666.7	1700000000	1333333333	1366666667
150000000	133333333.3	350000000	1533333333	1466666667	1400000000
200000000	150000000	183333333.3	1666666667	1483333333	1383333333
1533333333	1450000000	316666666.7	1633333333	983333333.3	1333333333
2000000000	1666666667	1366666667	700000000	633333333.3	1383333333
1966666667	2166666667	1500000000	550000000	733333333.3	866666666.7
2333333333	2166666667	1283333333	500000000	766666666.7	766666666.7
2016666667	2000000000	1700000000	750000000	700000000	833333333.3
1833333333	2166666667	2000000000	966666666.7	850000000	916666666.7
2016666667	2000000000	1666666667	833333333.3	766666666.7	833333333.3

Table 6.28: **Data presented in figures (4.1h).** The obtained experimental data reflects the evolution between the interacting populations of SH1000 and TU3298, starting from equal initial frequencies.

Bibliography

[1] Abell, M., Braselton, J. and Braselton, L., 2006. A model of allelopathy in the context of bacteriocin production. *Applied Mathematics and Computation*, 183(2), pp.916-931.

[2] Adams, E. and Traniello, J., 1981. Chemical interference competition by Monomorium minimum (Hymenoptera: Formicidae). *Oecologia*, 51(2), pp.265-270.

[3] Adams, J., Kinney, T., Thompson, S., Rubin, L. and Helling, R., 1979. Frequency-dependent selection for plasmid-containing cells of *Escherichia coli*. *Genetics*, 91 (4), pp.627-637.

[4] Alex van Belkum, Nelianne J. Verkaik, Corné P. de Vogel, Hélène A. Boelens, Jeroen Verveer, Jan L. Nouwen, Henri A. Verbrugh, Heiman F. L. Wertheim, Reclassification of *Staphylococcus aureus* Nasal Carriage Types, The Journal of *Infectious Diseases*, Volume 199, Pages 1820 – 1826.

[5] J. Alvarez Pedro Jose and Illman, W.A. (2006) *Bioremediation and natural attenuation process fundamentals and mathematical models*. London u.a: Wiley.

[6] Amaral, S., Mathur, D. and Taft, E., 2008. *Advances in fisheries bioengineering*. Bethesda, Md.: American Fisheries Society.

[7] *Antibiotics*, 2021. Acknowledgment to Reviewers of Antibiotics in 2020. 10(2), p.111.

[8] Anton Paar. 2022. *Viscosity of Water – viscosity table and viscosity chart :: Anton Paar Wiki*. [online] Available at: <https://wiki.anton-paar.com/en/water/>

[9] Apte, A.J. (1974) *Systems analysis of ecosystem stability*. Ann Arbor, MI: University Microfilms International.

[10] Ashby M, Petkova A, Hilpert K. Cationic antimicrobial peptides as potential new therapeutic agents in neonates and children: a review. *Curr Opin Infect Dis*. 2014;27(3):258-267.

[11] Bacaer, N. (2011). Lotka, Volterra and the predator-prey system (1920-1926). In: *A Short History of Mathematical Population Dynamics*. Springer, London.

[12] Bacaer, N., 2011. *A Short History of Mathematical Population Dynamics*. London: Springer-Verlag London Ltd.

[13] Bagnoli F, Bertholet S, Grandi G. Inferring reasons for the failure of Staphylococcus aureus vaccines in clinical trials. *Front Cell Infect Microbiol*. 2012.

[14] Balsara, D. and Käppeli, R., 2019. von Neumann stability analysis of globally constraint-preserving DGTD and PNPM schemes for the Maxwell equations using multidimensional Riemann solvers. *Journal of Computational Physics*, 376, pp.1108-1137.

[15] Bao, J., Mao, X., Yin, G. and Yuan, C., 2011. Competitive *Lotka-Volterra* population dynamics with jumps. *Nonlinear Analysis: Theory, Methods & Applications*, 74(17), pp.6601-6616.

[16] Barkley, D., 1991. A model for fast computer simulation of waves in excitable media. Physica D: *Nonlinear Phenomena*, 49(1-2), pp.61-70.

[17] Bauer, T., Ofner, E., Just, H., Just, H. and Daschner, F., 1990. An epidemiological study assessing the relative importance of airborne and direct contact transmission of microorganisms in a medical intensive care unit. *Journal of Hospital Infection*, 15(4), pp.301-309.

[18] Bendahmane, M., Ruiz-Baier, R. and Tian, C., 2015. Turing pattern dynamics and adaptive discretization for a super-diffusive *Lotka-Volterra* model. *Journal of Mathematical Biology*, 72(6), pp.1441-1465.

[19] Bennett, J., Dolin, R. and Blaser, M., 2015. *Mandell, Douglas, and Bennett's Principles and Practice of Infectious Diseases*. Philadelphia, PA: Elsevier.

[20] Bermudez-Brito, M., Plaza-Diaz, J., Munoz-Quezada, S., Gómez-Llorente, C. & Gil, A. Probiotic mechanisms of action. *Ann. Nutr. Metab.* 61, 160–174 (2012).

[21] Berryman, A., 2002. *Population cycles*. Oxford: Oxford University Press.

[22] Blair, E., Emerson, J. and Tull, A., 1967. A New Medium, Salt Mannitol Plasma Agar, for the Isolation of *Staphylococcus aureus*.*American Journal of Clinical Pathology*, 47 (1), p.298.

[23] Bonnet, M., Lagier, J., Raoult, D. and Khelaifia, S., 2020. Bacterial culture through selective and non-selective conditions: the evolution of culture media in clinical microbiology. *New Microbes and New Infections*, 34, p.100622.

[24] Bridges, B., Foster, P. and Timms, A., 2001. Effect of endogenous carotenoids on "adaptive" mutation in Escherichia coli FC40. *Mutation Research/Fundamental and Molecular Mechanisms of Mutagenesis*, 473(1), pp.109-119.

[25] Buchanan RL, Whiting RC, Damert WC (1997) When is simple good enough: a comparison of the Gompertz, Baranyi, and three-phase linear models for fitting bacterial growth curves. *Food Microbiol*14: 313-326.

[26] Byrd, A., Belkaid, Y. and Segre, J., 2018. The human skin microbiome. *Nature Reviews Microbiology*, 16 (3), pp.143-155.

[27] Cakir, Z., 2012. Stability of Difference Schemes for Fractional Parabolic PDE with the Dirichlet-Neumann Conditions. *Abstract and Applied Analysis*, 2012, pp.1-17.

[28] Carroll, K.C. et al. (2019) *Manual of Clinical Microbiology*. Washington, DC: ASM Press.

[29] Centres for Disease Control and Prevention. Antibiotic Resistance Threats in the United States, 2013.

[30] Czárán, T., Hoekstra, R. and Pagie, L., 2002. Chemical warfare between microbes promotes biodiversity. *Proceedings of the National Academy of Sciences*, 99(2), pp.786-790.

[31] Chambers, H.F. and DeLeo, F.R. (2009) "Waves of resistance: *Staphylococcus aureus* in the antibiotic era," *Nature Reviews Microbiology*, 7(9), pp. 629–641.

[32] Chao, L. and Levin, B., 1981. Structured habitats and the evolution of anticompetitor toxins in bacteria. *Proceedings of the National Academy of Sciences*, 78 (10), pp.6324-6328.

[33] Chapman, G., 1945. The Significance of Sodium Chloride in Studies of *Staphylococci*. *Journal of Bacteriology*, 50 (2), pp.201-203.

[34] Chen, S. and Shi, J., 2020. Global dynamics of the diffusive *Lotka-Volterra* competition model with stage structure. *Calculus of Variations and Partial Differential Equations*, 59(1).

[35] Chessa, D., Ganau, G., Spiga, L., Bulla, A., Mazzarello, V., Campus, G. and Rubino, S., 2016. *Staphylococcus aureus* and *Staphylococcus epidermidis* Virulence Strains as Causative Agents of Persistent Infections in Breast Implants. *PLOS ONE*, 11(1), p.e0146668.

[36] Choi CS, Yin CS, Bakar AA, Sakewi Z, Naing NN, Jamal F, Othman N. 2006. Nasal carriage of *Staphylococcus aureus* among healthy adults. *J. Microbiol. Immunol.* 39:458-464.

[37] ClinicalTrials.gov. Evaluation of phage therapy for the treatment of *Escherichia coli* and *Pseudomonas aeruginosa* wound infections in burned patients (PHAGOBURN).

[38] Crank, J. (1956) *The mathematics of Diffusion.* Oxford: Clarendon.

[39] D. Jiang, N. Shi, A note on nonautonomous logistic equation with random perturbation, *Journal of Mathematical Analysis and Applications* 303 (2005) 164–172.

[40] Dagan R, Klugman KP. Impact of conjugate pneumococcal vaccines on antibiotic resistance. *Lancet Infect Dis.* 2008;8(12):785-795.

[41] Dashiff A, Junka RA, Libera M, Kadouri DE. Predation of human pathogens by the predatory bacteria Micavibrio aeruginosavorus and Bdellovibrio bacteriovorus. *J Appl Microbiol.* 2011;110 (2):431-444.

[42] Decoin, V., Barbey, C., Bergeau, D., Latour, X., Feuilloley, M., Orange, N. and Merieau, A., 2014. A Type VI Secretion System Is Involved in Pseudomonas fluorescens Bacterial Competition. *PLoS ONE*, 9 (2), p.e89411.

[43] Dehnel, T., 2010. Reacting to antibiotic resistance. *The Lancet Infectious Diseases*, 10(11), p.746.

[44] Diekema, D.J., et al. 2001. Survey of infections due to *Staphylococcus* species: frequency of occurrence and antimicrobial susceptibility of isolates collected in the United States, Canada, Latin America, Europe, and the Western Pacific region for the Sentry Antimicrobial Surveillance Program, 1997–1999. *Clin. Infect. Dis.* 32(Suppl. 2):S114–S132.

[45] Ditty, J., Mackey, S. and Johnson, C., 2009. *Bacterial circadian programs.* Berlin: Springer.

[46] Dosani, S., 2004. Penicillin Man: Alexander Fleming and the Antibiotic Revolution. *BMJ*, 330(7481), pp.50.2.

[47] Drobyshevich, V., 1994. Difference schemes with different time-steps in subdomains for solving parabolic equations. *Russian Journal of Numerical Analysis and Mathematical Modelling*, 9 (5).

[48] Dufour, P., Jarraud, S., Vandenesch, F., Greenland, T., Novick, R., Bes, M., Etienne, J. and Lina, G., 2002. High Genetic Variability of the agr Locus in *Staphylococcus* Species. *Journal of Bacteriology*, 184 (4), pp.1180-1186.

[49] ECDC, E., 2009. The bacterial challenge: time to react. *Stockholm: European Center for Disease Prevention and Control.*

[50] Elmesseri, R., Saleh, S., Elsherif, H., Yahia, I. and Aboshanab, K., 2022. Staphyloxanthin as a Potential Novel Target for Deciphering Promising Anti-*Staphylococcus aureus* Agents.*Antibiotics*, 11 (3), p.298.

[51] Everett B. S. & Shrondal A. (2010.) *The Cambridge Dictionary of Statistics*, 4e, Cambridge University Press, Cambridge, United Kingdom.

[52] Examples of how antibiotic resistance spreads. (2013). [image] Available at: https://articles.mercola.com/sites/articles/archive/2014/04/23/agricultural-antibiotic-overuse.aspx [Accessed 3 Jul. 2018].

[53] Fahnoe KC, Flanagan ME, Gibson G, Shanmugasundaram V, Che Y, Tomaras AP. Nontraditional antibacterial screening approaches for the identification of novel inhibitors of the glyoxylate shunt in gram-negative pathogens. *PLoS One.* 2012;7(12):e51732.

[54] Fife, P., 1979. *Mathematical Aspects of Reacting and Diffusing Systems.* Berlin, Heidelberg: Springer Berlin / Heidelberg.

[55] Fisher, R., 1937. The wave of advance of advantageous genes. *Annals of Eugenics*, 7(4), pp.355-369.

[56] Fisher, R., 1950. *Contributions to mathematical statistics.* New York: Wiley.

[57] Flannagan, S. and Clewell, D., 2002. Identification and characterization of genes encoding sex pheromone cAM373 activity in *Enterococcus faecalis* and *Staphylococcus aureus. Molecular Microbiology*, 44(3), pp.803-817.

[58] Fleming, V., Feil, E., Sewell, A., Day, N., Buckling, A. and Massey, R., 2006. Agr Interference between Clinical *Staphylococcus aureus* Strains in an Insect Model of Virulence. *Journal of Bacteriology*, 188 (21), pp.7686-7688.

[59] Fontana, M., de Bastos, M. and Brandelli, A., 2006. Bacteriocins Pep5 and *Epidermin* Inhibit *Staphylococcus epidermidis* Adhesion to Catheters. *Current Microbiology*, 52 (5), pp.350-353.

[60] Fowler VG, Allen KB, Moreira ED, et al. Effect of an investigational vaccine for preventing *Staphylococcus aureus* infections after cardiothoracic surgery: a randomized trial. *JAMA*. 2013;309 (13): 1368-1378.

[61] Frank DN, Feazel LM, Bessesen MT, Price CS, Janoff EN, Pace NR. 2010. The human nasal microbiota and *Staphylococcus aureus* carriage. *PLoS One* 5:e10598.

[62] Freeman-Cook, L. and Freeman-Cook, K., 2008. *Staphylococcus aureus infections*. Philadelphia, PA: Chelsea.

[63] Freney, J. et al. Recommended minimal standards for description of new staphylococcal species. Subcommittee on the taxonomy of staphylococci and streptococci of the International Committee on Systematic Bacteriology. *Int. J. Syst. Bacteriol.* 49, 489–502 (1999).

[64] G. Hu, K. Wang, On stochastic logistic equation with Markovian switching and white noise,*Osaka J. Math.* (2010) (preprint).

[65] Gaur RK. Antibiotic resistance: Alternative approaches. *Indian J Pharmacol*. 2017; 49 (2): 208-210.

[66] Gefen, O. et al., 2017. TDtest: Easy detection of bacterial tolerance and persistence in clinical isolates by a modified disk-diffusion assay. *Scientific Reports*, 7 (1).

[67] Ghabban, H.A. (2019) *Competition of Staphylococci as probe for novel antibiotics*. dissertation.

[68] Gibson AM, Baranyi J, Pitt JI, Eyles MJ, Roberts TA (1994) Predicting fungal growth: the effect of water activity on Aspergillus flavus and related species. *Int J Food Microbiol* 23: 419-431.

[69] Gill, S. R. et al. Insights on evolution of virulence and resistance from the complete genome analysis of an early methicillin-resistant *Staphylococcus aureus* strain and a biofilm-producing methicillin resistant *Staphylococcus epidermidis* strain. *J. Bacteriol.* 187, 2426–2438 (2005).

[70] Gomulkiewicz, R., Holt, R. and Barfield, M., 1999. The Effects of Density Dependence and Immigration on Local Adaptation and Niche Evolution in a Black-Hole Sink Environment. *Theoretical Population Biology*, 55 (3), pp. 283-296.

[71] Gourbeyre, P., Denery, S. & Bodinier, M. Probiotics, prebiotics, and synbiotics: impact on the gut immune system and allergic reactions. *J. Leukoc. Biol.* 89, 685–695 (2011).

[72] Grice, E. and Segre, J., 2011. The skin microbiome. *Nature Reviews Microbiology*, 9 (4), pp.244-253.

[73] Grindrod, P. and Grindrod, P., 1996. *The theory and applications of reaction-diffusion equations*. Oxford: Clarendon Press.

[74] Guarner, F. & Malagelada, J. R. Gut fora in health and disease. *Lancet* 361, 512–519 (2003).

[75] Gurcan, F., Kaya, G. and Kartal, S., 2019. Conformable Fractional Order *Lotka-Volterra* Predator–Prey Model: Discretization, Stability and Bifurcation. *Journal of Computational and Nonlinear Dynamics*, 14 (11).

[76] Habets, M., Czárán, T., Hoekstra, R. and de Visser, J., 2007. Spatial structure inhibits the rate of invasion of beneficial mutations in asexual populations. *Proceedings of the Royal Society B: Biological Sciences*, 274 (1622), pp. 2139-2143.

[77] Habets, M. G. J. L., Rozen, D. E., Hoekstra, R. F. & de Visser, J. A. G. M. 2006 The effect of population structure on the adaptive radiation of microbial populations evolving in spatially structured environments.*Ecol. Lett.* 9, 1041–1048.

[78] Hancock REW, Nijnik A, Philpott DJ. Modulating immunity as a therapy for bacterial infections. *Nat Rev Microbiol*. 2012; 10 (4): 243-254.

[79] Hardin, G. (1968). The Tragedy of the Commons. *Science* 162, 1243-1248.

[80] Harrison, F., Paul, J., Massey, R. and Buckling, A., 2007. Interspecific competition and siderophore-mediated cooperation in Pseudomonas aeruginosa. *The ISME Journal*, 2 (1), pp. 49-55.

[81] Harvard Publishing.*Deviated Septum - Harvard Health*.[online] Available at: https://www.health.harvard.edu/diseases-and-conditions/deviated-septum.

[82] Héchard, Y. and Sahl, H., 2002. Mode of action of modified and unmodified bacteriocins from Gram-positive bacteria. *Biochimie*, 84 (5-6), pp. 545-557.

[83] Heilman C. Vaccines: an innovative approach to combating antimicrobial resistance. Published July 2015.

[84] Henrichsen, J., 1972. Bacterial surface translocation: a survey and a classification. *Bacteriological Reviews*, 36 (4), pp. 478-503.

[85] Hiramatsu, K., et al. 1997. Methicillin-resistant *Staphylococcus aureus* clinical strain with reduced vancomycin susceptibility. *J. Antimicrob. Chemother.* 40:135–136.10.

[86] Hoffman, A. (1991) "Testing the red queen hypothesis," *Journal of Evolutionary Biology*, 4(1), pp. 1–7.

[87] Holscher, T. & amp; Kovács, Á.T., 2017. Sliding on the surface: Bacterial spreading without an active motor. *Environmental Microbiology*, 19 (7), pp. 2537–2545.

[88] Holt, R. and Gaines, M., 1992. Analysis of adaptation in heterogeneous landscapes: Implications for the evolution of fundamental niches. *Evolutionary Ecology*, 6(5), pp. 433-447.

[89] Holt, R., Gomulkiewicz, R. and Barfield, M., 2003. The phenomenology of niche evolution via quantitative traits in a 'black-hole' sink. *Proceedings of the Royal Society of London. Series B: Biological Sciences*, 270 (1511), pp. 215-224.

[90] Hsu, S. and Waltman, P., 1998. Competition in the chemostat when one competitor produces a toxin. *Japan Journal of Industrial and Applied Mathematics*, 15 (3), pp. 471-490.

[91] Hsu, S. and Waltman, P., 2004. A survey of mathematical models of competition with an inhibitor. *Mathematical Biosciences*, 187 (1), pp. 53-91.

[92] Ingraham JL, Maaloe O, Neidhardt FC (1983) *Growth of the bacterial cell*. Sinauer Associates, Sunderland.

[93] Ingraham, J. and Ingraham, C., 2000. *Introduction to microbiology*. Pacific Grove, CA: Brooks/Cole.

[94] Ito, K. and Kappel, F., 2002. *Evolution Equations and Approximations*. Singapore: World Scientific Publishing Company.

[95] Iwasa, Y., Nakamaru, M. and Levin, S., 1998. Allelopathy of bacteria in a lattice population: Competition between colicin-sensitive and colicin-producing strains. *Evolutionary Ecology*, 12 (7), pp. 785-802.

[96] Iwase, Tadayuki et al. "*Staphylococcus epidermidis* Inhibits *Staphylococcus aureus* Biofilm Formation And Nasal Colonization". *Nature*, 465.7296 (2010): 346 – 349. Web.

[97] *JAC-Antimicrobial Resistance*, 2019. Antimicrobial resistance and infections. 1 (2).

[98] Jack, R., Tagg, J. and Ray, B., 1995. Bacteriocins of gram-positive bacteria. *Microbiological reviews* , 59 (2), pp. 171-200.

[99] Jarraud, S., Lyon, G., Figueiredo, A., Lina, G., Vandenesch, F., Etienne, J., Muir, T. and Novick, R., 2011. Exfoliatin-Producing Strains Define a Fourth agr Specificity Group in *Staphylococcus aureus. Journal of Bacteriology*, 193 (24), pp. 7027-7027.

[100] Ji, G., Beavis, R. and Novick, R., 1997. Bacterial Interference Caused by Autoinducing Peptide Variants. *Science*, 276 (5321), pp. 2027-2030.

[101] *Journal of Global Antimicrobial Resistance*, 2019. The Journal of Global Antimicrobial Resistance meets the World Health Organization (WHO). 18, pp. 305-308.

[102] Kamada, N., Chen, G. Y., Inohara, N. & Nunez, G. Control of pathogens and pathobionts by the gut microbiota. *Nat. Immunol.* 14, 685-690 (2013).

[103] Kim, J. and Kim, K., 2017. Effects of minimal media vs. complex media on the metabolite profiles of *Escherichia coli* and *Saccharomyces cerevisiae. Process Biochemistry*, 57, pp. 64-71.

[104] Kingsland S. Alfred J. *Lotka* and the origins of theoretical population ecology. *Proc Natl Acad Sci U S A*. 2015 Aug 4; 112 (31): 9493-5.

[105] Kirby, B., 2010. *Micro- and Nanoscale Fluid Mechanics*. Cambridge: Cambridge University Press.

[106] Kluytmans J, van Belkum A, Verbrugh H. 1997. Nasal carriage of *Staphylococcus aureus*: epidemiology, underlying mechanisms, and associated risks. *Clin. Microbial. Rev.* 10: 505-520.

[107] Kolmogoroff, A. (1937). Zur Umkehrbarkeit der statistischen Naturgesetze. *Mathematische Annalen*, 113 (1), pp. 766-772.

[108] Kolmogorov, A.N., Petrovsky, I.G. and Piskunov, N.S. (1937) Investigation of the Equation of Diffusion Combined with Increasing of the Substance and Its Application to a Biology Problem. Bulletin of Moscow State University Series A: Mathematics and Mechanics, 1, 1-25.

[109] Konangi, S., Palakurthi, N. and Ghia, U., 2018. von Neumann stability analysis of first-order accurate discretization schemes for one-dimensional (1D) and two-dimensional (2D) fluid flow equations. *Computers & Mathematics with Applications*, 75 (2), pp. 643-665.

[110] Korona, R., Nakatsu, C. H., Forney, L. J. & Lenski, R. E. 1994 Evidence for multiple adaptive peaks from populations of bacteria evolving in a structured habitat. *Proc. Natl Acad. Sci. USA* 91, 9037–9041.

[111] Kovarova-Kovar, K. and Egli, T., 1998. Growth Kinetics of Suspended Microbial Cells: From Single-Substrate-Controlled Growth to Mixed-Substrate Kinetics. *Microbiology and Molecular Biology Reviews*, 62 (3), pp. 646-666.

[112] Kreft, J., 2004. Biofilms promote altruism. *Microbiology*, 150 (8), pp. 2751-2760.

[113] Labrum, E., 1953. The Effect of Generation Time on the Delayed Appearance of Induced Mutants in *Escherichia Coli. Proceedings of the National Academy of Sciences*, 39 (12), pp. 1221-1227.

[114] Laitila, J. and Moilanen, A., 2013. Approximating the dispersal of multi-species ecological entities such as communities, ecosystems or habitat types. *Ecological Modelling*, 259, pp. 24-29.

[115] Leão, P., Vasconcelos, M. and Vasconcelos, V., 2009. Allelopathy in freshwater cyanobacteria. *Critical Reviews in Microbiology*, 35 (4), pp. 271-282.

[116] leavingcertbiology (2018). *Binary Fission*. [image] Available at: http://www.leavingcertbiology.net/chapter-20-kingdom-monera.html.

[117] leavingcertbiology (2018). *Growth curve of microorganisms*. [image] Available at: http://www.leavingcertbiology.net/chapter-20-kingdom-monera.html.

[118] Lenski, R. and Hattingh, S., 1986. Coexistence of two competitors on one resource and one inhibitor: A chemostat model based on bacteria and antibiotics. *Journal of Theoretical Biology*, 122 (1), pp. 83-93.

[119] Levin, B. and Udekwu, K., 2010. Population Dynamics of Antibiotic Treatment: a Mathematical Model and Hypotheses for Time-Kill and Continuous-Culture Experiments. *Antimicrobial Agents and Chemotherapy*, 54 (8), pp.- 3414-3426.

[120] Li H, Xie G, Edmondson A (2007) Evolution and limitations of primary mathematical models in predictive microbiology. *Br Food J* 109: 608-626.

[121] Libberton, B., Coates, R., Brockhurst, M. and Horsburgh, M., 2014. Evidence that Intraspecific Trait Variation among Nasal Bacteria Shapes the Distribution of *Staphylococcus aureus. Infection and Immunity*, 82 (9), pp. 3811-3815.

[122] Libberton, B., Horsburgh, M. and Brockhurst, M. (2015). The effects of spatial structure, frequency dependence and resistance evolution on the dynamics of toxin-mediated microbial invasions. *Evolutionary Applications*, 8 (7), pp. 738 – 750.

[123] Licata, N., Mohari, B., Fuqua, C. and Setayeshgar, S., 2016. Diffusion of Bacterial Cells in Porous Media. *Biophysical Journal*, 110 (1), pp. 247-257.

[124] Lina, G., Boutite, F., Tristan, A., Bes, M., Etienne, J. and Vandenesch, F. (2003). Bacterial Competition for Human Nasal Cavity Colonization: Role of *Staphylococcal* agr Alleles. *Applied and Environmental Microbiology*, 69 (1), pp. 18-23.

[125] Ling LL, Schneider T, Peoples AJ, et al. A new antibiotic kills pathogens without detectable resistance. *Nature*. 2015; 517 (7535): 455-459.

[126] Lowy, F. D. *Staphylococcus aureus* infections. *N. Engl. J. Med*. 339, 520–532 (1998).

[127] Lowy, F., 2003. Antimicrobial resistance: the example of *Staphylococcus aureus*. *Journal of Clinical Investigation*, 111 (9), pp. 1265-1273.

[128] Lubelchek, R. (2008). Arms Race With a Superbug — *NOVA | PBS*. [online] Pbs.org.

[129] M. Liu, K. Wang, Persistence and extinction in stochastic non-autonomous logistic systems, *Journal of Mathematical Analysis and Applications* 375 (2011) 443–457.

[130] Macpherson, A. J. & Harris, N. L. Interactions between commensal intestinal bacteria and the immune system. *Nat. Rev. Immunol*. 4, 478-485 (2004).

[131] Majeed, H., Gillor, O., Kerr, B. and Riley, M., 2010. Competitive interactions in *Escherichia coli* populations: the role of bacteriocins. *The ISME Journal*, 5 (1), pp. 71-81.

[132] Manges AR, Steiner TS, Wright AJ. Fecal microbiota transplantation for the intestinal decolonization of extensively antimicrobial resistant opportunistic pathogens: a review. *Infect Dis*. 2016; 48 (8): 587-592.

[133] Mashburn, L., Jett, A., Akins, D. and Whiteley, M., 2005. *Staphylococcus aureus* Serves as an Iron Source for *Pseudomonas aeruginosa* during In Vivo Co-culture. *Journal of Bacteriology*, 187 (2), pp. 554-566.

[134] Massey, R., Horsburgh, M., Lina, G., Höök, M. and Recker, M., 2006. The evolution and maintenance of virulence in *Staphylococcus aureus*: a role for host-to-host transmission?. *Nature Reviews Microbiology*, 4 (12), pp. 953-958.

[135] Mattsson, K. and Rydin, Y., 2022. Implicit Summation by Parts Operators for Finite Difference Approximations of First and Second Derivatives. *SSRN Electronic Journal*

[136] Mazumdar, P., 1984. Fleming as Bacteriologist: Alexander Fleming. *Science*, 225 (4667), pp. 1140-1140.

[137] Evans, G.A., Blackledge, J.M. and Yardley, P.D. (2001) *Numerical methods for partial differential equations*. Berlin: Springer.

[138] McKellar RC, Lu X (eds) (2004) Modeling microbial responses in foods. *CRC Press, Boca Raton*.

[139] McPeek, M.A. (2017) *Evolutionary community ecology*. Princeton, NJ: Princeton University Press.

[140] Milne, W., 1949. *Numerical calculus*. Princeton: Princeton University Press.

[141] Milo, R., Phillips, R. and Orme, N. (2016) *Cell biology by the numbers*. New York, N.Y: Garland Science, Taylor & Francis Group.

[142] Mitchell, D., von Meien, O., Krieger, N. and Dalsenter, F., 2004. Recent developments in modeling of microbial growth kinetics and intraparticle phenomena in solid state fermentation. *ChemInform*, 35 (27).

[143] Moran, J., Crank, E., Ghabban, H. and Horsburgh, M., 2016. Deferred growth inhibition assay to quantify the effect of bacteria-derived antimicrobials on competition. *Journal of Visualized Experiments*, 115.

[144] Moran, J.C. & amp; Horsburgh, M.J., 2016. Whole-genome sequence of *Staphylococcus epidermidis* TU3298. *Genome Announcements*, 4 (2).

[145] Morin, P. J. (1999). *Community Ecology*. England: Blackwell Science.

[146] Morton, K. W., & Mayers, D. F. (2010). *Numerical solution of partial differential equations: An introduction*. Cambridge University Press.

[147] Muhammad haji, A., Halik, A. and Li, H., 2021. Dynamics in a ratio-dependent *Lotka-Volterra* competitive-competitive-cooperative system with feedback controls and delays. *Advances in Difference Equations*, 2021 (1).

[148] Murray, J., 2003. *Mathematical biology*. New York: Springer.

[149] Mylotte, J., McDermott, C. and Spooner, J., 1987. Prospective study of 114 consecutive episodes of *Staphylococcus aureus* bacteremia. *Clinical Infectious Diseases*, 9 (5), pp. 891-907.

[150] Nakayama, J., Igarashi, S., Nagasawa, H., Clewell, D., An, F. and Suzuki, A., 1996. Isolation and structure of staph-cAM373 produced by *Staphylococcus aureus* that induces conjugal transfer of *Enterococcus faecalis* Plasmid pAM373. *Bioscience, Biotechnology, and Biochemistry*, 60 (6), pp. 1038-1039.

[151] Nascimento, J. D., M. L. V. Coelho, H. Ceotto, A. Potter, L. R. Fleming, Z. Salehian, I. F. Nes et al. 2012. Genes involved in immunity to and secretion of *aureocin* A53, an atypical class II bacteriocin produced by *Staphylococcus aureus* A53. *Journal of Bacteriology* 194: 875–883.

[152] Neumann, G. and Schuster, S., 2007. Continuous model for the rock–scissors–paper game between bacteriocin producing bacteria. *Journal of Mathematical Biology*, 54 (6), pp. 815-846.

[153] Nguyen, D. and Yin, G., 2017. Coexistence and exclusion of stochastic competitive *Lotka-Volterra* models. *Journal of Differential Equations*, 262 (3), pp. 1192-1225.

[154] Novick, A., 1955. Growth of Bacteria. *Annual Review of Microbiology*, 9 (1), pp. 97-110.

[155] Olsen K, Falch BM, Danielsen K, Johannessen M, Sollid JUE, Thune I, Grimnes G, Jorde R, Simonsen GS, Furberg AS. 2012. *Staphylococcus aureus* nasal carriage is associated with serum 25- hydroxyvitamin D levels, gender and smoking status. The Tromso *Staph* and Skin Study. *Eur. J. Clin. Microbiol.* (31), pp. 465-473.

[156] Pankowski, J.A., Puckett, S.M. and Nano, F.E. (2016) "Temperature sensitivity conferred by *liga* alleles from psychrophilic bacteria upon substitution in mesophilic bacteria and a yeast species," *Applied and Environmental Microbiology*, 82 (6), pp. 1924–1932.

[157] Patel SJ, Saiman L. Antibiotic resistance in neonatal intensive care unit pathogens: mechanisms, clinical impact, and prevention including antibiotic stewardship. *Clin Perinatol*. 2010; 37 (3) :547–63.

[158] Pegu A, Asokan M, Wu L, et al. Activation and lysis of human CD4 cells latently infected with HIV-1. *Nat Commun*.

[159] Peleg M, Corradini MG (2011) Microbial growth curves: what the models tell us and what they cannot. *Crit Rev Food Sci Nutr* 51: 917-945.

[160] Peltola, H. (2000) "Worldwide *haemophilus influenzae* type b disease at the beginning of the 21st Century: Global analysis of the disease burden 25 years after the use of the polysaccharide vaccine and a decade after the advent of conjugates," *Clinical Microbiology Reviews*, 13 (2), pp. 302–317.

[161] Perez-Rodriguez F, Valero A (2013) *Predictive microbiology in foods*. Springer, New York.

[162] Perl TM, Cullen JJ, Wenzel RP, Zimmerman MB, P faller MA, Sheppard D, Twombley J, French PP, Herwaldt LA, Mupirocin and the Risk of *Staphylococcus aureus* study team. 2002. Intranasal mupirocin to prevent postoperative *Staphylococcus aureus* infections. *N. Engl. J. Med.* 346: 1871-1877.

[163] Perron, G., Gonzalez, A. and Buckling, A., 2008. The rate of environmental change drives adaptation to an antibiotic sink. *Journal of Evolutionary Biology*, 21 (6), pp. 1724-1731.

[164] Peschel, A., Schnell, N., Hille, M., Entian, K. and Götz, F., 1997. Secretion of the *lantibiotics epidermin* and *gallidermin*: sequence analysis of the genes gdmT and gdmH, their influence on *epidermin* production and their regulation by *EpiQ. Molecular and General Genetics MGG*, 254 (3), pp. 312-318.

[165] Piewngam, P., Zheng, Y., Nguyen, T., Dickey, S., Joo, H., Villaruz, A., Glose, K., Fisher, E., Hunt, R., Li, B., Chiou, J., Pharkjaksu, S., Khongthong, S., Cheung, G., Kiratisin, P. and Otto, M., 2018. Pathogen elimination by probiotic *Bacillus* via signalling interference. *Nature*, 562 (7728), pp. 532-537.

[166] Pizarro-Cerdá, J. and Cossart, P., 2006. Bacterial Adhesion and Entry into Host Cells. *Cell*, 124 (4), pp. 715-727.

[167] President's Council of Advisors on Science and Technology. Report to the President on combating antibiotic resistance.

[168] Press, M., Brown, N. and Barker, M., 1997. Photosynthetic characteristics of dipterocarp seedlings in three tropical rain forest light environments: a basis for niche partitioning?. *Oecologia*, 112 (4), pp. 453-463.

[169] Prestinaci, F., Pezzotti, P., & Pantosti, A. (2015). Antimicrobial resistance: a global multifaceted phenomenon. *Pathogens and global health*, 109 (7), 309–318.

[170] Pugliese, G. and Favero, M. (2001). Nasal Carriage as a Source of *Staphylococcus aureus* Bacteremia. *Infection Control & Hospital Epidemiology*, 22 (3), p. 185.

[171] Pugliese, G. and Favero, M. (2002). Intranasal Mupirocin to Prevent Postoperative *Staphylococcus aureus* Infections. *Infection Control & Hospital Epidemiology*, 23 (9), pp. 553-553.

[172] Quadram Institute. 2022. *Home - Quadram Institute.* [online] Available at: <https://quadram.ac.uk.

[173] Rainey, P. B. & Travisano, M. 1998 Adaptive radiation in a heterogeneous environment. *Nature* 394, 69–72

[174] Rao N, Cannella B, Crossett LS, Yates AJ, McGough R. 2008. A preoperative decolonization protocol for *Staphylococcus aureus* prevents orthopaedic infections. *Clin. Orthop. Rel. Res.* 466: 1343-1348.

[175] Rasool, K. and Wimpenny, J., 1982. Mixed continuous culture experiments with an antibiotic-producing *streptomycete* and *Escherichia coli*. *Microbial Ecology*, 8 (3), pp. 267-277.

[176] Rice, S., 2017. Interactions between microbial community members. *Environmental Microbiology Reports*, 9 (5), pp. 471-473.

[177] Ricker, W.E. (1979) *Growth rates and models.* In: Hoar, W.S., Randall, D.J. and Brett, J.R., Eds., Fish Physiology, III, Bioenergetics and Growth, Academic Press, New York, 677-743.

[178] Robinson, A., Ryu, D., Moller, G., Smith, B. and Abatzoglou, J., n.d. *Interdisciplinary approaches in food safety to expand mycotoxin detection, compare bacterial transfer rates, and forecast fungal inoculum under climate change.*

[179] Romsics, C., Makk, J., Palatinszky, M., Ács, É. and Jáger, K. (2013). Strain culture and cultivation-based techniques. In: *Practical Microbiology based on the Hungarian practical notes entitled "Mikrobiológiai Laboratóriumi Gyakorlatok".*

[180] Royama, T., 1992. *Analytical population dynamics.* London: Chapman & Hall.

[181] Sassone-Corsi, M. et al. (2016) "Microcins mediate competition among Enterobacteriaceae in the inflamed gut, *Nature*, 540 (7632), pp. 280–283.

[182] Schuch R, Lee HM, Schneider BC, et al. Combination therapy with lysin CF-301 and antibiotic is superior to antibiotic alone for treating methicillin-resistant *Staphylococcus aureus* induced murine bacteremia. *J Infect Dis.* 2014; 209 (9): 1469-1478.

[183] Stannard, D. (2014) "Procalcitonin to initiate or discontinue antibiotics in acute respiratory tract infections, *Critical Care Nurse*, 34 (2), pp. 75–76.

[184] Phoenix, D., Dennison, S.R. and Harris, F. (2013) *Antimicrobial peptides*. Weinheim: Wiley-VCH Verlag GmbH & Co. Kgaa.

[185] Shankar, P., 2016. Book review: Tackling drug-resistant infections globally. *Archives of Pharmacy Practice*, 7 (3), p. 110.

[186] Shui, Jr-Wen et al. "HVEM Signalling At Mucosal Barriers Provides Host Defence Against Pathogenic Bacteria". *Nature*, 488.7410 (2012): $222 - 225$. Web.

[187] Sieuwerts, S., de Bok, F., Mols, E., de Vos, W. and van Hylckama Vlieg, J., 2008. A simple and fast method for determining colony forming units. *Letters in Applied Microbiology*, 47 (4), pp. 275-278.

[188] Slopek S, Weber-Dabrowska B, Dabrowski M, Kucharewicz-Krukowska A. Results of bacteriophage treatment of suppurative bacterial infections in the years 1981-1986. *Arch Immunol Ther Exp (Warsz)*. 1987; 35 (5): 569-583.

[189] Sokolov, M., 2020. Kinematic viscosity vs temperature of fresh water: comparison of representation methods. *Transactions of the Krylov State Research Centre*, 1 (391), pp. 42-49.

[190] Spellberg, B., 2008. Antibiotic resistance and antibiotic development. *The Lancet Infectious Diseases*, 8 (4), pp. 211-212.

[191] Stoll BJ, Hansen NI, Bell EF, Shankaran S, Laptook AR, Walsh MC, et al. Neonatal outcomes of extremely preterm infants from the NICHD Neonatal Research Network. *Pediatrics*. 2010; 126 (3): 443–56.

[192] Tang, B. and Wolkowicz, G., 1992. Mathematical models of microbial growth and competition in the chemostat regulated by cell-bound extracellular enzymes. *Journal of Mathematical Biology*, 31 (1), pp. 1-23.

[193] Taylor & Francis. 2022. Alexander Fleming: Darvel and Antibiotics. *Journal of Biological Education*, 40 (3), pp. 141-144.

[194] Thambynayagam, R., 2011. *The diffusion handbook*. New York: McGraw-Hill.

[195] Tilman, D., 2020. *In Resource Competition and Community Structure.*, Volume 17. Princeton university press.

[196] Topsall, J., 1992. Basic Laboratory Procedures in Clinical Bacteriology. *Pathology*, 24 (4), p. 321.

[197] Tortora, G.J., Funke, B.R. and Case, C.L. (2021) *Microbiology: An introduction.* Harlow: Pearson Education Limited.

[198] Uehara, Y., Nakama, H., Agematsu, K., Uchida, M., Kawakami, Y., Abdul Fattah, A. S. M. & Maruchi, N. (2000). Bacterial interference among nasal inhabitants: eradication of *Staphylococcus aureus* from nasal cavities by artificial implantation of *Corynebacterium* sp. *J Hosp Infect* 44, 127-133.

[199] US Food and Drug Administration. Guidance for industry: early clinical trials with live bio-therapeutic products: chemistry, manufacturing, and control information. http://www.fda.gov /downloads/BiologicsBloodVaccines/Guidance -ComplianceRegulatoryInformation/Guidances /General/UCM292704.pdf. Published February 2012.

[200] Usher, M. and Williamson, M., 1974. *Ecological stability*. London: Chapman and Hall.

[201] Van Belkum A, Emonts M, Wertheim H, de Jongh C, Nouwen J, Bartels H, Cole A, Cole A, Hermans P, Boelens H, Toom NL, Snijders S, Verbrugh H, van Leeuwen W. 2007. The role of human innate immune factors in nasal colonization by *Staphylococcus aureus*. *Microbes Infect*. 9: 1471-1477.

[202] van Belkum A, Verkaik NJ, de Vogel CP, Boelens HA, Verveer J, Nouwen JL, Verbrugh HA, and Wertheim HF. 2009. Reclassification of *Staphylococcus aureus* nasal carriage types. *J. Infect. Dis.* 199: 1820–1826.

[203] van Opheusden, J., Hemerik, L., van Opheusden, M. and van der Werf, W., 2015. Competition for resources: complicated dynamics in the simple Tilman model. *SpringerPlus*, 4 (1).

[204] Vandermeer, J. (2010) How Populations Grow: The Exponential and Logistic Equations.*Nature Education Knowledge* 3 (10): 15

[205] Vasiev, B. and Weijer, C., 1999. Modelling Chemotactic Cell Sorting during Dictyostelium discoideum Mound Formation. *Biophysical Journal*, 76 (2), pp. 595-605.

[206] Verhulst, P.-F. "Recherches mathématiques sur la loi d'accroissement de la population." *Nouv. mém. de l'Academie Royale des Sci. et Belles-Lettres de Bruxelles*, 18, 1-41.

[207] Vito Volterra. Fluctuations in the abundance of a species considered mathematically. *Nature*, 118 (2972): 558–560, Oct 1926.

[208] Volterra, V.I.T.O. (1927) "Fluctuations in the abundance of a species considered mathematically," *Nature*, 119 (2983), pp. 12–13.

[209] Von Eiff C, Becker K, Machka K, Stammer H, Peters G. 2001. Nasal carriage as a source of *Staphylococcus aureus* bacteraemia. *N. Engl. J. Med.* 344: 11-16.

[210] von Eiff, C., Peters, G. & Heilmann, C. Pathogenesis of infections due to coagulase-negative *staphylococci. Lancet Infect. Dis.* 2, 677–685 (2002).

[211] Wei, Y., Wang, X., Liu, J., Nememan, I., Singh, A., Weiss, H. and Levin, B., 2011. The population dynamics of bacteria in physically structured habitats and the adaptive virtue of random motility. *Proceedings of the National Academy of Sciences*, 108 (10), pp. 4047-4052.

[212] Wos Oxley ML, Plumeier I, von Eiff C, Taudien S, Platzer M, Vilchez Vargas R, Becker K, Pieper DH. 2010. A poke into the diversity and associations within human anterior nare microbial communities. *ISME J.* 4: 839-851.

[213] Wright A, Hawkins CH, Anggard EE, Harper DR. A controlled clinical trial of a therapeutic bacteriophage preparation in chronic otitis due to antibiotic-resistant *Pseudomonas aeruginosa*: a preliminary report of efficacy. *Clin Otolaryngol.* 2009; 34 (4): 349-357.

[214] Mao, X., 2011. Stochastic Delay Population Systems. *Stochastic Differential Equations and Applications*, pp. 377-408.

[215] X. Mao, C. Yuan, Stochastic Differential Equations with Markovian Switching,*Imperial College Press.* 2006.

[216] X. Mao, G. Marion, E. Renshaw, Environmental noise suppresses explosion in population dynamics,*Stochastic Process.* Appl. 97 (2002) 95-110.

[217] Xu, P., 2019. Analytical solution for a hybrid Logistic-Monod cell growth model in batch and continuous stirred tank reactor culture. *Biotechnology and Bioengineering*, 117 (3), pp. 873-878.

[218] Xue, L., Chen, Y. Y., Yan, Z., Lu, W., Wan, D., & Zhu, H. (2019). *Staphyloxanthin*: a potential target for antivirulence therapy. *Infection and drug resistance*, 12, 2151–2160.

[219] Yan M, Pamp SJ, Fukuyama J, Hwang PH, Cho DY, Holmes S, Relman DA. 2013. Nasal micro-environments and interspecific interactions influence nasal microbiota complexity and *S. aureus* carriage. *Cell Host Microbe* 14: 631-640.

[220] Yano M, Doki Y, Inoue M, Tsujinaka T, Shiozaki H, Monden M. 2000. Preoperative intranasal mupirocin ointment significantly reduces postoperative infection with *Staphylococcus aureus* in patients undergoing upper gastrointestinal surgery. *Surg. Today Jpn. J. Surg.* 30: 16-21.

[221] Yosef I, Manor M, Kiro R, Qimron U. Temperate and lytic bacteriophages programmed to sensitize and kill antibiotic-resistant bacteria. *Proc Natl Acad Sci USA*. 2015; 112 (23): 7267-7272.

[222] Zaas AK, Burke T, Chen M, et al. A host-based RT-PCR gene expression signature to identify acute respiratory viral infection. *Sci Transl Med*. 2013; 5 (203)

[223] Zanger P, Nurjadi D, Gaile M, Gabrysch S, Kremsner PG. 2012. Hormonal contraceptive use and persistent *Staphylococcus aureus* nasal carriage. *Clin. Infect. Dis.* 55: 1625-1632.

[224] Zhang, J., Suo, Y., Zhang, D., Jin, F., Zhao, H. and Shi, C., 2018. Genetic and Virulent Difference Between Pigmented and Non-pigmented *Staphylococcus aureus*. *Frontiers in Microbiology*, 9.

[225] Zhou, P., Tang, D. and Xiao, D., 2021. On *Lotka-Volterra* competitive parabolic systems: Exclusion, coexistence and bistability. *Journal of Differential Equations*, 282, pp. 596-625.

[226] Zhu, L., Huang, X. and Su, H., 2007. Bifurcation for a functional yield chemostat when one competitor produces a toxin. *Journal of Mathematical Analysis and Applications*, 329 (2), pp. 891-903.

[227] Zwietering MH, Jongenburger I, Rombouts FM, vant Riet K (1990) Modelling of the bacterial growth curve. *Appl Environ Microbiol* 56: 1875-1881.

[228] Zwietering MH, Wijtzes T, De Wit JC, vant Riet K (1992) A decision support system for prediction of microbial spoilage in foods. *J Food Prot* 55: 973-979.